

UNIVERSITY OF OKLAHOMA
GRADUATE COLLEGE

INTEGRATED STUDY ON SEQUENCE STRATIGRAPHIC FRAMEWORK OF
DEEPWATER JACKFORK GROUP AND WOODFORD SHALE

A DISSERTATION
SUBMITTED TO THE GRADUATE FACULTY
in partial fulfillment of the requirements for the
Degree of
DOCTOR OF PHILOSOPHY

By
FUGE ZOU
Norman, Oklahoma
2015

INTEGRATED STUDY ON SEQUENCE STRATIGRAPHIC FRAMEWORK OF
DEEPWATER JACKFORK GROUP AND WOODFORD SHALE

A DISSERTATION APPROVED FOR THE
CONOCOPHILLIPS SCHOOL OF GEOLOGY AND GEOPHYSICS

BY

Dr.Roger M. Slatt, Chair

Dr.Matthew J. Pranter

Dr.Shankar Mitra

Dr.Xingru Wu

Dr.Erik D. Scott

© Copyright by FUGE ZOU 2015
All Rights Reserved.

I would like to dedicate this dissertation to my family and friends whose support, patience, and persistent encouragement was instrumental in allowing me to complete this degree program.

Acknowledgements

I would like to thank Dr. Roger Slatt, who is my mentor and advisor. He is one of the best geologists in the world with his life as a legend for others to follow. To me, he is not only a great academic advisor, but a career and life mentor. I treated him as my family and I am inspired by his hard work, optimism and responsibility, which will surely impact my future work and life. I also thank all committee members for their time and support for my PhD.

I would like to give my sincere thanks to my wife Lingxin (Cindy), without whose support I could not have completed the PhD dissertation. She helped me with lots of graphics and visualization work. And she supported me with her deep love. I thank my good friends Mr. Tao Huang, Mr. Hang Deng and Ms. Jing Zhang who helped me a lot during the research. I want to extend my gratitude to all of my parents and friends---thank you all for helping and supporting me.

Table of Contents

Acknowledgements	iv
List of Tables	ix
List of Figures	x
Abstract	xxvi
Chapter 1: Integrated outcrop reservoir characterization, modeling, and simulation of the Jackfork Group at the Baumgartner Quarry area, western Arkansas: Implications to Gulf of Mexico deep-water exploration and production	1
Abstract	1
Introduction	3
Geological Setting	6
Facies Definition	7
Stratigraphy and Architectural Elements	9
Lower Sandstones	9
Middle Shale	10
Upper Sandstones	11
Depositional Model	12
Three-Dimensional Geologic Model	13
Reservoir Simulation	16
Discussion	17
Conclusions	19
Acknowledgements	20

List of figures	21
References	36
Chapter 2: An Integrated Chemo- and Sequence- Stratigraphic Framework of the Early Pennsylvanian Deepwater Outcrops near Kirby, Arkansas, USA, and its Implications on Remnant Basin Tectonics and Hydrocarbon E&P	42
Abstract	42
Introduction	44
Geological Setting	46
Regional tectonic history	46
General stratigraphy	47
Characterization of Kirby Sections	49
Lower Jackfork Group	50
Middle Jackfork Group	52
Upper Jackfork Group	54
Johns Valley Shale	55
Regional Correlation	56
Review of DeGray Lake Area Geology	57
Review of Dierks Area Geology	59
Chemostratigraphy	60
Depositional Environments And Sequence Stratigraphy	64
Discussion	69
Conclusions	71
List of Figures	72

References	113
Chapter 3: Turbidite Petroleum Geology Updates in the Deepwater and Subsalt	
Gulf of Mexico.....	121
Abstract	122
Introduction	122
Sediment Gravity Flows (Turbidites)	123
Salt Structures And Traps.....	126
Casae Study.....	128
Exploration Updates.....	130
Neogene Play.....	134
Paleogene Play.....	135
Jurassic Norphlet Play	136
Drilling, Development And Production	137
Drilling	137
Development.....	139
Production.....	140
Vision Towards 2023	141
Conclusions	143
Acknowledgements.....	144
List of figures	145
References	170

Chapter 4: Relationship between Bioturbation, Microfacies and

Chemostratigraphy, and Its Implication on the Sequence Stratigraphic

Framework of the Woodford Shale, Oklahoma	173
Abstract	173
Introduction	176
The Woodford Shale Background	178
Methods of Study	180
<i>Chondrites</i>	182
<i>Paleodictyon</i>	183
<i>Planolites</i>	184
Radiolarian Chert and Fecal Pellets	186
Nodules	187
The Woodford Core Study	187
Lithofacies and Ichnofacies	188
Core A:	192
Core B:	195
Core C:	197
Sequence Stratigraphic Framework	197
Correlation in Anadarko Basin	203
Correlation with Woodford Shale in Permian Basin	204
Conclusions	205
List of figures	207
References	240

List of Tables

Table 2.1. List of the basic information of the key Jackfork Group outcrops.....	3
Table 2.2. General outcrop description and interpretation of the Lower Jackfork Group in Kirby Sections.....	77
Table 2.3. General outcrop description and interpretation of the Middle Jackfork Group in Kirby Sections.....	82
Table 2.4. General outcrop description and interpretation of the Middle Jackfork Group in Kirby Sections.....	87
Table 2.5. General outcrop description and interpretation of the Johns Valley Shale in Kirby Sections.....	91
Table 2.6. Summary of key chemostrata elements and proxies.....	98
Table 2.7. Categorization of the shale layers tested by ICP-MS, including 3rd and 4th order sequence boundary, local shale and their correlations.....	108
Table 2.8. Chemostrata correlation between Well A and B in deepwater GOM.....	113
Table 4.1. Comparing the relationship between type and abundance of Bioturbation in Woodford and key reservoir parameters.	236

List of Figures

Figure 1.1. Regional geologic map (including tectonic provinces) and cross section of the Ouachita Mountains and the locations of several major Jackfork Group outcrops: (1) DeGray Lakes Spillway, (2) Hollywood Quarry, (3) Dierks Spillway, and (4) Big Rock Quarry. Baumgartner Quarry is marked by a star. Modified from Slatt et al. (2000b), Suneson et al. (2008).	21
Figure 1.2. Regional stratigraphic column and tectonic events of study area in western Arkansas. The Jackfork Group was deposited during subsidence of the Ouachita Basin.	22
Figure 1.3. A complete Jackfork stratigraphic succession, including the Baumgartner Quarry. All the strata are steeply dipping toward the south. The lower, middle, and upper Jackfork Group boundaries were provided by Charles G. Stone, Arkansas Geological Commission (retired).	23
Figure 1.4. An overview of the Baumgartner Quarry, showing the location of the seven key measured sections.	24
Figure 1.5. Summary of lithofacies and architectural facies in the Baumgartner Quarry based on field observation and petrographic analysis.	25
Figure 1.6. Measured section face 2_lower in the Baumgartner Quarry, integrating lithofacies (A), outcrop gamma-ray measurements (B), architectural facies and grain sizes (C), and depositional environments (D). CPS = counts per second; F = finer grained; C = coarser grained.	26

Figure 1.7. Common sedimentary features of channel-fill sandstones in the lower sandstones, including megaflute (A1 in face 1 that can be correlated to A2 in face 2) and muddy debris-flow deposits with slump blocks (B). S = south.27

Figure 1.8. Measured section face 4_upper in the Baumgartner Quarry, integrating lithofacies (A), outcrop gamma-ray measurements (B), architectural facies and grain sizes (C), and depositional environments (D). F = finer grained; C = coarser grained..28

Figure 1.9. Sedimentary features of the upper sandstones, including unconfined channel cuts (A) and sandy debris flow (slurry beds) (B). Photographs C and D are located at the 100-m (328-ft) horizon of face 4_upper; these two photographs were taken 3 months apart. S = south..29

Figure 1.10. (A) Summary of sequence-stratigraphic units in the Baumgartner Quarry. (B) Depositional environment of the Baumgartner Quarry sequence over a larger area (sim2 times 2 km [sim1.2 times 1.2 mi])..30

Figure 1.11. Zones divided for reservoir modeling. The entire quarry is divided into 26 major zones for simulation, with thicknesses from 2 to 30 m (6.6–98 ft). Each zone is represented by a reservoir element, such as confined or semiconfined or unconfined channel fill, lobe or fan deposits, shale, and so on..31

Figure 1.12. Map view of the reservoir model, including the major reservoir elements and their composite subelements. The confined channel consists of channel axis and shale as background; the semiconfined channel is composed of channel axis and channel margin; the unconfined channel consists of channel axis, channel margin that is

much wider; lobe or fan deposits are presented by large fan-shaped sheet sandstones..
.....32

Figure 1.13. A three-dimensional view of the reservoir model of permeability with a salt surface and wells; the oil-water contact is set at 3900 m (12,795 ft). The producing well 1 and the injection well are connected through the channel axis facies, whereas the producing well 2 and the injection well are not..33

Figure 1.14. Reservoir simulation results from both upper and lower sandstones, upper sandstones only, and lower sandstones only, including cumulative production and production rate from producing well 1 (solid line) and well 2 (dashed line). Note that the (1) production volume and rate in well 1 is 60% more than those in well 2 in all cases; (2) the lower channelized sandstone package has a larger drop of production rate than does the upper sheet sandstone; and (3) the upper sandstones are more sustainable during a 10-yr production period, whereas the rate of the lower sandstones is close to zero after 10 yr..34

Figure 1.15. Comparison of pressure measurements (solid line and black dots) and prediction (dashed line) for Auger field, Garden Banks, Gulf of Mexico, and the Baumgartner Quarry modeled pressure..35

Figure 2.1. Map view of the reservoir model, including the major reservoir elements and their composite subelements. The confined channel consists of channel axis and shale as background; the semiconfined channel is composed of channel axis and channel margin; the unconfined channel consists of channel axis, channel margin that is much wider; lobe or fan deposits are presented by large fan-shaped sheet sandstones.....72

Figure 2.2. Regional stratigraphic column and tectonic events of the studied area in western Arkansas. Global sea-level curve is from Haq and Shutter, 2008. The Jackfork Group was deposited during the stage of Ouachita Basin subsidence.....75

Figure 2.3. An overview of complete Kirby sections, including Baumgartner Quarry. All the strata are steeply dipping towards the south. Lower, Middle and Upper Jackfork Group boundaries were provided by Charlie G. Stone, Arkansas Geological Commission (retired)..76

Figure 2.4. Outcrop photo, general description and outcrop gamma ray of the Kirby Roadcut 1.....78

Figure 2.5. Outcrop photo, general description and outcrop gamma ray of the Kirby Roadcut 2.79

Figure 2.6. Outcrop photo, general description and outcrop gamma ray of the Kirby Roadcut 3 and 4.80

Figure 2.7. Measured sections and interpretation (depositional model, environments, and relative sea-level)of the Lower Jackfork Group in the Kirby sections. See Figure 3.3 for locations. Locations of shale samples are marked as arrows.81

Figure 2.8. Outcrop photo, general description and outcrop gamma ray of the Kirby Roadcut 3 and 4.....83

Figure 2.9. Satellite image (Google Earth) showing the relationship between the Baumgartner Quarry and the Kirby Roadcuts, for locations see Figure 2.....84

Figure 2.10. Outcrop photo of the BQ_Section_2 on the hill of Baumgartner Quarry and Kirby Roadcut 7, the sandstones in these two sections are mostly with scoured surfaces.85

Figure 2.11. Measured sections and interpretation (depositional model, environments, and relative sea-level) of the Middle Jackfork Group in the Kirby sections. See Figure 2.3 for locations. Locations of shale samples are marked as arrows..86

Figure 2.12. Outcrop photo of the Kirby Roadcut 8...88

Figure 2.13. Outcrop photo, general description and outcrop gamma ray of the Kirby Roadcut 9..89

Figure 2.14. Measured sections and interpretation (depositional model, environments, and relative sea-level) of the Upper Jackfork Group in the Kirby sections. See Figure 2.3 for locations. Locations of shale samples are marked as arrows.....90

Figure 2.15. Outcrop photo of the Johns Valley Shale.....92

Figure 2.16. Measured sections and interpretation (depositional model, environments, and relative sea-level) of the Johns Valley Shale in the Kirby sections. See Figure 2.3 for locations. Locations of shale samples are marked as arrows...93

Figure 2.17. Paleogeography map of the Jackfork Group with key outcrop correlations, (Modified from Morris, 1971 and Pauli, 1994).94

Figure 2.18-A. An overview of Jackfork Group outcrops in the DeGray Lake area.....95

Figure 2.18-B. The measured sections in the DeGray Lake area, including Highway 7, DeGray Lake Spillway, Intake, Power Dam sections and Friendship roadcut(from Slatt et al., 2000a). Locations of shale samples are marked as arrows.....96

Figure 2.19. An overview of Jackfork Group outcrops in the Dierks Spillway area, including west and east walls. Most of the sandstone packages are flat-based, indicating a middle-distal basin-floor fan environment (lower right photo)...97

Figure 2.20. Preliminary test results of HHXRF on Roadcut 1, Kirby Section, including trace elements of Ni, Mo, Zr and Ti shown in ppm (parts per million)....	99
Figure 2.21. Preliminary test results of HHXRF on Roadcut 2, Kirby Section, including trace elements of Ni, Mo, Zr and Ti shown in ppm (parts per million)....	100
Figure 2.22. Preliminary test results of HHXRF on Roadcut 9, Kirby Section, including trace elements of Ni, Mo, Zr and Ti shown in ppm (parts per million).....	101
Figure 2.23. Preliminary test results of HHXRF on Highway 7, DeGray Lake Area Section, including trace elements of Ni, Mo, Zr and Ti shown in ppm....	102
Figure 2.24. Preliminary test results of HHXRF DeGray Lake Spillway Section, including trace elements of Ni, Mo, Zr and Ti shown in ppm ..	103
Figure 2.25. Preliminary test results of HHXRF Dierks Lake Spillway East Wall Section, including trace elements of Ni, Mo, Zr and Ti shown in ppm (parts per million)..	104
Figure 2.26. Plot of chemostrat data in the Lower, Middle and Upper Jackfork and Johns Valley Shale in the Kirby, DeGray and Dierks Sections with ICP-MS data...	105
Figure 2.27. Key trace element ratios that show a distinct data cloud for the Middle Jackfork Group using ICP-MS data....	106
Figure 2.28. Trace Elements plot of the Stanley Shale (Totten et al.,2000), Lower, Middle and Upper Jackfork Group, Johns Valley Shale (from this study) and averaged passive margin and active margins (Floyd, 1991)....	107
Figure 2.29. Chemostrata correlation between the Kirby and DeGray sections associated with Haq's (Haq and Shutter, 2008) global sea level curve....	109

Figure 2.30. Locations of sequence stratigraphic framework of the Jackfork Group, integrating all available data.....	110
Figure 2.31. Sequence stratigraphic framework of the Jackfork Group, integrating all available data	111
Figure 2.32. Evolution of Ouachita Basin from Jackfork Group to Johns Valley Shale integrating all available data... ..	112
Figure 3.1. Stratigraphic column of dGOM and key discoveries and fields (Halliburton Corp., 2010) (Ma = Million Years).	145
Figure 3.2. Major play trends and some key wells and discoveries in the deepwater Gulf of Mexico (Stars are important oil and gas discoveries or fields in each trend).bin number for anisotropy analysis.....	146
Figure 3.3. Turbidite facies in the dGOM (DeVay et al.,2000), showing major deepwater architectural elements from updip slope down to basin floor fans.....	147
Figure 3.4. Upper: west-east seismic cross section perpendicular to the direction of deposition in Mississippi Canyon, dGOM. Lower: interpreted cross section showing depositional elements and key surfaces (Sawyer, 2006). (v.e. = vertical exaggeration).	148
Figure 3.5. 5Static vs. dynamic onlaps of turbidite onto the edge of the basin or diapir (Haughton,2000).	149
Figure 3.6. Panorama of Hollywood Quarry, Jackfork Group in Arkansas, USA. It represents a channel-lobe system in a proximal fan setting which is one of the most common reservoirs in ultra dGOM Outcrop analogs have been widely used for the current ultra dGOM reservoir characterization. Three good examples for Wilcox	

reservoir analogs are Jackfork Group in USA, Ross Formation in Ireland, and Karoo Basin in South Africa.....149

Figure 3.7. Wilcox reservoir in the Baha 2 well within a sequence stratigraphic framework (Meyer et al.,2005). The vertical scale unit is in feet. The age is in million years. CS= Condensed Section..

.....150

Figure 3.8. Upper: top primary basin interpretation based upon 80,000 km² (31,000 mi²) of 3-D depth-processed seismic data, lower: schematic representation of salt-related geometries in the dGOM, GB = Garden Bank, GC = Green Canyon, AT = Atwater Valley, KC = Keathley Canyon, WR = Walker Ridge; (I) interpretation of the top primary basin surface and distinction between primary and secondary basins; (II) classification of the top primary basin surface according to the nature of the surface; (III) schematic salt geometry highlighting primary basin trap types with a turtle structure (T), bucket weld (B), salt feeder (F), salt ridge (R), base-of-salt truncation (S), and salt cored fold (C) (Pilcher et al.,2011).151

Figure 3.9. Evolution of salt mini-basins and distribution of deep water strata in the northern Gulf of Mexico (Mount et al.,2007). The age is from Jurassic (~150 million years ago) to present day..152

Figure 3.10. Schematic diagrams showing published aspects of sutures in (A) cross section and (B) map view (Dooley et al.,2012)..153

Figure 3.11. Summary of deepwater GOM reservoir development challenges (Halliburton Corp., 2010).154

Figure 3.12. Summary of major discoveries from 2008-2014 in the deepwater Gulf of Mexico (Halliburton Corp., 2010). N/A = Not Available.155

Figure 3.13. The structural model and map of the Tahiti field, Green Canyon Block 640, deepwater GOM (Swaston et al.,2012)..156

Figure 3.14. Summary of deepwater GOM reservoir development challenges (Halliburton Corp., 2010).157

Figure 3.15. Summary of major discoveries from 2008-2014 in the deepwater Gulf of Mexico (Halliburton Corp., 2010). N/A = Not Available.158

Figure 3.16. The structural model and map of the Tahiti field, Green Canyon Block 640, deepwater GOM (Swaston et al.,2012)..159

Figure 3.17. Lower Tertiary paleogeography and depositional styles in the northern Gulf of Mexico. Some discoveries are shown by red stars (Berman and Rosenfeld,2007)160

Figure 3.18. Wilcox discoveries and deepwater GOM resource potential (Chevron Corp., 2011). Orange color is the Miocene Trend, Green Color is the Paleogene (Lower Tertiary Wilcox) Trend, Deep purple color is the salt canopy, small red circles are key Paleogene fields.....161

Figure 3.19. The Norphlet play area in the eastern Mississippi Canyon and Desoto Canyon and the three most important discoveries by Shell (Shell Oil Company, 2014)...162

Figure 3.20. Summary of Wilcox pressure challenges (Shaker, 2010). PS =principle stress, FP= fracture pressure, OB = overburden, PP = pore pressure, SB = salt buoyancy.....163

Figure 3.21. Summary of the Wilcox reservoir development in Perdido fold belt (Chevron Corp., 2011). 164

Figure 3.22. Major trapped oil mechanisms for Paleogene Wilcox reservoirs in dGOM (Lach, 2010). 165

Figure 3.23. IOR deliverability forecast for Paleogene fields (Lach, 2010). Total near-term, mid-term and far-term IOR can contribute up to 42.1% of oil recovery by forecast. From a practical standpoint, the IOR process during Wilcox reservoir development should use the technology having a mature technical level and lower costs. Among the methods mentioned above, conventional water flood, subsea multiphase pumping, conventional hydrocarbon gas injection, in well ESP, and directional or horizontal drilling have the highest “technical readiness level”, and they should be applied regularly during the reservoir development phase. In the IOR process ranking, conventional water flooding and subsea multiphase pumping rank the highest. A combination of these IOR methods will unlock the recovery step by step through near, mid to far term field life cycle. Ideally, the ultimate recovery factor through the life cycle of the field can be up to 42%..... 166

Figure 3.24. Reservoir simulation results from both upper and lower sandstones, upper sandstones only, and lower sandstones only, including cumulative production and production rate from producing well 1 (solid line) and well 2 (dashed line). Note that the (1) production volume and rate in well 1 is 60% more than those in well 2 in all cases; (2) the lower channelized sandstone package shows a larger drop in production rate than does the upper sheet sandstone; and (3) the upper sandstones are more

sustainable during a 10-yr production period, whereas the rate of the lower sandstones is close to zero after 10 years (Zou et al.,2012)..167

Figure 3.25. Oil production and prediction of dGOM (Paganie, 2009)..168

Figure 3.26.Production from 2010-2020 by companies (Wood Mackenzie, 2014).Bnboe = billion of barrels oil equivalent, BP = British Petroleum, CVX = Chevron Corporation, RDS = Royal Dutch Shell, APC = Anadarko Petroleum Corporation, XOM = ExxonMobil Corporation, STL = Statoil Corporation, PBR = Petrobras Corporation, HES = Hess Corporation, ENI = Eni Corporation, APA = Apache Corporation, ME = Murphy Oil Company, DVN = Devon Corp, BHP = BHP Corp.169

Figure 3.27. NPV and breakeven oil prices (left), and NPV/boe and total Capex (right) for deepwater GOM plays (Wood Mackenzie, 2014). BOE = Barrel of Oil Equivalent, NPV = Net Present Value.....169

Figure 4.1.Gross isochore thickness map from top Woodford Shale to top Hunton Group in the study area (in feet, 100ft = 30m), with three well locations marked as A, B and C.....207

Figure 4.2.Stratigraphic column of the Woodford Shale based on global sea-level (Johnson et al. (1985), Slatt et al. (2013), and Spaw (2013)), biostratigraphy work is mainly from Conodonts by Dr. Jeffrey Over, Kerogen Type from Corelab.....208

Figure 4.3.Upper Left: Core photo of short Chondrites from Upper Woodford of Core A (43'). Upper Right: The same short Chondrites in the segmentation images of Micro CT-Scan. Middle: Zoom in photos of the pyritized Chondrites. Lower Left: Thin-Section

photo of the long Chondrites from Middle Woodford in Core C, Lower Right: 3-D CT Scan Segmentation images of the same interval. (Thin-Section and 2-D Core photos by Kimberly Hlava and Joan Spaw.).....209

Figure 4.4. Upper: Thin-section of short Chondrites in argillaceous shales from Middle Woodford of Core B (97'). Lower: Abundant pyritized short Chondrites in Middle Woodford of Core B (118') . (Thin-Section photos by Joan Spaw and CoreLab.).....210

Figure 4.5. Upper Left: Core photos of the Grazing Trails from Upper Middle Woodford of Core A. Upper Right: 2X reflected light of the same photo. Lower Left: Thin section photo of the same intervals. Note the burrows are filled by cherts. Lower Right: 3-D CT Scan Segmentation image of the same intervals.....211

Figure 4.6. Integrated trace fossil analysis at 30-31 ft (9.5m) of Core A. Left: 3-D segmentation of the Planolites with 2-D intersections. Red arrows points to the same Planolites feature to compare. Right: thin-section photo of the same interval, with Corelab parameters (lithology, XRD, TOC, and sequence.....212

Figure 4.7. Planolites example at 222ft (67.5m) of Core C. Upper Left: 2-D Micro CT image; Middle Left: 2-D Micro-CT image with 3-D Segmentation; Lower Left: 3-D Segmentation showing the 3-D geometry of Planolites. Upper Right: Core Photo at the same interval. There is obvious advantage of 3-D Micro CT-Scan in viewing the burrows.....213

Figure 4.8. Integrated trace fossil analysis at 181ft (55m) of Core C. Left: 3-D segmentation of the Planolites with 2-D intersections. Red arrows points to the same

Planolites features to compare. Right: thin-section photo of the same interval, with Corelab parameters (lithology, XRD, TOC, and sequence).....	214
Figure 4.9.Integrated trace fossil analysis at 98ft (30m) of Core C. Left: 3-D segmentation of the Planolites with 2-D intersections. Red arrows points to the same Planolites features to compare. Right: thin-section photo of the same interval, with Corelab parameters (lithology, XRD, TOC, and sequence).....	215
Figure 4.10.Examples of Thalassinoides in Core B and C, both examples are in Lower Woodford. The materials in vertical burrows are coarser grained than surrounding matrix, with occasionally pyritized framboid in them (Photos by Kimberly Hlava).....	216
Figure 4.11.Pyritized radiolarian chert examples in Core C. Left: thin-section photos by Kimberly Hlava. Right: 3-D Micro-CT-Scan Segmentation of the same interval.....	217
Figure 4.12. An example of the 3-D Micro-CT segmentation of nodules of 347-350ft (106m) in Core C (Upper Woodford). Left is the whole core image combined with nodules; middle is the noise and nodules; right is the filtered nodules.....	218
Figure 4.13.Upper: Shale classification by Gamero-Diaz et al. (2012)Lower: Ternary diagram plots showing how Lower, Middle and Upper Woodford Shale fall into their categories for Core A, B and C.....	219
Figure 4.14.A sophisticated schematic slope-to-basin depositional model for the Woodford Shale within a sequence stratigraphic framework. Modified from Slatt, 2013.Thin-section data by Joan Spaw, Kimberly Hlava and Corelab.....	220

Figure 4.15.Examples of the criteria of the abundance of trace fossils, using a Bioturbation Index (BI) measured from Micro-CT scan 3-D segmentation image and thin-section description. From left to right are: Absent (BI=0), Sparse (BI=1), Common (BI=2), and Abundance (BI=3). The values of the BI have been used for statistics and calculations.....221

Figure 4.16. Petrophysics logs of Corer A, including GR, Resistivity, Neutron-Density, Calculated TOC, VClay, Brittleness from dipole sonic logs and calculated water saturation.....222

Figure 4.17.Integrated description of Core A, with emphasis on bioturbation. Bioturbation Index (BI) is the sum of all four trace fossils (short Chondrites, long Chondrites, Paleodictyon, Planolites). Description and Interpretation are based on Dr. Joan Spaw, Kimberly Hlava and Fuge Zou’s work.....223

Figure4.18.Integration of bioturbation data for Core A, including GRI (Gas Research Institute) porosity, permeability, XRD and Geochemistry from CoreLab. Burrow Type: Chondrites (C), Paleodictyon and Grazing Trails (G), Planolites (P) and Thalassinoides (T).....224

Figure 4.19.Integration of bioturbation data for Core A with chemostrata data. The high resolution hand held X-Ray Fluorescence (XRF) data is from Dr. Harry Rowe of University of Texas at Austin.....225

Figure 4.20. Petrophysics logs of Corer B, including GR, Resistivity, Neutron-Density, Calculated TOC, VClay, Brittleness from dipole sonic logs and calculated water saturation.....226

Figure 4.21. Integrated description of Core B, with emphasis on bioturbation.
 Bioturbation Index (BI) is the sum of all four trace fossils (short Chondrites, long Chondrites, Paleodictyon, Planolites). Description and Interpretation are based on Dr. Joan Spaw, Kimberly Hlava and Fuge Zou’s work.227

Figure 4.22. Integration of bioturbation data for Core B with chemostrata data. The high resolution hand held X-Ray Fluorescence (XRF) data is from Dr. Harry Rowe of University of Texas at Austin. Burrow Type: Chondrites (C), Paleodictyon and Grazing Trails (G), Planolites (P) and Thalassinoides (T)228

Figure 4.23. Integration of bioturbation data for Core B with chemostrata data. The high resolution hand held X-Ray Fluorescence (XRF) data is from Dr. Harry Rowe of University of Texas at Austin.229

Figure 4.24. Petrophysics logs of Corer C, including GR, Resistivity, Neutron-Density, Calculated TOC, VClay, and calculated water saturation.230

Figure 4.25. Integrated description of Core C, with emphasis on bioturbation.
 Bioturbation Index (BI) is the sum of all four trace fossils (short Chondrites, long Chondrites, Paleodictyon, Planolites). Description and Interpretation are based on Dr. Joan Spaw, Kimberly Hlava and Fuge Zou’s work.231

Figure 4.26. Integration of bioturbation data for Core C with chemostrata data. The high resolution hand held X-Ray Fluorescence (XRF) data is from Dr. Harry Rowe of University of Texas at Austin. Burrow Type: Chondrites (C), Paleodictyon and Grazing Trails (G), Planolites (P) and Thalassinoides (T)232

Figure 4.27. Integration of bioturbation data for Core B with chemostrata data. The high resolution hand held X-Ray Fluorescence (XRF) data is from Dr. Harry Rowe of University of Texas at Austin.233

Figure 4.28. Cross-plotting of bioturbation intensity, permeability, porosity and lithofacies of 149 samples from three the Woodford corers. Upper Left is the permeability-porosity plot colored by bioturbation index. Upper Right is the permeability-porosity plot colored by lithofacies. Lower is the plotting of Porosity vs. Permeability colored by bioturbation types.234

Figure 4.29. Regional stratigraphic framework of Woodford Shale in the study area. Left is the reconstruction of basin history. Right is location map (including correlation to the Hall 2B well and Hunton Anticline Quarry) and global sea-level curve.236

Figure 4.30. Gross isochore maps of Lower Middle and Upper Woodford Shale, showing the transition of more restricted deposition in Lower Woodford to more extended deposition in Upper Woodford.237

Figure 4.31. Correlation from Marathon Oil Core C to Hunton Anticline Quarry (measured by Bryan and Slatt, 2013) ~25 Miles (40km) southeast to Core C. Gamma Ray and key chemostrata parameters matches the sequence stratigraphic framework.238

Figure 4.32. Correlation from Marathon Oil Core B to Hall 2B well (measured by Bryan and Slatt, 2013) ~30 Miles (48km) southwest to Core B. Gamma Ray and key chemostrata parameters matches the sequence stratigraphic framework. Note Hall 2B only cut Upper Woodford and Upper Middle Woodford Shale.239

ABSTRACT

Deepwater turbidites and unconventional shale reservoirs are two most important hydrocarbon resources in North America. To fully understand the hydrocarbon potentials of the deepwater reservoirs, we first need to utilize outcrops as analogs to help build good reservoir models because they are often easier to access and characterize than subsurface data. The Jackfork Group in Arkansas is a good example of deepwater turbidite outcrops. It has been studied for more than 40 years by both industry and academy. During my M.Sc. and early stage of PhD years (2009-2012), I successfully characterized the Jackfork Group at the Baumgartner Quarry and used it as an analog for reservoir modeling and simulation in real deepwater GOM fields. The Baumgartner Quarry work exhibits a good difference in simulated reservoir performance between channelized and sheet-like reservoirs. Following the Quarry work, I extended the outcrop characterization to the entire Jackfork Group within a large area from southeastern Oklahoma to western Arkansas. I compiled, described and characterized 20 nearby Jackfork outcrops and subsurface data including Kirby Section, DeGray Section, Shell Rex-Timber Well #1, Dierks Spillway, Mena Section, Big Rock Quarry, Friendship Roadcuts, Rich Mountain Anticline and Potato Hills gas fields. I tested chemostrata within Kirby; DeGray and Dierks sections in order to correlated them and build a sequence stratigraphic framework in the downdip basinal part of the Ouachita Basin. The final part of the Jackfork Group research is a complete sequence stratigraphic framework from updip slope to downslope basinal settings. This is the first time such a regional correlation has been completed for the Jackfork across the

Ouachita Mountains, and is of great value for understanding updip to downdip facies changes in the Jackfork.

After I finished the Jackfork Group research, I became interested in the 3 Woodford Shale cores from Marathon Oil Company, the company I am working for. Three Woodford cores, The Teague, Ridenour and Shi-Randall are located in the updip shelf, downdip slope and basin, respectively and they well represent the sequence stratigraphic framework during late Devonian time. Marathon Oil ran Micro-CT scan with the 3 cores. By reprocessing and segmenting on these 3-D raw Micro-CT scan data, one can quantitatively characterize the bioturbation and micro facies of the whole core. By comparing bioturbation Micro-CT results with well logs, geochemistry, routine core analysis and chemostrata, I built the regional sequence stratigraphic framework over the core area.

This dissertation mainly combines 3 **AAPG Bulletin** papers (one published, one in revision and one to be submitted). The first **AAPG Bulletin** paper (Chapter 1) is about reservoir modeling and simulation of the Jackfork Group in the Baumgartner Quarry, Arkansas. The second **AAPG Bulletin** paper (Chapter 2) is the research results on the integrated chemostrata and sequence stratigraphic framework of the Jackfork Group in Arkansas. The third **AAPG Bulletin** paper (Chapter 4) is the research results of bioturbation, chemostrata and integrated stratigraphic framework of Woodford Shale in southeast Anadarko basin, Oklahoma. One part of the Woodford Shale research (Chapter 4) has been also accepted by the **URTeC 2015 Conference** in San Antonio, Texas as an Oral Presentation. The dissertation also contains another published paper in **Journal of Earth Science and Engineering** which is a review of the deepwater Gulf of

Mexico (dGOM) exploration and production activities for the past 6 years (Chapter 3). In addition, I wrote two chapters about deepwater GOM E&P and geological modeling in the textbook: "**Stratigraphic Reservoir Characterization for Petroleum Geologists, Geophysicists, and Engineers, 2nd Edition**" by Dr. Roger M. Slatt published in 2013 by **Elsevier**. I have presented my PhD work in **AAPG, UrTEC, GCAGS** and **GSA** conferences with 6 abstracts from 2010-2015.

**Chapter 1: Integrated outcrop reservoir characterization, modeling,
and simulation of the Jackfork Group at the Baumgartner Quarry
area, western Arkansas: Implications to Gulf of Mexico deep-water
exploration and production***

Fuge Zou^{1,2}, Roger Slatt¹, Rodrigo Bastidas², Benjamin Ramirez²

¹ConocoPhillips School of Geology and Geophysics, University of Oklahoma, Norman,
Oklahoma

²Marathon Oil Company, Houston, Texas

**This paper has been published in AAPG Bulletin, August, 2012*

ABSTRACT

The lower Pennsylvanian Jackfork Group in Arkansas has been the subject of studies, field trips, and publications for many years because of excellent outcrop exposures of different deep-water architectural elements. This latest study is focused on the Baumgartner Quarry located near Kirby, Arkansas, which exposes a series of vertical walls in three dimensions. This quarry has not been as well documented as other popular exposures, although three-dimensional (3-D) quarry faces exist, and the quarry strata comprise part of a complete 600-m (1970-ft)-thick near-continuous Jackfork stratigraphic sequence not unlike younger deep-water stratigraphic exploration targets in the Gulf of Mexico and elsewhere. Subsurface problems including reservoir

uncertainties and reservoir performance of lobe versus channel-fill deposits are addressed based on our work in the quarry.

A 3-D sequence-stratigraphic model was developed using a correlation of seven measured stratigraphic sections in the quarry. The 180-m (590-ft)-thick quarry strata consist of a lower lowstand systems tract (LST) (lower sandstones) dominated by channel-fill sandstones, overlain by a shaly transgressive systems tract (condensed section), and then by an upper LST (upper sandstones) dominated by sheet or lobe sandstones.

This model was translated into an updip against salt field, which is analogous to some deep-water Gulf of Mexico reservoirs. Performance simulation was conducted on the model using a one-injector water well and two vertical producing wells, one of which was connected to the injector via a channel sandstone and the other of which was offset from the channel sandstone. Results yielded 60% more production from the connected injector-producer pair than from the nonconnected pair. Comparison between the lower (channel-prone) sandstones and the upper (sheet-prone) sandstones revealed that the sheet-prone sandstone is more sustainable, whereas the channel-prone sandstone exhibits a larger drop in production rate during a 10-yr production period. These results illustrate the value of 3-D outcrop models for reservoir performance simulation for development planning of deep-water fields with limited data control, such as in the deep-water Gulf of Mexico.

INTRODUCTION

Outcrops play an important function in providing two-dimensional (2-D) and three-dimensional (3-D) geologic models for understanding deep-water reservoir performance prediction (Slatt *et al.*, 2000b; Larue, 2004; Sullivan *et al.*, 2004; Stewart *et al.*, 2008; Jackson *et al.*, 2009; Sech *et al.*, 2009). Three-dimensional outcrop exposures, either horizontally bedded strata or long steeply dipping stratigraphic exposures, provide information that cannot be obtained from subsurface data, even when wells are closely spaced.

Sullivan *et al.* (2004) characterized large and long horizontal outcrops in the Ross Formation in Ireland and Skoorsteenberg Formation in South Africa and integrated bed continuity and connectivity measurements to solve reservoir uncertainties in the early stage of development of the Diana field, Gulf of Mexico. Larue (2004) evaluated different architectures (including variation in area, net to gross, and subseismic thin-bed effects) of multistory and multilateral channelized slope reservoirs for effects on volumes and waterflood recovery. Furthermore, Sech *et al.* (2009) and Jackson *et al.* (2009) compared the performance of a barrier versus a layer-cake model for a shoreface reservoir to best predict the oil in place and production rate. The Pennsylvanian Jackfork Group in Arkansas contains several excellent quarry and roadcut exposures of updip to downdip deep-water facies and architectural elements (Morris, 1971; Jordan *et al.*, 1991; Slatt *et al.*, 1997, 2000a, b; Al-Siyabi, 2000; Olariu *et al.*, 2008). Two such well-known exposures have been the subject of research studies and educational field trips for academia and industry for many years. The first is the 300-m (984-ft)-long upper Jackfork sequence at DeGray Lake Spillway (Slatt *et al.*,

2000a, b; Slatt and Stone, 2010, Schlichtemeier 2011). Slatt *et al.* (2000b) used several steeply dipping Jackfork Group outcrops and the ground surface in DeGray Lake, Arkansas, to simulate a “reservoir against unconformity topseal” with vertical and horizontal well scenarios.

The second is Hollywood Quarry (Slatt *et al.*, 2000a; Goyeneche *et al.*, 2006), a 400 times 200 times 23–m (1312 times 656 times 75–ft) outcrop, which exhibits deep-water channel and lobe stratigraphy, sealing and nonsealing faults (extensional, thrust, and strike slip), folds, fractures, and injectites. Hollywood Quarry has been documented sufficiently to build 3-D geologic models for simple reservoir performance simulation (Jordan *et al.*, 1991; Slatt, 2000a). Goyeneche *et al.* (2006) and Liceras (2010) characterized and modeled the stratigraphy and structures of the quarry in detail. They then tested reservoir performance of the quarry model from a simple tank model to a more sophisticated model with sealing and nonsealing fault scenarios. The sealing faults with shale barriers resulted in up to 30% reduction of production compared with the simple tank model.

The subject of this article is a less well-known, but equally spectacular, quarry near Kirby, Arkansas, named the Baumgartner Quarry (Figure 1.1). This quarry is cut into a series of benches oriented perpendicular to the strike of the beds, which comprise 180 m (590 ft) of steeply dipping sandstones and shales, thus providing 3-D exposures along its depositional trend. Duran (2007) completed a basic 3-D geologic model of part of the quarry and built a partial reservoir model. His work provided the foundation for the more detailed model and the accompanying reservoir performance simulation presented in this article.

It is particularly significant that this quarry contains both deep-water channel and lobe (sheet) sandstones that can be correlated in three dimensions from different quarry walls. Also, the geometry, orientation, width, and thickness of sheet and channelized sandstone beds can be measured, thus providing the opportunity to build a more sophisticated reservoir model.

The strata in the Baumgartner Quarry comprise the middle part of a continuous, easily accessible, 600-m (1970-ft)-thick section of alternating thick packages of sandstone and shale through the entire Jackfork from its basal contact with the Stanley Shale to its upper contact with the Johns Valley Shale (first described by Morris, 1971). This complete sequence is considered an excellent stratigraphic analog to deep-water sequences in the Gulf of Mexico and elsewhere.

The production performance of channelized versus sheet-prone reservoirs has always been a significant concern of deep-water field development and production in the Gulf of Mexico. Booth *et al.* (2000) described the Auger field in Garden Banks, Gulf of Mexico, as a sheet-prone reservoir; production performance was much better than originally expected because of a series of very uniform and continuous sheet sandstones across the Auger salt minibasin. However, channelized reservoirs commonly provide a faster than expected pressure drop because of a lack of aquifer support. Brushy Canyon outcrops have been used to resolve channel compartmentalization in the Ram-Powell field (Kendrick, 2000). A better understanding of the reservoir architectures of channel versus sheet sandstones and their related production performance using outcrops and field data remains an interesting spotlight for the remaining potentially very large global deep-water hydrocarbon resource.

The coexistence of channel and lobe sandstones in the Baumgartner Quarry provides a unique opportunity to compare and contrast their characteristics and simulated reservoir performance. The purpose of this article is to first describe the stratigraphy of the quarry then discuss how a geologic model was built to compare reservoir performance between lobe (sheet) and channel sandstones. Finally, we compare our model and simulations with present Gulf of Mexico deep-water exploration and production examples.

GEOLOGIC SETTING

The Jackfork Group in Arkansas has been described in publications by Morris (1971), Graham *et al.* (1975), Jordan *et al.* (1991), Roberts (1994), Slatt *et al.* (2000a) and others, so is not repeated here in any detail. It is part of the Ouachita Mountain fold and thrust belt (Figure 1.1) and is exposed along several high-angle imbricate thrust sheets generated by collision of North and South American plates during the Late Pennsylvanian–Permian Ouachita orogeny. Balanced reconstruction work implies that the Ouachita fold and thrust belt has been through a positive tectonic inversion process like many other exposed turbidite-rich foreland basins in the world (Ingersoll *et al.*, 2003; Suneson *et al.*, 2008). In the Early Pennsylvanian (Morrowan), Jackfork sediments were sourced from the north, south, and northeast and deposited in the west-east–trending Ouachita Basin (Figure 1.2). Sequence-stratigraphic analysis indicates that the Jackfork was deposited during a second-order relative sea level cycle beginning about 320 Ma with a major global drop of sea level; several third- and probably fourth-order sequences are superimposed (Slatt *et al.*, 2000a).

The 600 m (1970 ft) of Jackfork strata along the Highway 27 roadcut are composed of (1) the lower Jackfork (includes roadcuts 01 and 02); (2) the middle Jackfork (includes roadcuts 03 and 04 and Baumgartner Quarry); and (3) the upper Jackfork (includes roadcut 05) (Figure 1.3).

Locally, the 180 m (590 ft) of strata exposed at the Baumgartner Quarry strike northeast 70 to 75deg and dip 65 to 75deg south (Figures 3, 4). These strata are divided into three sequences: (1) 50 m (164 ft) of “lower sandstones,” (2) 30 m (98 ft) of “middle shale,” and (3) 100 m (328 ft) of “upper sandstones.” For descriptive purposes, the following names are used to define and discuss strata comprising the benches within the quarry. Lower sandstones = face 1, face 2, and face 3. Upper sandstones = face 2, face 3, face 4, and face 5. Duran (2007) described many of these faces. However, newer faces have been cut back 15 to 45 m (49–148 ft) since his work, adding more three dimensionality to our geologic model (Figure 1.4).

FACIES DEFINITION

The lower sandstones, middle shale, and upper sandstones were described along several transects at 0.3-m (1-ft) intervals. The Bouma sequence terminology was used to describe the lithofacies. The lithofacies were then integrated with architectural facies and hierarchy provided by Bouma (2000), Slatt *et al.* (2000a), and Campion *et al.* (2003).

Seven interpretive architectural facies were defined (Figure 1.5): channel-fill sandstone, channelized sheet sandstone (weakly confined sandstone), amalgamated sheet sandstone, layered sheet sandstone, thin-bedded sandstone and shale, parallel-

laminated shale, and muddy debris-flow deposits. These facies are described below and in more detail by Zou (2010).

Channel-fill sandstone is lenticular and exhibits scour surfaces, flute structures, soft-sediment deformation features, and tool marks. Shale clasts occur at the bases of individual beds. Grain size ranges from medium to coarse sand (0.2–0.8 mm). The thickness of a single bed ranges between 0.3 and 2.1 m (1–7 ft). Petrographic analysis indicates about 2% mud matrix and 98% quartz.

Channelized sheet sandstone (weakly confined sandstone) is a transition facies between channel and sheet sandstones. It exhibits a sheetlike geometry in outcrop and contains flute structures and irregular scoured bases. It has an aspect ratio (width/height ratio) between that of the typical channel-fill sandstone (lt100:1) and sheet sandstone (gt500:1). Grain size ranges from fine to coarse sand (0.2–0.6 mm). The single-bed thickness is 0.06 to 3 m (0.2–10 ft) and amalgamated intervals are up to 6 m (20 ft) thick. Petrographic analysis indicates about 5% mud matrix and 95% quartz.

Amalgamated sheet sandstone is laterally continuous and tabular in outcrop. Internal features include thick massive Bouma Ta beds with amalgamation surfaces. The beds are commonly flat based with minor or no flute structures. Grain size ranges from fine to medium sand (0.1–0.4 mm). The thickness is 0.15 to 0.6 m (0.49–2 ft) for single beds and 3 to 10 m (10–33 ft) for amalgamated bedsets. Petrographic analysis indicates more than 90 to 95% quartz.

Layered sheet sandstone consists of thin-bedded sandstones with thin shale intervals. The beds are generally flat based and lack flute structures. Grain size ranges from very fine to fine-grained sandstone (0.05–0.3 mm). Individual sandstone beds are

0.03 to 0.15 m (0.1–0.49 ft) thick. The net sand is relatively low (50–80%) because of the interbedded shale.

Interbedded thin-bedded sandstone and shale lithofacies is common. Grain size is silt to very fine sandstone (0.02–0.2 mm). Individual sandstone beds are 0.03 to 0.12 m (0.1–0.4 ft) thick and the net sand is low (20–60%). Multiple possible origins include levees, abandonment channels, and distal fans.

Parallel-laminated shale is also common and could represent basin floor shale as well as condensed sections.

Debris-flow lithofacies occurs as either massive or contorted shale matrix with contained sandstone blocks. This lithofacies is associated with both channelized and basin-floor deposits. When associated with channel deposits, it is the product of erosional collapse. When associated with basin-floor deposits, this lithofacies tends to be more of a slurry bed with a high sand content.

STRATIGRAPHY AND ARCHITECTURAL ELEMENTS

Lower Sandstones

The lower sandstones are mainly composed of a series of channelized Bouma Ta sandstone beds separated by Bouma Tc and Td beds (Figure 1.6A). Common sedimentary features in the sandstones include shale clasts, tool marks, flute marks, load structures, cross beds, and scour surfaces. Larger features include erosional megaflores (Elliott, 2000; Pyles, 2008; Kane *et al.*, 2009) (Figure 1.7A1, A2), irregular bed bases, and compensation stacking patterns. Muddy debris-flow deposits are also present (Figure 1.7B) at face 2_lower (2 m [6.6 ft] thick), face 1, and are more than 5 m (16.4

ft) thick at face 2 and face 3. Sandy, massive, medium-grained, siderite-cemented slump blocks, which are petrographically similar to underlying channel-fill sandstones, occur in the muddy matrix. Some of the discontinuous Bouma Tc-Td beds are interpreted as levee deposits associated with the channel sandstones, whereas fewer Bouma Tc-Td beds are interbedded with tabular Bouma Ta beds (Figure 1.6C). Structurally corrected paleoflow directions on several flutes range from 290 to 330deg Az for some of the channel-fill sandstones and 65 to 75degAz for channelized sheet sandstone (weakly confined sandstone).

According to the hierarchy system by *Campion et al.* (2003), the entire lower sandstone section is interpreted as a weakly confined and retrogradational channel complex that consists of at least three possible channel fills. The first channel fill is located from 0 to 10 m (0–33 ft), with two to three stories in between. It is overlain by a 5- to 7-m (16.4- to 23-ft)-thick muddy debris-flow deposit, then another compensationally stacked channel fill from 12 to 26 m (39–85 ft). This second channel fill is followed by a 1-m (3.3-ft)-thick shale drape and a 2-m (6.6-ft)-thick tabular sandstone package. The third channel was cut into the tabular sandstones with retrogradational patterns from 30 to 45 m (98–148 ft). The aspect ratio (width/thickness) of single-story channelized sandstones decreases from channel fill 1 to channel fill 3.

Middle Shale

This 30-m (98-ft)-thick shale separates the lower sandstones from the upper sandstones. It is dark brown to black and finely laminated. The upper part of the shale

contains large, detached, floating blocks of sandstone that are similar in appearance to the underlying lower sandstones. The middle shale is considered a marine condensed section because of its thickness, uniform lithology, and high gamma-ray API values. The detached blocks near the top of the shale may be the product of slumping of slope strata during initiation of a sea level drop.

Upper Sandstones

The upper sandstones are dominated by tabular Bouma Ta sandstones interbedded with a 5-m (16.4-ft)-thick dark shale (Bouma Te) and several other thinner shaly Bouma Td beds (Figure 1.8A). The upper sandstones are interpreted as a series of stacked, amalgamated, and layered sheet sandstones (Figure 1.8C). The upper part of the upper sandstones consists of thick amalgamated sheet sandstones with several channel-fill sandstones at the top.

Flute marks in the upper sandstones indicate flow from the northeast to the southwest at 60 to 80deg Az (Figure 1.9A). This is different from the paleoflow directions in the lower sandstones, probably because they represent two different architectural elements. The main transport direction of strata within the Ouachita Basin in the Early Pennsylvanian was mainly from north-northeast to west-southwest (Slatt *et al.*, 2000a), which coincides with the sheet-prone upper sandstones and some parts of channelized sheet sandstone (weakly confined sandstone) in the lower sandstones. The northwest-southeast flow direction measured in the channel-fill sandstone in the lower sandstones is probably a more local feature caused by channel stacking and/or sinuosity.

Debris-flow deposits within the upper sandstones are thinner and sandier than those in the lower sandstones (Figure 1.9B). Thicknesses range from 0.3 to 0.5 m (1–1.6 ft) over a very short distance. These beds are interpreted as having formed by local autocyclic processes (Weimer and Slatt, 2006). Sandy slurry beds are believed to be more common in a more distal environment (Lowe *et al.*, 2003; and evidence of common slurry beds in Cascade reservoir cores in Walker Ridge, Gulf of Mexico). In the uppermost part of the section (75–95 m [246–312 ft]), channel-fill sandstones, levee deposits, and channel-margin facies exhibit sand-on-sand contacts along the interpreted channel axis, whereas the interpreted channel margin contains a shale drape between channel sandstones (Figure 1.9C, D). These figures show a thick interval (gt3 m) of debris-flow deposits overlain by a channel-levee complex. The whole quarry wall was cut farther east by more than 10 m (gt33 ft) in a 3-month period, which revealed along-strike lateral discontinuity over a short distance.

More sheet-prone distal sandstone facies and shale in the upper sandstones suggest that the depositional environment was relatively farther downdip than that of the lower sandstones. The section from 0 to 70 m (0–230 ft) is interpreted as three separate basin-floor fan deposits. The overlying section is interpreted as possible prograding channel-fan complex with a muddy debris-flow deposit on top.

DEPOSITIONAL MODEL

Figure 1.10A summarizes the interpreted architectural facies of the Jackfork Group in the Baumgartner Quarry. The vertical facies stacking of sheet sandstones on top of channel sandstones in the lower sandstones indicates a shift of depositional

environment from channels to sheets caused by retrogradation or lateral avulsion. Retrogradation continued with deposition of the thick middle shale (condensed section), which can also be interpreted as complete avulsion and decrease of sand into this area (not very likely for a 30-m [98-ft]-thick shale in the Jackfork Group). In the upper sandstones, channel-fill sandstones with slump deposits stacked above sheet sandstones are caused by progradation of more proximal channel sandstones over more distal sheet deposits.

Figure 1.10B shows a stratigraphic model closer to the size of a deep-water reservoir (sim2 times 2 km [sim1.2 times 1.2 mi]) based on the sequence-stratigraphic framework. Depositional environments and aspect ratios of thickness versus length are based on the Baumgartner Quarry stratigraphy. This model provided the basis for reservoir modeling and simulation described below.

The presence of thick channel-fill sandstone and amalgamated sheet sandstones is caused by either allocyclic processes such as small-scale sea level drops at third- or fourth-order scales (see Slatt *et al.*, 2000a, based on sedimentation rate by Morris, 1974) or autocyclic processes such as avulsion (for the channel-fill system) and compensational stacking (for the lobe or fan system). The large sandstone blocks in the top of the shaly condensed section signifies an early drop of sea level, which later produced the upper sandstones.

THREE-DIMENSIONAL GEOLOGIC MODEL

The entire measured sections in the Baumgartner Quarry have been divided into 26 zones ranging from 2 to 30 m (6.6–98 ft) based on the depositional model (Figure

1.11). Five reservoir elements were defined: (1) confined stacked channel fill, (2) unconfined or semiconfined channel fill, (3) lobe or fan deposits, (4) levee or overbank deposits, and (5) parallel-laminated shale. Also, five subelements were defined to characterize each reservoir element: axial channel-fill sandstone, margin channel-fill sandstone, sheet sandstone, siltstone, and parallel-laminated shale.

The global positioning system coordinates of seven measured sections were input into a 3-D geologic model after calculating the true stratigraphic thickness. All steeply dipping structures of the Baumgartner Quarry were corrected and transferred into a horizontal model to distribute the interpreted facies. The measured sections were considered as pseudovertical wells and placed close to the center of a 5 times 5-km²-shaped area (the size of the model is close to a deep-water Gulf of Mexico outer continental shelf (OCS) block or a general deep-water field).

Geometry of the channel-fill sandstone story was best estimated based on the aspect ratio and sedimentary structures. For example, the channel sandstone shown in Figure 1.7A in face 1_lower and face 2_lower exhibits an about 30% thickness change over a 100-m (328-ft) lateral distance. Thus, the width of the channel is probably from 500 to 1000 m (1640–3280 ft). Usually, semiconfined and unconfined channel sandstones have larger widths because only minor (0–10%) thickness changes have been observed, and the width of such a channel can be up to 2 to 4 km (1.2–2.4 mi). Sheet sandstone intervals, which typically exhibit less than 1% thickness change over a few kilometers distance, can be either represented in the model by a large fan-shaped body or a layer-cake interval, depending on their position within the sequence (e.g., middle vs. proximal fan in a lowstand systems tract or distal turbidite in a transgressive

systems tract). In general, the channel-fill sandstones in the lower sandstones are more confined than those in the upper sandstones because of different depositional environments. An exception is the confined channel-fill deposit (elements) located at the top of the upper sandstones (Figure 1.11).

We tested both stochastic and deterministic modeling of the reservoir elements and subelements. For example, an unconfined channel fill (reservoir elements) has three subelements: channel axis, channel margin, and siltstone (subelements). For deterministic modeling, the boundaries between the different subelements were drawn by hand with respect to the flow direction and measured sections located at the center of the model. For stochastic modeling, object-based algorithms were used (e.g., sequential indicator simulation). We found that, for very limited data control over a large area, a deterministic model is more geologically reasonable (Zou, 2010). In this case, sparse well control is similar to early stages of field development in the deep-water Gulf of Mexico, where data from only two to three exploration and appraisal wells may be available. General paleoflow direction (which was from east to west in Arkansas) was set to be from north to south to facilitate the modeling process for the Gulf of Mexico. Based on these settings and assumptions, subelements were distributed zone by zone using a deterministic method (Figure 1.12).

Jackfork Group strata have long been used as an outcrop analog for deep-water architectural element observation and measurement. However, porosity and permeability of these rocks are very low. Thus, for this article, we incorporated porosity values from a subsurface Gulf of Mexico reservoir to simulate reservoir performance, as was previously done for other Jackfork outcrops (Slatt, 2000; Slatt *et al.*, 2000b;

Goyeneche *et al.*, 2006). To obtain reasonable porosity and permeability values for the model, grain size was determined for the different subelements from thin-section analyses (Zou, 2010) then related to field porosity and permeability data from deep-water Gulf of Mexico reservoirs (Weimer and Slatt, 2006). Simple properties data were then assigned to the model (Figure 1.12).

After constructing the reservoir elements model in a layer-cake setting, topography of the surface, pseudo oil-water contact, and lateral seal boundaries were added to model a simple trap against a salt wall in a deep-water setting (Figure 1.13). The 3-D surfaces of reservoirs and salt were created based on studies of a three-way closure-type (which is an updip structural or stratigraphic trap against a salt feeder or canopy) fields such as Auger, Mars-Ursa, Troika, and Droshky in the Gulf of Mexico.

RESERVOIR SIMULATION

Parameters of oil and water saturation, pressure, compressibility, fluid saturations, and sedimentary and stratigraphic features were derived in a similar manner and imported into the model to simulate the production performance (Slatt *et al.*, 2000b). For simplistic modeling, some very thin beds such as shale drape, levee, or overbank deposits were upscaled and grouped into related channel or sheet sandstones, although this may result in up to 20% difference in production performance (Larue, 2004; Goyeneche *et al.*, 2006; Zou, 2010). Larue (2004) investigated the effect of lateral barriers inside a channel complex by comparing different permeabilities across channel boundaries versus homogeneous permeability. Goyeneche *et al.* (2006) simulated a uniform tank model versus a model with barriers in the Hollywood Quarry.

Other parameters used in our simulation represent a deep-water reservoir at 3600 m (11,811 ft) depth with the initial pressure of 8000 psia (Slatt *et al.*, 2000b; Zou, 2010). A typical trap against the salt field case with two producing wells and one injection well was simulated. Oil-water contact was set at 3900 m (12,795 ft). Channel sandstones penetrated by the injection well are connected to producing well 1 along the flow direction (north-south) but not connected to producing well 2 (Figure 1.13), which is offset to flow direction. Simulation was set for the 10-yr production with 8650 bbl (1000 m³) per day water injection.

Three production cases were simulated: both upper and lower sandstones, upper sandstones only, and lower sandstones only. Figure 1.14 shows the cumulative production and production rate from well 1 (solid line) and well 2 (dash line). Note that (1) in all cases, production volume and rate in well 1 is 60% more than those in well 2; (2) the lower channelized sandstone package has a larger drop of production rate than the upper sheet sandstone package; (3) production rate for the upper sandstones is more sustainable during the 10-yr production period, whereas the rate for the lower sandstones is close to zero after 10 yr.

DISCUSSION

High and sustainable production rate depends on several factors, including reservoir architecture (channel fill vs. sheet), sandstone thickness, areal extent, and internal connectivity (Kendrick, 2000). Our simulation results show that the sheet-prone upper sandstones can provide sustained field production for a much longer period than the channel-prone lower sandstones (Figure 1.15). Generally, the sheet-prone upper

sandstones not only have better aquifer support to maintain reservoir pressure but also have a better continuity for internal migration of hydrocarbons. One classical example of this scenario is the Auger field in Garden Banks, Gulf of Mexico (Booth *et al.*, 2000; Kendrick, 2000), where a history match indicates a potential aquifer volume 53 times the size of the petroleum volume (Figure 1.15). The production performances indicate that the sheet sandstone reservoirs are continuous across the entire Auger minibasin. Lower sandstones, however, have more internal barriers because of a channel-levee setting. Our simple model indicated a high initial production rate and a faster decline, which is mainly caused by a higher permeability along the channel axis and limited areal extent of channel geometry. More barriers and lateral heterogeneities are present in the Baumgartner Quarry than in the model, and they have been ignored in the upscaling process. However, these barriers will decrease the sweep efficiency of waterflood production. In our model, channel-fill facies perforated in production well 1 have a 60% higher production volume and rate than in well 2, which is completely separated from the injector well. In a real case, water breakthrough may also occur during this period for producing well 1, but not for well 2 (Stewart *et al.*, 2008). Kendrick (2000) pointed out that the perched water trapped in the bottom of channelized sandstones may adversely impact one's estimate of in-place hydrocarbon volumes because they are isolated from the aquifer. One example is the Ram-Powell field in Mississippi Canyon, Gulf of Mexico.

Slatt *et al.* (2000b) proposed two factors that are particularly relevant to deep-water reservoir management: proportion of facies and their lateral continuity. The proportion of channelized facies versus sheet sandstone facies in the Baumgartner

Quarry strata are shown to vary in a systematically and geologically plausible way, particularly when placed within a sequence-stratigraphic context. As our model suggests, the difference between channel and sheet architectures observed in the outcrop will greatly affect aquifer pressure support, sweep efficiency, and recovery efficiency in the model. Recognizing the causes and effects listed above will be critical in the reservoir development stage.

CONCLUSIONS

This article presents an integrated approach to characterization and modeling of deep-water Jackfork Group strata in the Baumgartner Quarry area, western Arkansas. An entire 3-D geologic modeling workflow, from outcrop data collection, to petrographic analysis, to computer modeling and simulation is presented. The geologic model is noteworthy because at Baumgartner, two different sandstone packages are present and separated by a thick shale. One package is channel prone and the other is sheet prone, thus making it possible to compare and contrast their characteristics and simulated reservoir performance. Results of simulations indicate that the sheet-prone upper sandstones can provide sustained production for a much longer period than the channel-prone lower sandstones.

The Baumgartner Quarry reservoir model can serve as an outcrop analog for various deep-water reservoirs in the Gulf of Mexico, North Sea, offshore Brazil, offshore west Africa, and elsewhere. Although the active margin tectonic setting of the Jackfork Group differs from these other deposits, the combination and order of architectural elements remain similar at the reservoir scale. Thus, outcrops of deep-

water successions such as at the Baumgartner Quarry can be used as analogs to deep-water reservoirs for input into geologic models, reservoir performance simulation, and management planning.

ACKNOWLEDGEMENTS

Fuge Zou thanks the School of Geology and Geophysics for supporting his graduate research and Roger M. Slatt as his graduate thesis adviser. We thank Charlie Stone for guidance and discussion of Arkansas fieldwork. We also thank Staffan Van Dyke and David Pyles for their discussion and inspiration. We thank Abousleiman for his generous support on the core-plug tests in his laboratory. We thank Jonathan Funk for his support on the research. We thank Majia Zheng and Shanshan Liu who helped us with three-dimensional geologic modeling using Petrel. We thank Henry Badra, John Brumley, Nabanita Gupta, Rafael Sierra, and Supratik Sarkar for technical support. We thank Kui Zhang for kindly helping us with seismic forward modeling. We thank Xiaochun Jin for kindly helping us with reservoir simulation. We thank the turbidite trip class of 2010 for participating in measuring the Kirby sections. We thank Colin North, Jonathan Stewart, and Kirt Campion for great reviews to improve this article.

LIST OF FIGURES

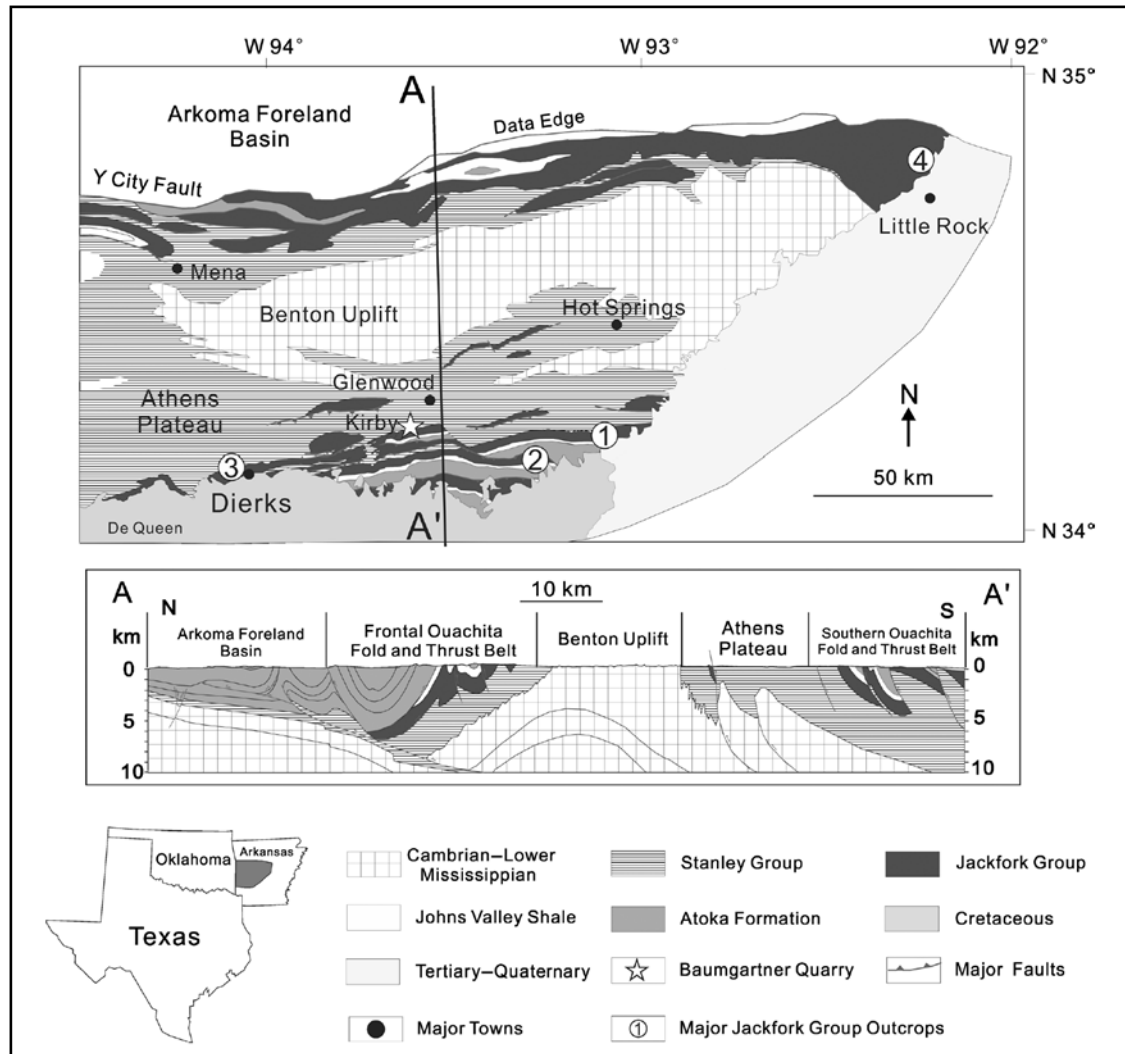


Figure 1.1. Regional geologic map (including tectonic provinces) and cross section of the Ouachita Mountains and the locations of several major Jackfork Group outcrops: (1) DeGray Lakes Spillway, (2) Hollywood Quarry, (3) Dierks Spillway, and (4) Big Rock Quarry. Baumgartner Quarry is marked by a star. Modified from Slatt *et al.* (2000b), Suneson *et al.* (2008).

Ma	System		Formation	Tectonic Events
65	Tertiary–Quaternary			Craton
290	Cretaceous			Igneous Intrusion
310 323 354 417 443 495 545	Pennsylvanian	Desmoinesian		Late Pennsylvanian Ouachita Orogeny
		Atokan	Atoka Formation	Orogenic Foreland Basin Subsidence
		Morrowan	Johns Valley Shale	
			Jackfork Group	
		Mississippian	Chestertian	Stanley Group
	Merrimacian			
	Osagean		Kindehookian	
	Kindehookian			
	Devonian			
	Silurian			
Ordovician				
Cambrian				
Precambrian			Rifting	

Figure 1.2. Regional stratigraphic column and tectonic events of study area in western Arkansas. The Jackfork Group was deposited during subsidence of the Ouachita Basin.

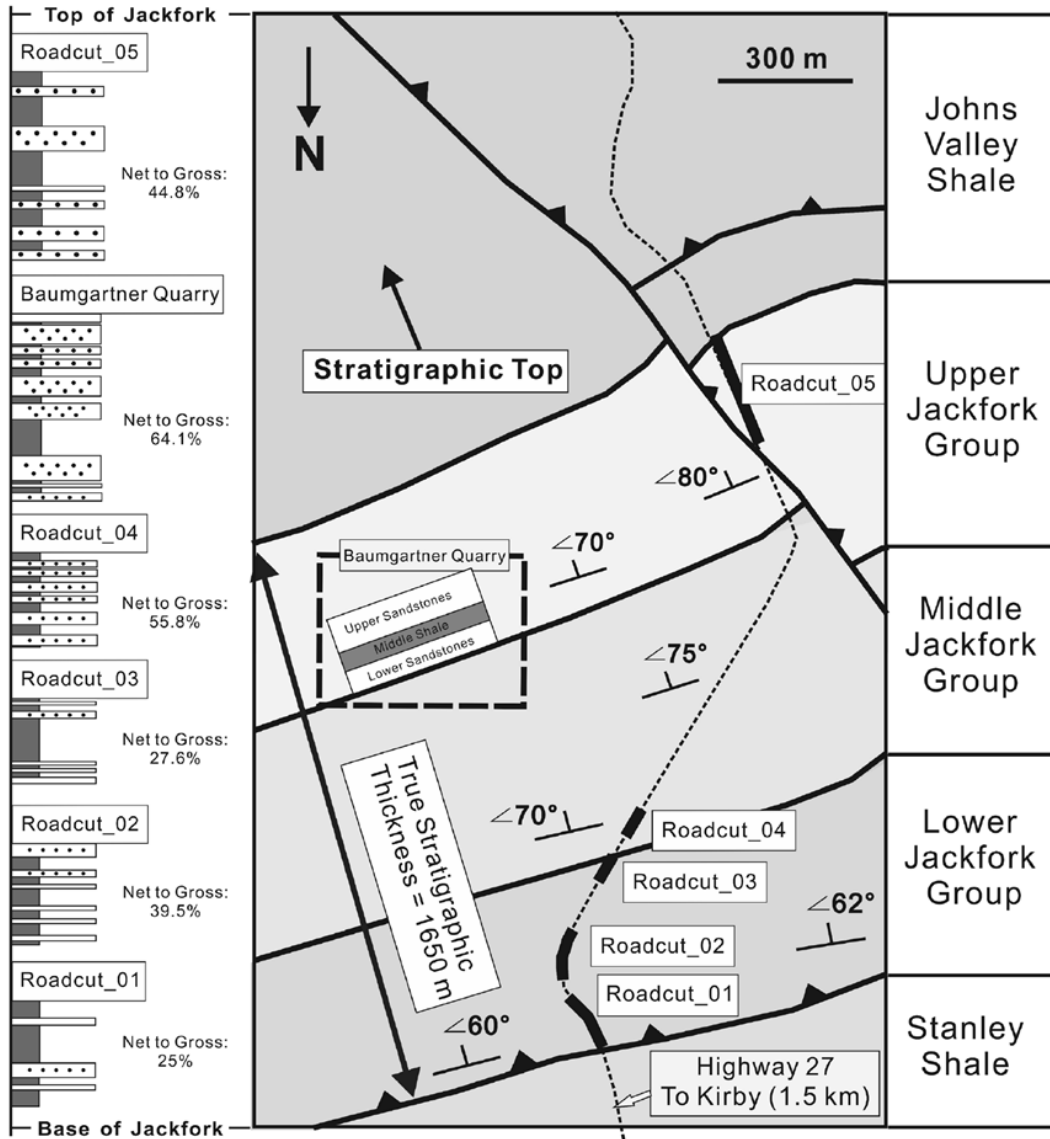


Figure 1.3.A complete Jackfork stratigraphic succession, including the Baumgartner Quarry. All the strata are steeply dipping toward the south. The lower, middle, and upper Jackfork Group boundaries were provided by Charles G. Stone, Arkansas Geological Commission (retired).

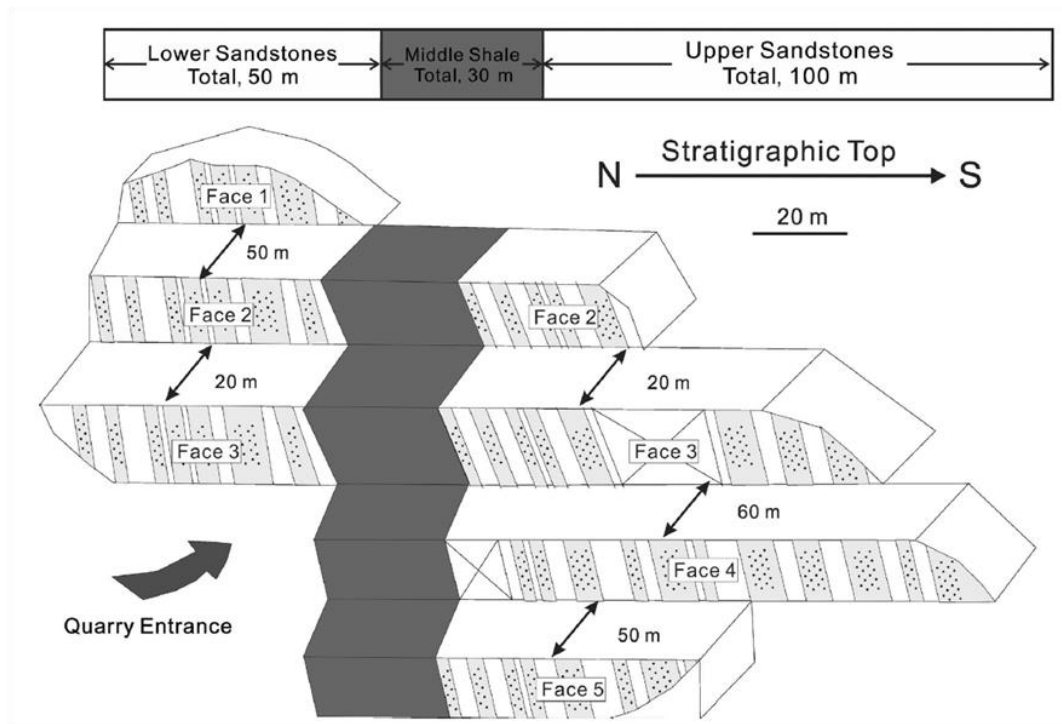


Figure 1.4.An overview of the Baumgartner Quarry, showing the location of the seven key measured sections.




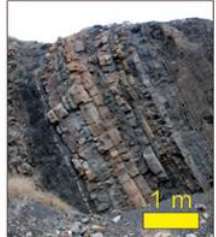
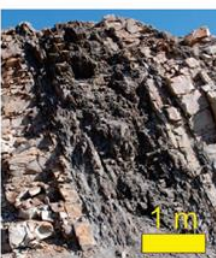

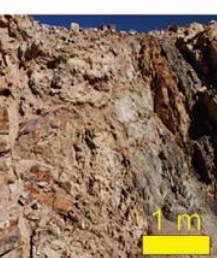
Channel-Fill Sandstone	Channelized Sheet Sandstone	Amalgamated Sheet Sandstone	Layered Sheet Sandstone
			
Thin-Bedded Sandstone and Shale	Parallel-Laminated Shale	Muddy Debris-Flow Deposits	
			

Figure 1.5. Summary of lithofacies and architectural facies in the Baumgartner Quarry based on field observation and petrographic analysis.

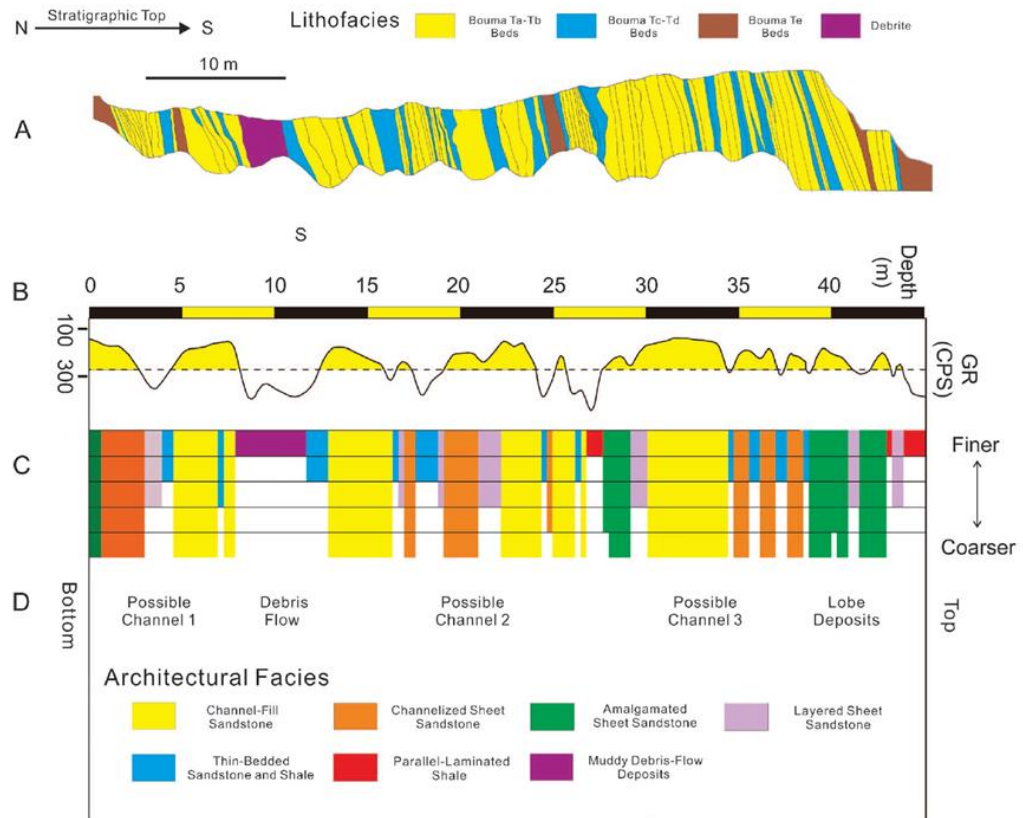


Figure 1.6. Measured section face 2_lower in the Baumgartner Quarry, integrating lithofacies (A), outcrop gamma-ray measurements (B), architectural facies and grain sizes (C), and depositional environments (D). CPS = counts per second; F = finer grained; C = coarser grained.

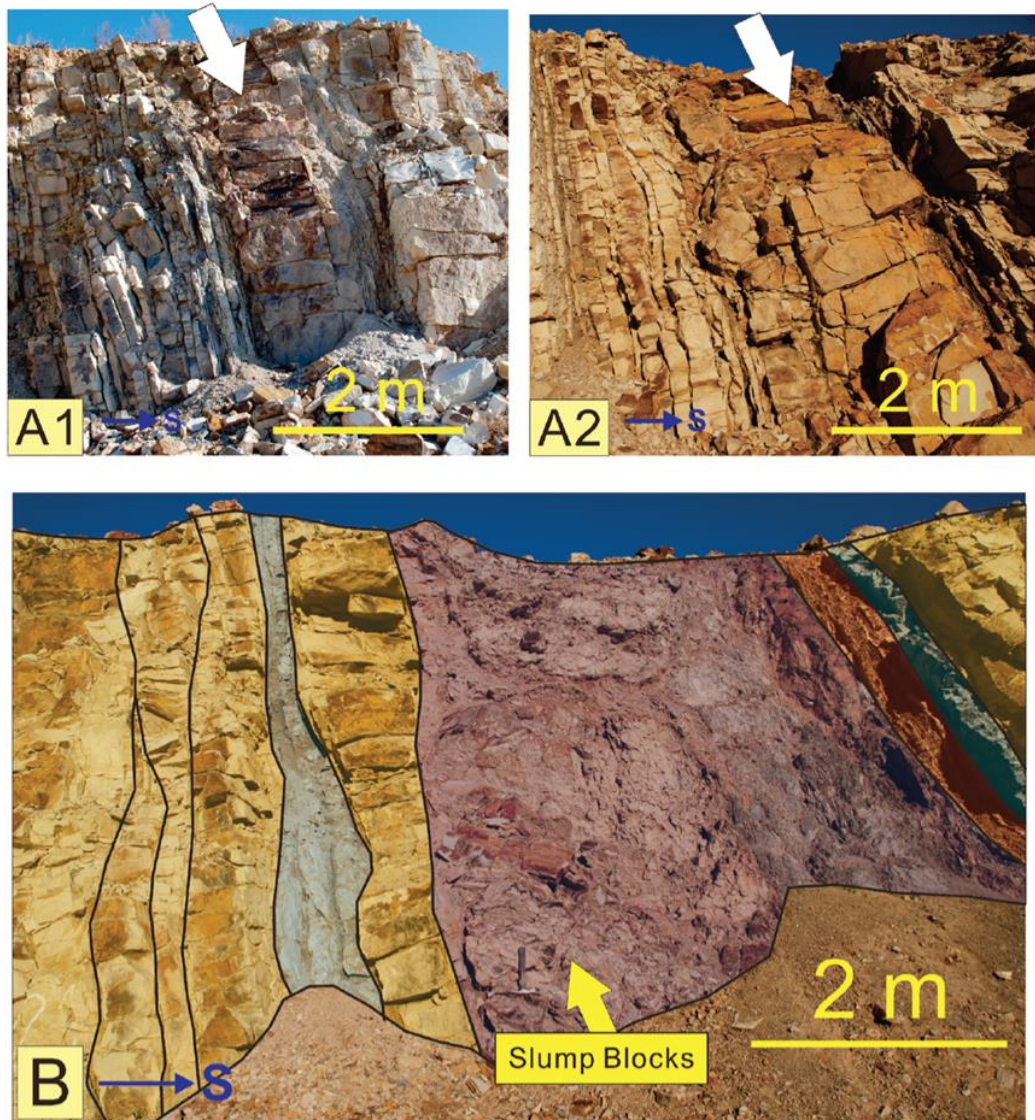


Figure 1.7. Common sedimentary features of channel-fill sandstones in the lower sandstones, including megafloor (A1 in face 1 that can be correlated to A2 in face 2) and muddy debris-flow deposits with slump blocks (B). S = south.

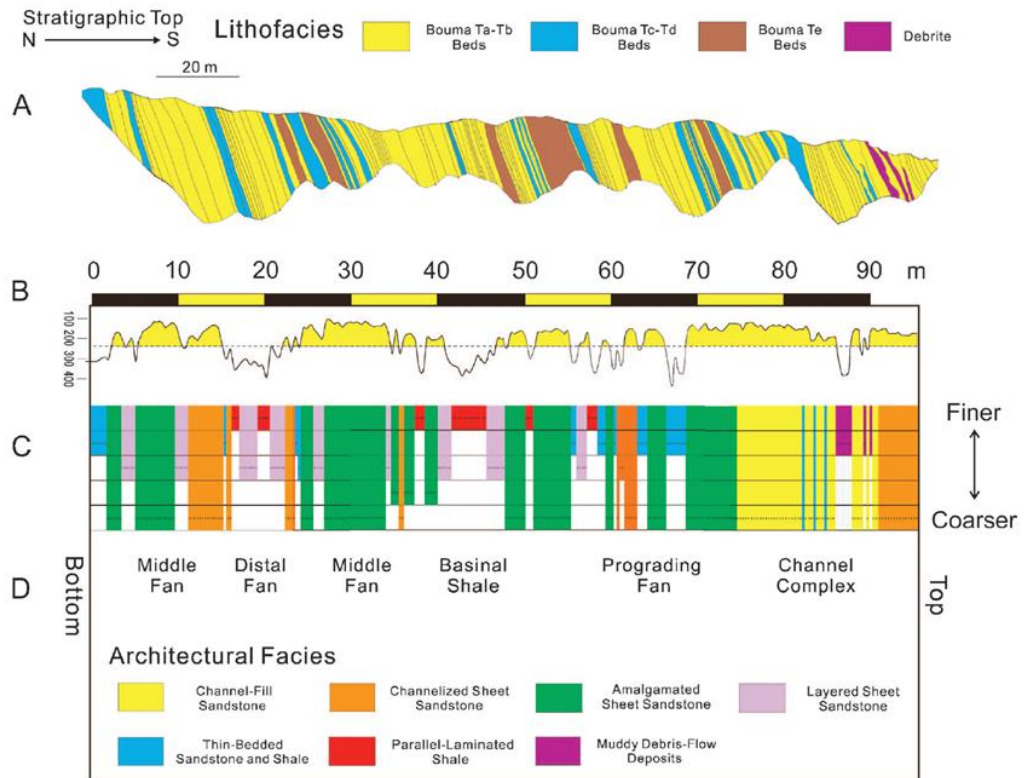


Figure 1.8. Measured section face 4_upper in the Baumgartner Quarry, integrating lithofacies (A), outcrop gamma-ray measurements (B), architectural facies and grain sizes (C), and depositional environments (D). F = finer grained; C = coarser grained.

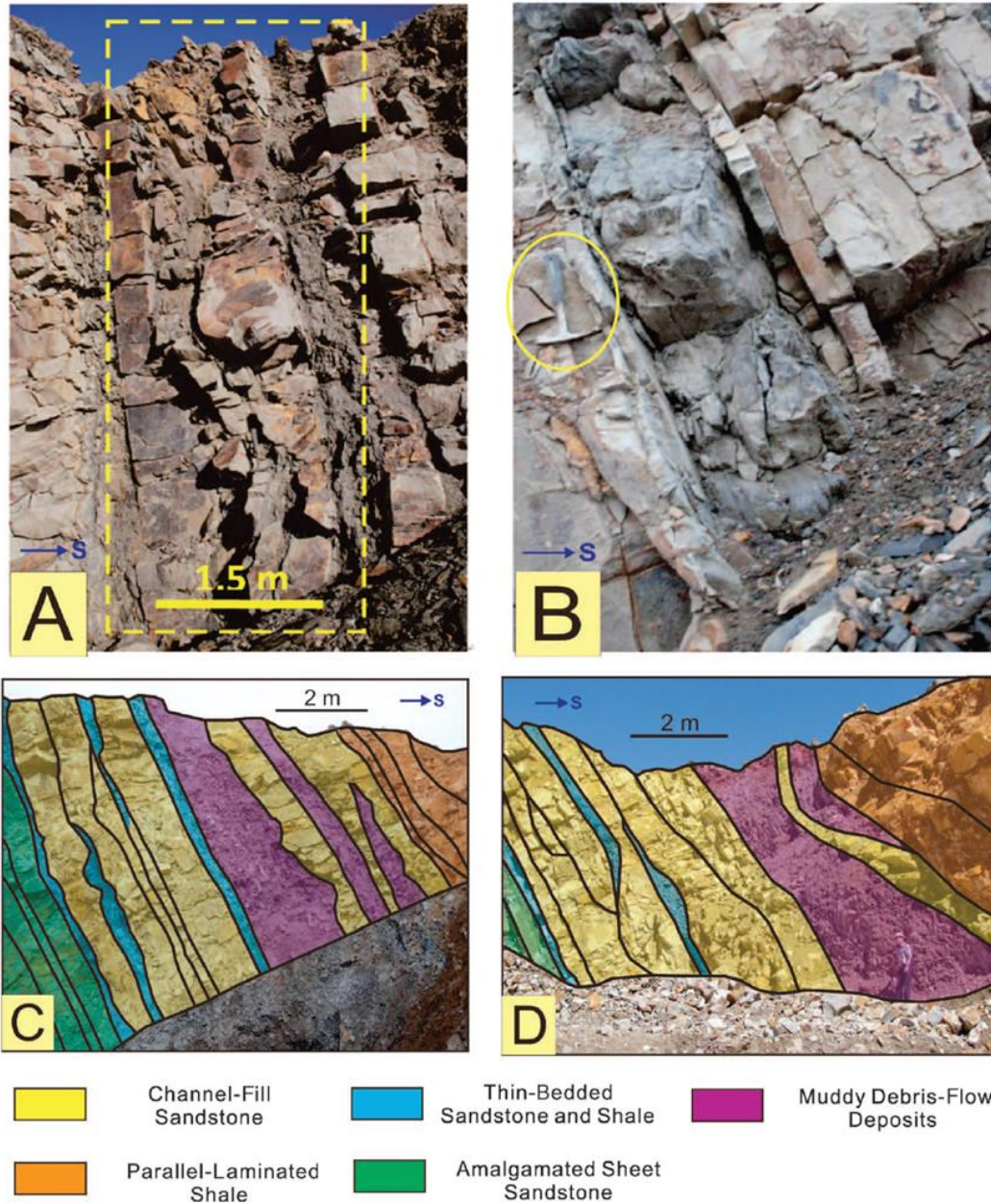


Figure 1.9. Sedimentary features of the upper sandstones, including unconfined channel cuts (A) and sandy debris flow (slurry beds) (B). Photographs C and D are located at the 100-m (328-ft) horizon of face 4_upper; these two photographs were taken 3 months apart. S = south.

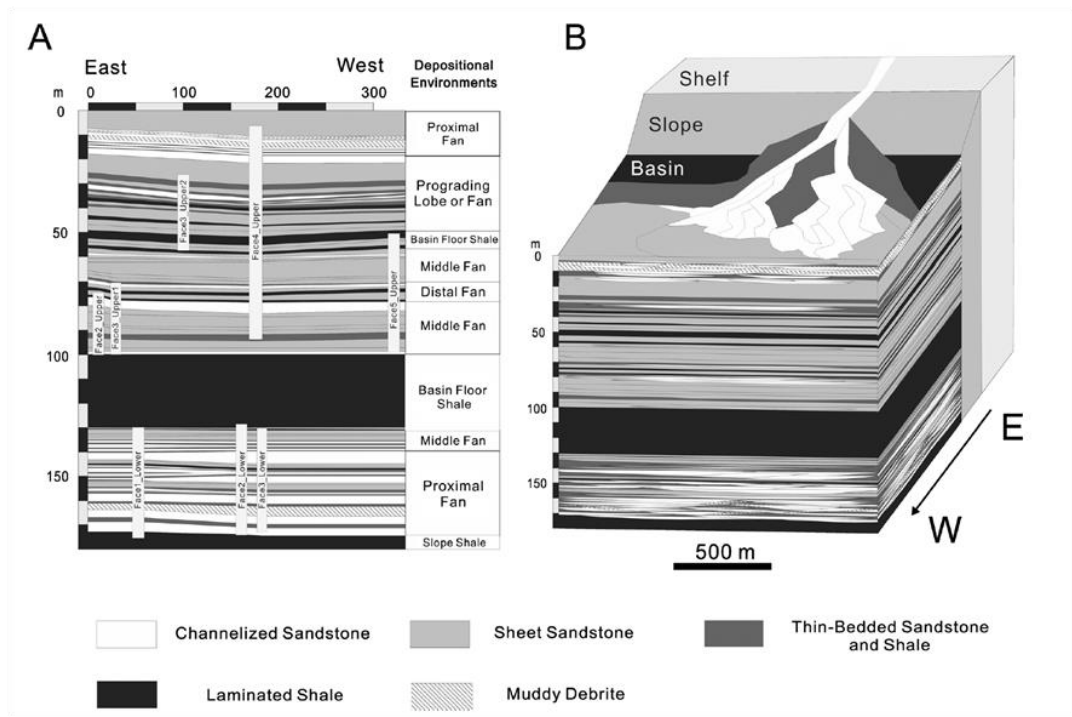


Figure 1.10. (A) Summary of sequence-stratigraphic units in the Baumgartner Quarry. (B) Depositional environment of the Baumgartner Quarry sequence over a larger area (sim2 times 2 km [sim1.2 times 1.2 mi]).

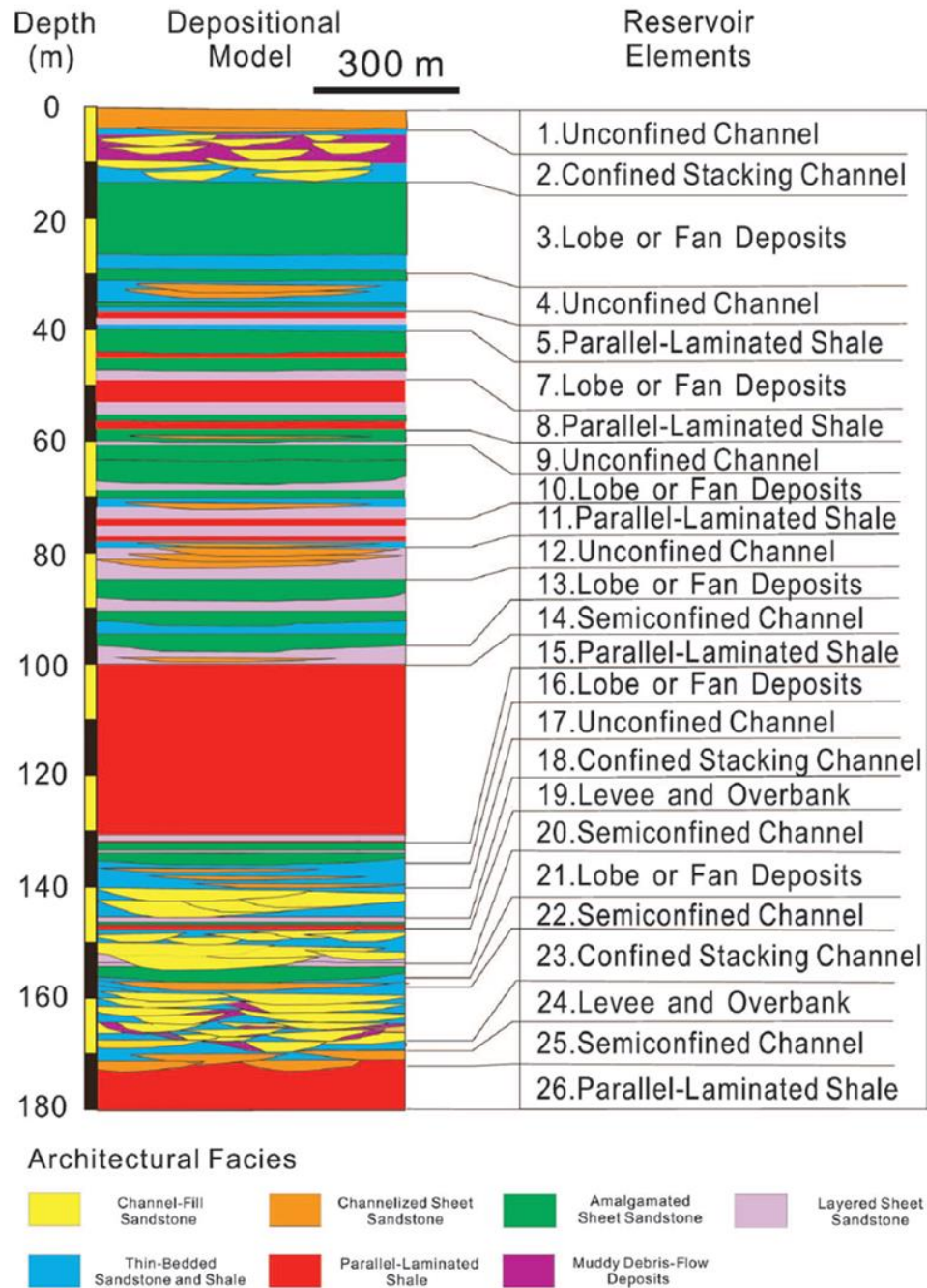


Figure 1.11. Zones divided for reservoir modeling. The entire quarry is divided into 26 major zones for simulation, with thicknesses from 2 to 30 m (6.6–98 ft). Each zone is represented by a reservoir element, such as confined or semiconfined or unconfined channel fill, lobe or fan deposits, shale, and so on.

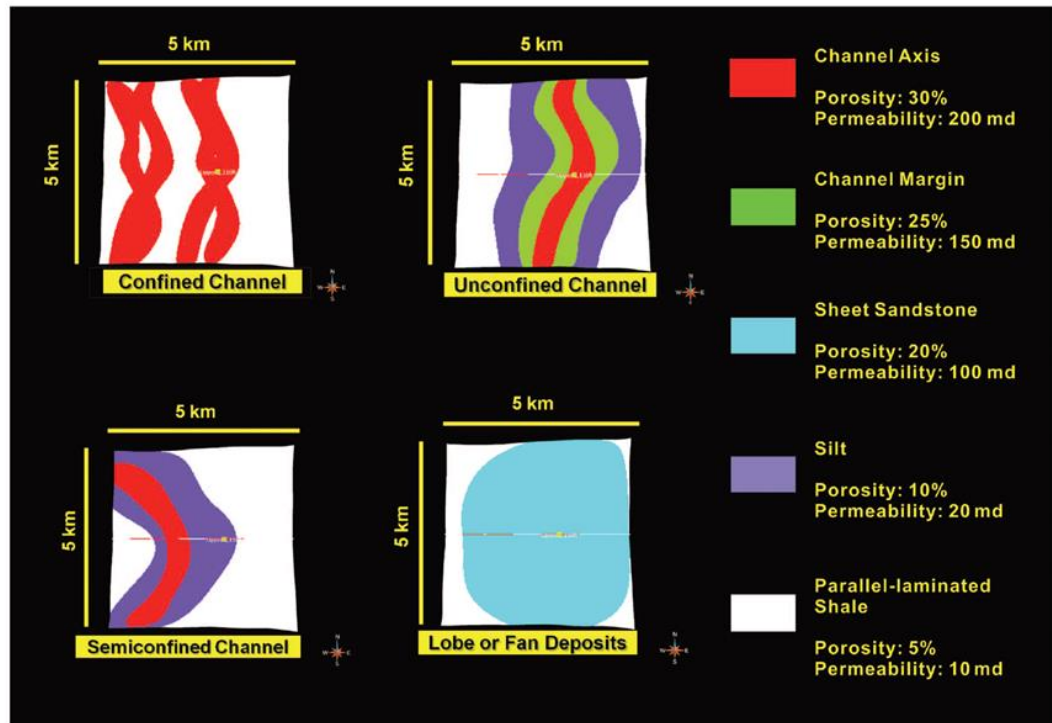


Figure 1.12. Map view of the reservoir model, including the major reservoir elements and their composite subelements. The confined channel consists of channel axis and shale as background; the semiconfined channel is composed of channel axis and channel margin; the unconfined channel consists of channel axis, channel margin that is much wider; lobe or fan deposits are presented by large fan-shaped sheet sandstones.

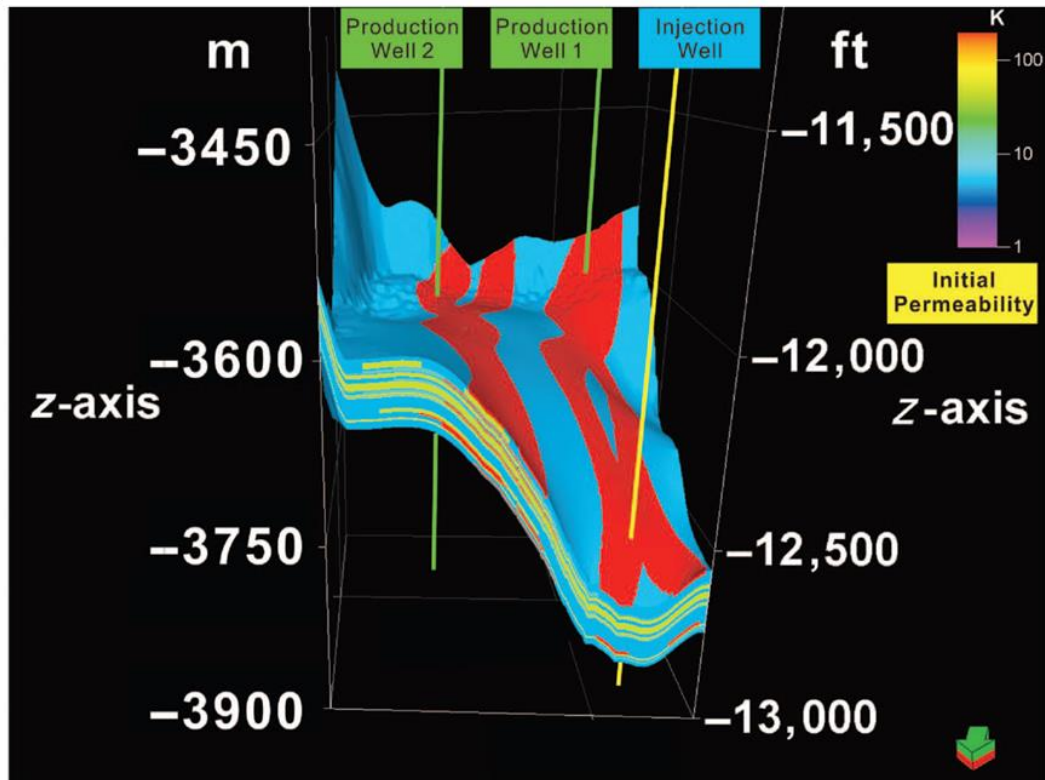
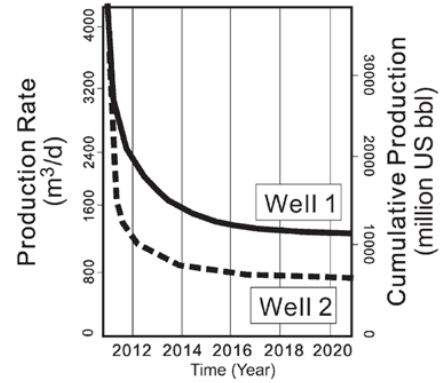
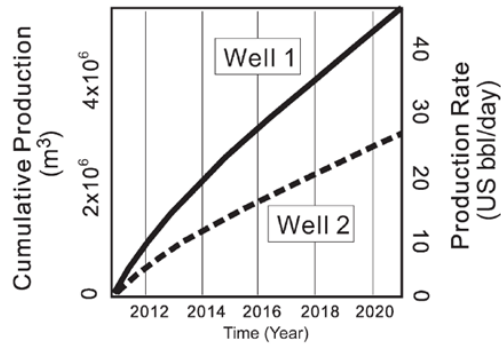
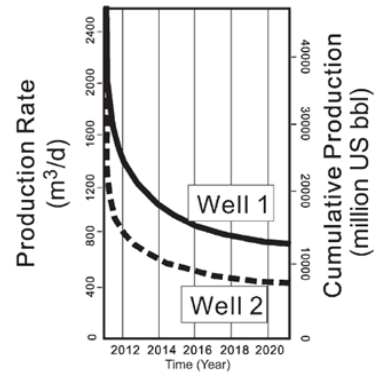
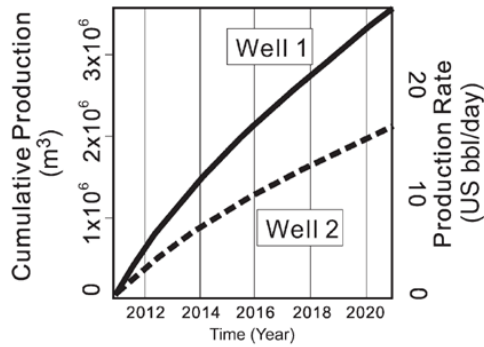


Figure 1.13.A three-dimensional view of the reservoir model of permeability with a salt surface and wells; the oil-water contact is set at 3900 m (12,795 ft). The producing well 1 and the injection well are connected through the channel axis facies, whereas the producing well 2 and the injection well are not.

Both Upper and Lower Sandstones



Upper Sandstones Only (Sheet-Prone)



Lower Sandstones Only (Channel-Prone)

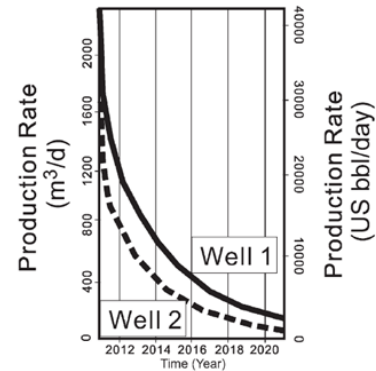
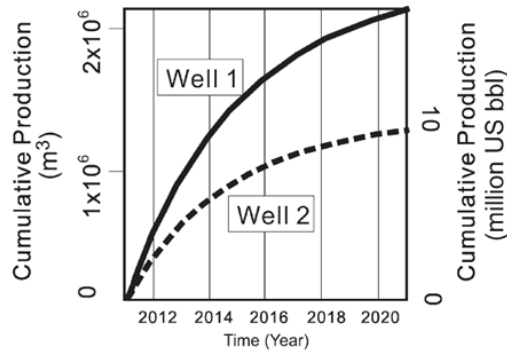


Figure 1.14. Reservoir simulation results from both upper and lower sandstones, upper sandstones only, and lower sandstones only, including cumulative production and production rate from producing well 1 (solid line) and well 2 (dashed line). Note that the (1) production volume and rate in well 1 is 60% more than those in well 2 in all cases; (2) the lower channelized sandstone package has a larger drop of production rate than does the upper sheet sandstone; and (3) the upper sandstones are more sustainable during a 10-yr production period, whereas the rate of the lower sandstones is close to zero after 10 yr.

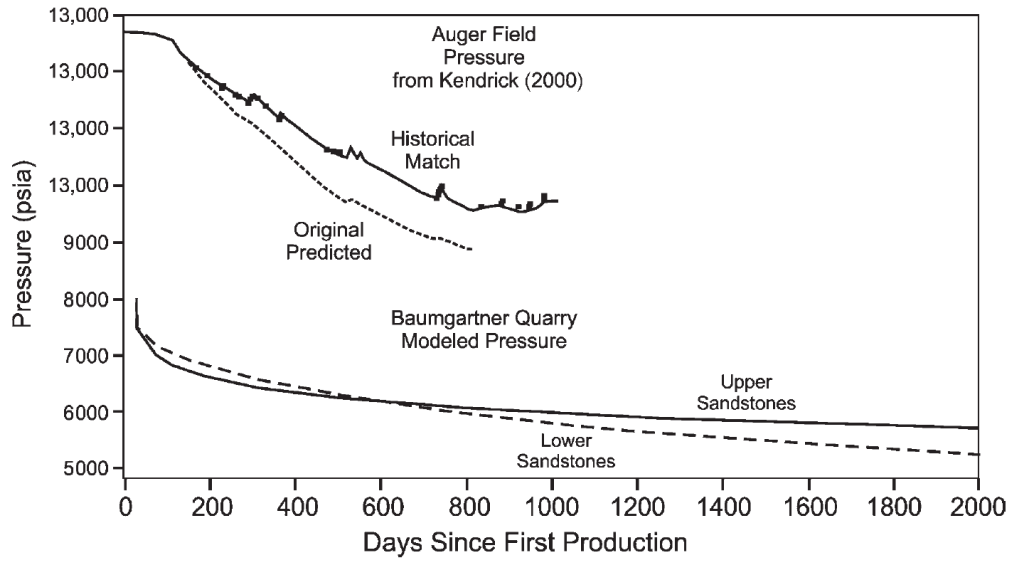


Figure 1.15. Comparison of pressure measurements (solid line and black dots) and prediction (dashed line) for Auger field, Garden Banks, Gulf of Mexico, and the Baumgartner Quarry modeled pressure.

REFERENCES

- Al-Siyabi, H. A., 2000, Anatomy of a type II turbidite depositional system: Upper Jackfork Group, Degray Lake area, Arkansas, in A. H. Bouma and C. G. Stone, eds., *Fine-grained turbidite systems: AAPG Memoir 72/SEPM Special Publication 68*, p. 245–262.
- Booth, J. R., A. E. DuVernay III, D. S. Pfeiffer and M. J. Styzen, 2000, Sequence-stratigraphic framework and stacking patterns of ponded and slope fan systems in the Auger Basin: Central Gulf of Mexico Slope: Gulf Coast Section SEPM Foundation 20th Annual Research Conference, Deep-Water Reservoirs of the World, p. 82–102.
- Bouma, A. H., 2000, Fine-grained, mud-rich turbidite systems: Model and comparison with coarse-grained, sand-rich systems, in A. H. Bouma and C. G. Stone, eds., *Fine-grained turbidite systems: AAPG Memoir 72/SEPM Special Publication 68*, p. 9–20.
- Campion, K. M., A. Sprague, and M. Sullivan, 2003, San Clemente State Beach, California: A classic example for stratal hierarchy and prediction within deep-water channels: AAPG Annual Convention Abstracts, Salt Lake City, Utah, v. 12, p. A25.
- Duran, W. J., 2007, Outcrop-based geologic model of the Jackfork Group at Baumgartner Quarry, Kirby, Arkansas, U.S.A.: Master's thesis, University of Oklahoma, Norman, Oklahoma, 118 p.
- Elliott, T., 2000, Megaflute erosion surfaces and the initiation of turbidite channels: *Geology*, v. 28, p. 119–122, doi:10.1130/0091-7613(2000)282.0.CO;2.

- Goyeneche, J. C., R. M. Slatt, A. C. Rothfolk, and R. J. Davis, 2006, Systematic geological and geophysical characterization of a deep-water outcrop for reservoir simulation: Hollywood Quarry, Arkansas, in R. M. Slatt, N. C. Rosen, M. Bowman, J. Castagna, T. Good, R. Loucks, R. Latimer, M. Scheihing, and R. Smith, eds., Reservoir characterization: Integrating technology and business practices: 26th Annual Gulf Coast Section SEPM Foundation Bob F. Perkins Research Conference, Houston, Texas, p. 685–728.
- Graham, S. A., W. R. Dickinson and R. V. Ingersoll, 1975, Himalayan-Bengal model for flysch dispersal in the Appalachian-Ouachita system: Geological Society of America Bulletin, v. 86, no. 3, p. 273–286, doi:10.1130/0016-7606(1975)862.0.CO;2.
- Ingersoll, R. V., W. R. Dickinson, and S. A. Graham, 2003, Remnant-marine submarine fans; largest sedimentary systems on Earth (in extreme depositional environments; mega end members in geologic time): Geological Society of America Special Paper 370, p. 191–208.
- Jackson, M. D., G. J. Hampson, and R. P. Sech, 2009, Three-dimensional modeling of a shoreface-shelf parasequence reservoir analog: Part 2. Geologic controls on fluid flow and hydrocarbon recovery: AAPG Bulletin, v. 93, no. 9, p. 1183–1208, doi:10.1306/05110908145.
- Jordan, D. W., D. R. Lowe, R. M. Slatt, C. G. Stone, A. D'Agostino, M. H. Scheihing, and R. H. Gillespie, 1991, Scales of geological heterogeneity of Pennsylvanian Jackfork Group, Ouachita Mountains, Arkansas: Applications to field

- development and exploration for deep-water sandstones: Dallas Geological Society Field Trip, 320 p.
- Kane, I. A., W. D. Mccaffrey, and O. J. Martinsen, 2009, Allergenic vs. autogenic controls on megaflute formation: *Journal of Sedimentary Research*, v. 79, p. 643–651, doi:10.2110/jsr.2009.072.
- Kendrick, J. W., 2000, Turbidite reservoir architecture in the northern Gulf of Mexico deep water: Insights from the development of Auger, Tahoe, and Ram-Powell fields: Gulf Coast Section SEPM Foundation 20th Annual Research Conference, Deep-Water Reservoirs of the World, p. 450–468.
- Larue, D. K., 2004, Outcrop and waterflood simulation modeling of the 100-foot channel complex, Texas, and the Ainsa II channel complex, Spain: Analogs to multistory and multilateral channelized slope reservoirs, in G. M. Grammer, P. M. Harris, and G. P. Eberli, eds., *Integration of outcrop and modern analogs in reservoir modeling: AAPG Memoir 80*, p. 337–364.
- Liceras, V., 2010, Outcrop-based 3-D modeling and upscaling of the Jackfork Group turbidites in Hollywood Quarry, Arkansas: Master's thesis, University of Oklahoma, Norman, Oklahoma, 148 p.
- Lowe, D. R., M. Guy, and A. Palfrey, 2003, Facies of slurry-flow deposits, Britannia Formation (Lower Cretaceous), North Sea: Implications for flow evolution and deposit geometry: *Sedimentology*, v. 50, no. 1, p. 45–80, doi:10.1046/j.1365-3091.2003.00507.x.
- Morris, R. C., 1971, Stratigraphy and sedimentology of Jackfork group, Arkansas: *AAPG Bulletin*, v. 55, no. 3, p. 387–402.

- Olariu, M. I., J. F. Ferguson, C. L. V. Aiken, and X. Xu, 2008, Outcrop fracture characterization using terrestrial laser scanners: Deep-water Jackfork sandstone at Big Rock Quarry, Arkansas: *Geosphere*, v. 4, no. 1, p. 247–259, doi:10.1130/GES00139.1.
- Pyles, D. R., 2008, Multiscale stratigraphic analysis of a structurally confined submarine fan: Carboniferous Ross Sandstone, Ireland: *AAPG Bulletin*, v. 92, no. 5, p. 557–587, doi:10.1306/01110807042.
- Roberts, M. T., 1994, Geologic relations along a regional cross section from Spavinaw to Broken Bow, eastern Oklahoma, in N. H. Suneson and L. A. Hemish, eds., *Geology and resources of the eastern Ouachita Mountains frontal belt and southeastern Arkoma Basin, Oklahoma*: Oklahoma Geological Survey Guidebook 29, p. 137–159.
- Rothfolk, A. C., 2006, Characterization of a fractured turbidite channel sandstone: the Jackfork Group, Hollywood Quarry, Arkansas: Master's thesis, University of Oklahoma, Norman, Oklahoma, 149 p.
- Schlichtemeier, B. D., 2011, LIDAR characterization of a Jackfork Group basin floor fan deposit and implications to analog reservoir modeling and production: Master's thesis, University of Oklahoma, Norman, Oklahoma, 126 p.
- Sech, R. P., M. D. Jackson, and G. J. Hampson, 2009, Three-dimensional modeling of a shoreface-shelf parasequence reservoir analog: Part 1. Surface-based modeling to capture high-resolution facies architecture: *AAPG Bulletin*, v. 93, no. 9, p. 1155–1181, doi:10.1306/05110908144.

- Slatt, R. M., 2000, Why outcrop characterization of turbidite systems, in A. H. Bouma and C. G. Stone, eds., *Fine-grained turbidite systems: AAPG Memoir 72/SEPM Special Publication 68*, p. 181–186.
- Slatt, R. M., and C. G. Stone, 2010, *Geology of the DeGray Spillway, Arkansas: A geologic excursion through rocks deposited in an ancient marine basin: Arkansas Geological Survey Guidebook 2010*, 98 p.
- Slatt, R. M., P. Weimer, and C. G. Stone, 1997, Reinterpretation of depositional processes in a classic flysch sequence (Pennsylvanian Jackfork Group), Ouachita Mountains, Arkansas and Oklahoma: Discussion: *AAPG Bulletin*, v. 81, no. 3, p. 449–491.
- Slatt, R. M., C. G. Stone, and P. Weimer, 2000a, Characterization of slope and basin facies tracts, Jackfork Group, Arkansas, with applications to deep-water (turbidite) reservoir management, in P. Weimer, R. M. Slatt, J. L. Coleman, and A. H., Bouma, eds., *Deep-water reservoirs of the world: Gulf Coast Section SEPM Foundation 20th Annual B. F. Perkins Research Conference*, p. 940–980.
- Slatt, R. M., H. A. Al-Siyabi, C. W. VanKirk, and R. W. Williams, 2000b, From geologic characterization to “reservoir simulation” of a turbidite outcrop, Arkansas, U.S.A., in A. H. Bouma and C. G. Stone, eds., *Fine-grained turbidite systems: AAPG Memoir 72/SEPM Special Publication 68*, p. 187–194.
- Stewart, J., P. Dunn, C. Lyttle, K. Campion, and A. Oyerinde and B. Fischer, 2008, Improving performance prediction in deep-water reservoirs: Learning from outcrop analog, conceptual models and flow simulation: *International Petroleum*

Technology Conference, Kuala Lumpur, Malaysia, paper 12892-MS, 9 p.,
doi:10.2523/12892-MS.

Sullivan, M. D., J. L. Foreman, D. C. Jennette, D. Stern, G. N. Jensen, and F. J.

Goulding, 2004, An integrated approach to characterization and modeling of deep-water reservoirs, Diana field, western Gulf of Mexico, in G. M. Grammer, P. M. Harris, and G. P. Eberli, eds., *Integration of outcrop and modern analogs in reservoir modeling: AAPG Memoir 80*, p. 215–234.

Suneson, N., I. Cemen, D. R. Kerr, M. T. Roberts, R. M. Slatt, and C. G. Stone, 2008,

Stratigraphic and structural evolution of the Ouachita Mountains and Arkoma Basin, southeastern Oklahoma and west-central Arkansas: Applications to petroleum exploration: Oklahoma Geological Survey Guidebook 34, p. 50–72.

Weimer, P., and R. M. Slatt, 2006, *Introduction to the petroleum geology of deep-water settings: AAPG Studies in Geology 57*, 850 p.

Zou, F., 2010, *An integrated approach to characterization and modeling of the Jackfork Group at the Baumgartner Quarry area, western Arkansas and its implications to deep-water exploration and production: Master's thesis, University of Oklahoma, Norman, Oklahoma, 154 p.*

**Chapter 2: An Integrated Chemo- and Sequence- Stratigraphic
Framework of the Early Pennsylvanian Deepwater Outcrops near
Kirby, Arkansas, USA, and its Implications on Remnant Basin
Tectonics and Hydrocarbon E&P**

Fuge Zou^{1,2}, Jing Zhang¹, Tao Huang³, and Roger M. Slatt¹

¹ConocoPhillips School of Geology and Geophysics, University of Oklahoma, Norman,
Oklahoma, 73019

²Marathon Oil Corporation, Oklahoma City, Oklahoma, 73132

³Sinopec Corporation, U.S.A, Oklahoma City, Oklahoma, 73112

**This paper has been submitted to AAPG Bulletin, and it is now in revision process.*

ABSTRACT

The Kirby sections in western Arkansas, U.S.A provide a unique opportunity to build a complete and continuous sequence stratigraphic framework for Early Pennsylvanian time in the ancient Ouachita Basin. They consist of 25 outcrops, including 12 roadcuts on Highway 27 and 13 sections in the Baumgartner Quarry. All the measurements and interpretations on the outcrops were integrated with previous work using modern concepts of deepwater turbidite geology, including (1) regional tectonic and sequence stratigraphic framework of the Stanley Group, Jackfork Group, and Johns Valley Shale in the Ouachita Basin, (2) deepwater outcrop characterization and correlation from the DeGray Lake Section, Dierks Section and Big Rock Quarry which is on the trend of the depositional fairway, and (3) chemical stratigraphic data

from key shale layers which are considered as potential condensed sections for assisting correlation.

Twenty-five key shale samples from Kirby, DeGray and Dierks sections have been tested using Inductively Coupled Plasma and Mass Spectrometry (ICP-MS) tests. Along with 475 samples were collected for Handheld X-Ray Fluorescence (HHXRF) tests for both major and trace elements. Results of sequence and chemostrata analysis indicate that the entire Kirby sections consist of at least three 3rd order sequences from the bottom of the Jackfork Group to the middle of the Johns Valley Group, and over ten 4th order sequences caused by a combined effect of tectonic uplift, eustatic sea-level change, mixed sediment provenance and shifting of depositional fairways when the Ouachita Basin was transitioning from a passive margin to a remnant marine basin. Rare Earth and Trace Element results are compared with known tectonic data to further pinpoint the tectonic environment of the Ouachita Basin during early Pennsylvanian time, which is dominantly a continental arc setting.

A direct reservoir analog of the Jackfork Group outcrops in Arkansas is the subsurface Jackfork Potato Hills gas field in southeastern Oklahoma. Previous well-based stratigraphic interpretations have been tied to the established and complete sequence stratigraphic framework of the Jackfork Group from outcrop to subsurface. With the sequence stratigraphic framework established in the Jackfork Group, the interpretation, correlation and reservoir modeling of the Jackfork reservoirs will gain more confidence and accuracy.

INTRODUCTION

The ancient Ouachita Basin consists of 15,000m of Carboniferous deepwater strata which covered an area of 246,592 km² from Little Rock, Arkansas to southeastern Oklahoma, U.S.A. The Early Pennsylvanian Jackfork Group in the Ouachita Mountains (Figure 2.1) has been studied for over forty years. The outcrops display an excellent example of different types of turbidite reservoirs from *updip slope deposits* to *downdip basinal deposits* (Slatt *et al.*, 2000a). The regional tectono-stratigraphic framework of the Jackfork Group in the Ouachita Mountains was described by Walthall, 1967; Morris, 1971; Graham *et al.*, 1975). Over the last two decades, various Jackfork outcrops (including roadcuts, rock quarry faces, lake spillways etc.) in the Ouachita Mountains region have been documented in detail. These studies have helped geoscientists to develop analogs for deepwater reservoir characterization and development (Jordan *et al.*, 1991; Pauli, 1994; Al-Siyabi, 1998; Slatt *et al.*, 2000a; Slatt *et al.*, 2000b; Omatsola and Slatt, 2003; Goyeneche *et al.*, 2005; Shear, 2006; Duran, 2007; Schlichtemeier, 2011; Zou, *et al.*, 2012). The Kirby Section, which was partially described by Morris (1971), is located on Highway 27-3km south of Kirby, Arkansas (Figure 2.1). This section contains a ~1200m exposure of Chickasaw Creek (top of Stanley Shale), Jackfork Group and Johns Valley Shale strata (Figure 2.2). Recently, the Baumgartner Quarry has become active, adding over ~500m of new exposures to the Kirby section which belongs to the Middle and Upper Jackfork Group.

All related regional Jackfork outcrops are summarized in Table 2.1. In the past, a regional sequence stratigraphy of the Jackfork was difficult to complete because of lack of exposures and structural complications within the Ouachita Mountain area.

Correlation of the different outcrops within the Ouachita Basin has been a challenging task. Coleman *et al.* (1994) established a qualitative correlation of the Jackfork Group in southeast Oklahoma and DeGray area. The Arkansas Geological Commission has mapped the Jackfork outcrops as Upper, Middle and Lower units, which provides basic guidance for correlation. Coleman (2000) discussed the general evolution of the Ouachita deepwater basin with a series of basin-wide paleogeography maps. However, the stratigraphic units inside the Jackfork Group were not differentiated. Recently, more Jackfork Group outcrops have been studied using a quantitative approach such as at Baumgartner Quarry (Duran, 2007; Zou *et al.*, 2012), Hollywood Quarry (Goyeneche *et al.*, 2005), DeGray Lake Spillway (Slatt *et al.*, 2000b; Schlichtemeier, 2011) and Big Rock Quarry (Olariu *et al.*, 2008; Funk *et al.*, 2012). These detailed characterizations provide a solid base for developing a regional stratigraphic framework.

The main scope of this paper is to study the Kirby section which includes the Jackfork Group and the lower half of John Valley Shale with chemostratigraphic measurements. The results (description and interpretation) are used to conduct regional correlation to other outcrops nearby. And re-establish a sequence stratigraphic framework integrating our data and previous work.

One direct reservoir analog of Jackfork outcrops in Arkansas would be the subsurface Jackfork tight gas fields in southeastern Oklahoma because they are the same formation in the same basin (Roberts, 1994; Montgomery, 1996; Omatsola, 2003; Romero, 2004; Suneson and Slatt, 2004). Roberts (1994) first described outcrops near Rich Mountains, Oklahoma containing friable sandstones (Figure 2.1). Omatsola (2003) further investigated the relationship between channelized friable sandstone and

subsurface reservoir intervals with good production performance. Romero (2004) built a sequence stratigraphic framework in Potato Hills (Figure 2.1) area with well logs, borehole image and mud logs data. The previous well-based stratigraphic interpretations can be tied to the established and complete sequence stratigraphic framework across the basin.

GEOLOGICAL SETTING

Regional tectonic history

The Ouachita Basin in the southern-central United States is a distinct Paleozoic remnant marine basin. It is bounded by the Arkoma Basin to the north, and the Gulf Coastal Plain to the south, and extends from Little Rock, Arkansas westward to Atoka, Oklahoma (Figure 2.1). In the Ouachita region, rifting during the Late Precambrian and Early Cambrian resulted in a continental margin along the southern boundary of North America (Hatcher *et al.*, 1989). Deposition started with carbonate shelf deposits, but as the rifting advanced in the Early Paleozoic, the depositional environment began to evolve into a deepwater clastic basin (Hatcher *et al.*, 1989). During Middle-Late Pennsylvanian time, the entire basin began to close in response to the approach of the Gondwana continental plate front to the south. As the Ouachita Basin closed, all the strata from Late Cambrian to Carboniferous were deformed to a foreland fold and thrust belt (which defines the Ouachita Mountains).

General Stratigraphy

The stratigraphy in the Ouachita Mountains is generally divided into two distinct units (Figure 2.2). The older units are "pre-orogenic" strata which consist of Late Cambrian to Early Mississippian siliceous shales, cherts and sandstones (Hatcher *et al.*, 1989). The sedimentation rate for these strata in the deep basin was very low (<4m per million years) (Lowe, 1989).

The younger units are "syn-orogenic" strata which consist of Early Mississippian to Pennsylvanian deepwater deposits (Stanley Group, Jackfork Group, Johns Valley Formation and Atoka Formation). These rocks make up more than 80% of the surface exposure (Roberts, 1994) and are about 10,000m thick. These syn-orogenic rocks represent pre-foreland basin deepwater detrital fill which was deposited in water depth of 1,500 to 2,000m (Coleman, 2000).

The Mississippian Stanley Shale is composed of thick shales interbedded with fine-grained sandstone lenses which represent a highstand system tract (Coleman, 2000; Slatt *et al.*, 2000a). It is sub-divided into three formations, the Tenmile Creek, Moyers and Chickasaw Creek Formations. The sandstones display numerous sedimentary features such as flute, load and groove casts (Morris, 1971). The thickness varies from 1,800-3,600m with an average depositional rate of 160m per million years (Slatt *et al.*, 2000a).

Details of the Jackfork Group in Arkansas have been described in publications by Morris (1971), Graham *et al.* (1975), Jordan *et al.* (1991), Roberts (1994), Slatt *et al.* (2000a) among others, and is not repeated here. In Early Pennsylvanian (Morrowan) time, Jackfork sediments were mainly sourced from the north and northeast, and were deposited in the west-east trending Ouachita Basin. U-Pb dating at the top of Stanley

Shale (Shaulis *et al.*, 2012) and the global sea-level curve (Haq *et al.*, 2008) indicate that the Jackfork Group was deposited during a 2nd order global sea level drop beginning at 320 million years ago, with several 3rd and probably 4th order sequences superimposed (Ross and Ross, 1988; Slatt *et al.*, 2000a). The Jackfork Group was interpreted as a large major lowstand system tract (LST) consisting of stacked turbidite deposits (Pauli, 1994; Tillman, 2000; and Slatt *et al.*, 2000a) which are dominated by medium-to-fine-grained sandstones.

The Jackfork Group is subdivided into five units in Oklahoma (from the youngest to the oldest: the Game Refugee Sandstone, Wesley Shale, Markham Mill Formation, Prairie Mountain Formation, and Wildhorse Mountain Formation) and two units in Arkansas (from the youngest to the oldest: Brushy Knob Formation and Iron Fork Mountain Formation). The difference between Oklahoma and Arkansas strata is the absence of thick shale layers in the more proximal facies in Arkansas. Practically, the stratigraphic units of the Jackfork Group in Arkansas and Oklahoma in the last two decades have been informally termed as the "Upper Jackfork", "Middle Jackfork", and "Lower Jackfork". The thickness varies from 350-2,200m with a maximum depositional rate of 150m per million years (Lowe, 1989).

The Pennsylvanian Johns Valley Shale is a poorly exposed unit dominated by shale and thin sandstone beds which overlie the Jackfork Group. It represents a transgressive systems tract following a sea-level drop during Jackfork Group time. The thickness varies from 60-300m. However, the formation is difficult to distinguish from the underlying Jackfork Group due to similar lithology. Morris (1989) suggests the presence of olistostromal deposits is a good way to identify the Johns Valley Shale.

The Pennsylvanian Atoka Formation is another thick turbidite sequence which is a good reservoir in the Arkoma Basin in eastern Oklahoma. The formation exhibits a thickness variation of 500-6,000m with a maximum sedimentation rate of 900m per million years (Morris, 1989). The likely cause of the increasing sedimentation rates is local uplift associated with the closing of the remnant Ouachita marine basin, where large volumes of sediments were dumped into the deep basin.

Since Late Pennsylvanian time, the Ouachita Mountain region has been uplifted and eroded. Cretaceous conglomerates unconformably overlie some of the Jackfork Group strata, forming a distinct regional unconformity in places such as DeGray Lake Spillway (Shear, 2006).

CHARACTERIZATION OF KIRBY SECTIONS

Slatt *et al.* (2000) and Zou *et al.* (2012) developed a systematic way to describe the Jackfork Group in the Ouachita Basin. It is used here to describe the Kirby sections. The descriptive lithofacies of the Kirby sections are classified as (1) Bouma Ta-Tb beds with amalgamated, scoured (lenticular) or tabular geometry; (2) Bouma Tc-Td beds which are thin-bedded sandstones and shale; and (3) Bouma Te beds with shaly units.

Seven interpretive, generic architectural facies were also identified in the Kirby section: channel fill sandstone, channelized sheet sandstone (weakly confined sandstone), amalgamated sheet sandstone, layered sheet sandstone, thin-bedded sandstone and shale, parallel laminated shale and muddy debrites deposits. Details regarding these facies are described by Slatt *et al.*, (2000a), Zou (2010) and Zou *et al.* (2012) and are not repeated here.

The Kirby Section consists of 25 outcrops, including 12 roadcuts along Highway 27 and 13 sections located in Baumgartner Quarry (Figure 2.3). Total true stratigraphic thickness from the base of the Jackfork to the middle of the Johns Valley Shale (including vegetation covers) is 2400m. It is measured and presented in a universal scale from 0m at the base to 2400m at the top. The entire Jackfork Group in the Kirby Section has been divided into the Lower, Middle and Upper Jackfork. The Lower Jackfork Group includes Roadcut 1, 2, 3 and 4; the Middle Jackfork Group includes Roadcut 5, 6, 7, BQ_Section_1, 2 and lower part of BQ_Section_3; the Upper Jackfork Group includes the upper part of BQ_Section_3, Roadcut 8 and 9. The overlying Johns Valley Shale section includes JV_Roadcut_1, 2, and 3.

Lower Jackfork Group

General outcrop description and interpretation of the Lower Jackfork Group in Kirby Sections is summarized in Table 2.2. Approximately 370m of mostly continuous exposures including Roadcut 1, 2, 3 and 4 of Jackfork Group strata occur in the northernmost part of the Kirby section from 0-370m.

Description

The lowermost 20m of Roadcut 1, the transition between the Stanley Group and the Jackfork Group, is characterized by thin-bedded, fine-grained sandstone, siltstone and shale. An abrupt change in lithology occurs at 20m, where a 5-m thick medium- to fine-grained sandstone that exhibits a tabular geometry with a flat base and top overlies the shaly units (Figure 2.4). Similar tabular sandstones interbedded with shaly units continue up the section to 225m (Figure 2.5). Tabular sandstone beds with scour surfaces locally occur at 57m, 63m, 165m and 182m.

At the top of Roadcut 2 (230 m, Figure 2.5), thick, massive and amalgamated sandstones with clear scour surfaces occur for the first time. Each scour surface is 2-3m apart with dish structures and angular mudstone clasts in the deposits above. This transition continues up to Roadcuts 3 and 4 (Figure 2.6), where massive scoured (lenticular) sandstones are found with debrites at 360m. The top of Roadcut 4 is composed of a major unit of thin-bedded sandstones and mudstones, followed by a shale unit that is over 20m thick.

Interpretation

The bottom of this section is the boundary between the Lower Jackfork Group and the Stanley Group. Beneath this boundary is the Chickasaw Creek Siliceous Shale Member of the Stanley Group, which was interpreted as a condensed section within a transgressive systems tract (Coleman 2000; Slatt *et al.*, 2000a). Zircon dating from a Chickasaw Creek tuff unit indicated an absolute age of 320.6 ± 2.7 Ma (Shaulis *et al.*, 2012). The tabular sandstone at 20m is the oldest turbidite sandstone found in the Jackfork Group, which marks the transition from a 'starved basin' to classic orogenic flysch deposition in Early Pennsylvanian time (Shaulis *et al.*, 2012).

In the first 230m's of section, all the tabular sandstones with minor or no scour surfaces are interpreted as layered sheet sandstones which represent a basin floor fan environment at the early stage of sea-level fall (Figure 2.7). The thicker amalgamated scour sandstones at 230m are interpreted as amalgamated channel sandstones in proximal fan setting. The muddy debris flow deposits associated with the channel deposits at Roadcut 4 indicate the increase of sea-bottom relief or further drop of sea-

level. A potential minor transgressive systems tract and sequence boundary may occur at the top of Roadcut 4 as indicated by a 20-m shale.

Middle Jackfork Group

General outcrop description and interpretation of the Middle Jackfork Group in Kirby Sections is summarized in Table 2.3. Approximately 625m of mostly continuous exposures include Roadcut 5, 6, 7, BQ_Section_1, 2, and 3 (Lower) from 500m to 1120m.

Description

Roadcut 5 is about 100m above the top shaly package in Roadcut 4 (Figure 2.8). The boundary between the Lower and Middle Jackfork Group is covered by vegetation. Unlike the mostly-tabular Lower Jackfork Group, the Middle Jackfork Group is characterized by massive sandstones with scoured (lenticular) surfaces. In Roadcut 5, individual sandstone bed thickness is typically 1-2 m with frequent scour surfaces, and amalgamated sandstones up to 6m thick. Roadcut 6 is poorly exposed and is partially covered by vegetation. However, one can still observe most exposed sandstones with massive scoured (lenticular) beds.

BQ_Section_1, 2 and 3 are in the Baumgartner Quarry (Figure 2.9), with BQ_Section_1 beginning at the entrance of the quarry (near the pond). BQ_Section_1 is along the drainage of the quarry, with only a 2-3m narrow exposure of strata. BQ_Section_2 is up on the hill and is about 270m wide and 130m thick (Figure 2.10). Three major, thick, and distinct shale packages occur at 870m, 935m and 1120m, and are 17m, 21m and 30m thick, respectively. Friable sandstones occur from 920m to

930m. The main quarry (BQ_Section_3) has been divided into the "Lower Sand", "Middle Shale" and "Upper Sand". The Lower Channelized Sand and Upper Sheet-prone Sand have been described, modeled and simulated using a deepwater Gulf of Mexico field case. The results indicate a faster decline of channelized sands with higher initial rates versus a slower decline of sheet sands. These have been discussed in detail by Zou *et al.* (2012), so BQ_Section_3 is not repeated here in any detail.

Roadcut 7 is at the turn of Highway 27 southwest of the quarry (Figure 2.10). It is 1600m away from the Lower Sand of BQ_Section_3 along the strike direction. Similar to the Lower Sand in BQ_Section_3, it is mostly amalgamated sandstones with scour surfaces. With 1600m distance along strike, direct bed-level correlation to BQ_Section_3 is difficult.

Interpretation

Roadcut 5 is bounded by shaly units above and below, indicating that it belongs to a potential proximal distributary complex, which is similar concept by Sprague *et al.* (2002) except that Jackfork channels are in deeper water. Roadcut 6, BQ_Section_1 and 2 all have thicker massive channelized sandstones, indicating a potential drop of sea-level or regression associated with large amount of sediment input and basin subsidence (Figure 2.11). Three thick parallel laminated shale packages at 870m, 935m and 1120m, indicate potential condensed sections. These are higher-order transgression stacked on a lower-order regression during Early Pennsylvanian time. The 270m lateral exposure of BQ_Section_2 shows good continuities against lenticular geometries of all channelized sandstones along strike, indicating a more weakly confined channel and splays

environment. In summary, the entire Middle Jackfork Group is an unconfined channelized sequence located at the downslope environment, with three exposed potential condensed sections in the upper interval, and some intervals of unconsolidated sands caused by surface weathering. These friable sandstone are interpreted as close to the axis of a distributary system (Omatsola, 2003).

Upper Jackfork Group

General outcrop description and interpretation of the Upper Jackfork Group in Kirby Sections is summarized in Table 2.4. The boundary between Middle and Upper Jackfork Group is defined as the 30-m thick “Middle Shale” at 1120m (Figure 2.11, Zou *et al.*, 2012). Approximately 490m of mostly continuous exposures include Roadcut 8, 9, and BQ_Section_3 (Upper) from 1160m to 1650m.

Description

The Upper Jackfork Group is dominated by quartz cemented, tabular sandstones and associated shaly units. BQ_Section_3 (Upper Sand) can be qualitatively correlated 1600m along strike to Roadcut 8 through satellite image and quadrangle maps. Roadcut 8 begins with a 15m-thick amalgamated tabular sandstone, followed by 10m thin-bedded sandstone sequences (Figure 2.12). Roadcut 8 and 9 are separated by a 50m gap, where an interpreted strike-slip fault cut through (Figure 2.3, Godo *et al.*, 2008). This dominant tabular sandstone trend continues towards the top of the Jackfork Group in Roadcut 9 (Figure 2.13).

Interpretation

Upper Jackfork is an interval with sheet-prone deposits (Zou *et al.*, 2012). The depositional environment is relatively further downdip than that of the Middle Jackfork. No major shale break was observed throughout the section except for the 4-m thick section at 1215m in BQ_Section_3 (Upper Sand), indicating a more continuous deposition period. The channel complex with muddy debris flow deposits at the top of BQ_Section_3 (Zou *et al.*, 2012) may indicate a higher order regression event or compositional stacked distributary system. At Roadcut 9, the sandstone to shale ratio decreases upward towards the top of the Jackfork Group, indicating a major transgression event transition to the Johns Valley Shale (Figure 2.14).

Johns Valley Shale

General outcrop description and interpretation of the Johns Valley Shale in Kirby Sections is summarized in Table 2.5. Approximately 700m of partially covered exposures include JV_Section_1 to 3 from 1700m to 2400m.

Description

JV_Roadcut_1, which is the first section of Johns Valley Shale, occurs at 1700m. It is 50m above the top of Roadcut 9. It begins with a 15m thick amalgamated tabular sandstone package, followed by a 10m shaly and thin-bedded section (Figure 2.15). A 3m-thick scoured (lenticular) sandstone occurs at 1725m. In JV_Section_2 and 3, sandstone packages are located from 1770~1820m (amalgamated tabular sandstones), 1900~2000m (amalgamated scoured sandstones) and 2280~2310m (mixed tabular and scoured sandstones). The top of the section (from 2310~2400m) is over 90% shale (Figure 2.16).

Interpretation

The Johns Valley Shale above the Jackfork Group represents the major transgression after the first global sea-level drop during Early Pennsylvanian time. Steel *et al.* (2012) proposed that significant slope sediment delivery and basin floor fan growth can occur during sea level rise and highstand due to high sediment influx. The thin channelized and sheet sandstones found in the Johns Valley Shale are such examples. The 90% shale interval at the top of BQ_Section_3 represents the most highly transgressive system in the middle of the Johns Valley Shale (Figure 2.16).

REGIONAL CORRELATION

Slatt *et al.* (2000a) described more than 15 outcrops of the Jackfork Group in Arkansas from the Little Rock and Hot Springs area. In the Ouachita Basin from northeast to the southwest, the Jackfork Group exhibits a change from updip slope channelized facies to downdip basin floor fan facies. Similar studies have also been made by Jordan *et al.* (1991) and Coleman *et al.* (1994). However, little effort has been made to regionally correlate these separate Jackfork outcrops at a finer scale due to complex structural geology and a lack of continuous outcrop exposures. In order to build a more accurate sequence stratigraphic framework of the Jackfork Group, we started with three of the most continuous and well-exposed downdip-basinal Jackfork outcrops: DeGray Lake, Kirby and Dierks (from east to west) as study examples. These three outcrops are 40-50km apart, and sub-parallel to the regional sediment transport direction (Figure 2.1 and 2.17).

Correlation of these outcrops is based on an integration of chemical stratigraphy, lithology and generic facies analysis. Correlations using isotope geochemistry and biostratigraphy were investigated, but were not successful. These two methods were ineffective because of a lack of fossils and difficulty obtaining U-Pb dates from Jackfork Group rocks. A handheld scintillometer was used to collect shale samples from the intervals with highest gamma-ray reading (in counts per second, or CPS). These shales are the most likely candidates for condensed sections with maximum flooding surfaces (Slatt *et al.*, 2000a). Shale samples were tested by ICP-MS (Inductively Coupled Plasma –Mass Spectrometry), and shales with similar chemical components were correlated.

Review of DeGray Lake Area Geology

Outcrop at DeGray Lake Spillway, which is 50 km east to the Kirby Section, exposes a series of sandstone-prone sections separated by shales. This section has been studied by many geologists and is well documented (Morris, 1971; Jordan *et al.*, 1991; DeVries, 1992; Shanmugam and Moiola, 1995; Slatt *et al.*, 1997; Al-Siyabi, 2000; Slatt *et al.*, 2000a; Schlichtemeier, 2011). For many years it has been a classic outcrop for oil and gas geoscientists and engineers to study deepwater reservoir analogs because of the Jackfork Group's excellent exposure with a relatively long and continuous vertical section (~1000m) in several separate outcrops (Figure 2.18-A). One of the key goals for previous researchers on DeGray Lake was to develop an appropriate depositional and sequence stratigraphic model for the Jackfork Group in the DeGray Lake area (Figure 2.18-A).

Beginning with the base of the Jackfork Group at the roadcut of Highway 7 (Figure 2.18-A), the contact between the underlying Stanley Shale and the Lower Jackfork Group is identified by a boundary separating shaly strata at the bottom of the section from sandy strata above. This boundary is interpreted as a global eustatic boundary dated at ~320 Ma (Slatt *et al.*, 2000a). In the Lower Jackfork Group, channelized facies and sheet-prone facies are both present, which implies a general down slope proximal fan environment. The Highway-7 section is followed by Lakeview Section and Old Roadcuts (Figure 2.18-A) along Arkansas Highway 283 (Coleman *et al.*, 1994). However, the exposures of these two outcrops are too poor to be effectively measured and described. Thus only a qualitative lithology description is available here.

The Middle Jackfork Group outcrop has been characterized in detail by Slatt *et al.* (2000a) and Shear (2006). The Middle Jackfork Group is characterized by sheet sandstones at the bottom and friable channel sandstones with relatively thin-bedded levee facies at the top. Shell Exploration Corporation drilled the Rex Timber No. 1-9 well to test their Moccasin prospect in 1985 (Figure 2.18-B). Detailed analysis of the well was done by Shear (2006) and then by Godo *et al.* (2008), including the well log evaluation, lithology description, petrology, and geochemistry. Coleman *et al.*, (1994) and Shear (2006) proposed correlations between the well and the outcrop sections of the Upper and Middle Jackfork Group. They correlated DeGray Lake Middle Jackfork Group section and Spillway Lower Jackfork Section from 500-1200m to the well interval from 800-1500m. Clay, feldspar and carbonate are more abundant in the Middle Jackfork and secondary dissolution porosity development can be the cause of friability of the Middle Jackfork Group in both DeGray outcrops, Rich Mountain outcrops and in

the wells (Omatsola, 2003; Romero, 2004, Godo *et al.*, 2008). In contrast, the Upper Jackfork Group consists of mostly quartz cemented sandstone.

The Upper Jackfork Group has over 300m of excellent exposure in the DeGray Lake Spillway, plus several dam and intake exposures. DeVries (1992) studied the bedding associations and depositional cycles at DeGray Lake Spillway, and placed depositional environments into a middle fan depositional environment. Al-Siyabi (2000) also interpreted depositional environments based on analysis of facies distributions, vertical facies trends and downcurrent relationships. He proposed that the Upper Jackfork Group in DeGray Lake Spillway is a Type II depositional system (Mutti and Normark, 1991), which is characterized by channel fill and lobate sandstone sequences. Schlichtemeier (2011) used LIDAR (Laser imaging and ranging) technology to scan both the west and east walls of DeGray Lake Spillway, adding much detail and confidence to the correlation of strata between the two walls.

Based on the previous work and our measurements, all related measured sections were combined to form a complete section of the Jackfork Group (Figure 2.18-A and B). In general, the whole sequence is characterized by a sheet-prone Lower Jackfork member with mainly quartz-cemented sandstones, a channelized Middle Jackfork member with relatively friable sandstones, and an Upper Jackfork member with mixed facies of sheet and channel sandstones that are quartz cemented.

Review of Dierks Area Geology

The Dierks Spillway is a continuous outcrop of the Jackfork Group located 44 kilometers to the west of Kirby (Figure 2.17). It represents a more downdip and distal

facies than at the Kirby Section. The Dierks Spillway has two measured sections (the West Wall and the East Wall) that are 240m apart (Figure 2.19, Jordan *et al.*, 1991). The West Wall is 140m thick and the East Wall is 70m thick. The majority of the facies are flat-based sheet sandstones (Figure 2.9 photo), and thin beds separated by parallel laminated shales. Most of these sandstones are well cemented "hammer-ringers" with few friable sandstone beds present. Interpreted channelized sheet sandstone (weekly confined sandstone) account for 8% of the entire section. The sandstone package at Dierks is interpreted as compensationally stacked middle-distal fan deposits.

CHEMOSTRATIGRAPHY

475 samples mainly from shaly intervals in Kirby Section, DeGray Lake Sections and Dierks sections were collected to test chemostratigraphy (both trace and major elements) with the Hand-Held XRF. In addition, for calibration purposes, 10 shale samples from DeGray Sections, 12 shale samples from Kirby and 3 shale samples from Dierks sections were collected with the highest outcrop gamma ray responses. They were sent to the State Key Laboratory at China Academy of Geosciences (Beijing) for high resolution X-Ray Fluorescence (XRF) and Inductively Coupled Plasma and Mass Spectrometry (ICP-MS) tests. The main chemical elements tested include all *Major Oxides, Trace Elements and Rare Earth Elements (REEs)*.

These elements have proven useful from both deepwater turbidites [e.g., Australia Paleozoic turbidites, Bhatia (1983), and Bhatia (1985)] and unconventional plays [e.g., Eagle Ford, Ratcliffe *et al.*, (2012); Longmaxi Shale in Sichuan, China, Mu *et al.*, (2013)] for developing a sequence stratigraphic framework. The elements and

proxies proposed in this research are summarized in Table 2.6 (Tribovillard *et al.*, 2006; Radcliffe *et al.*, 2012; and Mu *et al.*, 2013):

Based on these existing criteria for chemostratigraphic analysis, three key problems were to be investigated with these data:

1. The vertical change in Stanley Shale, Lower, Middle, Upper Jackfork and Johns Valley Shale regarding eustatic sea-level changes versus tectonic events.
2. The lateral correlation between Dierks, Kirby, and DeGray sections with similarities and differences along depositional dip and strike;
3. Characters of local shale versus regional condensed sections (generic sequence boundary) to better restrict a sequence stratigraphic framework.

Preliminary results of HXRF (Hand Held X-Ray Florescence) are shown from Figure 2.20-2.25, including Roadcut 1, 2, 7, 8 and 9 of Kirby Sections, Highway 7 and DeGray Spillway sections. Future work includes additional samples collected and tested in the area to build a complete chemostratigraphic logs within the shale units in the Jackfork Group.

The raw results of whole rock geochemistry tests are shown in Figure 2.26 with key elements and proxies. In the Lower Jackfork Group, the Th/U ranges from 3.85 to 6.60 with an average of 5.15. Deep basin-floor indicators such as Ni, Mo, Mn and V vary dramatically. Ni, which is sensitive to sea-level change, ranges from 28.9 to 128 ppm (parts per million). The relatively high Th/U and low Ni in the Kirby section indicate high sediment supply with shallower water depth than the underlying Stanley Shale. The data also implies derivation from a mafic provenance (Totten *et al.*, 2000).

In the Middle Jackfork Group, Th/U ranges from 4.44 up to 6.24 with an average of 5.4. A large increase of Nb/Y (Figure 2.27) occurs from 0.46 to 0.69 with an average of 0.62, indicating a major change in detrital sediments within these intervals. Sea bottom indicators vary, including Ni (17 to 90ppm with an average of 43ppm) and Co (2.9 to 27.8ppm with an average of 8.6ppm), and detrital indicators such as Th/U and Terr. In. (see Table 2.6 for definition) show a generally inverse relationship against Co and Ni.

In the Upper Jackfork Group section, the Th/U decreases, ranging from 3.8 to 5.2 with an average of 4.6. Ni and Co increase dramatically, with Ni ranging from 57.2 to 81.9ppm, averaging 68.1ppm. These changes indicate both a reduction of the amount of detrital components and an increase in water depth. As the Kirby section grades into the Johns Valley Shale, Ni and Co reach their peak level, with Ni ranging from 80.2 to 97.5, averaging 88.9, which indicates that the Johns Valley Group was deposited in the deepest water.

Not only do the elements vary vertically, but also they change along the dip and strike. Ni in the Kirby Section is 28.9 ppm and 44.6 ppm, while in DeGray Lake it varies from 36.7 to 128 ppm. The values of Th/U of these two locations are generally at the same level. However, the shale sample DG-08, which was taken from the shale within the channelized intervals at the top of the DeGray Lake Spillway section, shows low Ni and Co coincident with rounded to sub-rounded conglomerates (Slatt *et al.*, 2000a). The low values for DG-08 indicate a different provenance and a higher order regressive sequence from the south (Slatt *et al.*, 2000a). The equivalent channelized sequence has been found near the top of the Baumgartner Quarry section (Zou *et al.*,

2012). However, that section has been mined since 2011 and is no longer available for sampling.

The Dierks Spillway section is 140m thick. Without exposure of the top and base of the Jackfork Group, direct lithological correlation is difficult. The Dierks area Quadrangle map from the Arkansas Geological Commission shows the bottom of the Dierks section is 450m above the base of the Jackfork, thus the main sandstone package in the Dierks section is likely to be in the Middle Jackfork. Chemostratigraphic data improved this interpretation, where the trace element data fit in the range of the Middle Jackfork from Kirby and DeGray Lake sections (Figure 2.26 and 27). Moreover, seabottom indicators such as Co, Ni and U are much higher than in its equivalent intervals at Kirby and DeGray Lake section, indicating a downdip basinal environment.

Figure 2.28 is the trace elements plot against the average upper crust (Taylor and McLennan, 1985), with the Stanley shale data overlay from Totten *et al.* (2000). Average continental arc, active margin and passive margin data are from Floyd (1991). The trace elements results from the Stanley Shale (Totten and Blatt, 1993; Totten *et al.*, 2000) indicate enrichment in Cs-V-Cr-Ni-Yb-Ti and depletion in Sr-Ta-Nb relative to the standard average upper crust content (Taylor and McLennan, 1985; Floyd, 1991). Totten *et al.* (2000) compared the trace elements of the Stanley Shale to active margin, continent arc and passive margin settings and they concluded that the Stanley shale in the Ouachita Basin is a result of a dominant passive margin source with sediments from an active margin setting. Our results deliver similar trace element patterns to the previous work on the Stanley shale such as:

1. The low Sr level is consistent across all the tested intervals, which in an indication of passive margins (Floyd, 1991; Totten *et al.*, 2000).

2. The enrichment of Ti is higher in the Jackfork and Johns Valley shale than Stanley Shale. They are related to both mafic tectonic provenance and high terrestrial input into the basin (Totten *et al.*, 2000).

3. Similar values of key provenance indicators La-Sc-Th were used by many geologists to indicate the similar tectonic environment (Bhatia, 1983; Bhatia, 1985; Totten *et al.*, 2000; Meng *et al.*, 2007).

However, there are also differences such as:

1. The negative P and positive Cs of the Jackfork Group and Johns Valley shale. Negative P is caused by lowstand sediment input during Early Pennsylvanian time, which reduces the surface productivity. Positive Cs is consistent with large-ion lithophile elements (LILEs) such as K and Rb, which indicate that the tectonics of the provenance shifted from a passive margin towards an active margin environment.

2. The separations in Ni-Hf-Zr in Lower, Middle, Upper Jackfork Group and Johns Valley shale are consistent with the division of the intervals which are different from Stanley Shale. The Ni increases from the Stanley shale into the Lower Jackfork Group, then decreases into Middle Jackfork Group, increases again into Upper Jackfork Group, and reaches the highest value in the Johns Valley shale. Hf and Zr share a common trend as high field-strength elements (HFSE). Their range is between passive margin and active margin. They also follow the same trend as Ni from the Stanley shale to the Johns Valley Group. The fundamental control of these separations is a result of

tectonic environment of the provenance, which also has an impact on sedimentation and sequence stratigraphy.

DEPOSITIONAL ENVIRONMENTS AND SEQUENCE STRATIGRAPHY

We integrated lithological and chemostratigraphic information in order to build a continuous sequence stratigraphic framework across the Ouachita basin. In all the sections measured, the distinct shale layers are categorized into those that are regional and those that are local (Table 2.7), including 3rd and 4th order sequence boundaries, local shales (caused either by compensational stacking patterns or by shutdown of sandy depositional fairways), and their correlations confidence (Figure 2.29). In addition, there are unsampled shales which could be higher order sequence boundaries or local shales. The outcrop exposures are limited in extent so gaps exist between roadcuts and sections.

The Lower Jackfork Group was deposited when sea-level began falling during Early Pennsylvanian time. The depositional environment in the Kirby area is interpreted as middle fan with no major depositional break. The shale units found in the Lower Jackfork Group are all likely to be local (i.e., shutdown of depositional fairways) without any noticeable higher order transgressions. Both channelized and sheet-prone facies are present in this interval (Figure 2.31 and 2.32).

The Middle Jackfork Group is an interval with a large amount of sediment input associated with sea-level fluctuations. Channelized sandstones are most common across the DeGray Lake area to the Kirby sections. At least three confident and major regional

3rd order transgressions can be correlated across DeGray Lake to the Kirby sections (Table 3 and Figure 2.13). Architectural elements are dominated by low-relief erosional channel deposits. The depositional environments are interpreted as mainly downslope channels to proximal fan (Figure 2.31 and 2.32).

The Upper Jackfork Group corresponds to a significant rise in sea level. The Upper Sand in the BQ_Section_3 is likely correlated to the lower part of the DeGray Lake Spillway section. The top of the Upper Sand is characterized by debris flow and slump deposits as well as channel fill sandstones (Zou *et al.*, 2012). Such higher order sequence fluctuation in the Kirby section can be correlated to the top of the DeGray Lake Spillway section, where a shift in chemostrata and lithology occur. The provenance of these channelized sandstones was interpreted to be from the south (Proctor, 1974; Graham *et al.*, 1976; Morris, 1977; Miller, 1985; Owen and Carozzi, 1986; and Danielson *et al.*, 1988). Moreover, according to the bottom current indicators from Hollywood Quarry (an Upper Jackfork quarry close to DeGray Lake, Goyeneche *et al.*, 2006), it is also likely that sediment transport was from the southern active margin. Other than this regression higher order sequence, most of the Upper Jackfork is dominated by sheet sandstones and associated shales. Depositional environments are most likely middle and distal fan (Figure 2.31 and 2.32).

From previous regional work (Morris, 1974; Slatt *et al.*, 2000a; Coleman, 2000; and Shaulis *et al.*, 2012), the age from the bottom of the Jackfork to the top of Johns Valley Group (Morrowan) is likely to be from 323Ma to 311Ma. Haq's (Haq and Shutter, 2008) global sea-level curve indicates at least 13 significant 3rd order sea-level fluctuations that can be dated during this time period. An effort to correlate these well-

documented time intervals to the Jackfork sequences has been made (Figure 2.29) using an estimated depositional rate from Slatt *et al.* (2000a).

In addition to the local correlation, various efforts have been made to correlate the major downdip basinal facies of the Jackfork Group to the upper slope channelized facies near Little Rock. Because of the distance (90km from Big Rock quarry to DeGray Lake), structural complexity, and lack of stratigraphic control, the correlation remains qualitative (Slatt *et al.*, 2000a).

The Upper Jackfork stratigraphy at the Big Rock Quarry has been studied in detail by Olariu *et al.*, (2008 and 2011) with major erosional channel contacts highlighted with a 3-D laser scanner and photo real models. The Middle Jackfork Group in Big Rock Quarry consists of only slope shale on the quarry floor (Jordan *et al.*, 1991; Slatt *et al.*, 2000a). Other well-documented outcrops such as Pinnacle Mountain State Park (Slatt *et al.*, 2000a), Maumelle chaotic zone (Viele, 1973), Mena forest road in Arkansas (Morris, 1971), and Rich Mountain in Oklahoma (Pauli, 1994; Montgomery, 1996; Tillman, 2000 and Omatsola and Slatt, 2003) are also included in the correlation. The southeast Oklahoma outcrops are beyond the distal Dierks spillway and interfered by a northern source with channelized friable sandstones (Figures 2.31 and 32).

One direct analog to the outcrops of the Jackfork Group is the Potato Hills-Jackfork Group gas field in southeastern Oklahoma (Pauli, 1994; Montgomery, 1996; Tillman, 2000 and Omatsola and Slatt, 2003; Romero, 2004). Figure 2.15 includes a correlation between the Potato Hills and Kirby sections. These two sections exhibit the following similarities and differences: (1) the unconfined Lower Jackfork Group, where sheet sandstones and unconfined channels dominate; (2) a major eastern source during

Middle Jackfork Group time, where the updip Kirby section is mostly channel sandstone and shifts into shaly intervals downdip at Potato Hills; (3) the lithology, bed thickness, net to gross ratio of the sandstone packages, as well as the presence of the shale layers; (4) the Jackfork Group in Potato Hills is much thinner than at the Kirby section, which indicates that the majority of sediments from the eastern source did not reach to the west; (5) the dominant channelized sandstones in the Upper Jackfork Group of Potato Hills correlate to the dominant sheet sandstones in the Kirby section. This further supports that the Jackfork Group in Oklahoma is mainly sourced from the northern paleo-shelf as the depocenter shifted towards present Arkoma basin to the north (Figure 2.32).

The Jackfork Group in Oklahoma has been developed as a tight sandstone gas reservoir for over a decade (Montgomery, 1996; Suneson and Slatt, 2004). As horizontal drilling and hydraulic fracture technology thrives in the unconventional boom, the Jackfork Group tight gas reservoirs may get more petroleum industry attention. Previously the major productions have been from the friable channelized sandstones facies. As the sequence stratigraphic model indicates, the more sheet prone sandstones in the Lower and Middle Jackfork Group in Oklahoma may be applicable for unconventional development when economics become more favorable.

DISCUSSION

Tectonic Activity versus Eustatic Sea-Level

The Kirby sections illustrate the hierarchical nature of sequence stratigraphy in Early Pennsylvanian time. Based on Coleman's analysis (Coleman, 2000), the Jackfork Group was deposited during a 2nd order major eustatic lowstand during a time of maximum climatic precipitation and weathering. Regional tectonic activity in the basin was probably minor, although it gradually increased throughout Jackfork deposition (Coleman, 2000). This macro-scale tectonic background provided some basis for our detailed sequence stratigraphic framework. We can assume the dominant control is eustatic sea-level with minor tectonic overprint.

However, the time of deposition of the Upper Jackfork and Johns Valley Group, corresponds to a time of rise in sea-level coupled with increased tectonic activity. At a certain time when uplift (induced by foreland folding and thrusting) outpaced the rise in sea-level, the deepwater deposits were dumped into the basin during transgressive and highstand stages. Key evidence includes the conglomerate found at the top of the DeGray Spillway section (Slatt *et al.*, 2000a) and the massive channelized sandstones in the Upper Kirby section. It also explains the presence of massive channelized sandstones in the Johns Valley shale at the Kirby section.

Most of the 4th order cycles found in the Kirby section can be interpreted to be close to the end member of out-of-grade system (Pyles *et al.*, 2011). The Kirby sections are initialized by aggradational and retrogradational stacking patterns in the Lower Jackfork Group (out-of-grade). The basin margin is over steepened by sea-level drop and sediments bypass large sections of the margin and are deposited in the basin, where

most sandstone was deposited on the basin floor. The system is also characterized by an elongate fan with little longitudinal changes in reservoir architecture (Pyles *et al.*, 2011).

CONCLUSIONS

The Kirby sections in western Arkansas, U.S.A provide the opportunity to build the most complete and continuous sequence stratigraphic framework during Early Pennsylvanian time in the ancient Ouachita Basin. The Kirby sections consist of 25 outcrops, including 12 roadcuts in Highway 27 and 13 sections in the Baumgartner Quarry. All the measurements and interpretations on the outcrops were integrated with all previous Jackfork work using modern concepts of deepwater turbidite geology, including (1) regional tectonic and sequence stratigraphic framework of the Stanley Group, Jackfork Group, and Johns Valley Shale in the Ouachita Basin, (2) deepwater outcrop characterization and correlation from the DeGray Lake Section, Dierks Section and Big Rock Quarry which is parallel to the depositional fairway, (3) chemostratigraphic data from key shale layers which are considered as potential condensed sections for assisting correlation.

Outcrop and chemostratigraphic data indicate that the entire Kirby sections consist of at least three confident 3rd order sequences from the bottom of the Jackfork Group to the middle of the Johns Valley Group caused by a combined effect from tectonic uplift, eustatic sea-level change, mixed sediment provenance and shifting of depositional fairways, when the Ouachita Basin was transitioning from a passive margin to a remnant marine basin.

One direct reservoir analog of Jackfork outcrops in Arkansas is the subsurface Jackfork gas field in southeastern Oklahoma. Previous well-based stratigraphic interpretations have been tied to the established and complete sequence stratigraphic framework.

LIST OF FIGURES AND TABLES

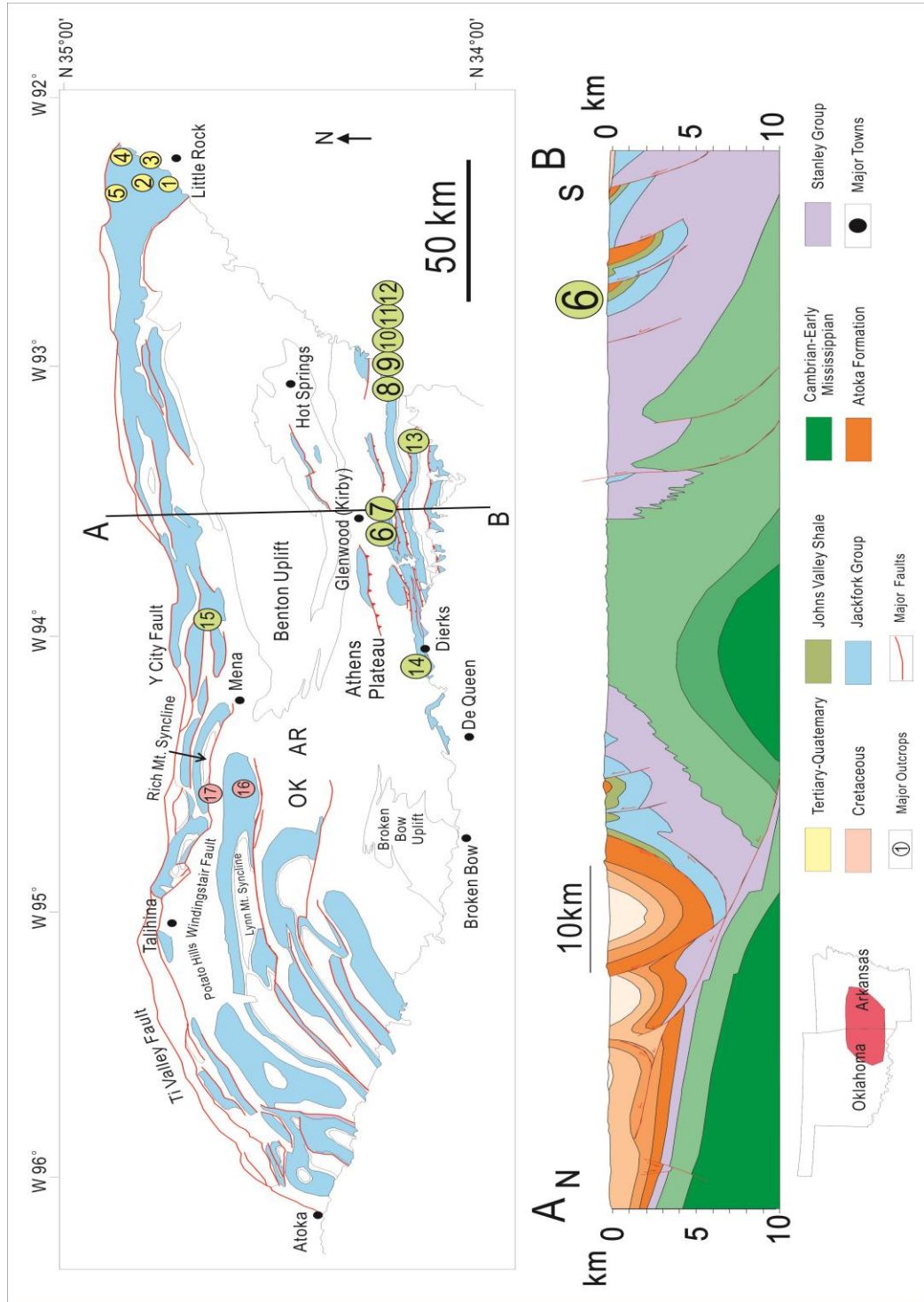


Figure 2.1. Overview map of the Jackfork Group and the location of the key outcrops (to be introduced in Table 2.1)

	Outcrop	Location	Description	Interpretation	Reference
Upland Slope Facies Tract, Arkansas	1: Big Rock Quarry	Little Rock Area, AR	Upper Jackfork Group sandstones rest unconformably on Middle Jackfork Group Shales. 3000ft (1000m) long quarry face with 200ft vertical exposure. Lower 2/3 of the quarry is amalgamated massive sandstones, and upper 1/3 is thin bedded lenticular sandstones and shales.	Lower 2/3 is interpreted as slope canyon-fill turbidite near the entry point into the deepwater system. Upper 1/3 is interpreted as channel levee/overbank deposits. Paleo-flow direction is generally from east to the west.	Slatt et al., 2000
	2: I-430 Roadcut	Little Rock Area, AR	450ft (135m) near vertical Upper Jackfork Group strata rest unconformably on deformed Middle Jackfork Shales. Bioturbated and thinning upward sequence	Similar to Big Rock Quarry so is not repeated here.	Slatt et al., 2000
	3: McCain Mall	North Little Rock Area, AR	70+ ft (21+m) thick and 500ft (150m) wide outcrop wall. Lower thick massive amalgamated sandstone overlain by interbedded sandstone and shales	The entire section is interpreted as two separated slope channel fill. Between the channel fill are levee and overbank (crevasse splay) deposits.	Slatt et al., 2000
	4: Sherwood Outcrop	Sherwood, North Little Rock Area, AR	50+ ft (15m) thick and 400ft (120m) wide outcrop wall behind Wal-Mart Supercenter. Scoured and amalgamated sandstones are interbedded with siltstones and shales.	Similar to McCain Wall, the section is interpreted to be channel complex with 2-3 channel fills and associated levees/overbanks.	Newly discovered Jackfork outcrop (2013) with Mr. Charlie Stone from Arkansas Geological Survey
	5: Pinnacle Mountain State Park	Little Rock Area, AR	130ft (40m) thick clean, amalgamated and tabular Middle Jackfork sandstones sitting on 200ft (60m) highly deformed shales. Large blocks of sandstones are interspersed within the contorted shales.	The shale interval below is interpreted as a muddy slump deposit and the overlying tabular sandstones are interpreted as ponded slope fan.	Slatt et al., 2000
Downdip Basinal Facies Tract, Arkansas	6 Baumgartner Quarry	Kirby, AR	600ft (180m) of Middle-Upper Jackfork Group turbidite sections with 150 (45m) Lower Sandstone, 100ft (30m) Middle Shale and 350ft (105m) Upper Sandstones. Lower Sandstone has more scoured surface and lenticular geometries than Upper Sandstones.	Lower Sandstones is more channel-prone and Upper Sandstones is more sheet-prone. Middle Shale is a major transgression separating Upper and Middle Jackfork Group.	Zou et al., 2012
	7 Kirby Roadcuts	Kirby, AR	5000ft (1600m) gross thickness with a few separated Jackfork Group roadcuts. It is the most continuous and complete Jackfork Group outcrop in the entire basin.	A wide variety of architecture elements and depositional environments that is going to be described and discussed in this paper.	Morris, 1974; Zou et al., 2012; This paper
	8 DeGray Lake Highway 7	DeGray Lake Area, AR	350ft (105m) Lower Jackfork Group in Highway 7 near the entrance of DeGray Lake resort. The sandstones are a mixture of amalgamated tabular sandstones and interbedded lenticular sandstones.	The section is interpreted as unconfined channel system in a proximal basin setting. The depositional process is "fill and spill" for interbedded channel fills and sheet sandstones.	Slatt et al., 2000
	9 DeGray Resort	DeGray Lake Area, AR	This is a shallow quarry (which no longer exist due to mining). It is ~1000ft (300m) above Lower Woodford Highway 7 section. It exposed 660ft (200m) of Middle Jackfork sections. The lower part comprises thin-to-thick bedded sandstones with ripple bedding, shale rip-up clasts and lenticular bedding. It is overlain by two shale packages and tabular dominated sandstones on top	The basal 160ft (50m) is interpreted as channel-fill sandstones in Middle Jackfork Group followed by two condensed sections and unconfined sheet sandstones.	Slatt et al., 2000

Table 2.1-A. List of the basic information of the key Jackfork Group outcrops.

	Outcrop	Location	Description	Interpretation	Reference
Downdip Basinal Facies Tract, Arkansas	10: DeGray Spillway	DeGray Lake Area, AR	1000ft (300m) thick, most famous outcrop in the area. Very thick turbidite sequence with multiple lithofacies. In the broader sense, the succession tends to thicken and becomes coarser grained and cleaner stratigraphically upward.	Multiple sequence boundary and condensed sections found in the section. The major sandstone package is most likely of a base of slope setting with proximal fans and unconfined channel fills.	Slatt et al., 2000; Al-Siyabi, 2000
	11: DeGray Dam	DeGray Lake Area, AR	800ft (240m) of the Uppermost Jackfork Group, Amalgamated tabular sandstones are the dominated lithofacies separated by parallel laminated shales. Most of the massive tabular sandstones have flat bases except for the ones on top and bottom.	Right above DeGray Spillway, the depositional environment is also similar which is proximal fan.	Slatt et al., 2000
	12: Friendship	DeGray Lake Area, AR	440ft (130m) thick Uppermost Jackfork Group section. Massive sandstones dominated with both laminated and contoured shales.	100-200ft (30-60m) above DeGray Spillway, the depositional environment is also similar.	Slatt et al., 2000
	13: Hollywood Quarry	Hollywood, AR	3-dimensional exposure of the Upper Jackfork Group including 4 major sandstone unites above the quarry floor. The strata is stratigraphically above the DeGray Lake Spillway section. Both basal and upper sandstones have erosional and scour surfaces. The 2 middle sandstones are more extensive and tabular looking	This interval is interpreted to be mostly channel fill-sandstones. Tabular looking sandstones with interbedded shale in the middle is caused by the fill and spill of the underlying major channel.	Slatt et al., 2000
	14: Dierks Spillway	Dierks, AR	The 500ft (150m)-thick Dierks Spillway section is located at the distal part of the basin. Geological map indicate the section belongs to Middle Jackfork Group. Most of the sandstones are tabular with much less scoured surfaces.	The Dierks Spillway section is interpreted as middle to distal basin floor fan environment.	Slatt et al., 2000, This paper
	15: Mena Forest Roadcut	Mena, AR	2000ft (600m) section with heavily covered vegetation, measurements no longer available.	Located at the distal part of the basin.	Morris, 1974
Oklahoma	16: Highway 270, Rich Mountain	Rich Mountain, OK	600ft (180m) continuous roadcuts in the Rich Mountains. Friable sandstones are dominant in the Middle Jackfork Group that has visible porosities. Scour surfaces and lenticular bedding are common	The Friable sandstones are interpret to be mainly channelized sandstones sourced from the north.	Roberts, 1994; Pauli, 1994; Slatt et al., 2000; Omatsola, 2003; Romero, 2004.
	17: Highway 1, Rich Mountain	Rich Mountain, OK	180ft (54m) continuous roadcuts in the Rich Mountains. Friable sandstones are dominant in the Middle Jackfork Group that has visible porosities. Scour surfaces and lenticular bedding are common	The Friable sandstones are interpreted to be mainly channelized sandstones sourced from the north.	Roberts, 1994; Pauli, 1994; Slatt et al., 2000; Omatsola, 2003; Romero, 2004.

Table 2.1-B. List of the basic information of the key Jackfork Group outcrops.

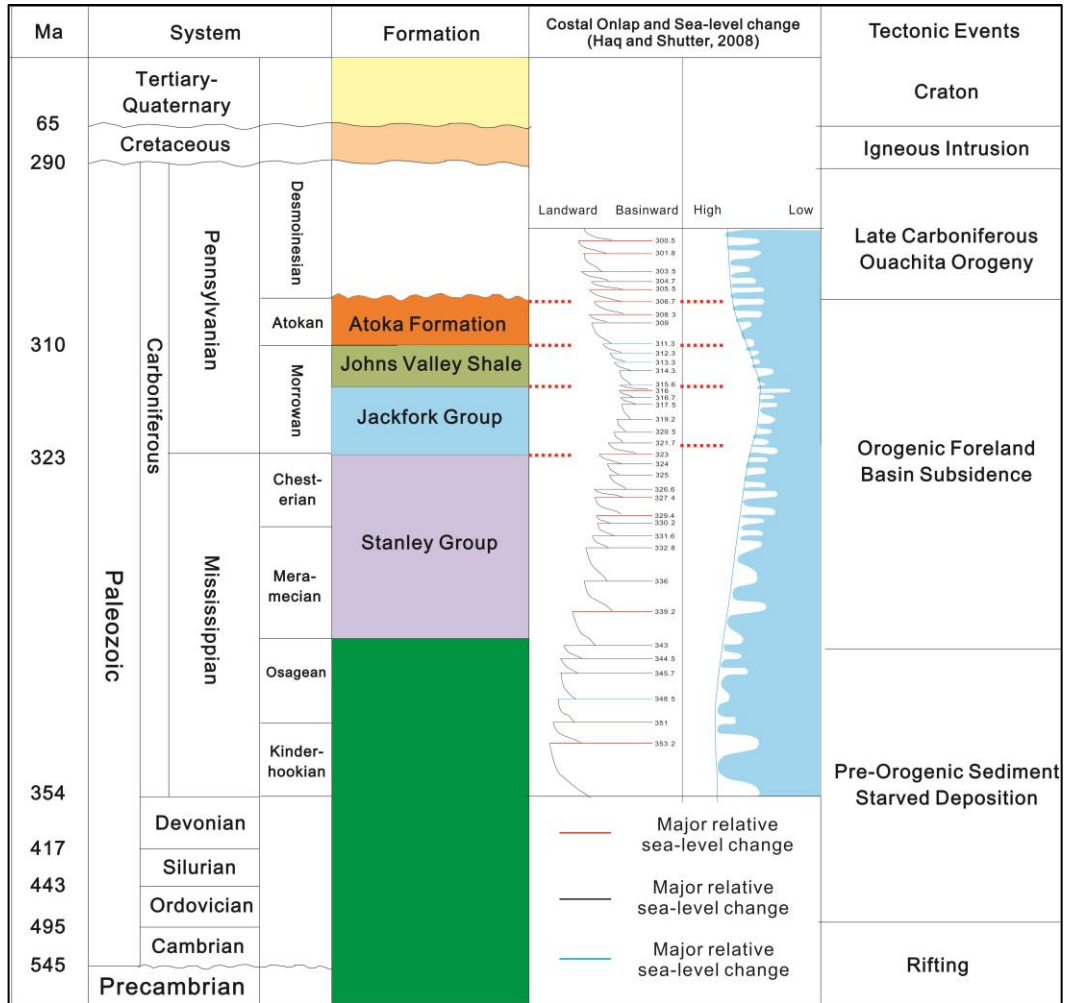


Figure 2.2. Regional stratigraphic column and tectonic events of the studied area in western Arkansas. Global sea-level curve is from Haq and Shutter, 2008. The Jackfork Group was deposited during the stage of Ouachita Basin subsidence.

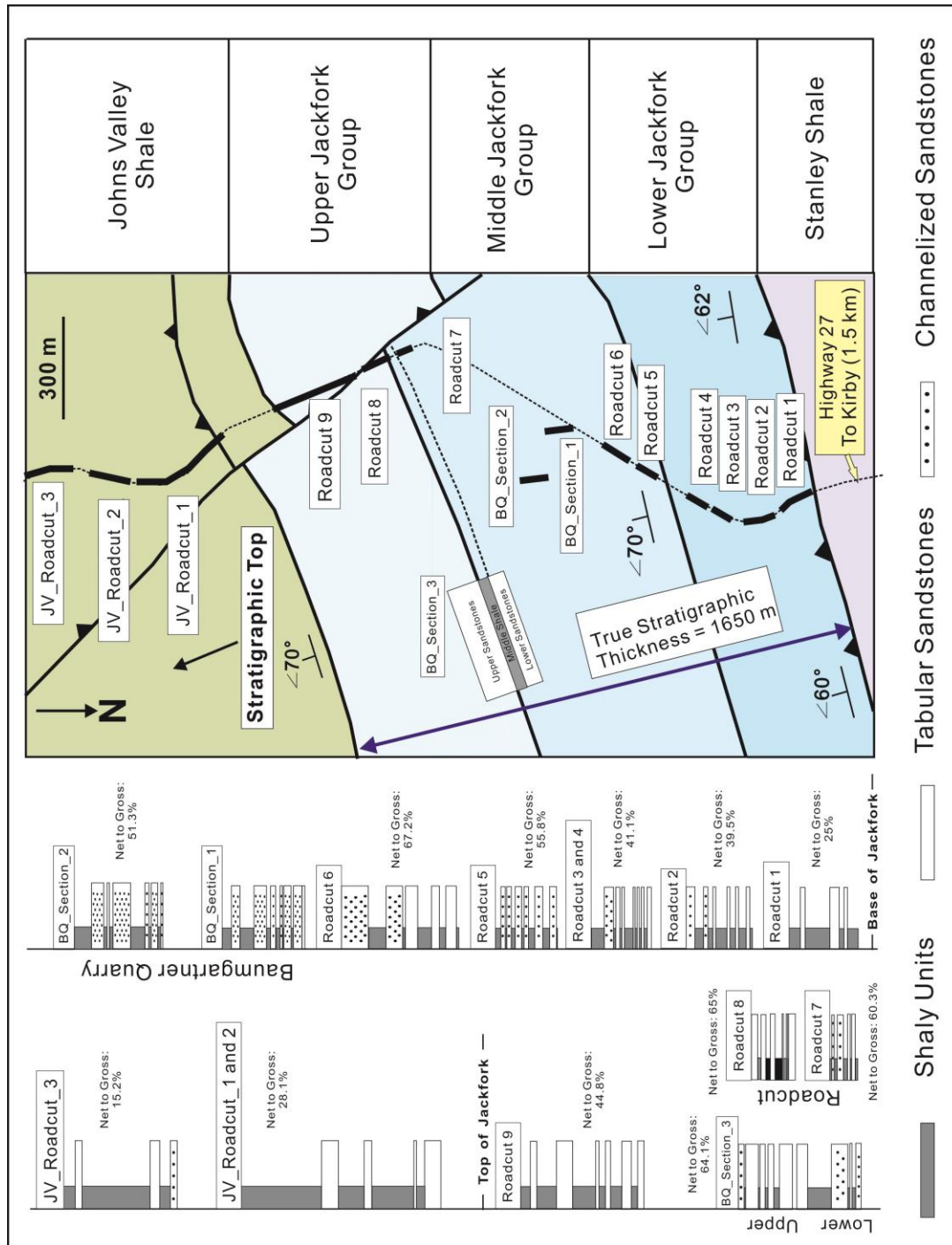


Figure 2.3.An overview of complete Kirby sections, including Baumgartner Quarry. All the strata are steeply dipping (60-70 degree) towards the south. General Lower, Middle and Upper Jackfork Group boundaries were provided by Charlie G. Stone, Arkansas Geological Commission (retired).

Outcrop Name	Universal Thickness from Base of Jackfork (m)	True Stratigraphic Thickness (m)	Outcrop Exposure Condition	General Description	General Interpretation	Chemstrata Samples
Roadcut 1	0-130	130	Good Vertical Section along the east side of the road	Lowermost Jackfork Group underlain by Staley Shale. 130m thick section with dominated fine-grained tabular sandstones (Bouma Ta beds) interbedded with shaly units (Bouma Tc-Te beds). Scour surfaces at the bottom of the sandstone beds observed at 57m and 63m	Most sandstones are layered sheet sandstones which represent a basin floor fan environment at the early stage of sea-level fall. The observed scour surfaces represent high energy flows.	Thoroughly sampled all shales for HHXRF, 1 sample for ICP-MS compare
Roadcut 2	150-275	125	Good Vertical Section along the east side of the road	125m of Lower Jackfork Group is dominated by amalgamated massive sandstones (Bouma Ta beds) interbedded with shale units (Bouma Tc-Te beds). Scour surfaces observed at 165m and 182m. Thick, massive and massive sandstones with clean and scour surfaces occur at 230m for the first time.	Amalgamated sheet and channelized sandstones. More sandstones against shales, more scour surfaces and amalgamation indicate more channelization and higher sediment input and energy flows. The depositional environment shifted from middle/distal fan to proximal fan in a basin floor environment.	Thoroughly sampled all shales for HHXRF, 1 sample for ICP-MS compare
Roadcut 3	300-330	30	Medium Vertical Section along the east side of the road	Poorer exposure of 30m-thick Lower Jackfork Group is dominated by tabular looking sandstones with minor scoured surfaces. The lithology is similar to Roadcut2.	Similar facies and environment with Roadcut2.	Not Sampled
Roadcut 4	340-370	30	Medium Vertical Section along the west side of the road	Massive amalgamated sandstones with shale interbeds. Massive and lenticular sandstones with scoured surfaces at 360m, interbedded with massive shales (debrites) with chaotic bedding at the same depth.	The majority of the sandstones are interpreted to be amalgamated channelized sandstones. The muddy debris flow deposits associated with the channelized deposits indicate the increase of sea-bottom relief. The environment of deposition shift further towards proximal basin floor (and potential base of slope) fan.	Not Sampled

Table 2.2. General outcrop description and interpretation of the Lower Jackfork Group in Kirby Sections.

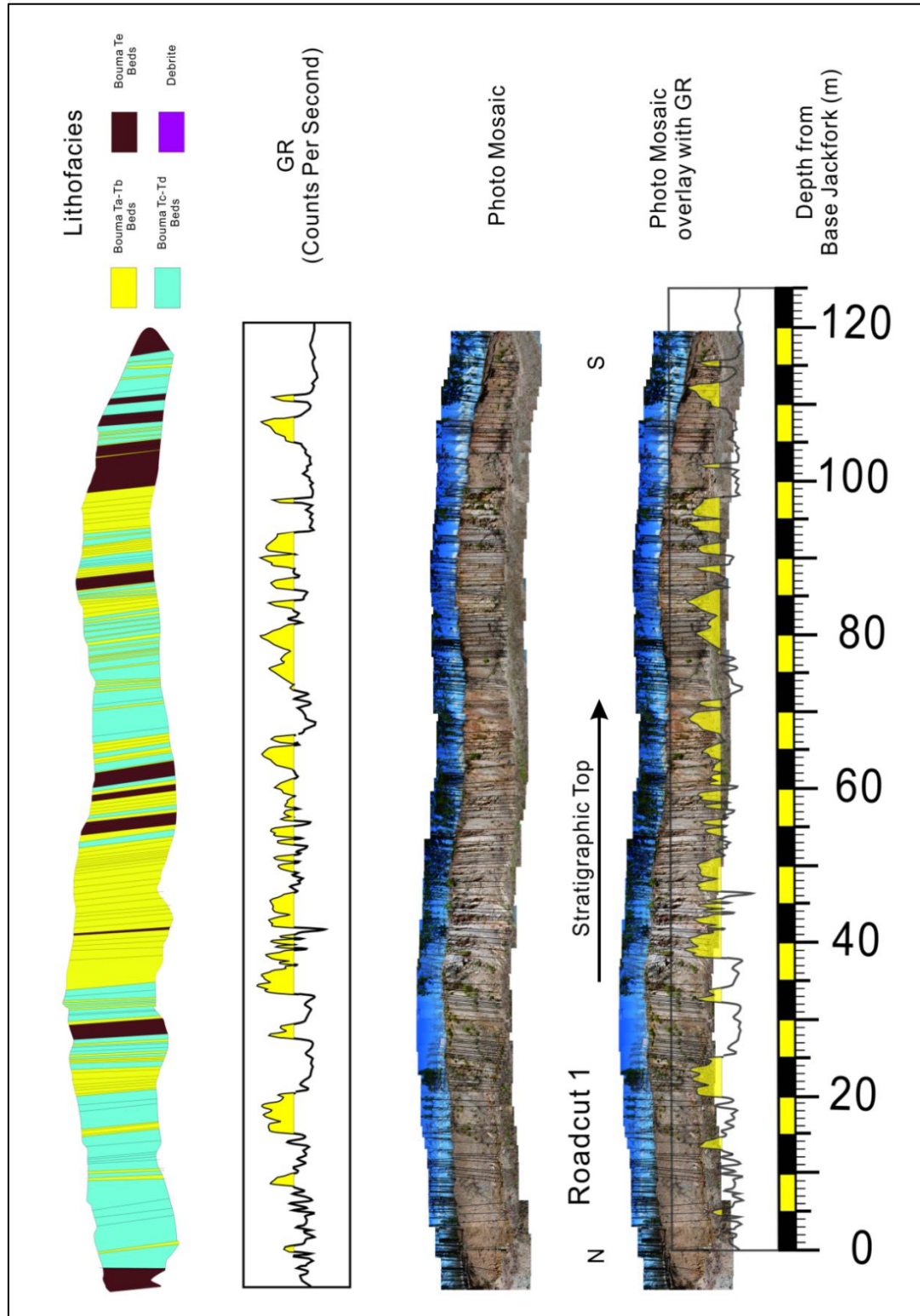


Figure 2.4. Outcrop photo, general description and outcrop gamma ray of the Kirby Roadcut 1

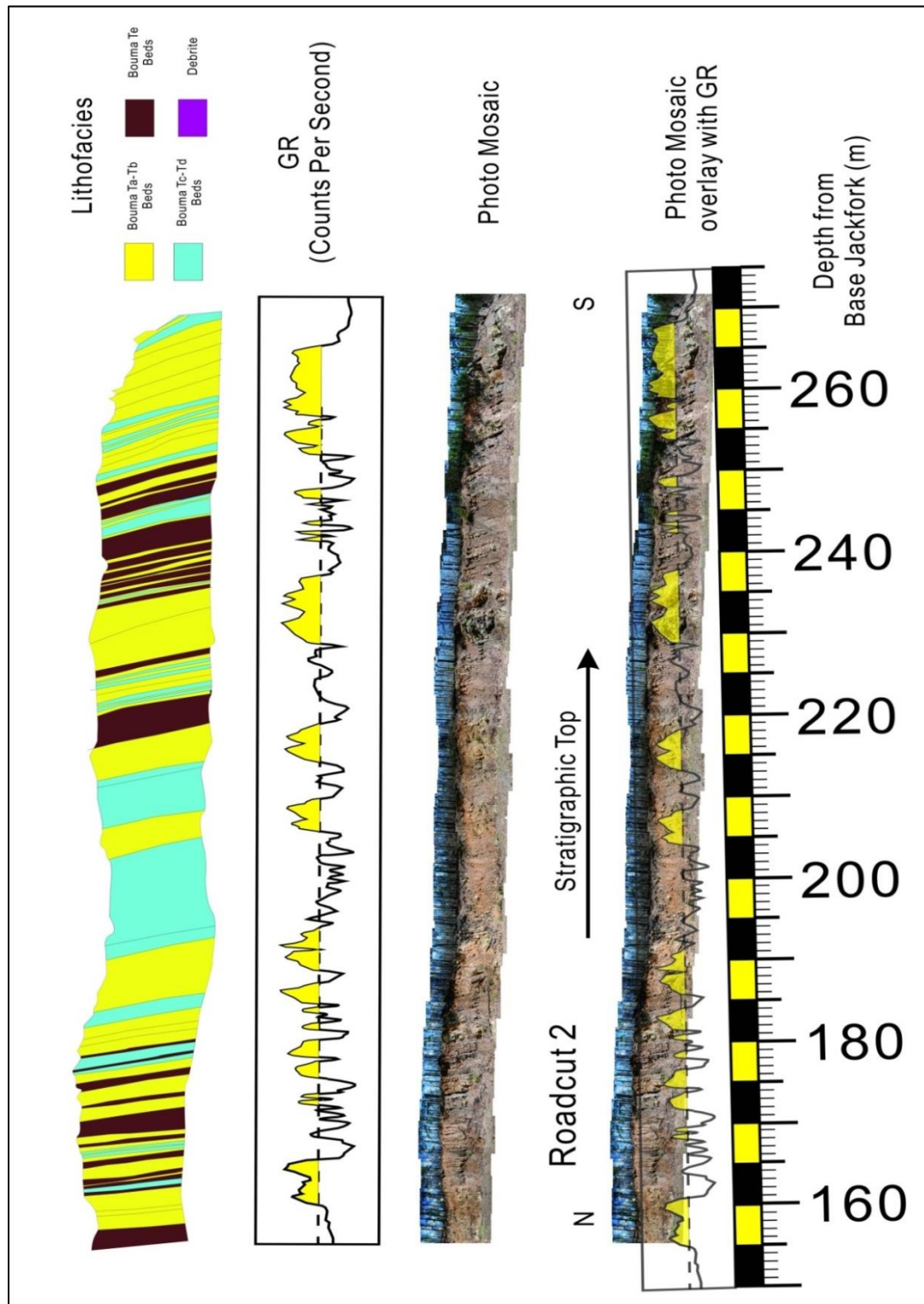


Figure 2.5. Outcrop photo, general description and outcrop gamma ray of the Kirby Roadcut 2

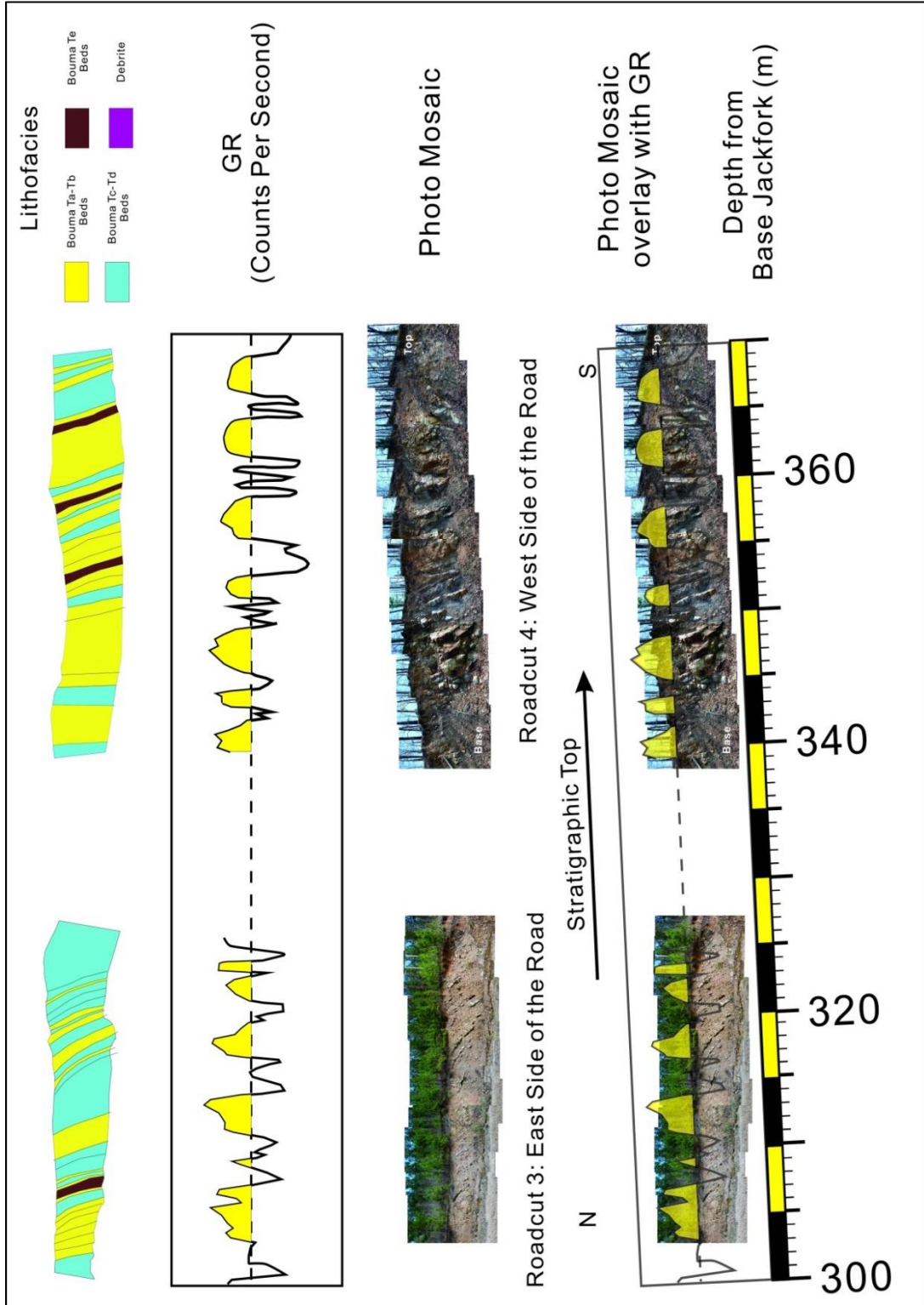


Figure 2.6. Outcrop photo, general description and outcrop gamma ray of the Kirby Roadcut 3 and 4

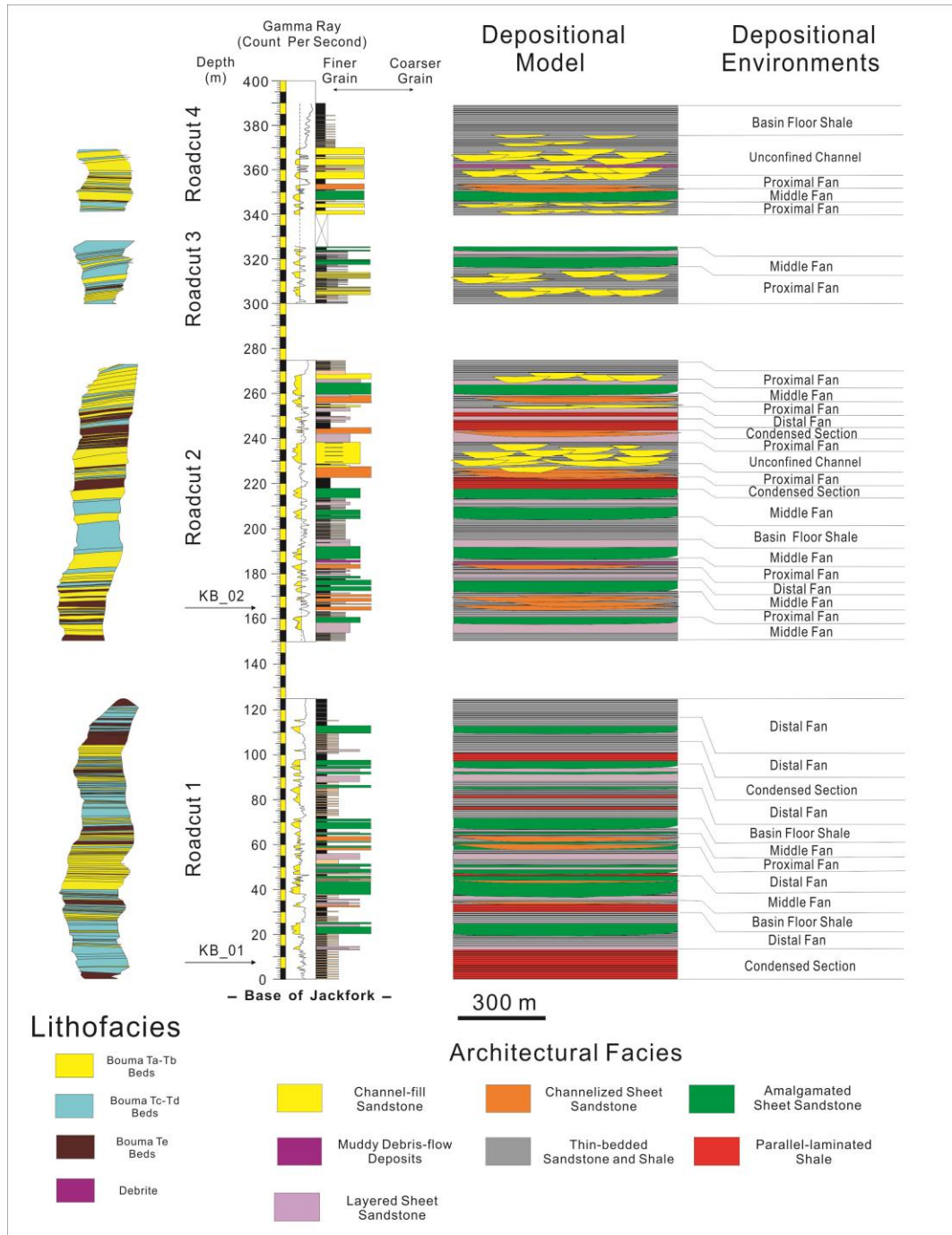


Figure 2.7. Measured sections and interpretation (depositional model, environments, and relative sea-level) of the Lower Jackfork Group in the Kirby sections. See Figure 2.3 for locations. Locations of shale ICPMS samples are marked as arrows.

Outcrop Name	Universal Thickness from Base of Jackfork (m)	True Stratigraphic Thickness (m)	Outcrop Exposure Condition	General Description	General Interpretation	Chemostrata Samples
Roadcut 5	500-545	45	Good Vertical Section along the east side of the road	45m thick massive and amalgamated sandstones (Bouma Ta) with shale interbeds (Bouma Tc-Te). Most of the sandstone beds are lenticular-shaped with clasts and scoured surfaces at the bottom. Individual sandstone bed thickness is typically 1-2m with frequent scoured surfaces.	The sandstones are interpreted to be channel filled sandstones with associated shaly interbeds. The 45m exposed section has similar facies patterns without major changes. Thus they belong to one single channel complex.	Not Sampled
Roadcut 6	580-660	80	Poor Vertical Section along west side of the road which no Longer Exst	80m of poor vertical section which is no longer available after the road re-construction. However, massive, amalgamated and scoured (lenticular) sandstones were observed and documented.	Based on large amount of amalgamated sandstones against shale, and scoured surfaces, the facies patterns is similar to Roadcut5.	Not Sampled
BQ_Section_1	790-840	50	Medium Vertical Section near the entrance of the quarry (Section start at the pond)	The section exposed along the drainage of the quarry, with only 2-3m wide narrow exposure.	Based on large amount of amalgamated sandstones against shale, and scoured surfaces, the facies are amalgamated channel-fill sandstones with associated shales. They are most likely proximal fan or lobe in the downslope environment.	1 Sample for ICP-MS Compare
BQ_Section_2	850-950	100	Good Both Vertical and Lateral Section on the hill of the quarry	The section is up on the hill with 270m wide and 130m thick. It is dominated by massive amalgamated sandstones with scoured surfaces. Two major, thick and distinct shale packages occur at 870m and 935m and are 17m and 21m thick respectively. The shales are all dark colored and parallel laminated. Thick Friable sandstones occur from 920-930m.	Most sandstones are interpreted to be channel filled sandstones. They are most likely represent proximal fan or lobe in the downslope environment. The thick shale are interpreted as transgression events separating two major channel complexes.	3 Samples for ICP-MS Compare
Lower Sand of BQ_Section_3 (Below Middle Shale)	1070-1125	55	Good Both Vertical and Lateral Section at the quarry face	The section is the 55m-thick Lower Sand which is well documented by Zou et al. (2012). Most of them are thick, massive and scoured sandstones with interbedded shale facies.	Most sandstones are interpreted to be channel filled sandstones. They are most likely represent proximal fan or lobe in the downslope environment. The thick shale are interpreted as transgression events separating two major channel complexes.	2 Samples for ICP-MS Compare
Roadcut 7	1090-1120	30	Medium Vertical Section along the east side of the road	According to satellite image and quadrangle (detailed geological) map, it is likely be correlated to the Lower Sand in the Baumgartner Quarry (BQ_Section_3) that is 1600m along the strike. Lithology is mainly massive, amalgamated sandstones with scour surfaces.	Facies are similar to the Lower Sand in BQ_Section_3	Thoroughly sampled all shales for HXRF

Middle Jackfork Group

Table 2.3. General outcrop description and interpretation of the Middle Jackfork Group in Kirby Sections.

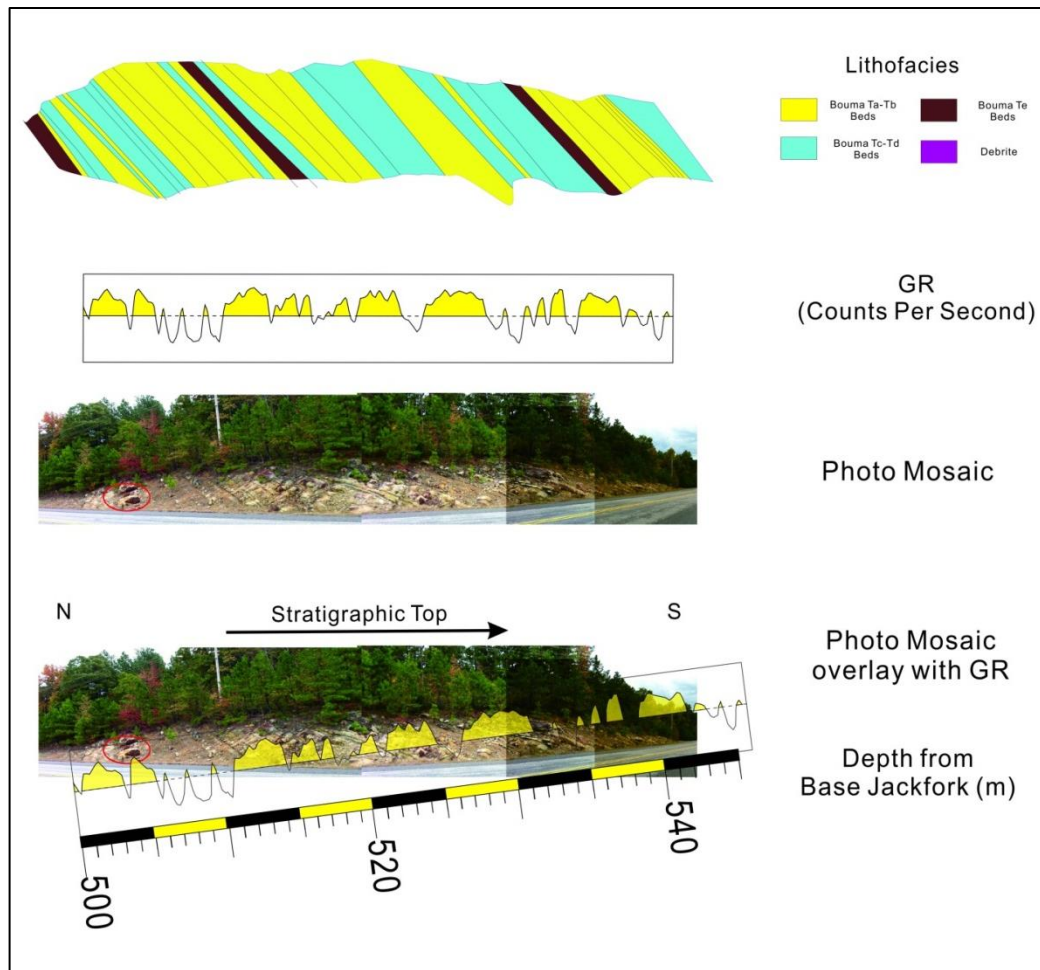


Figure 2.8. Outcrop photo, general description and outcrop gamma ray of the Kirby Roadcut 3 and 4

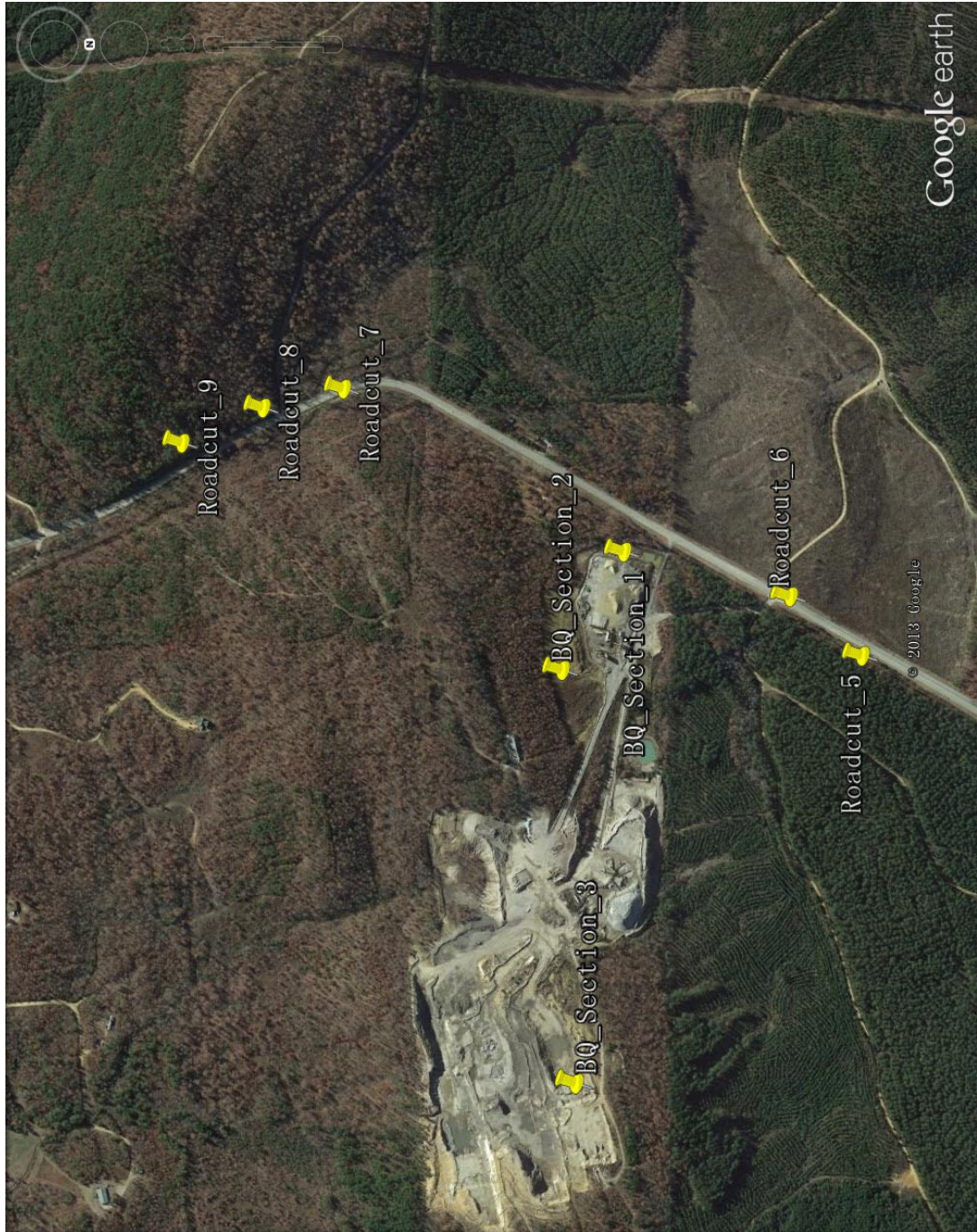


Figure 2.9. Satellite image (Google Earth) showing the relationship between the Baumgartner Quarry and the Kirby Roadcuts, for locations see Figure 2.3

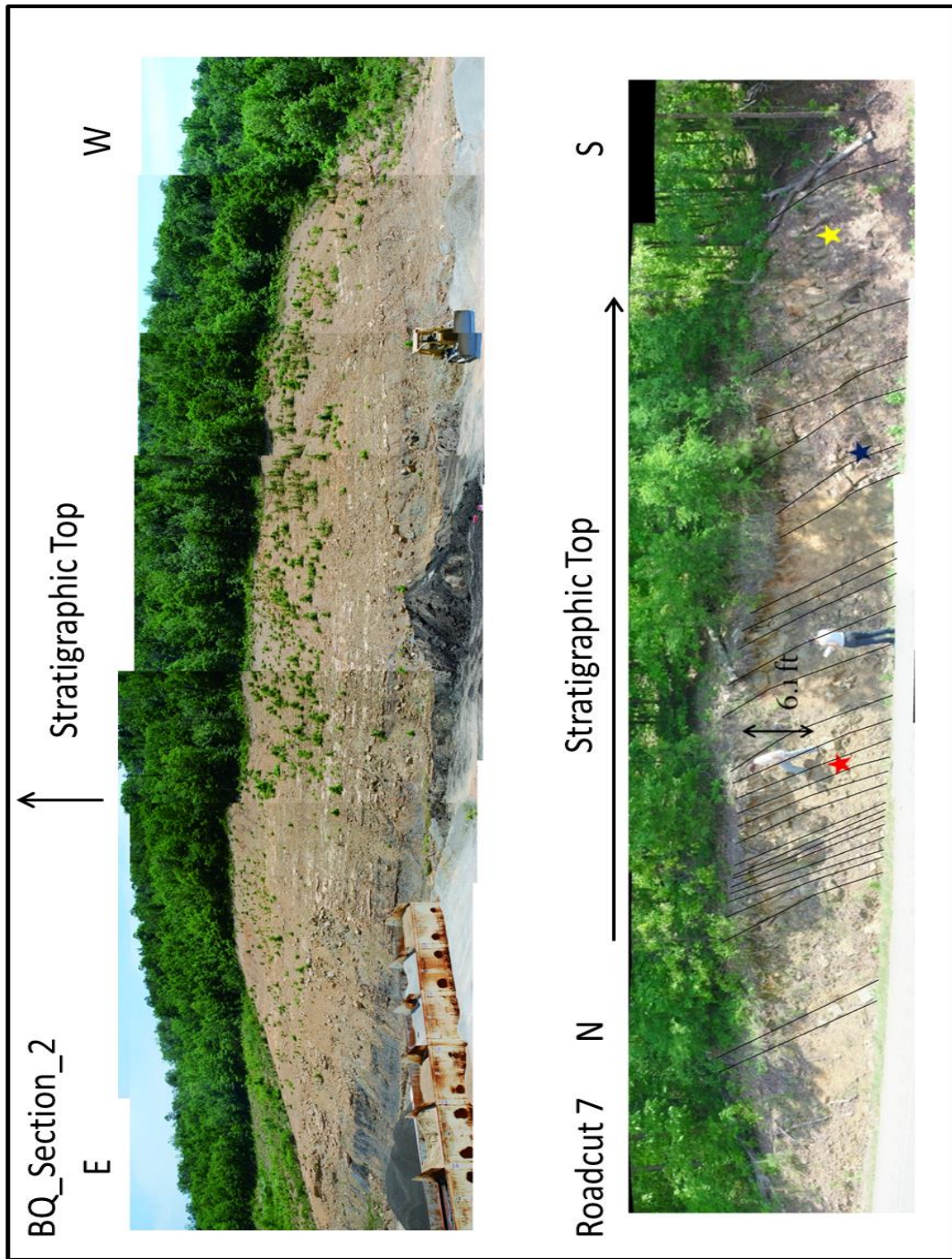


Figure 2.10. Outcrop photo of the BQ_Section_2 on the hill of Baumgartner Quarry and Kirby Roadcut 7, the sandstones in these two sections are mostly with scoured surfaces.

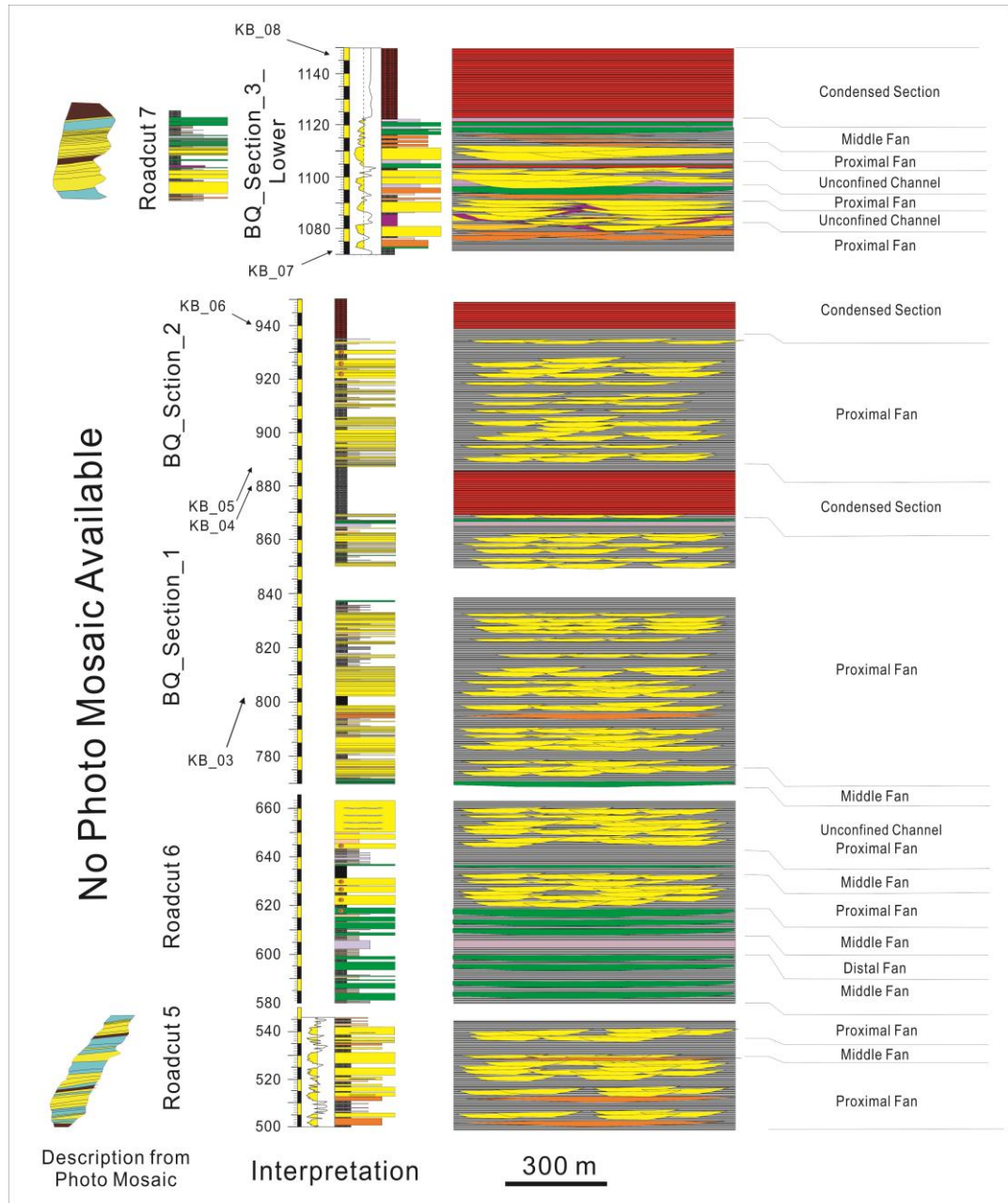


Figure 2.11. Measured sections and interpretation (depositional model, environments, and relative sea-level) of the Middle Jackfork Group in the Kirby sections. See Figure 2.3 for locations. Locations of shale samples are marked as arrows.

Outcrop Name	Universal Thickness from Base of Jackfork (m)	True Stratigraphic Thickness (m)	Outcrop Exposure Condition	General Description	General Interpretation	Chemostrata Samples
Upper Sand of BQ_Section_3 (Above Middle Shale)	1160-1260	100	Good Both Vertical and Lateral Section at the quarry face	The section is 100m-thick Upper Sand which is well documented by Zou et al. (2012). Most of them are thick, massive and tabular sandstones (Bouma Ta beds) with interbedded shale facies. Sandy debris flow (Slurry beds) are common with the tabular sandstones. Lenticular sandstones with muddy debris flow deposits occur at the top.	The Upper Sand interpreted to be dominated by amalgamated and layered sheet sandstones. Because of the dominated sheet deposits (in contrast to the underlain channel dominated interval), the depositional environment is interpreted to be relatively further downdip than that of Middle Jackfork Group. The top lenticular sandstones are interpreted as Channels caused by another turbidite flow cycle (or a higher order transgression event).	2 Samples for ICP-MS
Roadcut 8	1170-1270	100	Medium Vertical Section along the west side of the road	The section is stratigraphically equivalent to Upper Sand in the BQ_Section_3. It begins with a 15m thick massive, amalgamated and tabular-looking sandstone (Bouma Ta beds), followed by 10m thin-bedded sandstone interval. The rest of the section is poorly exposed with observed tabular and massive looking sandstones.	The facies interpretation is similar to Upper Sand of BQ_Section_3. Lack of scoured surfaces indicate amalgamated and layered sheet sandstones facies. The depositional environment is interpreted as proximal and middle basin floor fan.	Thoroughly sampled all shales for HHXRF
Roadcut 9	1450-1650	200	Good Vertical Section along the west side of the road	Stratigraphically, Roadcut 9 is 180m above Roadcut 8 due to a strike-slip fault from Arkansas Geological Survey. It is dominated by massive, tabular-looking, amalgamated sandstones with interbedded shales. However, the sandstone to shale ratio decreases.	The dominated massive, tabular looking sandstones are interpreted as amalgamated sheet sandstones. The depositional environment is likely middle basin floor fan. The decrease of sandstone-to-shale ratio may indicate a transgression towards Johns Valley Shale.	Thoroughly sampled all shales for HHXRF, 1 sample for ICP-MS compare
Upper Jackfork Group						

Table 2.4. General outcrop description and interpretation of the Middle Jackfork Group in Kirby Sections.

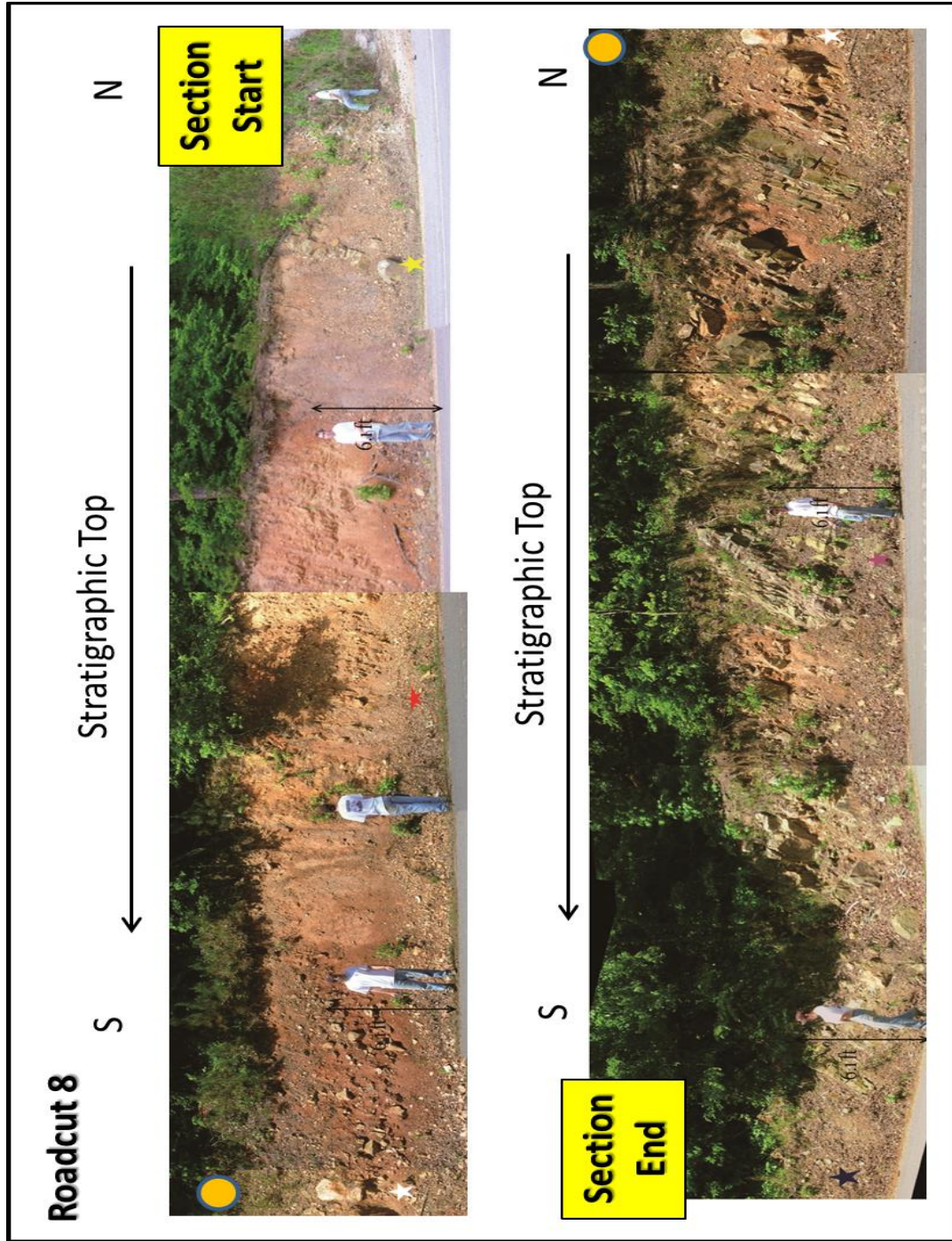


Figure 2.12. Outcrop photo of the Kirby Roadcut 8.

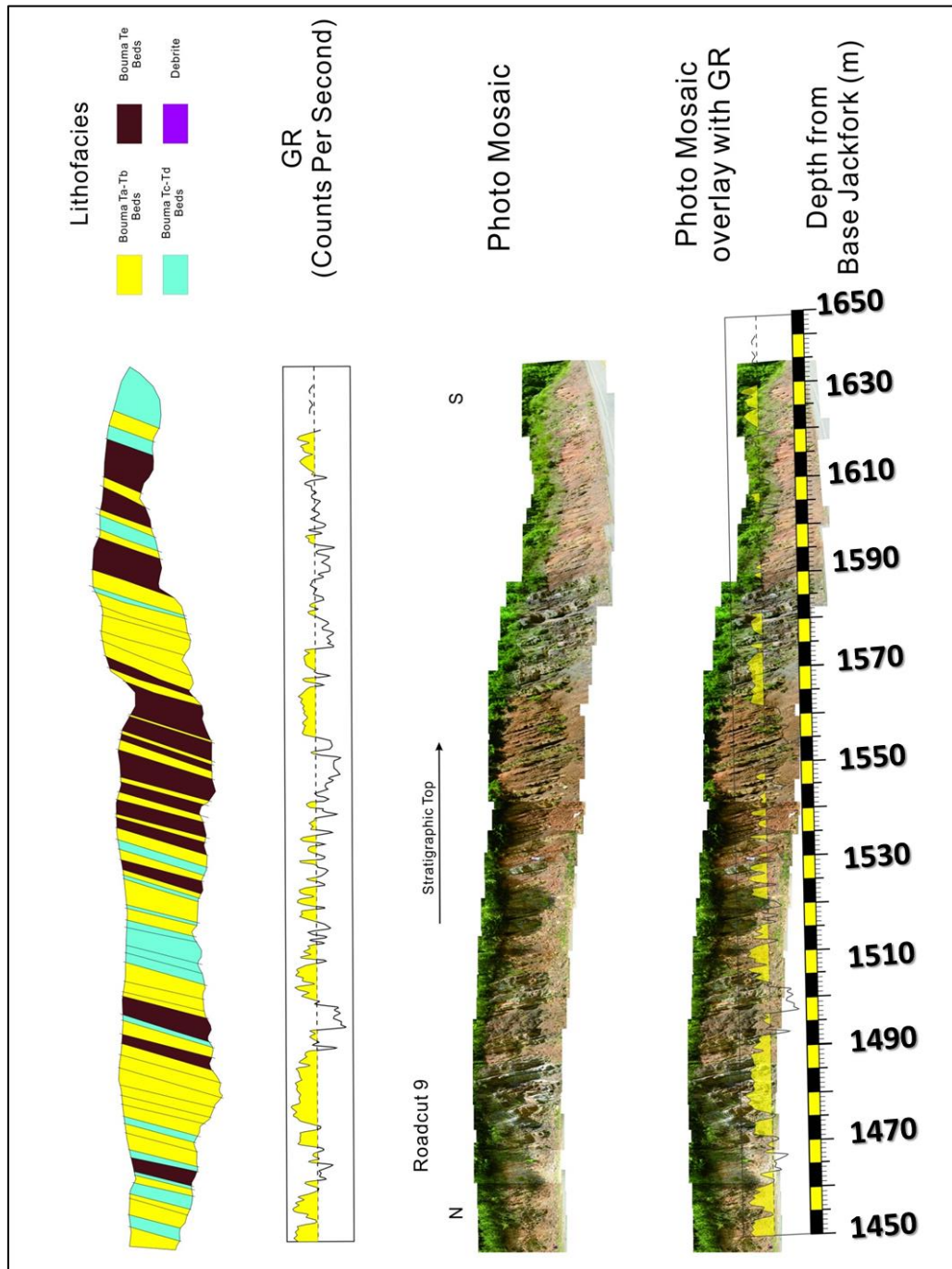


Figure 2.13. Outcrop photo, general description and outcrop gamma ray of the Kirby Roadcut 9

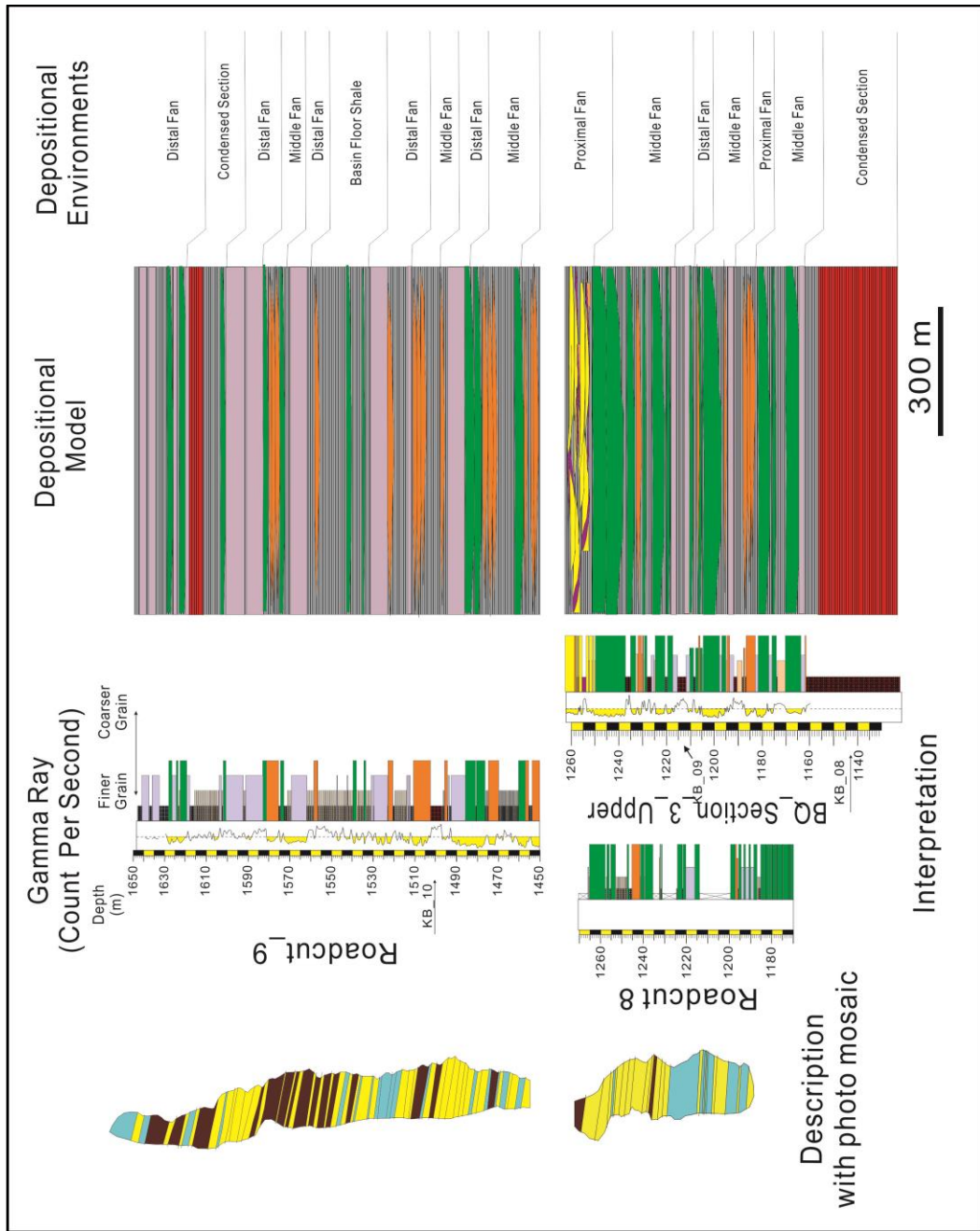


Figure 2.14. Measured sections and interpretation (depositional model, environments, and relative sea-level) of the Middle Jackfork Group in the Kirby sections. See Figure 2.3 for locations. Locations of shale samples are marked as arrows.

Johns Valley Shale						
Outcrop Name	Universal Thickness from Base of Jackfork (m)	True Stratigraphic Thickness (m)	Outcrop Exposure Condition	General Description	General Interpretation	Chemostrata Samples
JV_Section_1	1700-1780	80	Good Vertical Section along the west side of the road	This section has much lower sand to shale ratio, and is dominated by tabular looking sandstones. The lowermost Johns Valley Shale section occur 250m above the top of Roadcut 9. It begins with a 15m-thick amalgamated tabular sandstone package (Bouma Ta beds), followed by a 10m shaly and thin-bedded section. A 3m thick scoured (lenticular) sandstone occur at 1925m	Most of the sandstones are interpreted to be layered sheet sandstones. The depositional environment is middle to distal fan in a transgression period.	1 sample for ICP-MS compare
JV_Section_2	1800-1900	100	Medium Vertical Section along the west side of the road	The Lower part of this section is 20-m thick tabular-looking sandstones, followed by 80m shaly interval.	Similar facies and environment with JV_Section_1. Lack of sandstones and dominated shale in the section indicate a transgressional and hemipelagic period.	Not Sampled
JV_Section_3	2280-2400	120	Good Vertical Section on both sides of the road.	The Lower part of this section is 10-m thick scoured sandstones, followed by 20m tabular looking sandstones. The upper 100m (2310-2400m) is 90 shale.	The section is probably Middle Johns Valley Shale. The dominated shale component indicate a transgressional or highstand period with minor turbidite dumped into the basin.	1 sample for ICP-MS compare

Table 2.5. General outcrop description and interpretation of the Johns Valley Shale in Kirby Sections.

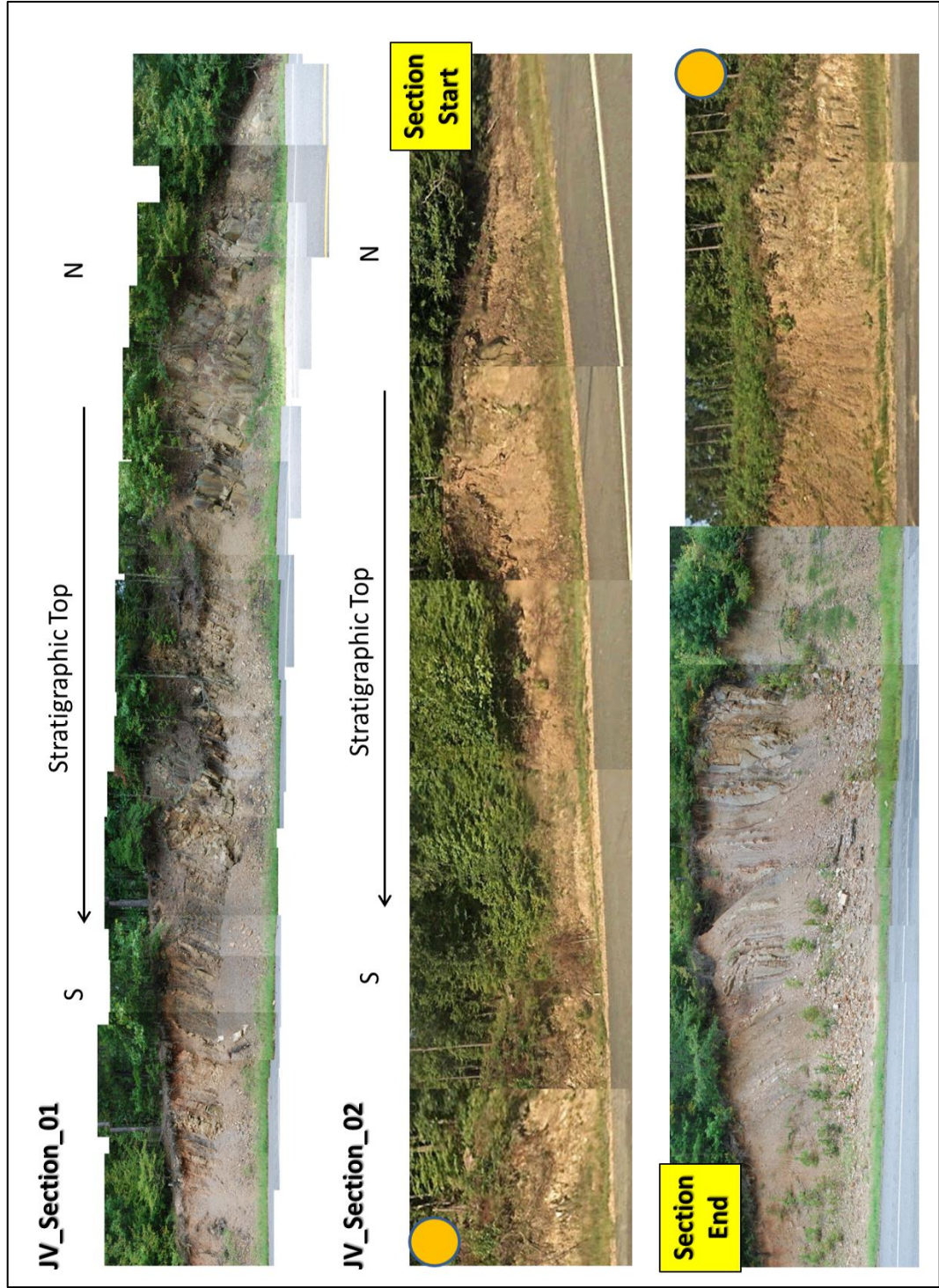


Figure 2.15. Outcrop photo of the Johns Valley Shale

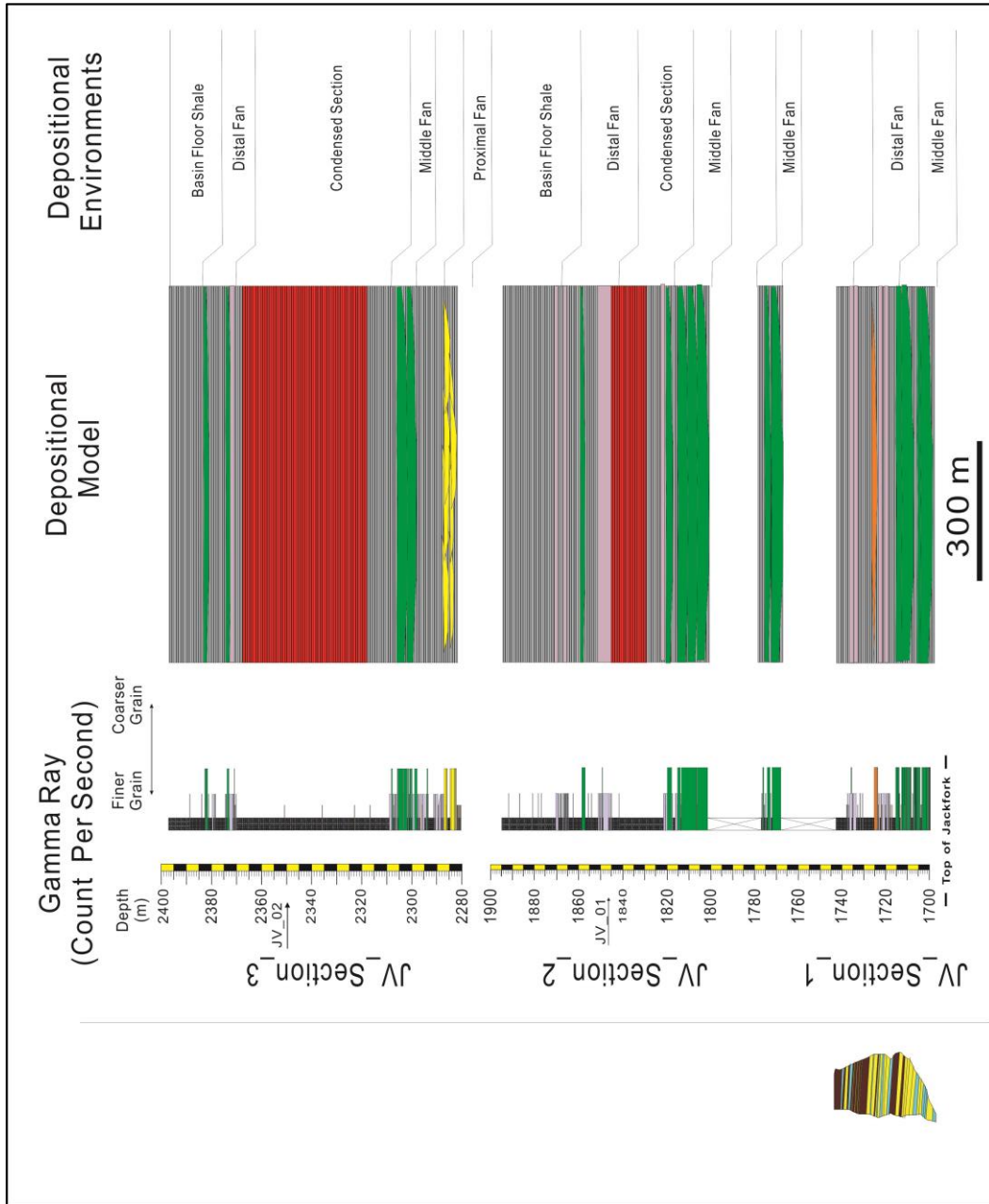


Figure 2.16. Measured sections and interpretation (depositional model, environments, and relative sea-level) of the Johns Valley Shale in the Kirby sections. See Figure 2.3 for locations. Locations of shale samples are marked as arrows.

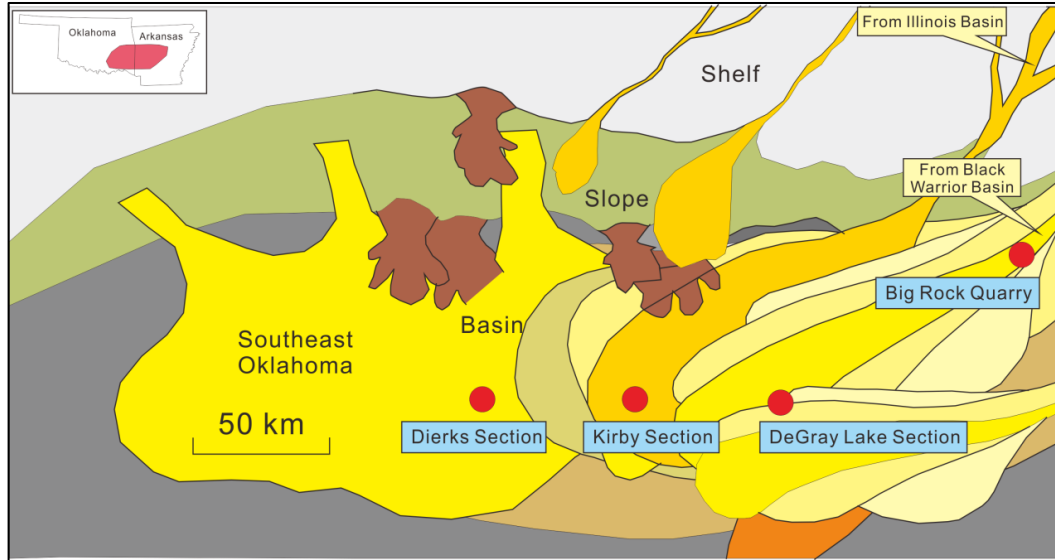


Figure 2.17. Paleogeography map of the Jackfork Group with key outcrop correlations, (Modified from Morris, 1971 and Pauli, 1994).

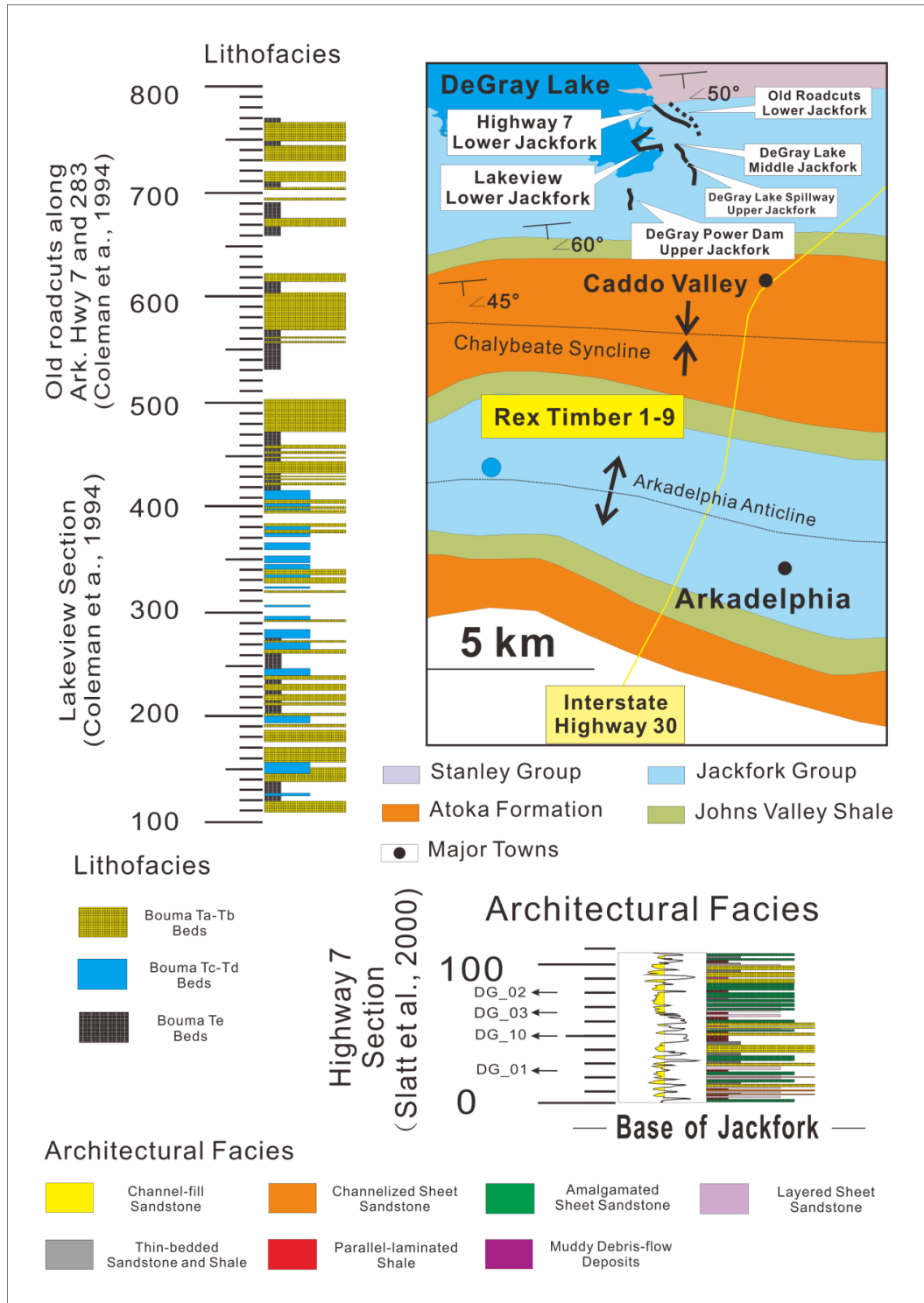


Figure 2.18-A. An overview of Jackfork Group outcrops in the DeGray Lake area,

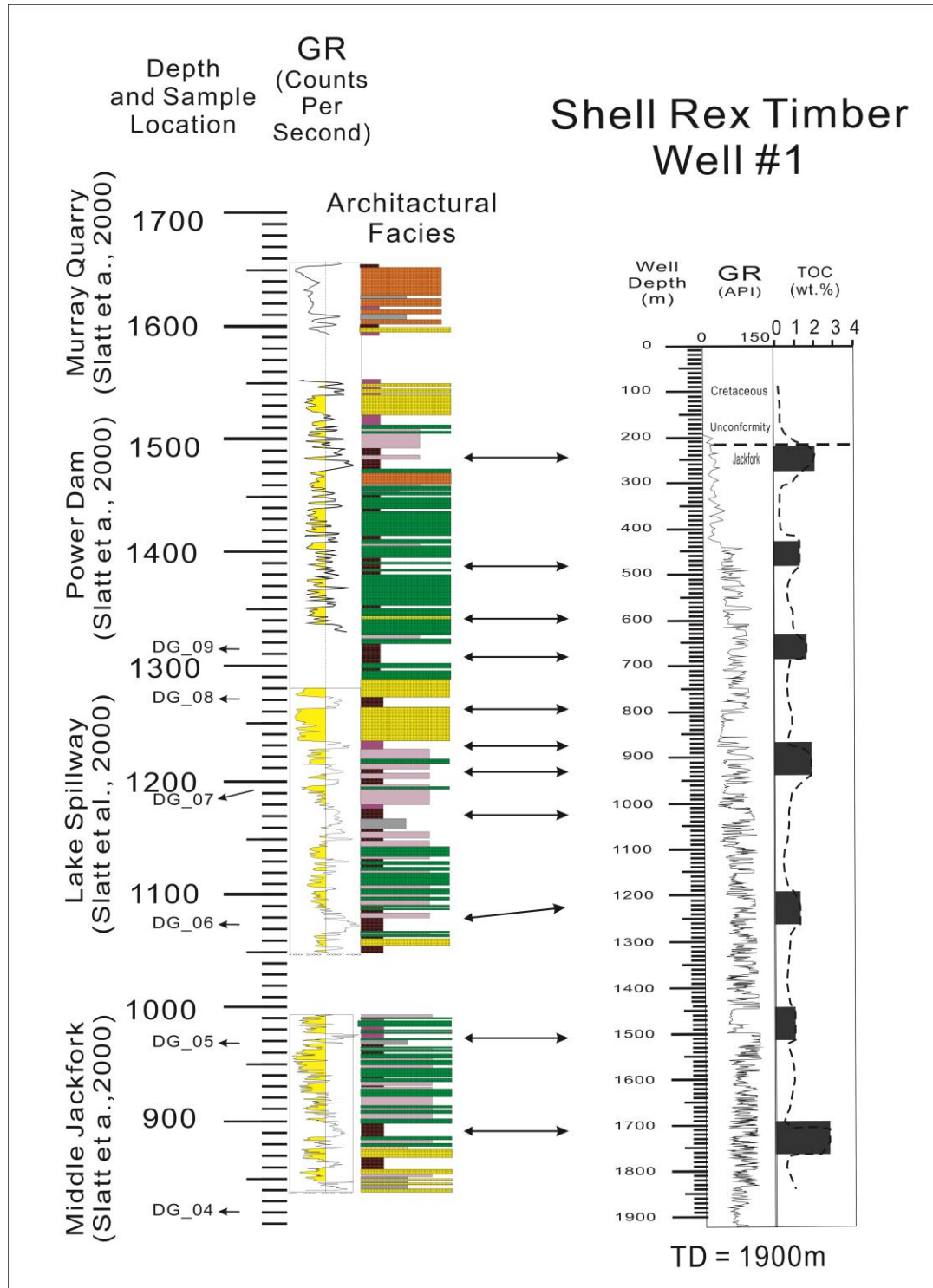


Figure 2.18-B. The measured sections in the DeGray Lake area, including Highway 7, DeGray Lake Spillway, Intake, Power Dam sections and Friendship roadcut (from Slatt *et al.*, 2000a). Locations of shale samples are marked as arrows.

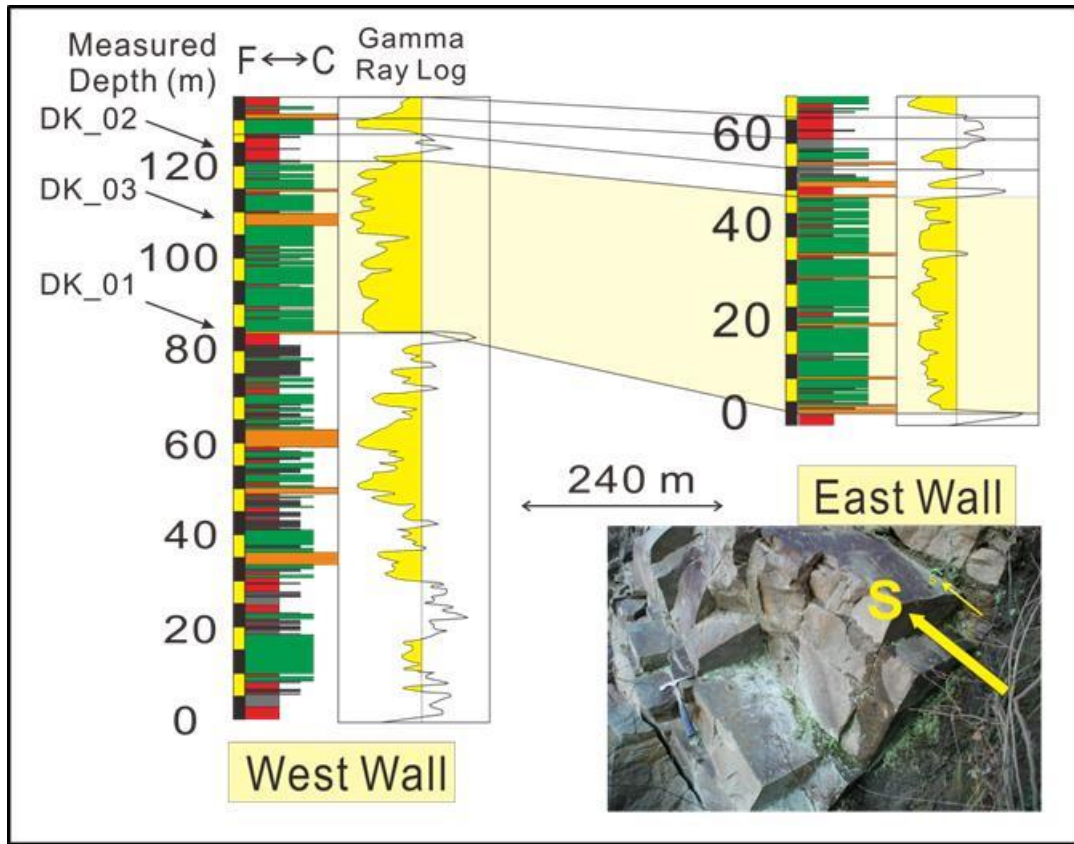


Figure 2.19.An overview of Jackfork Group outcrops in the Dierks Spillway area, including west and east walls. Most of the sandstone packages are flat-based, indicating a middle-distal basin-floor fan environment (lower right photo).

Element and Proxy	Interpretation
P ₂ O ₅	Biogenic apatite related to surface productivity
V Enrichment Factor (EFV) = (V _{Sample} /Al ₂ O ₃ _{Sample})/(V _{SMS} /Al ₂ O ₃ _{SMS})	Oxygenation of bottom waters (>=1 is anoxic, <1 is oxic)
U	Organic carbon content (TOC)
Th/U	Amount of clastic input versus organic input
TiO ₂ /Nb	Composition of clastic material entering the basin
Cr/Th	Changes in oxygenation of bottom waters versus clastic material entering the basin
Th	Amount of clastic input
Trace elements (e.g. Mn, Cu, Ni, Co and Pb)	Significantly enriched in deep sea sediments compared with nearshore shales
Terr. In = TiO ₂ + Al ₂ O ₃ + K ₂ O + Na ₂ O	Terrestrial input
SiO ₂ /Zr	Organic Matter Abundance
Fe ₂ O ₃	Suboxic paleo-environment
U, V, Cr	Anoxic paleo-environment
Mo, Ni	Euxinic paleo-environment
Zr, Zr/Al, Zr/Cr	Grain Size and Heavy Mineral

Table 2.6. Summary of key chemostrata elements and proxies.

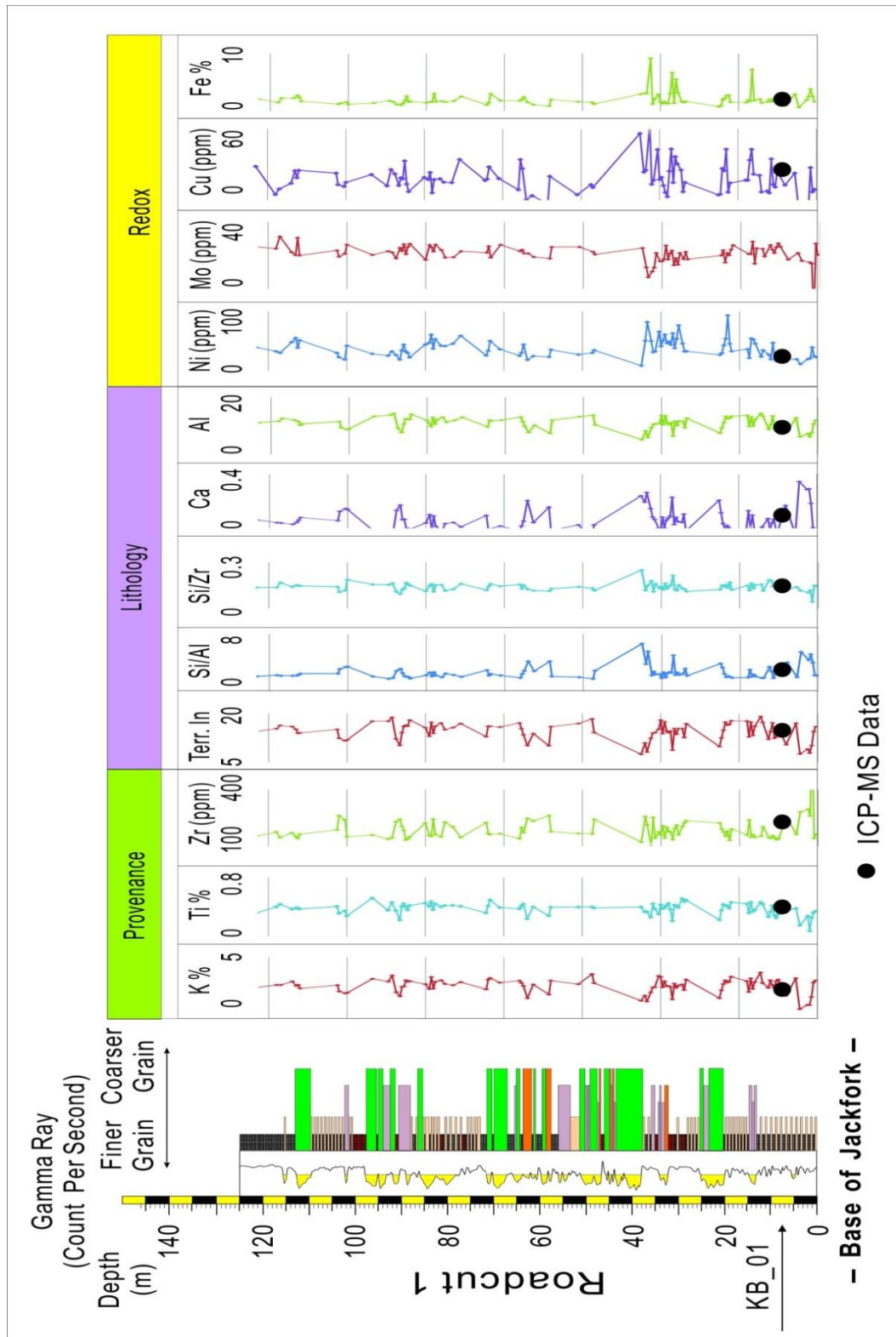


Figure 2.20. Preliminary test results of HHXRF on Roadcut 1, Kirby Section, including trace elements of Ni, Mo, Zr and Ti shown in ppm (parts per million).

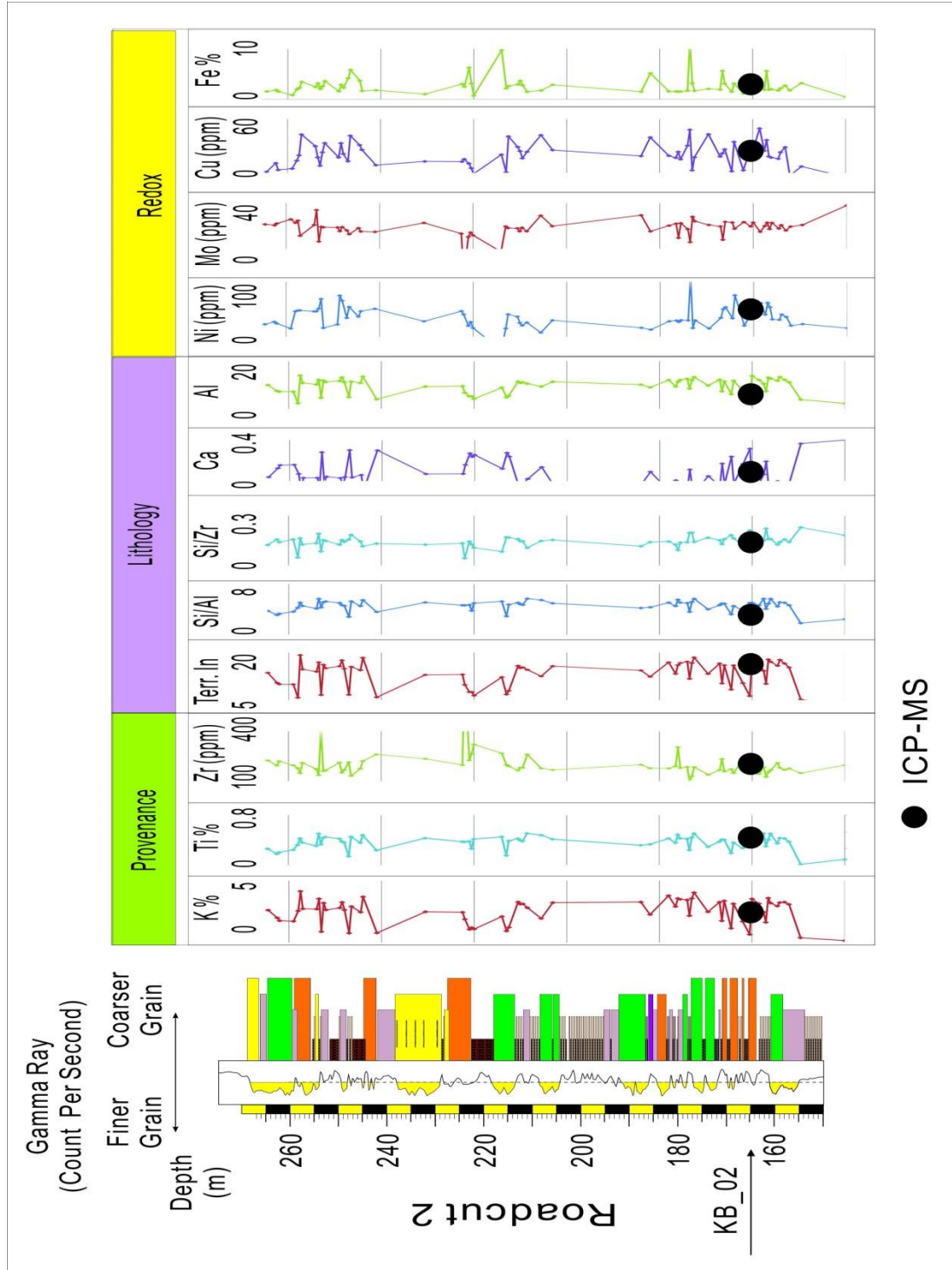


Figure 2.21. Preliminary test results of HHXRF on Roadcut 2, Kirby Section, including trace elements of Ni, Mo, Zr and Ti shown in ppm (parts per million).

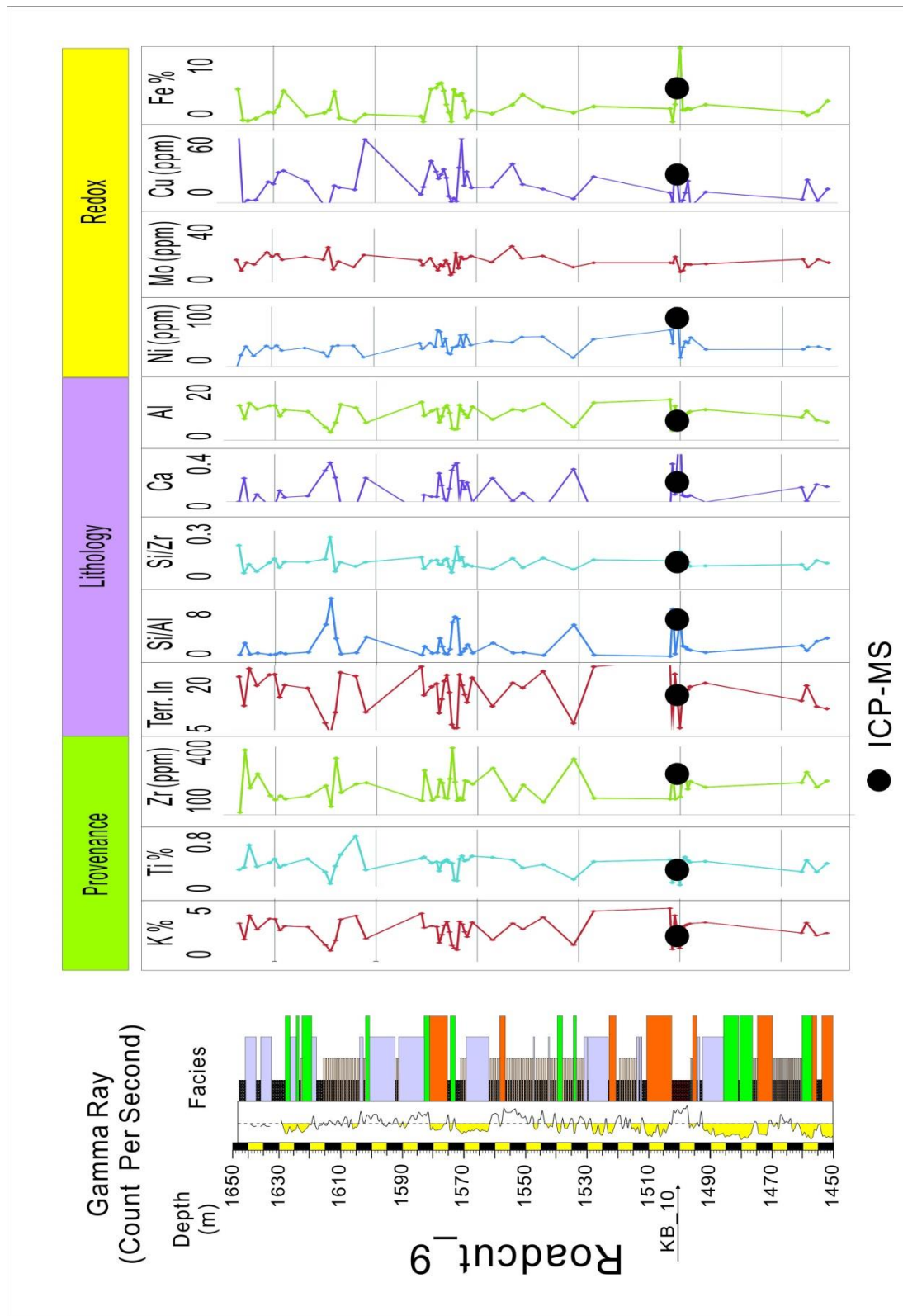


Figure 2.22. Preliminary test results of HHXRF on Roadcut 9, Kirby Section, including trace elements of Ni, Mo, Zr and Ti shown in ppm (parts per million).

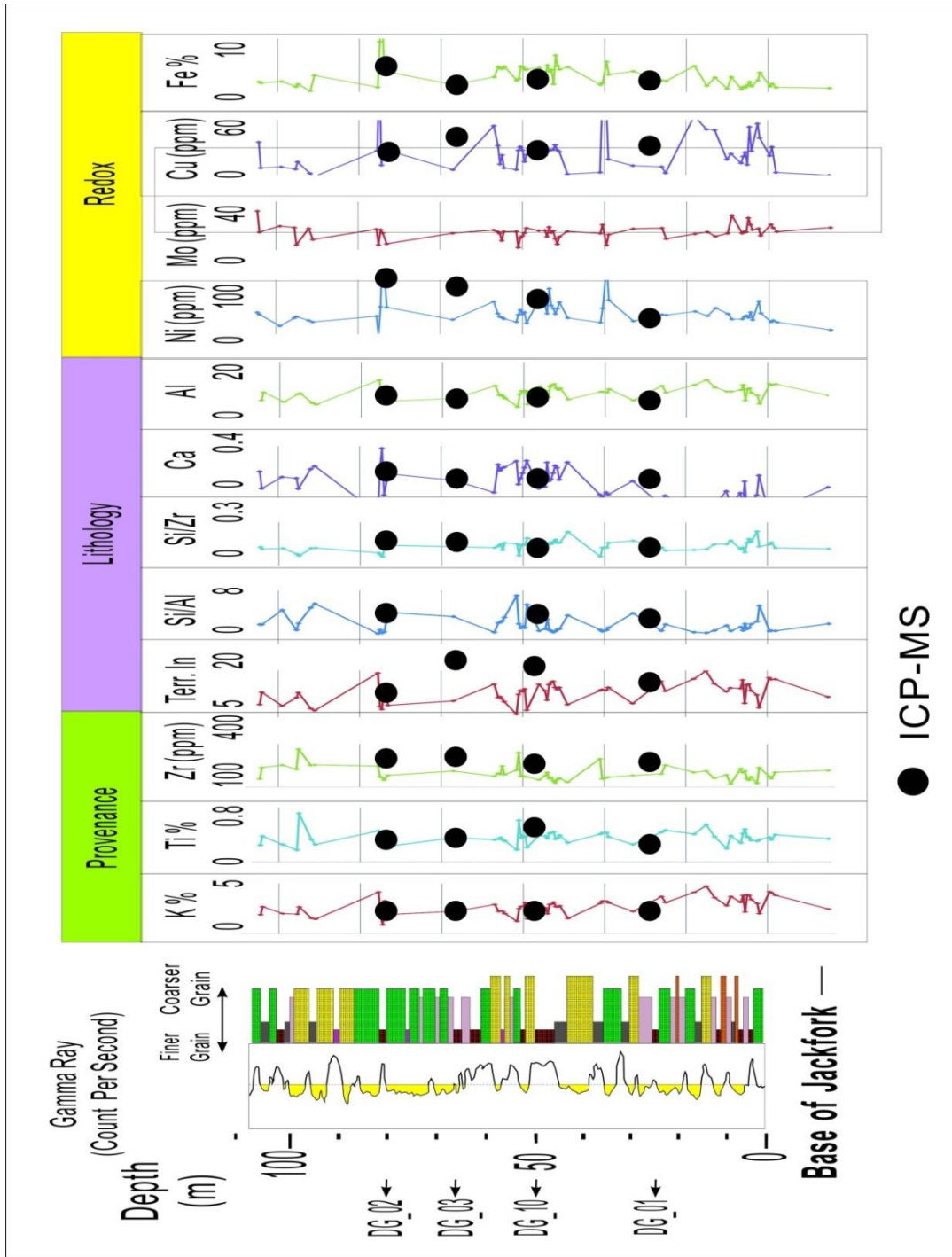


Figure 2.23. Preliminary test results of HHXRF on Highway 7, DeGray Lake Area Section, including trace elements of Ni, Mo, Zr and Ti shown in ppm (parts per million).

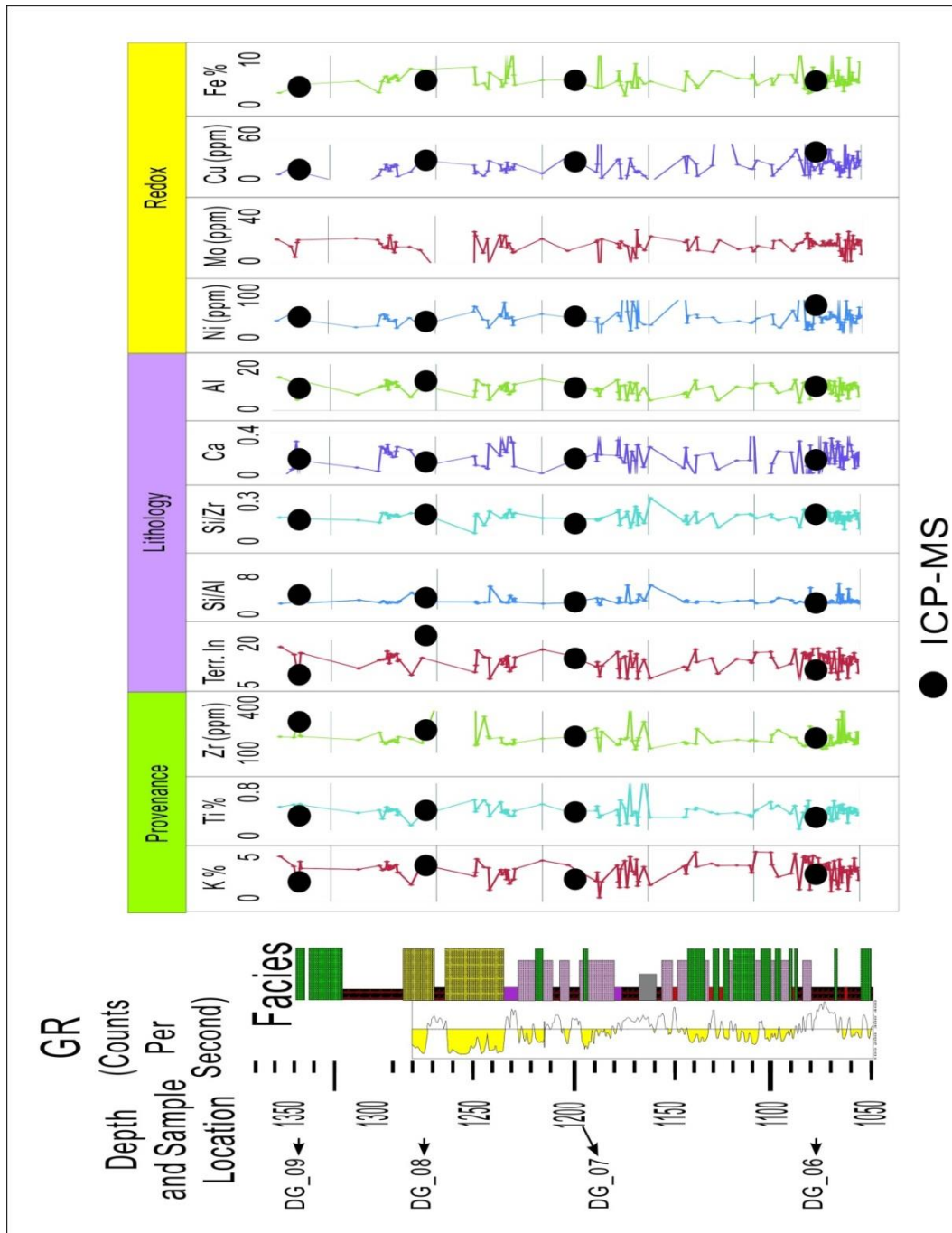


Figure 2.24. Preliminary test results of HHXRF DeGray Lake Spillway Section, including trace elements of Ni, Mo, Zr and Ti shown in ppm (parts per million).

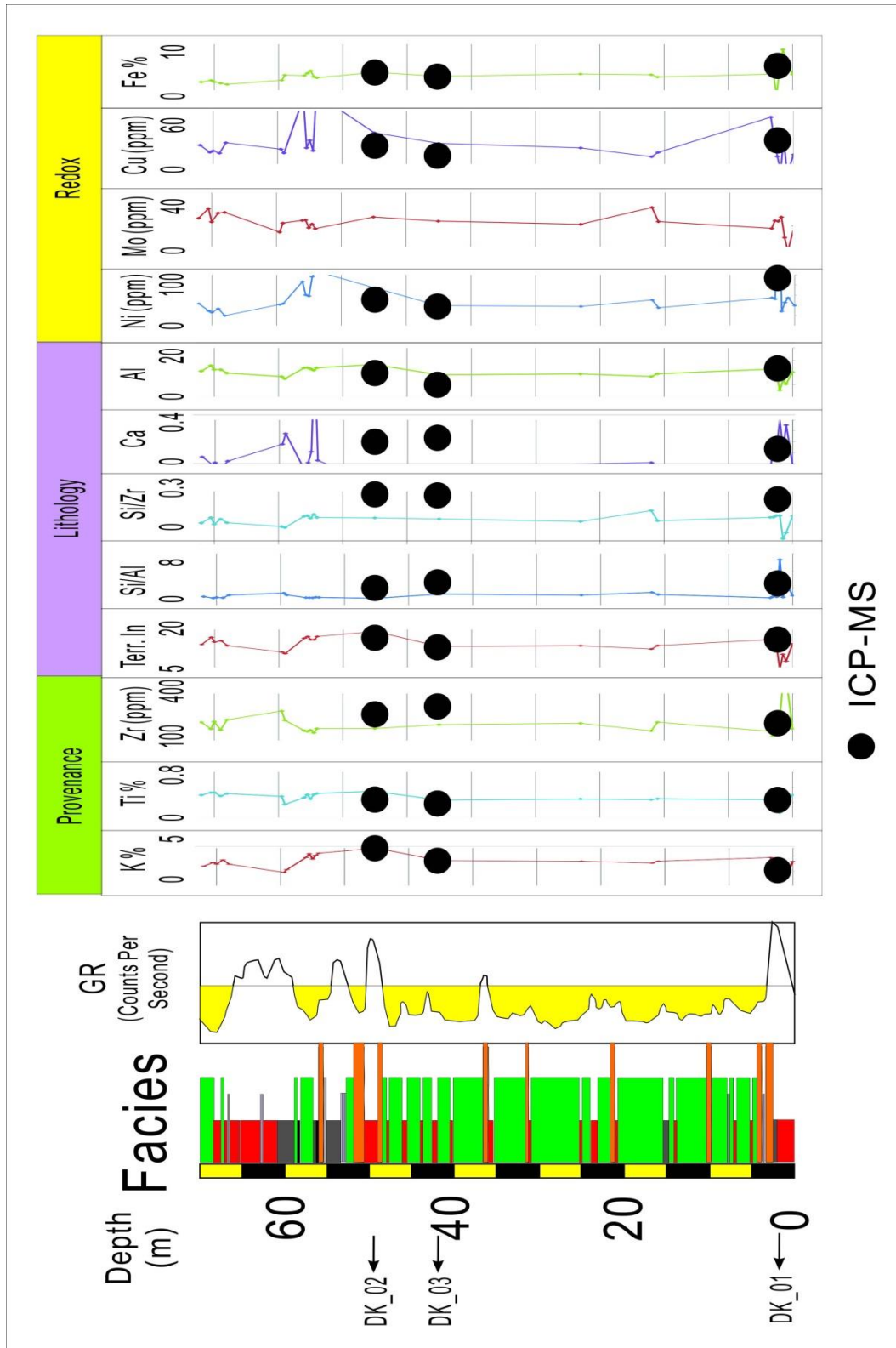


Figure 2.25. Preliminary test results of HHXRF Dierks Lake Spillway East Wall Section, including trace elements of Ni, Mo, Zr and Ti shown in ppm (parts per million).

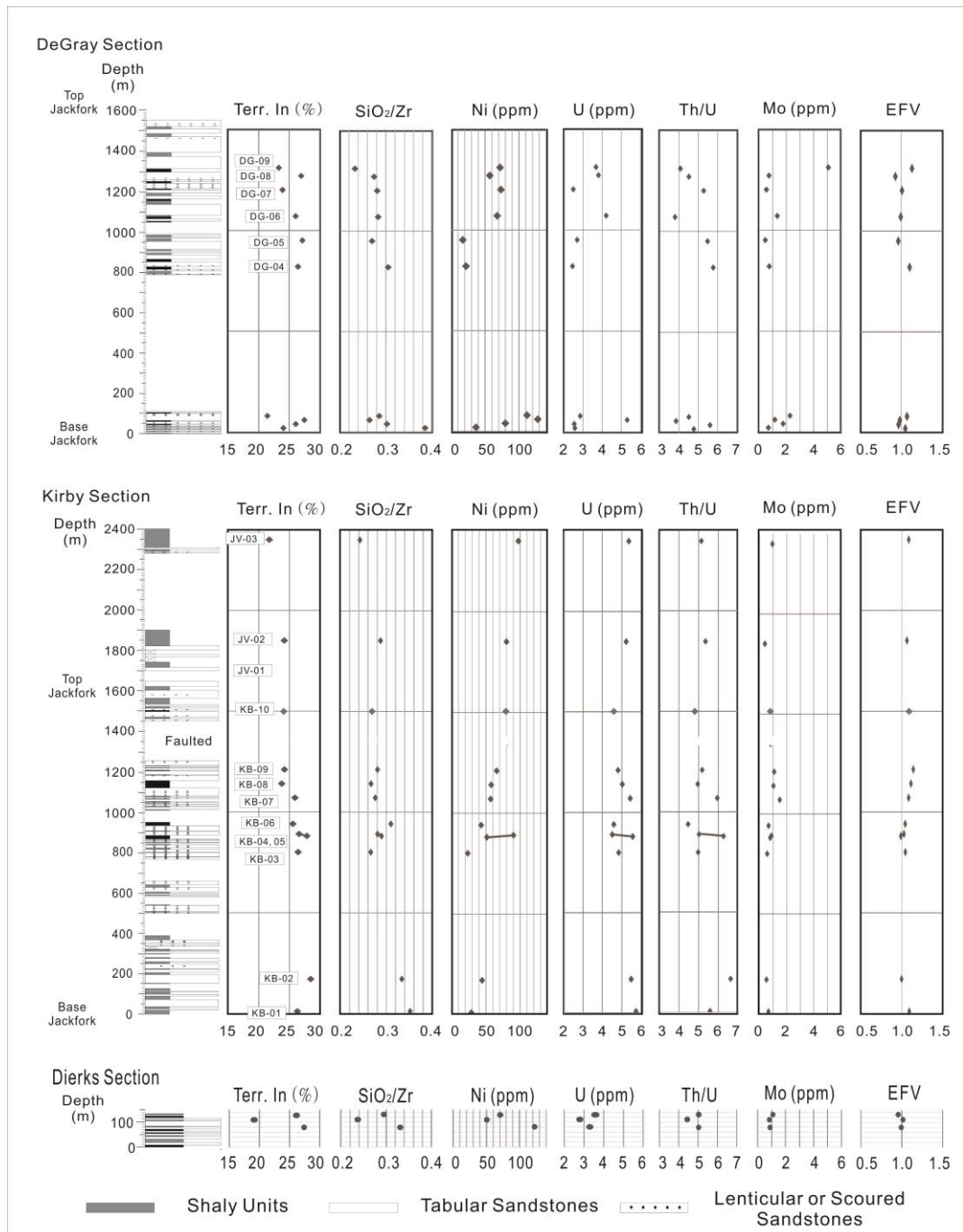


Figure 2.26. Plot of chemostrat data in the Lower, Middle and Upper Jackfork and Johns Valley Shale in the Kirby, DeGray and Dierks Sections with ICP-MS data.

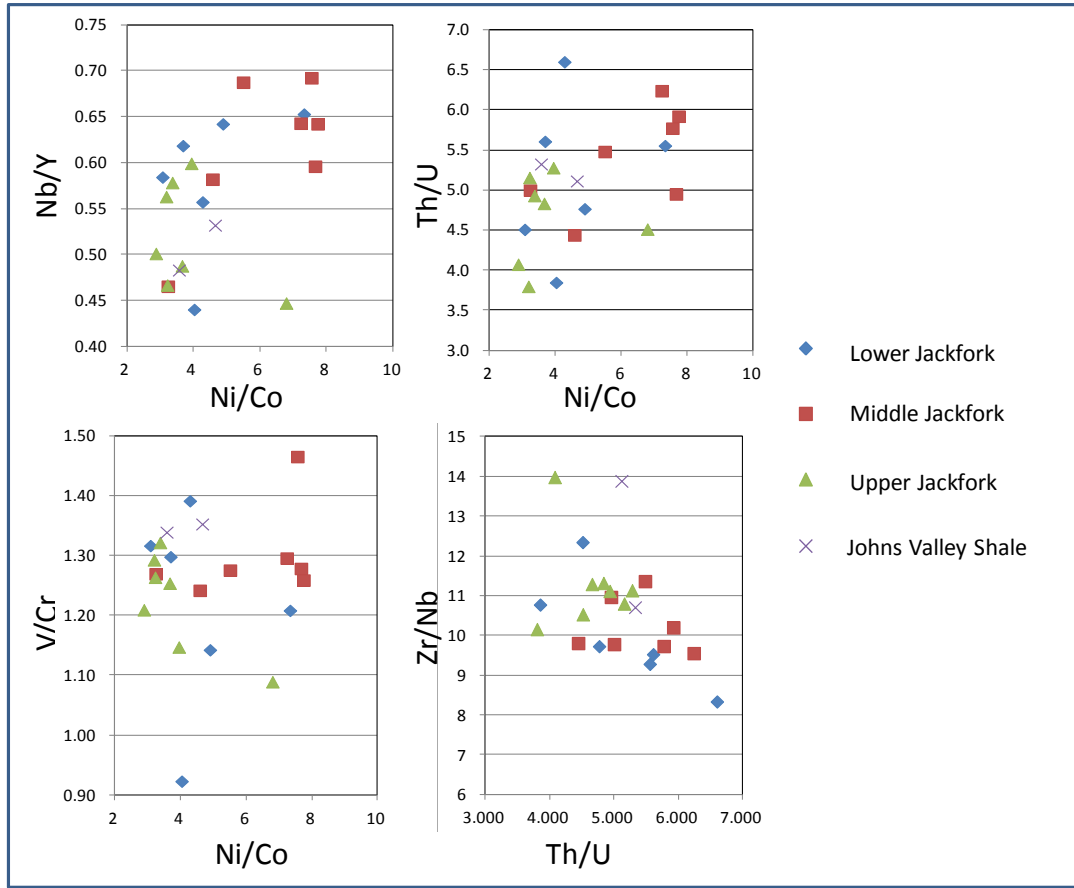


Figure 2.27. Key trace element ratios that show a distinct data cloud for the Middle Jackfork Group using ICP-MS data.

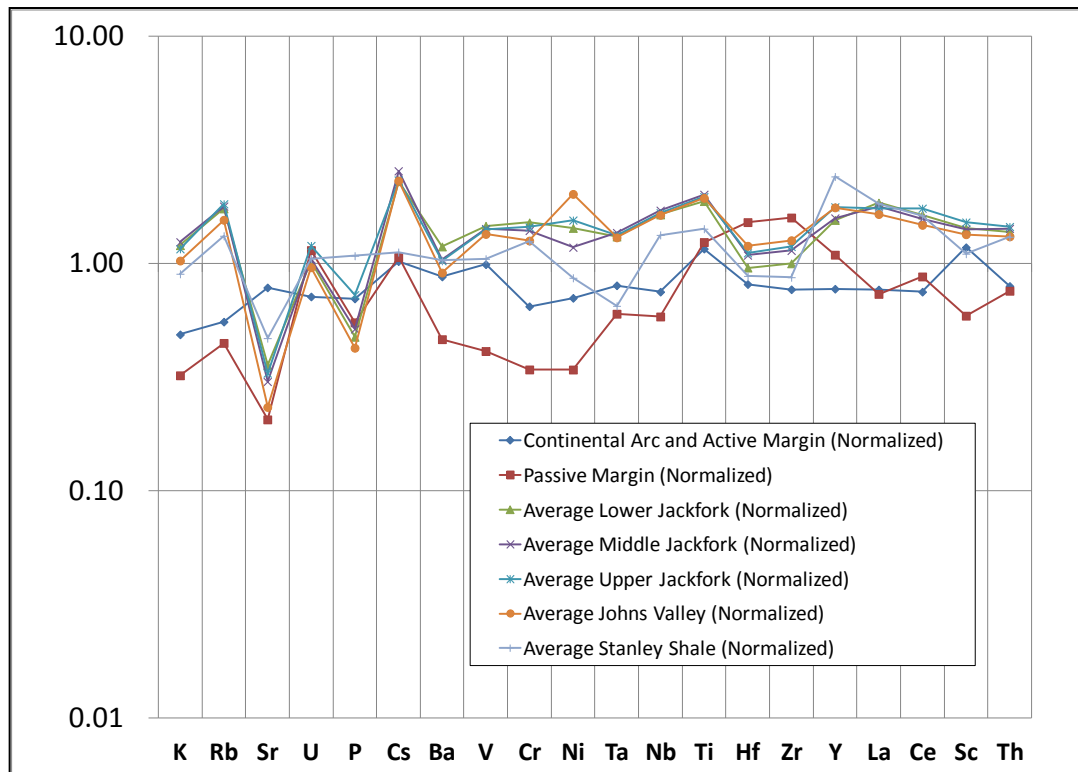


Figure 2.28. Trace Elements plot of the Stanley Shale (Totten *et al.*, 2000), Lower, Middle and Upper Jackfork Group, Johns Valley Shale (from this study) and averaged passive margin and active margins (Floyd, 1991).

Correlation Number and Confidence	Correlation Depth and Sample No.	Chemostrat Analysis	Lithology and Facies Analysis	Sequence Stratigraphy Interpretation
Correlation 7 (High)	KB-09 at 1213m (Kirby) and DG-07 at 1195m (DeGray)	Almost Same: Terr. In (1.4% difference) SiO ₂ /Zr (0.1% difference) Th/U(2.2% difference)	DeGray: 5m thick shale packages separated by one finely bedded tabular sandstones, large and thick lenticular sandstones above;	This top of this shale layer is a minor 3rd sequence boundary, and is the Maximum Flooding Surface (MFS). Below this shale layer is the massive sheet sandstones (LST associated with this TST). Above this shale is the massive amalgamated channelized sandstones, which is a another LST of the younger sequence. It potentially correlates to 316.7Ma in Haq's global sea-level curve.
		Slightly difference: Ni(10.3% difference) V(7.6% difference)	Kirby: 5m thick shale between tabular sandstones, large and thick lenticular sandstones above with debris flow deposits	
		Largely difference: U(21.3% difference) Mo(50% difference)		
Correlation 6 (High)	KB-08 at 1140m (Kirby) and DG-06 at 1070m (DeGray)	Almost Same: V(3.8% difference) SiO ₂ /Zr (5.6% difference) Terr. In (8.6% difference)	DeGray: 30m thick black laminated shale at the base of DeGray Spillway section, correlated well with the high TOC zones in Shell Rex Timber #1 well 10km to the south	This shale layer is a major 3rd order TST, and the top of the shale is the MFS, which separate the Upper and Middle Jackfork Group Below this shale layer is the massive and amalgamated channelized sandstones in Middle Jackfork Group. And it is overlain by sheet prone sandstones above. It potentially correlates to 317.5Ma in Haq's global sea-level curve.
		Slightly difference: Th/U(10% difference) Ni(15.1% difference)	Kirby: 30m thick black laminated shale in Baumgartner Quarry, separating Upper and Middle Jackfork	
		Largely difference: U(29.7% difference) Mo(23.1% difference)		
Correlation 4 (High)	KB-04 at 880m (Kirby) and DG-04 at 820m (DeGray)	Almost Same: V(5.8% difference) SiO ₂ /Zr (7.9% difference) Terr. In (7.8% difference)	DeGray: 15m thick shale package between two unconfined channel complex	This shale layer is a minor 3rd order TST in the Middle Jackfork Group. The top of the shale is the MFS. Below this layer is the thick and massive channelized sandstones in the Middle Jackfork. Above this layer is another sequence of friable channelized sandstones. It potentially correlates to 320.5Ma in Haq's global sea-level curve.
		Slightly difference: Th/U(13.3% difference) Mo(13.7% difference)	Kirby: 15m thick shale package between two unconfined channel complex	
		Largely difference: U(29.3% difference) Ni(43.9% difference)		
Correlation 1 and 9 (High)	Top and Base of Jackfork Group	Not Available	Well known top and base of Jackfork Group from Geological Map and regional correlation.	Top and Base of Jackfork Group are the boundaries between 2nd order TST (Stanley Group) to LST (Jackfork Group), and to TST (Johns Valley Group). The base and top of Jackfork Group correlate to ~323Ma and 316Ma in Haq's global sea-level curves respectively.
Correlation 2,3 and 5 (Low)	Internal correlations in Jackfork Group	Inconsistent	Correlation of shale layers using lithostratigraphic analysis. Either Data or outcrop exposures are limited.	Potential time intervals (MFS) or local shales generated by compensational stacking of lobes.
Correlation 10 and 11	Correlation from Haq's curve to Johns Valley Group	Not Available	Shale layers correspond to sea-level high and massive sandstone packages correspond to sea-level low. However, some sections are missing.	Potential 3rd order MFS above the sandstone packages.

Table 2.7. Categorization of the shale layers tested by ICP-MS, including 3rd and 4th order sequence boundary, local shale and their correlations.

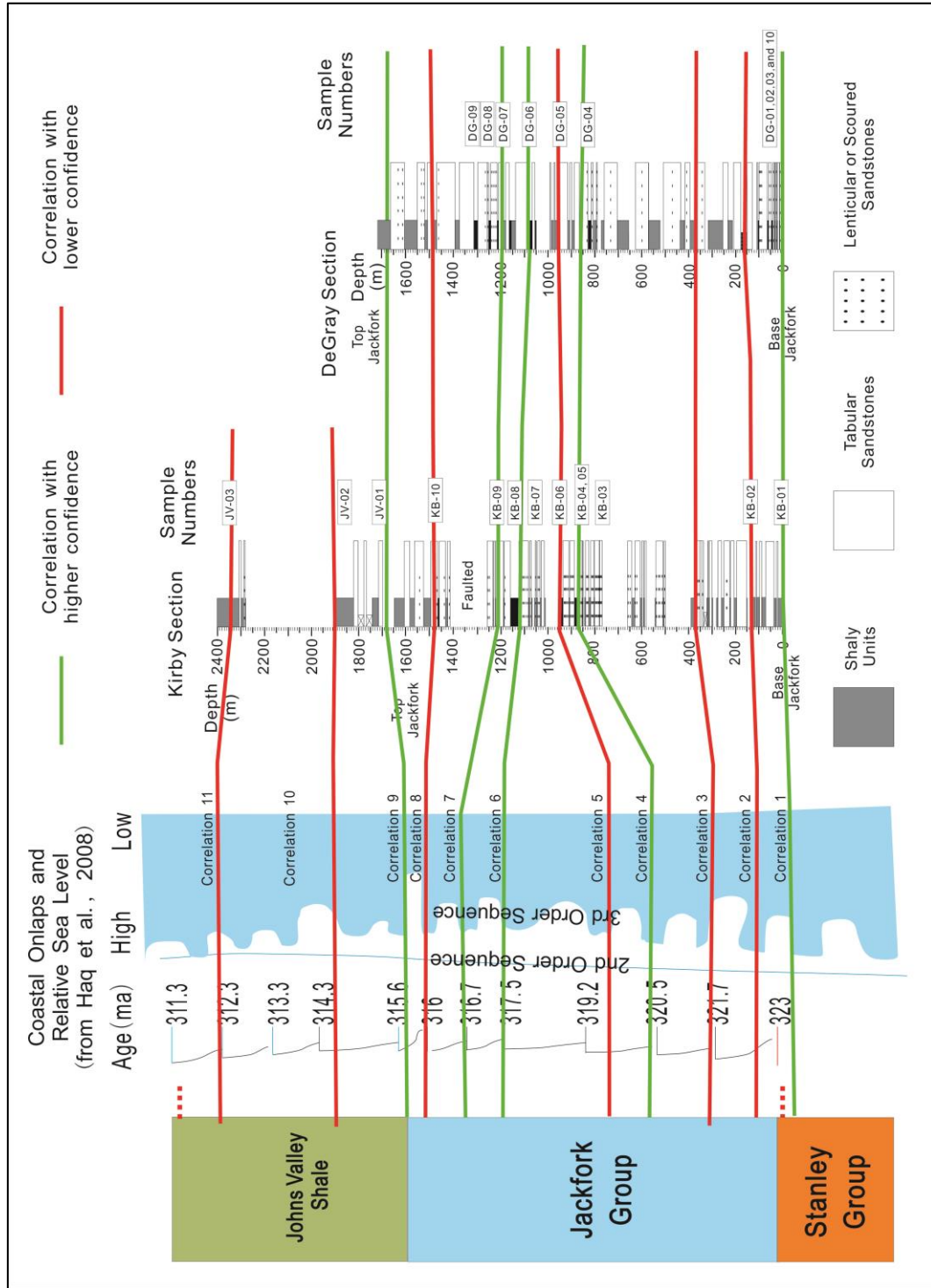


Figure 2.29. Chemostrata correlation between the Kirby and DeGray sections associated with Haq's (Haq and Shutter, 2008) global sea level curve.

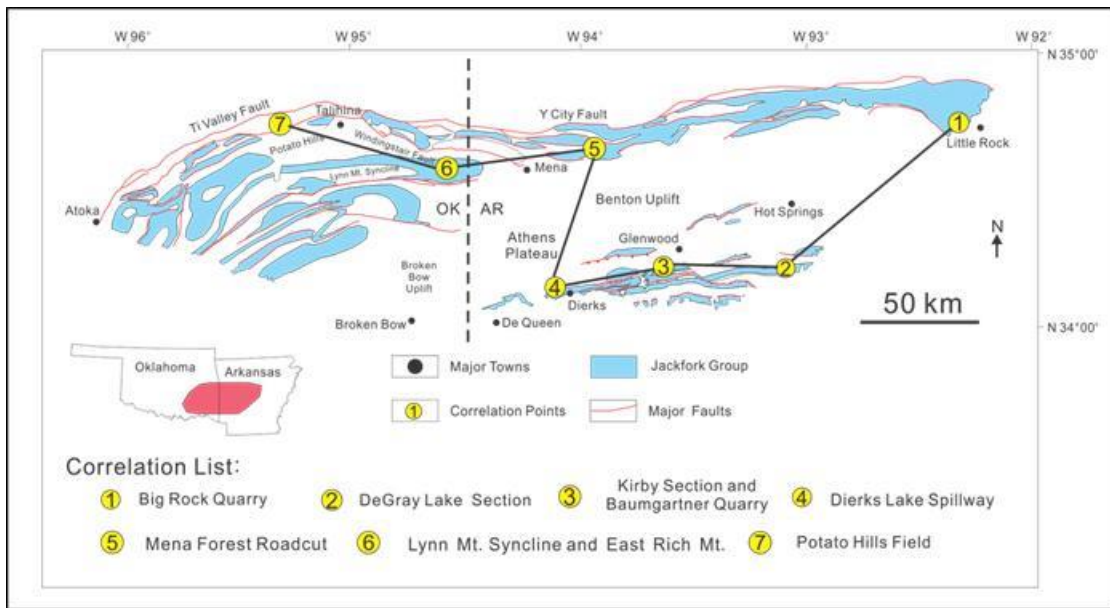


Figure 2.30. Locations of sequence stratigraphic framework of the Jackfork Group, integrating all available data.

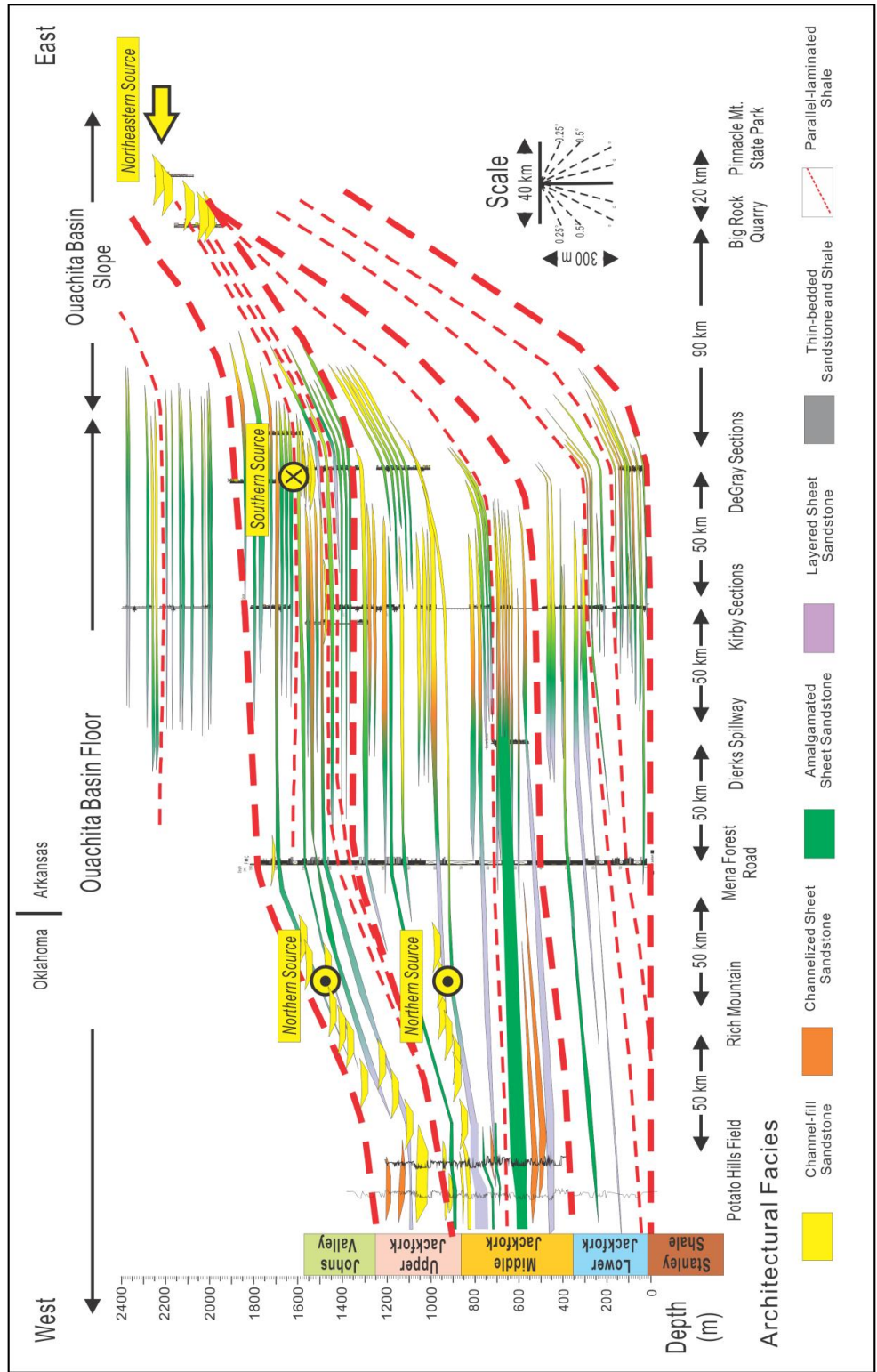


Figure 2.31. Sequence stratigraphic framework of the Jackfork Group, integrating all available data.

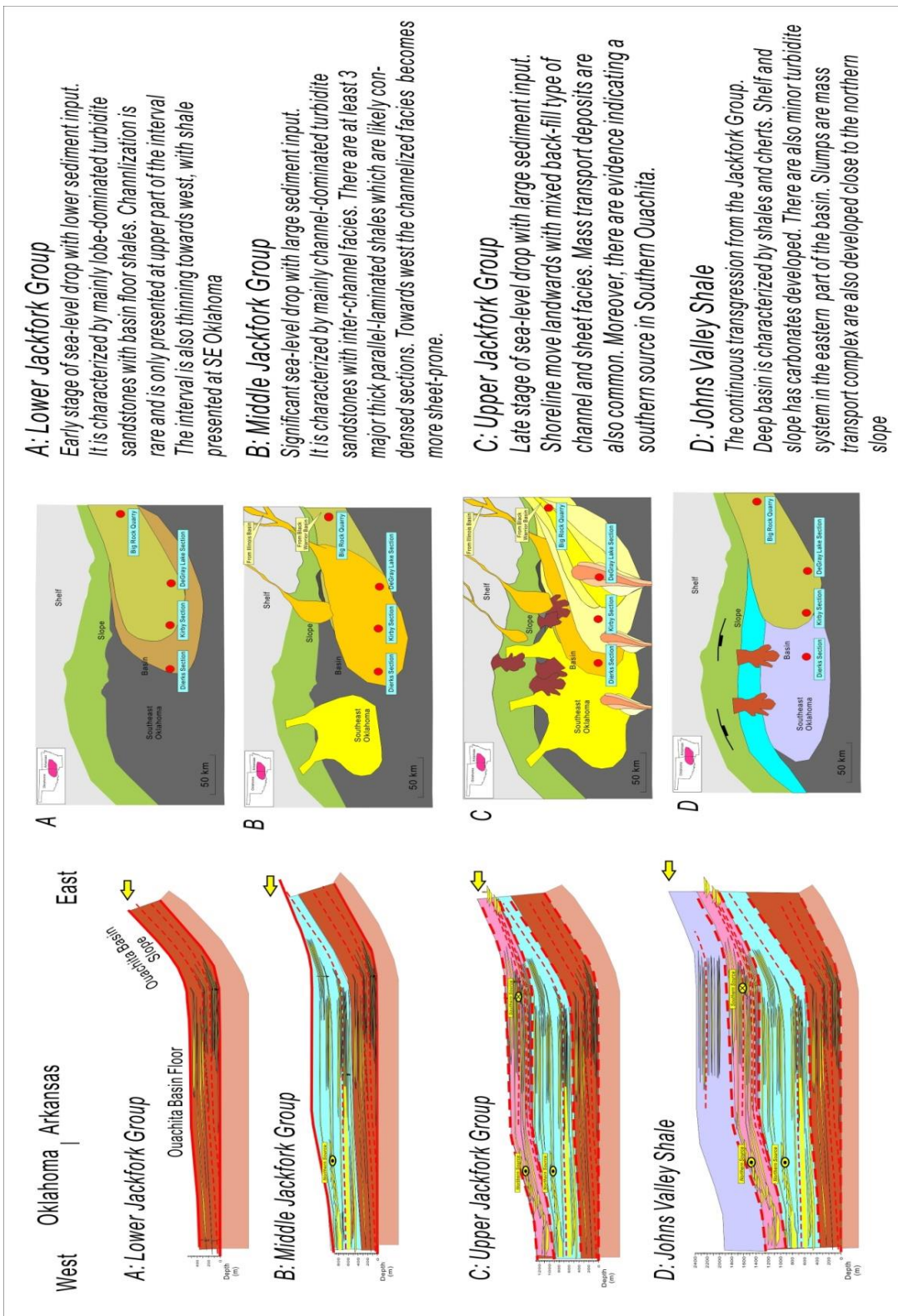


Figure 2.32. Evolution of Ouachita Basin from Jackfork Group to Johns Valley Shale integrating all available data

REFERENCES

- Al-Siyabi, H. A., 2000, Anatomy of a type II turbidite depositional system: Upper Jackfork Group, DeGray Lake area, Arkansas, in A. H. Bouma and C. G. Stone, eds., Fine-grained turbidite systems, AAPG Memoir 72/SEPM Special Publication 68, p. 245–262.
- Berman, A.E and J.H. Rosenfeld, 2007, A new depositional model for the deepwater Willcox-equivalent Whopper sand - changing the paradigm, World Oil, Vol. 228, No.6.
- Bhatia, M.R., 1983, Plate tectonics and geochemical composition of sandstones, the Journal of Geology, vol.91, no.6, pp. 611-627
- Bhatia, M.R., 1985, Rare earth element geochemistry of Australian Paleozoic graywackes and mudocks: provenance and tectonic control, Sedimentary Geology, vol.45, pp.97-113.
- Coleman, J.L., G.V. Swearomgem. and C.E. Breckon, 1994, The Jackfork formation of Arkansas, a test of the Walker- Mutti -Vail models for deep-sea fan deposition, Arkansas Geological Commission, pp.1-65.
- Coleman, J.L., 2000, Carboniferous submarine basin development of the Ouachita Mountains of Arkansas and Oklahoma (in Fine-grained turbidite systems) AAPG Memoir 72, pp.21-32
- Danielson, S.E., P.K. Hankinson, K.D. Kitchings, and A. Thompson, 1988, Provenance of the Jackfork Sandstone, Ouachita Mountains, Arkansas and eastern Oklahoma, in J. D. McFarland, ed. Arkansas Geol. Comm., Contributions to the Geology of Arkansas Misc. Publs. V. 3, No. 18-C, p. 95-112.
- DeVries, M.B., 1992, Correlation trends in thinner-bedded turbidites, Chatsworth Formation, Simi Hills, California and Jackfork Group, DeGray Lake, Arkansas Louisiana State University, Baton Rouge, LA, Master's thesis
- Duran W. J., 2007, Outcrop-based Geologic Model of the Jackfork Group at Baumgartner Quarry, Kirby, Arkansas, USA, Master Thesis, the University of Oklahoma.

- Floyd, P.A., 1991, Rhenohercynian sandstone chemistry, in Morton, A.C., Todd, S.P., and Haughton, P.D.W., eds., *Developments in sedimentary provenance studies: Geological Society Special Publication 57*, pp. 173-188.
- Funk, J.E., R.M. Slatt, and D.R. Pyles, 2012, Quantification of static connectivity between deep-water channels and stratigraphically adjacent architectural elements using outcrop analogs, *AAPG Bulletin*, v. 96, p. 277-300, oi:10.1306/07121110186
- Godo, T., P. Li and M. Ed Ratchford, 2008, Structural and Stratigraphic Analysis of the Shell Rex Timber No. 1-9 Well, Southern Ouachita Fold and Thrust Belt, Clark County, Arkansas, Information Circular 39A, Arkansas Geological Survey, December 2008
- Goyeneche, J. C., R.M. Slatt, A.C. Rothfolk, and R.J. Davis, 2006, Systematic geological and geophysical characterization of a deepwater outcrop for “Reservoir” Simulation: Hollywood Quarry, Arkansas, in Slatt, R.M., N.C. Rosen, M. Bowman, J. Castagna, T. Good, R. Loucks, R. Latimer, M. Scheihing, and R. Smith (eds.), *Reservoir Characterization: Integrating Technology and business practices: 26th Annual GCSSEPM Foundation Bob F. Perkins Research Conf.*, Dec. 3-6, Houston, p. 685-728.
- Graham, S.A., W. R. Dickinson and R. V. Ingersoll, 1975, Himalayan-Bengal Model for Flysch Dispersal in the Appalachian-Ouachita System, *GSA Bulletin*, March; v. 86; no. 3; p. 273-286
- Graham, S. A., R. V. Ingersoll, and W. R. Dickinson, 1976, Common provenance for lithic grains in Carboniferous sandstones from Ouachita Mountains and Black Warrior Basin: *Journal of Sedimentary Research*, v. 46, p. 620-632.
- Haq, B. U. and Shutter, S. R., 2008. A chronology of Paleozoic sea-level changes, *Science*, Vol. 322, October 2008, p. 64-68.
- Hatcher, R.D., W. A. Thomas and G. W. Viele, 1989, The Appalachian-Ouachita Orogen in the United States, *Geol. Soc. Am.*, Boulder, CO, United States, pp. 700-800.

- Jordan, D. W., D. R. Lowe, R. M. Slatt, C. G. Stone, A. D'Agostino, M. H. Scheihing, and R. H. Gillespie, 1991, Scales of geological heterogeneity of Pennsylvanian Jackfork Group, Ouachita Mountains, Arkansas: applications to field development and exploration for deep-water sandstones: Dallas Geological Society Field Trip
- Lowe, D.R., 1989, Stratigraphy, sedimentology, and depositional setting of pre-orogenic rocks of the Ouachita Mountains, Arkansas and Oklahoma (in *The Appalachian-Ouachita Orogen in the United States* Hatcher, Thomas, Viele, Robert D., William A., v. F-2, George W., Geol. Soc. Am., Boulder, CO, United States, pp. 575-590
- Lowe, D. R., M. Guy, A. Palfrey, 2003, Facies of slurry-flow deposits, Britannia Formation (Lower Cretaceous), North Sea: implications for flow evolution and deposit geometry, *Sedimentology*, Volume 50, Issue 1, pages 45–80.
- Mattis, A.F., 2008, Geological challenges in reservoir modeling, Tahiti Field, Green Canyon 596/640, Gulf of Mexico, 28th Annual GCSSEPM Bob Perkins Research Conference Publication.
- Meng, W., J. Li, and S. Liu, 2007, Minor element geochemistry of Triassic mudstone in the Zoige massif and its tectonic setting, *Acta Geologica Sichuan*, Vol. 27, No.1, pp. 2-6.
- Miller, M.E., 1985, The use of cathodoluminescence colors for interpreting the provenance of the Jackfork Sandstones, Arkansas, Univ. Cincinnati, unpubl. M.S. thesis, 145p.
- Montgomery, S.L., 1996, Jackfork Group, southern Oklahoma: New gas play in the Ouachita overthrust, *AAPG Bulletin*, Vol. 80, No. 11.
- Morris, R.C., 1971, Stratigraphy and sedimentology of Jackfork group, Arkansas, *The American Association of Petroleum Geologists Bulletin*, vol.55, no.3, pp.387-402.
- Morris, R. C., 1977, Petrography of Stanley-Jackfork sandstones, Ouachita Mountains, Arkansas, in C. G. Stone, ed., *Symposium on the geology of the Ouachita Mountains*: Little Rock, Arkansas Geological Commission, p. 146-157.

- Morris, R.C., 1989, Stratigraphy and sedimentary history of post-Arkansas Novaculite Carboniferous rocks of the Ouachita Mountains (in *The Appalachian-Ouachita Orogen in the United States* Hatcher, Thomas, Viele, Robert D., William A., George W., F-2, Geol. Soc. Am., Boulder, CO, United States, pp. 591-602
- Mutti, E. and W.R. Normark, 1991, An integrated approach to the study of turbidite systems (in Weimer, P., H. Martin and A.H. Bouma eds. , *Seismic facies and sedimentary processes of submarine fans and turbidite systems*, New York, NY, United States, pp. 75-106
- Olariu M. I., J. F. Ferguson, C. L.V. Aiken, and X. Xu, 2008, Outcrop fracture characterization using terrestrial laser scanners: Deep-water Jackfork sandstone at Big Rock Quarry, Arkansas, *Geosphere*, vol. 4, no. 1, pp.247-259
- Olariu M. I., C. L. V. Aiken, J. P. Bhattacharya, and X. Xu, 2011, Interpretation of channelized architecture using three-dimensional photo real models, Pennsylvanian deep-water deposits at Big Rock Quarry, Arkansas, *Marine and Petroleum Geology*, v. 28, p. 1157-1170.
- Omatsola, B., 2003, Origin and distribution of friable and cemented sandstones in outcrops of the Pennsylvanian Jackfork Group, southeast Oklahoma: Master's thesis, University of Oklahoma, Norman, 227p.
- Owen, M. R., and A. V. Carozzi, 1986, Southern provenance of upper Jackfork Sandstone, southern Ouachita Mountains: cathodoluminescence petrology: *Geological Society of America Bulletin*, v. 97, p. 110-115.
- Pack, L.B., 2010, Facies control on production in the Jackfork Group, Latimer and Pushmataha Counties, Oklahoma, unpubl. M.S. thesis, Univ. Oklahoma, 126p.
- Pauli, D., 1994, Friable submarine channel sandstones in the Jackfork Group, Lynn Mountain Syncline, Pushmataha and Le Flore Counties, Oklahoma (in *Geology and resources of the eastern Ouachita Mountains frontal belt and southeastern Arkoma Basin, Oklahoma; Part II, Contributed papers*) *Guidebook - Oklahoma Geological Survey*, pp. 179-202

- Proctor, K. E., 1974, The petrography and gas-reservoir potential of Stanley-Jackfork sandstones, Ouachita Mountains, Arkansas and Oklahoma: Master's thesis, Northern Illinois University, De Kalb, 302 p.
- Pyles D. R., 2008, Multiscale stratigraphic analysis of a structurally confined submarine fan: Carboniferous Ross Sandstone, Ireland, AAPG Bulletin, vol. 92, no. 5, pp.557-587.
- Pyles, D.R., J.P.M. Syvitski and R. M. Slatt, 2011, Defining the concept of stratigraphic grade and applying it to stratal (reservoir) architecture and evolution of the slope-to-basin profile: An outcrop perspective, Marine and Petroleum Geology, Vol. 28, No.3, pp. 675–697
- Ratcliffe, K. T., A.M. Wright and K. Schmidt, 2012, Application of inorganic whole-rock geochemistry, to shale resource plays: an example from the, Eagle Ford Shale Formation, Texas, the Sedimentary Record, Vol. 10, No.2, pp. 4-10.
- Roberts, M. T., 1994, Geologic relations along a regional cross section from Spavinaw to Broken Bow, eastern Oklahoma, in N. H. Suneson and L. A. Hemish, eds., Geology and resources of the eastern Ouachita Mountains frontal belt and southeastern Arkoma basin, Oklahoma: Oklahoma Geological Survey Guidebook 29, p. 137–159
- Romero, G.A., 2004, Identification of architectural elements of turbidite deposits, Jackfork Group, Potato Hills eastern Oklahoma, Master Thesis of the University of Oklahoma, pp.238p.
- Ross, C.A. and J.R.P. Ross, 1988, Late Paleozoic sea levels and depositional sequences: Cushman Found. for Foram. Res. Special Publication 24, p. 137-149.
- Schlichtemeier, B.D., 2011, Lidar Characterization of a Jackfork Group Basin Floor Fan Deposit and Implications to Analog Reservoir Modeling and Production, Master Thesis, the University of Oklahoma.

- Shanmugam, G. and R. J. Moiola, 1995, Reinterpretation of depositional processes in a classic flysch sequence (Pennsylvanian Jackfork Group), Ouachita Mountains, Arkansas and Oklahoma, AAPG Bulletin, May 1995; 79: 672 – 69
- Shaulis, B.J., T. J. Lapen, J. F. Casey, and D. R. Reid, 2012, Timing and Rates of Flysch Sedimentation In the Stanley Group, Ouachita Mountains, Oklahoma and Arkansas, U.S.A.: Constraints from U-Pb Zircon Ages of Subaqueous Ash-Flow Tuffs, Journal of Sedimentary Research, v. 82, p. 833-840, doi:10.2110/jsr.2012.68
- Shear, A.C., 2006, Stratigraphy and petrology of the Cretaceous-Pennsylvanian unconformity at DeGray Lake, Master Thesis, the University of Oklahoma, pp.1-100.
- Slatt, R. M., P. Weimer; C.G. Stone, 1997, Reinterpretation of depositional processes in a classic flysch sequence (Pennsylvanian Jackfork Group), Ouachita Mountains, Arkansas and Oklahoma; discussions and reply AAPG Bulletin, vol.81, no.3, pp.449-491,
- Slatt, R.M., C.G. Stone, and P. Weimer, 2000a, Characterization of slope and basin facies tracts, Jackfork Group, Arkansas, with applications to deepwater (turbidite) reservoir management, in Weimer, P., Slatt, R.M., Coleman, J. L. Jr. and., Bouma, A.H (eds.) Deep-water reservoirs of the world, Gulf Coast Sect. Soc. Econ. Paleon.& Mineral. Found. 20th Ann. B.F. Perkins Research Conference, p. 940-980.
- Slatt, R. M, H. A. Al-Siyabi, C. W. VanKirk, and R. W. Williams, 2000b, From geologic characterization to "reservoir simulation" of a turbidite outcrop, Arkansas, U.S.A. (in Fine-grained turbidite systems) AAPG Memoir, 72 187-194
- Slatt, R. M., 2000c, Why outcrop characterization of turbidite systems, in A. H. Bouma and C. G. Stone, eds., Fine-grained turbidite systems, AAPG Memoir 72 /SEPM Special Publication 68, p. 181–186.
- Sprague, A. R., P. E. Patterson, R.E. Hill, C.R. Jones, K. M. Champion, J.C. Van Wagoner, M. D. Sullivan, D.K. Larue, H.R. Feldman, T.M. Demko, R.W. Wellner, and J.K. Geslin, 2002, The Physical stratigraphy of Fluvial strata: A Hierarchical Approach to the

- Analysis of Genetically Related Stratigraphic Elements for Improved Reservoir Prediction, Abstract of AAPG Annual Meeting, Houston, Texas.
- Steel, R.J., C. Olariu, and M. Olariu, 2012, Basin-floor fan architecture: signals of sea level behavior, Abstract in 2012 GSA Annual Meeting in Charlotte.
- Stone, C., 2012, Ireland Outcrops Still Yield Deep Secrets, AAPG Explorer, March, 2012.
- Suneson, N., I. Cemen, D.R. Kerr, M.T. Roberts, R.M. Slatt, and C.G. Stone, 2008, Stratigraphic and structural evolution of the Ouachita Mountains and Arkoma Basin, southeastern Oklahoma and west-central Arkansas: applications to petroleum exploration: Oklahoma Geological Survey Guidebook 34, p.50-72
- Suneson, N. and R.M. Slatt, 2004, the Jackfork Sandstone: The Next Big Oklahoma Exploration Play, Shale Shaker, Vol. 55, No. 3., (November and December), Pages 71-79
- Sullivan, M. D., J. L. Foreman, D. C. Jennette, D. Stern, G. N. Jensen, and F. J. Goulding, 2004, An integrated approach to characterization and modeling of deep-water reservoirs, Diana field, western Gulf of Mexico, in Integration of outcrop and modern analogs in reservoir modeling: AAPG Memoir 80, p. 215– 234.
- Tillman, R.W., 2000, Sedimentology and sequence stratigraphy of Jackfork Group, U.S. Highway 259, Le Flore County, Oklahoma (in Marine clastics in the southern Midcontinent, 1997 symposium) Circular - Oklahoma Geological Survey (2000), pp.65-85
- Totten and Blatt, 1993, Alterations in the nonclay-mineral fraction of pelitic rocks across the diagenetic to low-grade metamorphic transition, Ouachita Mountains, Oklahoma and Arkansas, Journal of Sedimentary Petrology, v.63, pp. 899-908.
- Totten, M.W., M.A.Hanan, and B.L.Weaver, 2000. Beyond whole-rock geochemistry of shales: The importance of assessing mineralogical controls for revealing tectonic discriminants of

- Multiple sediment sources for the Ouachita Mountain flysch deposits. Geological Society of America Bulletin 112, 1012–1022.
- Taylor, S.R. and S.M. McLennan, 1985, The continental crust: its composition and evolution, Blackwell Scientific Publications, Oxford, pp.1-300.
- Vail, P.R., R.M. Mitchum, and S. Thompson, 1977. Seismic stratigraphy and global changes of sea level, part 4: global cycles of relative changes of sea level, AAPG Bulletin, v. 26, p.83–97.
- Viele, G.W., 1973, Structure and tectonic history of the Ouachita Mountains, Arkansas, in Delong, K., and Scholten, R., eds., Gravity and tectonics: John Wiley and Sons, New York, p. 361-377,
- Walthall, B. H., 1967, Stratigraphy and structure, part of Athens Plateau, southern Ouachitas, Arkansas, AAPG Bulletin, v. 51, p. 504-528
- Weislogel, A. L., S. A. Graham, and E. Z. Chang, 2007, Accumulation of the Middle to Upper Triassic Songpan-Ganzi turbidite Complex, China, in T. H. Nilsen, R. D. Shew, G. S. Steffens, and J. R. J. Studlick, eds., Atlas of deep-water outcrops: AAPG Studies in Geology 56, CD-ROM, 20 p.
- Zou F., 2010, An integrated approach to characterization and modeling of the Jackfork Group at the Baumgartner quarry area, western Arkansas and its implications to deepwater exploration and production, Master Thesis of University of Oklahoma.
- Zou F., R.M. Slatt, R. Bastidas and B. Ramirez, 2012, Integrated outcrop reservoir characterization, modeling, and simulation of the Jackfork Group at the Baumgartner Quarry area, western Arkansas: Implications to Gulf of Mexico deep-water exploration and production, AAPG Bulletin, v. 96, p. 1429-1448.

Chapter 3: Turbidite Petroleum Geology Updates in the Deepwater and Subsalt Gulf of Mexico*

Fuge Zou^{1,2} and Roger M. Slatt²

¹Marathon Oil Corporation, Oklahoma City 73132, USA

²ConocoPhillips School of Geology and Geophysics, University of Oklahoma, Norman
73019, USA

**Part of this chapter has been published in*

1) Journal of Earth Science and Engineering, Issue 9, 2014, ISSN 2159-581X;

*2) Textbook: "Stratigraphic Reservoir Characterization for Petroleum Geologists,
Geophysicists, and Engineers, 2nd Edition" by Dr. Roger M. Slatt published in 2013 by
Elsevier, ISBN: 978-0-444-56365-1*

ABSTRACT

The past six years (2008-2014) was a prosperous time for exploration and production in the dGOM (deepwater Gulf of Mexico). Recent exploration and production activities can be divided into three major categories: drilling new wildcat wells, appraising and developing newly discovered fields and enhanced oil recovery of mature fields. Seismic imaging, complex geology, high pressure drilling, greater depth, and higher temperature are key challenges for the exploration and production of dGOM reservoirs. Complex geology includes salt-related structures and traps, reservoir compartmentalization, and the sequence stratigraphy of turbidite reservoirs. Turbidite

sequence stratigraphy helps the asset team to find the best target intervals. Sheet and channelized sandstones with good downdip aquifer support are preferred reservoir conditions. All the drilling, development and production challenges are related to high pressure, greater depth, higher temperature and lack of existing field analogs. Various IOR (improved oil recovery) methods are studied and applied in the development stage of the Wilcox fields, which have an average primary recovery factor of 10%~15%. With ideal tabular reservoir geometry and IOR methods, recovery factor of the Wilcox reservoirs can reach up to 42% of OOIP (Original Oil in Place) through the field life cycle.

INTRODUCTION

The dGOM (deepwater Gulf of Mexico) basin is a large Cenozoic deepwater basin formed on a passive margin tectonic setting. The petroleum reservoirs cover a wide range of geologic ages including the Norphlet (Jurassic), Tuscaloosa (Cretaceous), Wilcox (Paleogene), Miocene, Pliocene and Pleistocene (Figure 3.1). The Jurassic Louann salt serves as a buoyant and ductile layer that can rise up to form various salt structures. These salt structures would then result in complicated features with relief which drive the generation, migration and seal of hydrocarbons.

It has been more than 10 years since the largest fields in dGOM, including Mars-Ursa, Thunder Horse, Tahiti, Mad Dog, and Cascade, were found. Currently, dGOM is thriving with increased drilling activities and production. The rig count has not only returned to where it was before the Macondo Tragedy in 2010, but also continues to grow with newly built rigs entering the region. The giant Middle-Lower

Miocene fields such as Tahiti, Mad Dog and Thunder Horse are entering or are about to enter their peak production. Younger Upper Miocene and Pliocene fields such as Auger, Conger and Mars-Ursa are being rejuvenated by secondary and enhanced oil recovery. Appraisal of deeper targets in existing fields is also common, adding tremendous upside potential, such as Cardamom Deep, Mad Dog Deep, and Mars-Ursa. Paleogene fields, such as Jack, Cascade and Chinook, are still in their early stages of development with recent start-up production (Figure 3.2).

This paper will first discuss the updates on the turbidite petroleum geology in dGOM, followed by the recent exploration, development and production activities.

SEDIMENT GRAVITY FLOWS (TURBIDITES)

Deepwater sediment gravity flows, often referred to as turbidity current deposits, are the dominant reservoir type over the entire dGOM. Characterizing the deepwater turbidites, including their origin, composition, 3-D geometry and depositional environments, is critical in the exploration and production of these reservoirs. Figure 3.3 illustrates a complete deepwater system from updip shelf, to slope then down to the basin floor (DeVay *et al.*, 2000). To date, almost all “shelf edge”, “upper slope” and “mid to upper slope” turbidite reservoirs have been discovered and produced within ~150 miles (240 km) of the shoreline. Our focus here on the dGOM is the “mid to lower slope” and “lower slope to basin floor” environments. Major architectural elements of the reservoirs are summarized below:

(1) Confined and depositional channels on the mid slope and in minibasins: These reservoirs are often amalgamated channel sands with low aspect ratio (width

divided by thickness). Debris flow and slump deposits are also common due to very steep slope topography. Large mass transport complexes can be clearly defined on 3-D seismic as toe-thrusted chaotic zones. These reservoirs are also discontinuous with very high heterogeneity. Levees, scours and injection dikes can either improve reservoir connectivity or result in reservoir compartmentalization depending upon their geometries. Fields in eastern Mississippi Canyon, northern Green Canyon and Garden Banks are such cases. The best reservoir of this kind consists of several stacked channel sandstones up to several-hundred-ft. (meters) thick with a high percentage of sand-on-sand contacts, resulting in a large hydrocarbon-filled reservoir volume (e.g., Mars-Ursa, Figure 3.4) (Sawyer, 2006).

(2) Weekly confined and distributary channel fills in down slope, primary and secondary basins. These reservoirs, compared to the confined ones, have more continuous geometries and better lateral continuity, but poorer vertical connectivity. These channel fills are wider with aspect ratio > 100 . The ideal reservoir consists of several separate channelized and tabular sandstones within a formation up to 1,000ft (300m) thick. Fields in central Green Canyon and Mississippi Canyon are such examples, including Thunder Horse and Tahiti.

(3) Distributary lobes in basin floor and primary basins: These reservoirs reach far into the basin floor; some of them extend to near the Sigsbee Escarpment. These are very large basin-floor fan systems covering hundreds of square kilometers/miles. They are sheet dominated sandstones with very good lateral continuity, but very poor vertical connectivity due to interbedded thick shales. A 4-way turtle structure or a 3-way structure against a salt feeder trap could result in billions of barrels of oil in place.

Another critical issue of turbidite reservoirs is how they trap hydrocarbons when close to a basin margin or the edge of a diapir. The margin or edge can be as follows: (a) A natural pinch-out of the sandstone lense due to decreasing depositional energy. In this case the sandstones may not be in contact with the salt. The success of the trap depends on the seal capacity of the associated shale; (b) A sandstone package that is truncated by a salt diapir or canopy. In this case, sandstones may be in contact with the salt body. The successful trap depends on the pore pressure and seal capacity. There is a likelihood that the hydrocarbons may leak along the sediment-salt interface. However, in most cases, the interaction between the salt and turbidites is a dynamic process: they are the cause and result of each other (Figure 3.5).

Data collection during exploration and development activities improve the understanding of structure and stratigraphy in dGOM. Comparison of such data with deepwater outcrop analogs also aids in reservoir characterization, modeling and simulation (Slatt *et al.*,2000). A good outcrop analog of the deepwater Wilcox reservoirs is the Pennsylvanian aged Jackfork Group in Arkansas, USA (Zou *et al.*,2012) (Figure 3.6) and the Karoo Basin Strata in South Africa (Sullivan *et al.*,2004). The Pennsylvanian Ross Formation in Ireland has been suggested as an analog for the more traditional minibasin in northern Gulf of Mexico and Mississippi Canyon areas (Pyles *et al.*,2011).

A robust Paleogene (Wilcox) reservoir database with well logs and cores has been established by the petroleum industry, with major inter-well correlations using seismic, paleontology, well logs and chemostrat data. However, the whole core of the pay zone (generally <300 ft, 100m) consists of only a small portion of the Wilcox

(>4,800 ft, 1,440m). This greatly increases the uncertainties of the lateral and vertical interpretation of reservoir architectures. One example is the Baha #2 well drilled on the crest of an anticline. A sequence stratigraphic framework has been established based on several well logs and limited cores, with large uncertainties on the extension and connectivity of the reservoir sands (Figure 3.7).

SALT STRUCTURES AND TRAPS

The concept of petroleum systems in the dGOM has changed dramatically in past decades. Classical trap concepts such as 4-way turtle and 3-way against salt have become more sophisticated. Ref. (Pilcher *et al.*, 2011) defined new trap types based on the concept of “top primary basin”, which ended up being a better solution to characterize the petroleum system and trap configuration in dGOM (Figure 3.8). Salt weld and carapace geometries have been investigated to evaluate the risk with traps. The successes of the Kaskida discovery in Keathley Canyon and the Tonga discovery in Green Canyon changed the traditional view that a “3-way trap against salt weld will not work”. In these two cases, the carapace above salt weld can be a good seal, leading up to 3,000 ft (900m) hydrocarbon columns. In addition, there is also a good geological chance of success on 3-way linear traps, but the economics of this type of trap is questionable.

Figure 3.9 illustrates the development of the outboard and inboard systems of Wilcox reservoirs (Mount *et al.*, 2007). The configuration of the primary basin usually formed before the deposition of the Wilcox, with Louann salt as the underlying pillows. Later formed Wilcox and Miocene turbidites drove the allochthonous salt both upward

and basinward. Hydrocarbon generally started to generate and migrate around 10 million years. One assumption geoscientists always have is that the 3-way updip against salt stock is a good place for a hydrocarbon trap. However, according to the recent dry hole results, the salt-sediment boundary can also serve as a conduit for hydrocarbons to leak towards the sea floor, especially when the near-salt reservoir beds are steep and overturned.

The success of the deepwater Wilcox trend began in the outboard trend (where there are no salt canopies above the traps), and moved towards inboard (where there are salt canopies above the traps). This is partly due to seismic imaging, but is also due to an improved understanding of the trap mechanism with salt related structures. The 4-way salt-cored anticlines were first recognized with discoveries such as Cascade-Chinook, Great White and Baha. Then the 3-way trap with a 4-way component was recognized (Tucker and Kaskida). The trapping mechanism also works for salt feeder, salt canopy and carapace types.

The salt sutures are important evidence of how salt interact with each other; (2) they are potential drilling hazards that need to be identified before drilling. Using 3-D seismic data, geoscientists can map the sutures in both section and map views (Figure 3.10), and restore the salt back to its origin. If a salt body has not moved far away from its feeder, one can clearly associate the salt body to its original feeder. However, the reality is that there are multiple salt feeders feeding multiple canopies, and they are mixed at the present time. Thus it remains uncertain when conducting a quantitative restoration.

CASE STUDY

Case A: Eastern Mississippi Canyon, Deepwater GOM

Field A and Field B are two medium-sized deepwater fields in the eastern Mississippi Canyon area, deepwater Gulf of Mexico. Field A is a smaller gas field which was discovered in 1999 with 75 BCF gas produced, Field B is a larger oil and gas field which was discovered in 1996 with 63MMBBL oil and 81 BCF gas produced (Figure 3.11). These two fields are 6 miles apart along a channel complex system. The reservoirs of the two fields both belong to one major channel complex system deposited along NW-SE direction. A whole core description from Field A #1 well indicates that the reservoir is a coarsening upwards channel complex. The lower 100ft part of the pay zone is characterized by mostly fine grained laminated sandstones with ripples and cross bedding with shales. They are interpreted as medium and slumped levee deposits. The main reservoir is 60ft clean channel sandstone in upper part of the core, with coarse-medium sized sandstone. Mud clasts, scour surfaces are common sedimentary features. Each bed is fining upward with Bouma A-C sequences stacked together. The key channel axis reservoir was overlain by slope mudstone and distal levees, forming a complete hydrocarbon trap. In addition, there is another major channel sandstone 100ft below the core bottom, which was filled by mostly water.

Field B (located 6 miles downdip from Field A) is a combined stratigraphic and structural trap. Structurally, there is one major W-E normal fault (5 miles long) cut through the northern part of Block 429. A large 3-way closure is likely to be sealed against the major fault. More importantly, from the 3-D seismic analysis (both section view and RMS amplitude extraction map), the channel system (same as Field A) cut

through the center of the fault-bounded closure. Thus the sealed closure is likely to have the best reservoir in the channel system. The gross thickness of the channel complex is >300ft, with more gamma-ray spikes than Field A. The reservoirs are likely to be naturally fractured with 6-7 compartments separated by inter-channel deposits. From RMS amplitude map of Figure 3.11, the topmost channel has very low amplitude, indicating a possible mud-filled bypass channels at the beginning of the transgression above.

Case B: Green Canyon, Deepwater GOM

Basin A is a secondary basin (minibasin) located at the northern Green Canyon, deepwater Gulf of Mexico. The basin is bounded by salt feeders in all directions (Figure 3.12). The deposition of turbidite reservoirs are strongly controlled by the development of salt structures. Basin A is also a petroleum-rich basin with producing oil and gas fields in the northwest and to the east (red and green dots on the map). Structures A, B and C are all salt-related features. Structure A is interpreted as a salt ridge caused by compression (analogous to the model from Pilcher *et al.*, 2012). Structure B is a huge salt stock (canopy) which is the southern and western boundary of Basin A. Structure C is a large salt feeder system which fed the salt canopies through the weld as salt conduits (black dots and pink lines on the cartoon section, Figure 3.12).

The turbidite deposits in Basin A generally come from the north (shelf). RMS amplitude extractions were run in both shallow and deep reservoirs to highlight the channelization features within Basin A using 3-D seismic data. In the Shallow Reservoir (Figure 3.13, Upper), the channelized features are clearly seen with higher amplitude on both the

gray-scale and color scaled maps. Depositional model was proposed as a distributary turbidite channel-lobe system inside a minibasin. The entire system consists of at least 4-5 major stacked lobes that are highly channelized. In the Deep Reservoir (Figure 3.13, Lower), the depositional patterns are similar, with major channelized input from the north. A well-reprocessed 3-D seismic cross section (AB) also reveals the stacked channel system in the reservoir interval. It is likely that these vertically and laterally stacked reservoirs are internally connected due to high energy flow. In addition, the TST isopach map indicates the basin center is in the south of Basin A.

EXPLORATION UPDATES

On the exploration side, the emerging play concepts keep the deepwater Gulf of Mexico evergreen for wildcat drilling. The depth of exploration has been extended from shallow to ultra deepwater (> 3,000 m), with several stacked reservoirs being targeted simultaneously. For the past decade, more than ten Paleogene fields have been discovered in the ultra deepwater area, mainly in Walker Ridge, Keathley Canyon and Alaminos Canyon. From west to east, successful exploration programs recently include the Perdido fold belt region (e.g., Great White, Tobago, Silvertip, and Baha) and the central region (Tiber, Kaskida, Stones, St. Malo-Das Bump, Jack and North Platte). Subsalt and ultra deepwater Pliocene and Upper Miocene fields were also found during the process of exploring deeper Paleogene targets, which unlocked another successful play (Figure 3.2). Further to the east, the Norphlet play began after the giant discovery (Probable reserve > 300 MMBBL, Million Barrels of Oil) at the Appomattox No.1 well near the Mississippi Canyon and De Soto Canyon boundary.

In addition, after the Cretaceous Tiber discovery in Keathley Canyon and the Davy Jones discovery in the northern Gulf of Mexico, the Cretaceous Tuscaloosa play began to receive much attention. Bids in the lease sale for Cretaceous blocks increased. The deepwater Cretaceous may become another new play in the near future.

As AVO (amplitude versus offset) technology becomes a routine and mature methodology in shallow supra-salt sections in the dGOM, and new shallow discoveries have been found with good rates of return (e.g., Galapagos development in the eastern Mississippi Canyon). Small discoveries have become commercial thanks to subsea tie-backs to facilities in existing from the larger fields (e.g., Aspen-Lorien-Droshky prospects in Green Canyon tie back to the Bullwinkle Platform).

Safety and environmental regulations have become one of the most important issues since the Macondo Tragedy. Due to the strict and rigid safety regulations, the business atmosphere in the dGOM no longer favors small to middle sized independent oil companies; many of these companies have either exited or reduced their dGOM business, shifting more to onshore unconventional resource plays. However, major oil companies not only remain active, but have even increased their portfolios significantly. In addition, national oil companies also have entered the dGOM through mergers and acquisitions.

Figure 3.14 summarizes the major challenges faced by reservoir development in the dGOM. Drilling, logging and completion technologies have also been improved to fit the challenges of the deep high pressure and high temperature environment (Halliburton Corp., 2010). LWD (logging while drilling) and modular formation dynamic tests have become routine for engineering, geological evaluation and

monitoring. However, the average drilling costs since the Macondo Tragedy have risen significantly over the last decade for ultra deepwater wells. The current average cost for one Paleogene well ranges from USD\$150MM up to USD\$350MM (Million US Dollars). Drilling problems such as overpressure, salt canopy inclusion and sutures, carapace/raft/overtuned sections near salt, sub-salt gouge zones, and sediment mass transport complexes all can cause a long non-operating time, lost circulation, low rate of penetration, bypassed wells, bad holes and in the worst scenario, a blowout.

Figure 3.15 is a summary of the major discoveries in the deepwater Gulf of Mexico during 2008-2014. The Macondo tragedy was in 2010, resulting in almost no drilling activities in 2010-2011. Beforehand, in 2008-2009, there were >10 discoveries each year. As the drilling activities have now restored to a pre-Macondo level, more and more discoveries covering a wide range of resources potential can be expected during the next 10 years.

These oil and gas discoveries during 2008-2014 can be divided into the following major categories:

(1) Shallow amplitude plays in the Upper Miocene, Pliocene and Pleistocene. The resource sizes of these discoveries are usually small (<50MMBOE, Million Barrels of Oil Equivalent), shallow and are surrounded by nearby existing production facilities. Thus the development costs of these wells are cheaper than dGOM wildcat exploration wells. Two good examples are the Condor and Droshky discoveries in Green Canyon (and several discoveries in Garden Banks).

(2) Conventional Miocene subsalt and amplitude driven discoveries, such as Heidelberg, Samurai, Vito, Deep Blue, Santiago and Santa Cruz. Most of the large

lower-middle subsalt and amplitude-driven fields are located in Green Canyon and Mississippi Canyon. These fields are often >100MMBOE and related to 4-way turtle anticlines, salt pillows or 3-way traps against salt feeders and canopies. Followed by the successes of Tahiti and Thunder Horse, more such discoveries have been made using the same concept and advanced seismic imaging technology. The depositional environments of these discoveries are often channelized sheet sandstone (weakly confined sandstone) in a proximal downslope and basin floor fan setting.

(3) Wildcat and appraisal wells of the emerging Paleogene trend. This is the continuing success of the trend and appears to be the future of dGOM exploration and production activities. Good examples include Shenandoah, North Platte, Tiber, Coronado, Phobos and Buckskin. Such ultra deepwater and expensive Paleogene wildcat wells push the play boundary both outboard to the south (Phobos) and inboard to the north (Shenandoah, North Platte). The appraisal activities of traditional Miocene fields such as Shenzi, Mad Dog and Big Foot have also found new opportunities in Paleogene reservoirs. Moreover, although the Paleogene Hadrian and Lucius wells drilled wet Wilcox reservoirs, they opened up new “subsalt” Upper Miocene and Pliocene oil plays in the ultra-deep Walker Ridge. The success of the Phobos well extends the Wilcox play into the Sigsbee Escarpment. Such a series of successes are exciting and beyond geoscientists' imagination ten years ago.

(4) The success of Appomattox, Vicksburg, Tiber and Davy Jones opened up whole new opportunities in the deepwater Norphlet and Tuscaloosa trends. The Jurassic Norphlet play comprises a dune sand reservoir located in the eastern Mississippi Canyon and De Soto Canyon in the ultra deepwater (>8,000 ft, 2,400 m) The

Appomattox wells in 2010 contained >300 ft, 90 m of oil pay in a Jurassic fault block. The preliminary resource size of Appomattox is > 300MMBOE.

There are two types of Cretaceous Tuscaloosa sandstones: the deepwater and the onshore deep gas. The Tiber well in Keathley Canyon found > 500ft (150 m) of oil pay in the Tuscaloosa sandstones, which is the milestone of the play. Davy Jones, drilled back in 2010, discovered a deep shelf gas play in the Wilcox aged reservoirs on the shallow shelf water zone, revitalizing a new deepwater shelf gas play.

In summary, all four of these major categories of discoveries from 2008-2014 have added multi-billion barrels of equivalent oil resource in the dGOM (Figure 3.15), and the future looks promising. Below, we discuss the latest progress on the petroleum geology of the dGOM, and associated operational, development, production, and economic challenges.

Neogene Play

The Neogene play in dGOM, which is mainly Miocene-aged reservoirs, has been heavily explored and produced, including giant fields such as Mars-Ursa, Tahiti, Mad Dog, Thunder Horse, Blind Faith, Auger, etc. These fields entered the production phase in recent years. There are many opportunities for development and enhanced oil recovery from them.

Tahiti (Green Canyon block 640) is one such example of a giant Lower-Middle Miocene oil field. It was discovered in 2002, which is a large 3-way closure against a salt feeder (Figure 3.16). The reservoirs consist of multiple channelized lobe turbidite sandstones. The sandstones are laterally continuous but are vertically separated. They

were deposited in a downslope environment. After the first discovery well drilled on the flank of the 3-way closure, 4-5 appraisal wells were drilled updip and downdip of the structure to delineate the hydrocarbon column and water contact (Figure 3.16, right). The hydrocarbon column from the oil-water contact to the top of the trap is over 3,000ft (1,000 m) high. The final reserve of the field is over 300 million barrels. The first oil flowed in 2010.

Paleogene Play

The Wilcox reservoirs in dGOM consist of Upper-Middle Paleocene and Lower-Middle Eocene turbidite sandstone packages (Figure 3.1). The primary sediment source of Wilcox reservoirs is related to the uplift of the Rocky Mountains and the Sierra Madre Oriental. Large volumes of sediments were transported down from the orogenic belts to build great fluvial-delta systems around the shelf. Shelf sediments were then dumped into the deepwater basin floor by sediment gravity flows (Figure 3.17). There are also secondary sources from the west in Mexico. Vertically, the Wilcox reservoirs are sub-divided into Upper and Lower Wilcox. Laterally, the Wilcox reservoirs have been divided into the Perdido fold belt play (in Alaminos Canyon) and the Walker Ridge-Keathley Canyon play. Deposition of the Lower Wilcox was focused in western Walker Ridge, Eastern Keathley Canyon and a small portion of Alaminos Canyon with average thickness from 2000-3000 ft (600-900m). The sources of these turbidite sediments were believed to come from the Houston embayment to the north (Lewis *et al.*,2007). The Upper Wilcox isopach shows a significant depocenter with over 4,000 ft (1,200 m) thickness in the western Alaminos Canyon and gradually thinning towards

Keathley Canyon and Walker Ridge to the east (Mathur,2008). The mixing of northern and western sources resulted in different stacking styles and distributions of the turbidities in the basin, which have a profound effect on reservoir properties.

Figure 3.18 illustrates the major Wilcox discoveries and their resources compared to Miocene fields. The Paleogene play has a higher success rate (46%) than the Miocene play (33%). This is partly due to a better seismic technology and a better understanding of trapping mechanism.

Jurassic Norphlet Play

The Jurassic Norphlet play extends from onshore to the deep waters of the eastern Gulf of Mexico. Appomattox is currently in the development phase and is moving forward with engineering design for a floating production system and subsea infrastructure. The Norphlet play is characterized by high pressures and well temperatures, where good quality oil can be found in high quality sandstone reservoirs. A series of major discoveries have been made in this emerging deep-water play (Figure 3.19).

A recent major discovery in the Norphlet play is the Rydberg exploration well. It is located 75 miles (120 kilometers) offshore in the Mississippi Canyon Block 525 in 7,479 ft (2,280 meters) of water. The discovery is within 10 miles (16 kilometers) of the planned Appomattox development and the 2013 Vicksburg discovery. It was drilled to a total depth of 26,371 ft (8,038 meters) and encountered more than 400 ft (122meters) of net oil pay. The resource base is expected to be approximately 100 million barrels of oil equivalent. Together with the Appomattox and Vicksburg discoveries, the total potential

Norphlet discoveries are over 700 million barrels of oil equivalent. As of this writing, an exploratory well is being drilled at Gettysburg, located in Desoto Canyon Block 398 which is within 10 miles (16 kilometers) of the planned Appomattox development (Shell Oil Company, 2014).

DRILLING, DEVELOPMENT AND PRODUCTION

Drilling

Drilling the dGOM wells is one of the toughest challenges facing the energy industry so far due to salt related structures, high pressure, greater depths, higher temperatures, blowout preventer investigation and narrow drilling margins. Average drilling time for one well is > 100 days for a 25,000 ft (7,500 m) well, with more than one million USD cost per day. The average “dry hole” cost of a Wilcox well is more than USD \$100MM. After the Macondo tragedy, the US government forced tough regulations for the operators in order to prevent another blowout. During drilling, the BOP (blowout preventer) now has to be tested every week or two. Checking the BOP usually requires a trip-out and trip- into of the wellbore, which takes up to a few days.

Salt related structures can have a big impact on drilling. Calculating the thickness, depth and geometry (dip and strike) of the top and base of a salt canopy near a well bore is one of the most important works during the well planning stage. In addition, geoscientists and drilling engineers need to identify all the potential drilling hazards such as shallow water flows, shallow faults, salt sutures and inclusions inside the salt canopy, shear gauge zones near the base of the salt, and overly steep or overturned beds

caused by salt movement. It is a long journey towards reaching the Wilcox reservoirs (Figure 3.20).

Overpressure can occur anywhere along the well path. Predicting and handling overpressure is another important task before and during drilling. BOP and cementing work need to be of good quality in order to control the overpressure effects. Usually in Wilcox drilling, the overpressure can be estimated by seismic velocity and offset logs. The deeper the drilling, the more likely that overpressure will cause a narrow drilling margin. For example, there may be less than 1.5 ppg difference between ECD (Estimated Circulation Density) and fracture gradient at the 16.0 ppg mud weights. This pressure situation will become worse when the well hits hydrocarbon bearing Wilcox sandstones.

Salt exit strategy is also one of the most important steps during drilling deepwater subsalt reservoirs (Figure 3.20). When a well is drilled close to the base of the salt canopy and is about to exit the salt and enter the sediment, drillers have to be very careful in executing appropriate strategy. Failure to do so will result in stuck pipe, lost circulation materials, kick, blowout, sidetrack, or bypass of the original hole. To better meet the challenges of executing the salt exit strategy, the geoscientists first need to provide the drilling engineers with the structural configuration near the base of salt zone. Pressures need to be calculated from methods such as (1) seismic velocity; (2) offset wells; (3) 3-D basin modeling; (4) hard measurements such as MDT (modular formation dynamics tester) or well log measurements. Whether to set the casing in the salt or out of the salt depends on the borehole instability condition. Successfully

executing the salt exit strategy can greatly reduce the overall drilling days and drilling costs.

Development

Reservoir development in dGOM is a long time process from exploration, appraisal, design, and execution to first oil production. The general time frame is usually 10 years. The Perdido fold belt field is the earliest Wilcox development which includes Great White, Silvertip, Tobago, Trident and Tiger fields with the average water depth from 8,500-9,500 ft (2,700 m). The production platform is 200 miles to onshore and 60 miles to the nearest infrastructure. The central platform can serve multiple fields, with a facility capacity of 130,000 barrels of oil per day. Key technologies include the seafloor caisson booster system to provide the artificial lift for increased productivity; and first use of subsea (located on the sea floor) multiphase flow meters. The central platform is also the deepest installed Truss Spar design in the world (Chevron Corp., 2011).

The Jack and St. Malo fields are located within 25 miles (40 km) of each other and are being jointly developed with a host floating production unit located between the two fields in 7,000 ft (2,134 m) of water, approximately 280 miles (450 km) south of New Orleans, Louisiana (Figure 3.21). The facility is planned to have a design capacity of 177,000 barrels of oil-equivalent per day to accommodate production from the Jack/St. Malo development, which is estimated at a maximum total daily rate of 94,000 barrels of oil-equivalent, plus production from third-party tiebacks. Total project costs for the initial phase of the development are estimated at \$7.5 billion.

It also includes seafloor boosting technology for late field life operations. In addition, the efficient multi-zone frac equipment enables complex completions over very large reservoir intervals. In March, 2013, the successful production test of St. Malo field at a daily rate of 13,000 barrels was announced, with emphasis that this production rate is limited due to the facility, i.e., there is much upside potential once it formally begins to produce in 2014. Other existing platforms and FPSOs (Floating Production, Storage and Offloading) such as Tahiti, Thunder Horse, Cascade, and Mad Dog are reaching their peak productions at present or will be in the near future.

Production

Lach (Lach, 2010) has conducted a comprehensive study for IOR (improved oil reservoir) in dGOM. They identified at least six trapped oil mechanisms for Paleogene Wilcox reservoirs (from high to low percentage of OOIP, Original Oil in Place): (1) communicating capillary bound oil (29% of OOIP), (2) limited displacement drive energy (24% of OOIP), (3) poor sweep efficiency (16% of OOIP), (4) non-connected to wells (15% of OOIP), and (5) high abandonment pressure (6% of OOIP). The total estimated ultimate recovery accounts for only 10% of the OOIP, giving much upside potential for the IOR strategies (Figure 3.22).

How to get oil and gas recovery beyond the initial 10% of primary recovery is the most important technical and strategic problems faced by the industry. First and the most important IOR method is water injection, including conventional and seafloor water injection (Lach, 2010). The technical recovery factor of these two methods can go up to 22% (conventional) and 15% (seafloor), respectively (Figure 3.23). Other

discussed IOR methods include low salinity water injection (7% RF, Recover Factor), conventional hydrocarbon gas injection (8% RF), nitrogen injection (12% RF), MEOR (microbial enhanced oil recovery) water injection diverters (7.5% RF), subsea multi-phase pumping (7.5% RF), in well ESP (electric submersible pumps), hydraulic fracturing (10% RF) and directional or horizontal drilling (5% RF).

The Wilcox reservoir simulation also best illustrates how an ideal tabular and continuous Wilcox reservoir behaves for water-flood recovery (Lach, 2010). This reservoir simulation also assumes an ideal downdip aquifer support. The initial production without water flood was about 8,000 barrels per day with reservoir pressure at 12,000 psi. The rate then dropped quickly to about 2,000 barrels per day after 11 months.

However, not all the reservoirs have the ideal tabular geometry with good aquifer support downdip. The difference between channel and sheet architectures will greatly affect aquifer pressure support, sweep efficiency, and recovery factors. Zou (*Zou et al., 2012*) discussed the reservoir performance between a channelized and a sheet prone reservoir using an outcrop example from the Jackfork Group, Arkansas. Results of simulations indicate that the sheet-prone upper sandstones can provide sustained production for a much longer period of time than the channel-prone lower sandstones (Figure 3.24)

VISION TOWARDS 2023

The crude oil production for offshore GOM was 1.3 million barrels per day in 2011, which accounts for 23% of total US crude oil production (source from EIA: US

Energy Information Administration, Figure 3.25). As the dGOM large discoveries turn into production, one would expect a steady increase in both oil production and share in total US oil production. The Wilcox field in the dGOM will become a major contribution to the US crude oil production in the near future. To unlock the production potential, the industry needs to better understand the reservoirs, development technology and strategy, and more importantly, the financial and economic environment. From the prediction of Wood McKenzie (Figure 3.26), BP (British Petroleum) is predicted to have the most production in the next 10 years. The key risks facing dGOM recovery include economic, environmental, regulatory and technical issues. A sustainable crude oil price above USD \$80 per barrel is considered as the most important factor. The environmental and regulatory factors also have notable impact on production recoveries. From the 2013 Wood Mackenzie report, currently the dGOM has five major plays which are: conventional Pliocene and Miocene, subsalt Pliocene and Miocene, Lower Miocene, Jurassic and Paleogene. The Paleogene play has the highest risk in reservoir quality, water depth, drilling costs, reservoir complexity, and infrastructure.

However, it also has the highest yet-to-find volume. Economics and commerciality are also at medium risk depending on the costs and crude oil price. From the commercial plot in Figure 3.27, the Paleogene play has the lowest NPV (net present value) at USD \$200MM and the highest breakeven prices (USD \$71/bbl, barrel), the NPV per barrel for Paleogene is less than USD \$1. And the total reservoir development Capex is more than USD \$16 billion. These are all negative commercial factors for developing Paleogene Wilcox reservoirs. However, successful online production of

Jack, St. Malo, Cascade-Chinook and Kaskida fields are encouraging news for Paleogene reservoirs. And there are substantial research and development activities both in industry and academia.

CONCLUSIONS

The past six years (2008-2014) were a prosperous time for exploration and production in the deepwater Gulf of Mexico (dGOM). Over 30 new discoveries were made, and many older discoveries have been through appraisal and development phases. Although there was a two year drilling moratorium due to the Macondo blowout tragedy, the dGOM is currently above its pre-Macondo rig count.

Recent deepwater exploration and production activities can be divided into three major categories: drilling new wildcat wells, appraising and developing newly discovered fields and enhanced oil recovery of mature fields. The Lower Tertiary Wilcox reservoirs have been a focus of exploration and development in the dGOM for the past decade, with major discoveries such as Cascade, Jack, Tiber, and Kaskida. Seismic imaging, complex geology, high pressure drilling, greater depth and higher temperature are key challenges for the exploration and production of Wilcox reservoirs. Complex geology includes salt-related structures and traps, reservoir compartmentalization, and the sequence stratigraphy of turbidite reservoirs. Salt-related structures include salt feeders, canopies, carapaces, welds, sutures and mini-basins. The combination of primary basin geometry and salt structure can have a large impact on reservoir geometries and properties. Reservoir compartmentalization can be caused by faults and fractures, as well as by sedimentary facies change. Turbidite sequence

stratigraphy helps the asset team to find the best completion intervals. Sheet and channelized sandstones with good downdip aquifer support are preferred reservoir conditions.

All the drilling, development and production challenges are related to high pressure drilling, greater depth, higher temperature and lack of existing field analogs. High well cost, narrow drilling margin, salt related drilling issues and extreme reservoir depth made drilling more difficult than anywhere on earth. High completion cost, poor reservoir quality and flow capability are key challenges for commercially developing the Wilcox fields. Various IOR methods are studied and applied in the development stage of the Wilcox fields, which have an average primary recovery factor of 10%~15%. With ideal tabular reservoir geometry and IOR methods, recovery factor of the Wilcox reservoirs can reach up to 42% of OOIP through the field life cycle.

ACKNOWLEDGEMENTS

This paper is a part of Fuge Zou's Ph.D. research with Dr. Roger Slatt at the University of Oklahoma. We thank the editors and reviewers who helped to greatly improve the quality of this paper.

LIST OF FIGURES

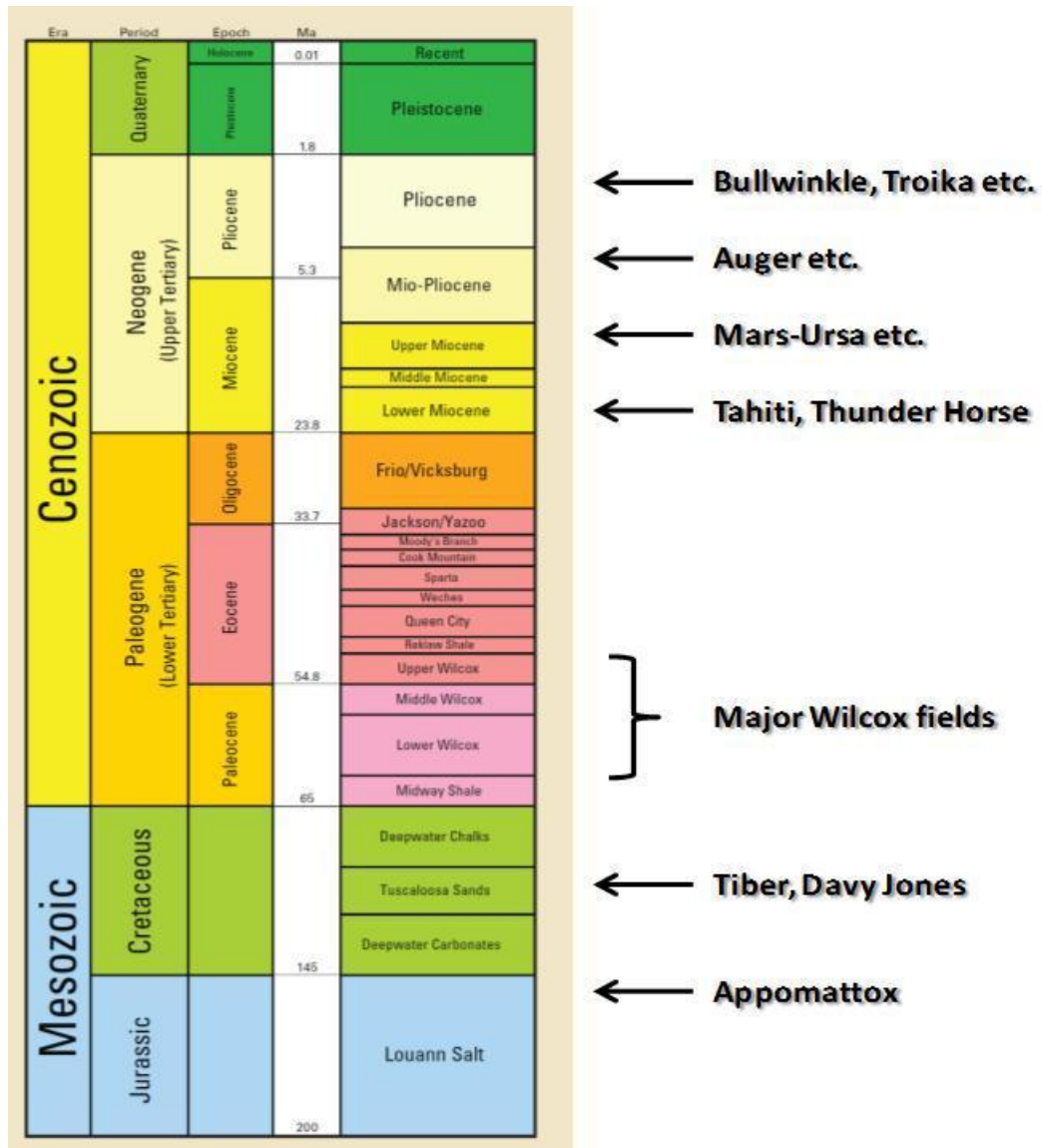


Figure 3.1. Stratigraphic column of dGOM and key discoveries and fields (Halliburton Corp., 2010) (Ma = Million Years).

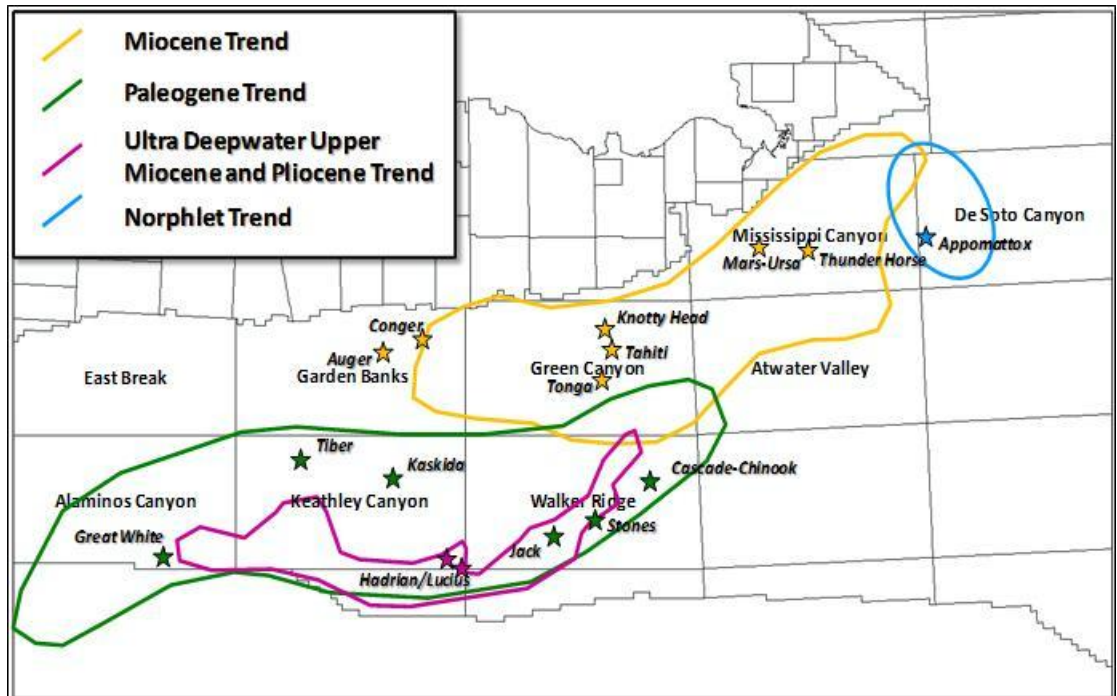


Figure 3.2. Major play trends and some key wells and discoveries in the deepwater Gulf of Mexico (Stars are important oil and gas discoveries or fields in each trend).bin number for anisotropy analysis.

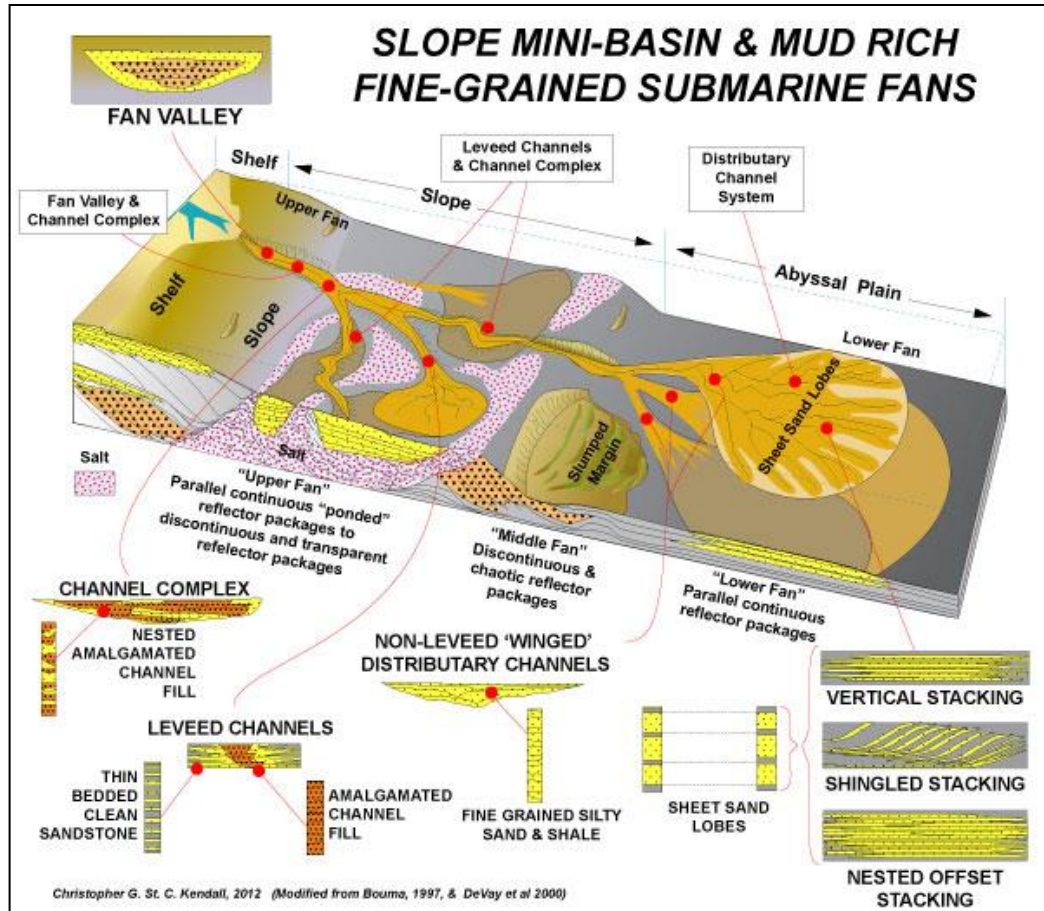


Figure 3.3. Turbidite facies in the dGOM (DeVay *et al.*, 2000), showing major deepwater architectural elements from updip slope down to basin floor fans.

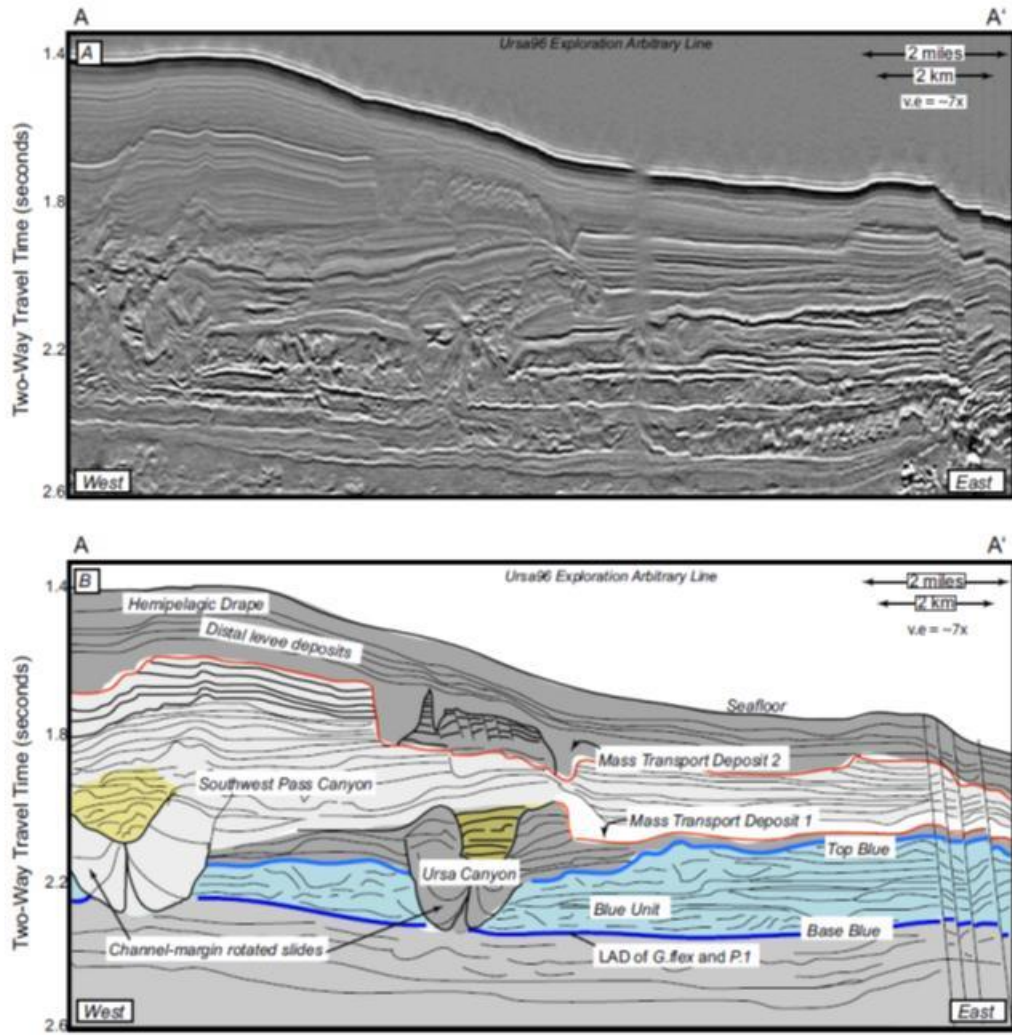


Figure 3.4. Upper: west-east seismic cross section perpendicular to the direction of deposition in Mississippi Canyon, dGOM. Lower: interpreted cross section showing depositional elements and key surfaces (Sawyer, 2006). (v.e. = vertical exaggeration)

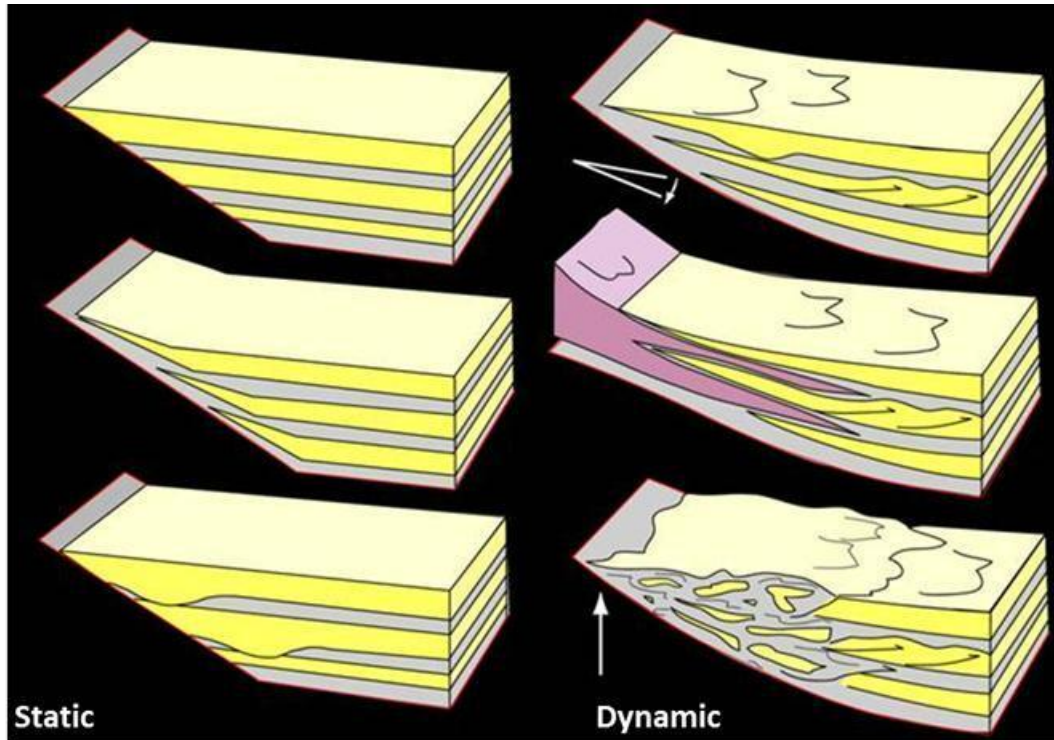


Figure 3.5. Static vs. dynamic onlaps of turbidite onto the edge of the basin or diaper (Haughton,2000).



Figure 3.6 .Panorama of Hollywood Quarry, Jackfork Group in Arkansas, USA. It represents a channel-lobe system in a proximal fan setting which is one of the most common reservoirs in ultra dGOM Outcrop analogs have been widely used for the current ultra dGOM reservoir characterization. Three good examples for Wilcox reservoir analogs are Jackfork Group in USA, Ross Formation in Ireland, and Karoo Basin in South Africa.

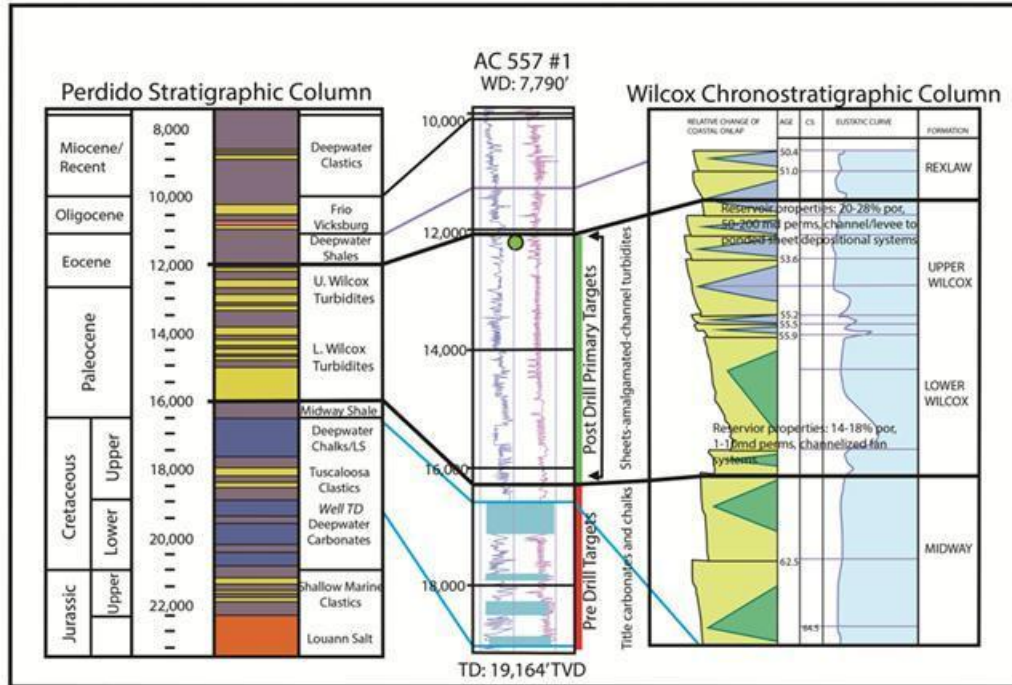


Figure 3.7. Wilcox reservoir in the Baha 2 well within a sequence stratigraphic framework (Meyer *et al.*, 2005). The vertical scale unit is in feet. The age is in million years. CS= Condensed Section.

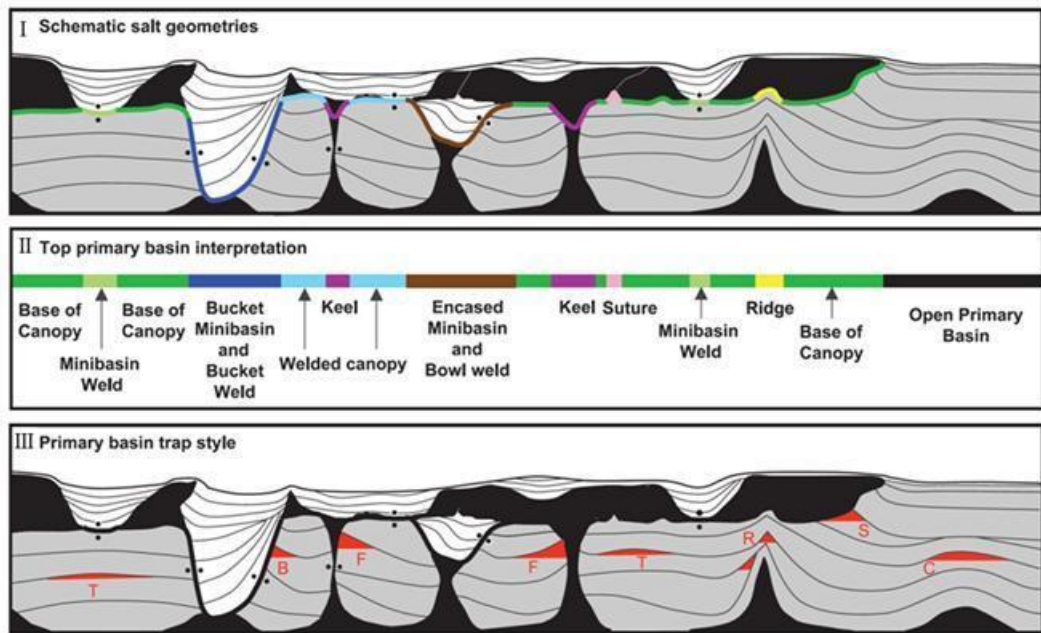
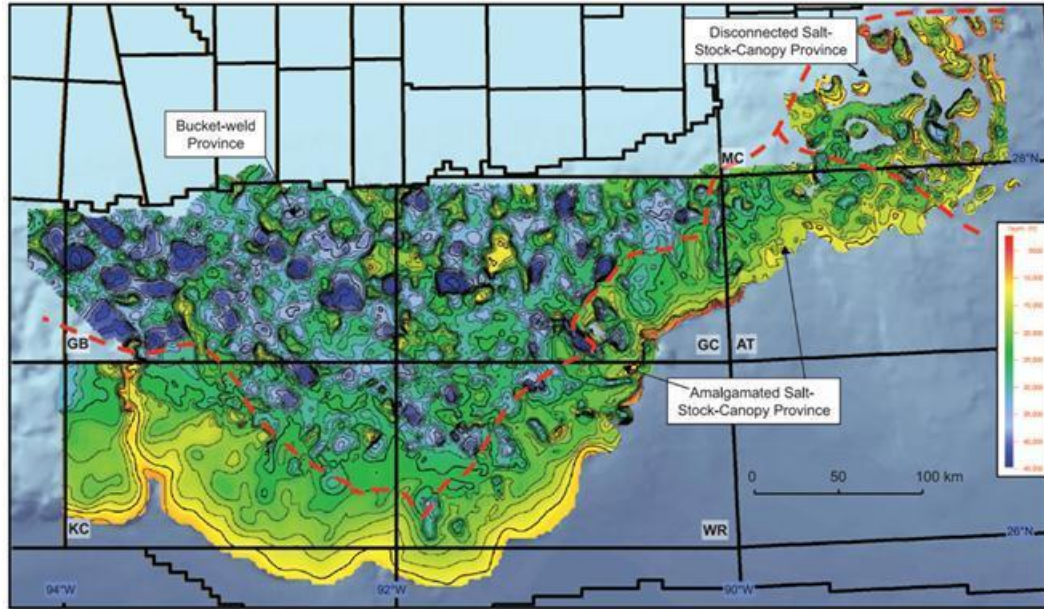


Figure 3.8.Upper: top primary basin interpretation based upon 80,000 km² (31,000 mi²) of 3-D depth-processed seismic data, lower: schematic representation of salt-related geometries in the dGOM, GB = Garden Bank, GC = Green Canyon, AT = Atwater Valley, KC = Keathley Canyon, WR = Walker Ridge; (I) interpretation of the top primary basin surface and distinction between primary and secondary basins; (II) classification of the top primary basin surface according to the nature of the surface; (III) schematic salt geometry highlighting primary basin trap types with a turtle structure (T), bucket weld (B), salt feeder (F), salt ridge (R), base-of-salt truncation (S), and salt cored fold (C) (Pilcher *et al.*,2011).

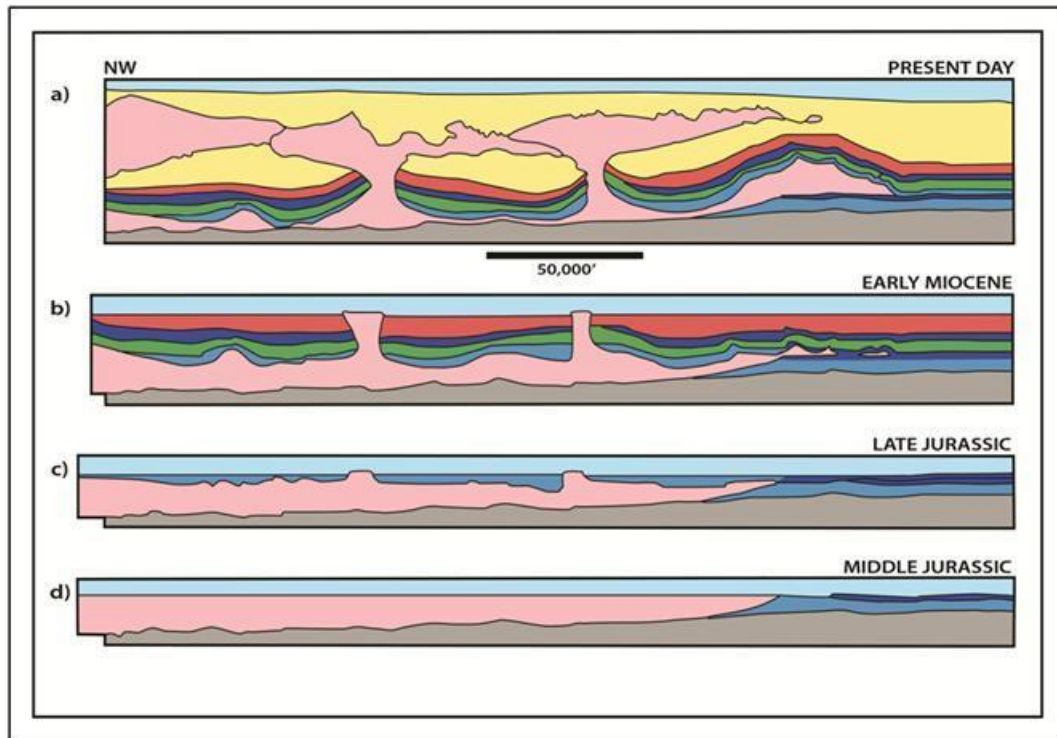


Figure 3.9. Evolution of salt mini-basins and distribution of deep water strata in the northern Gulf of Mexico (Mount *et al.*, 2007). The age is from Jurassic (~150 million years ago) to present day.

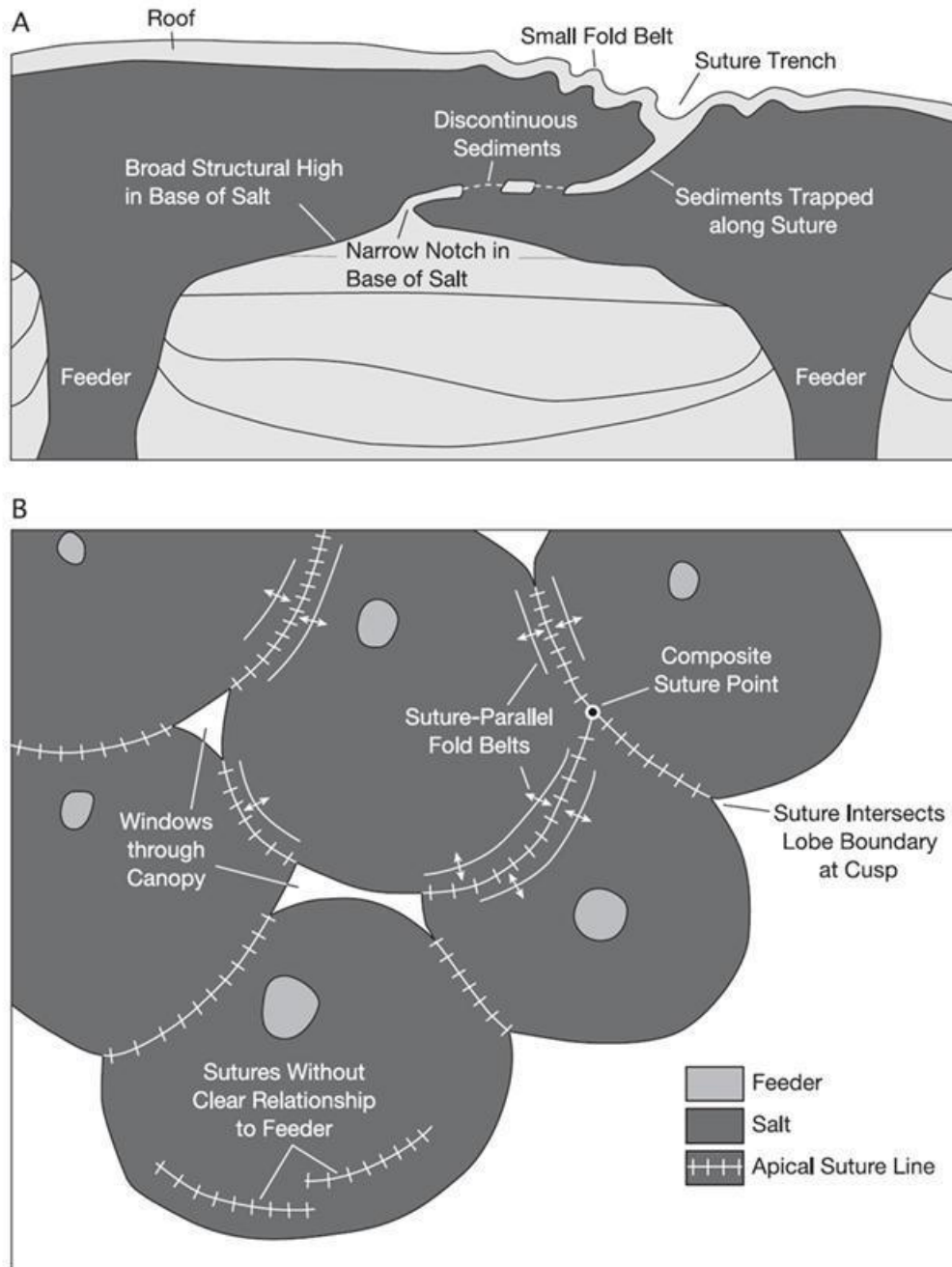


Figure 3.10. Schematic diagrams showing published aspects of sutures in (A) cross section and (B) map view (Dooley *et al.*, 2012).

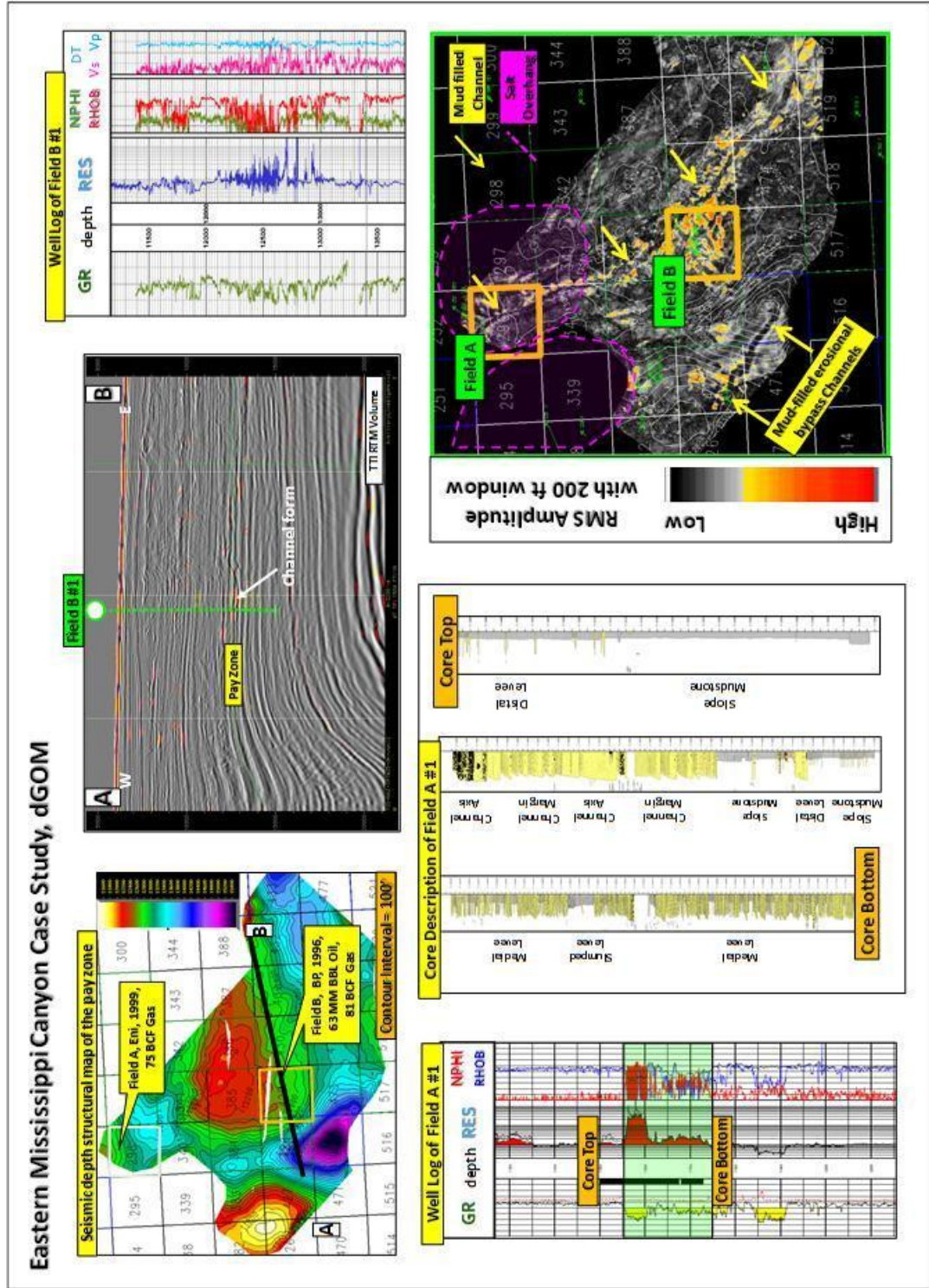


Figure 3.11. Case Study on the eastern Mississippi Canyon, deepwater GOM

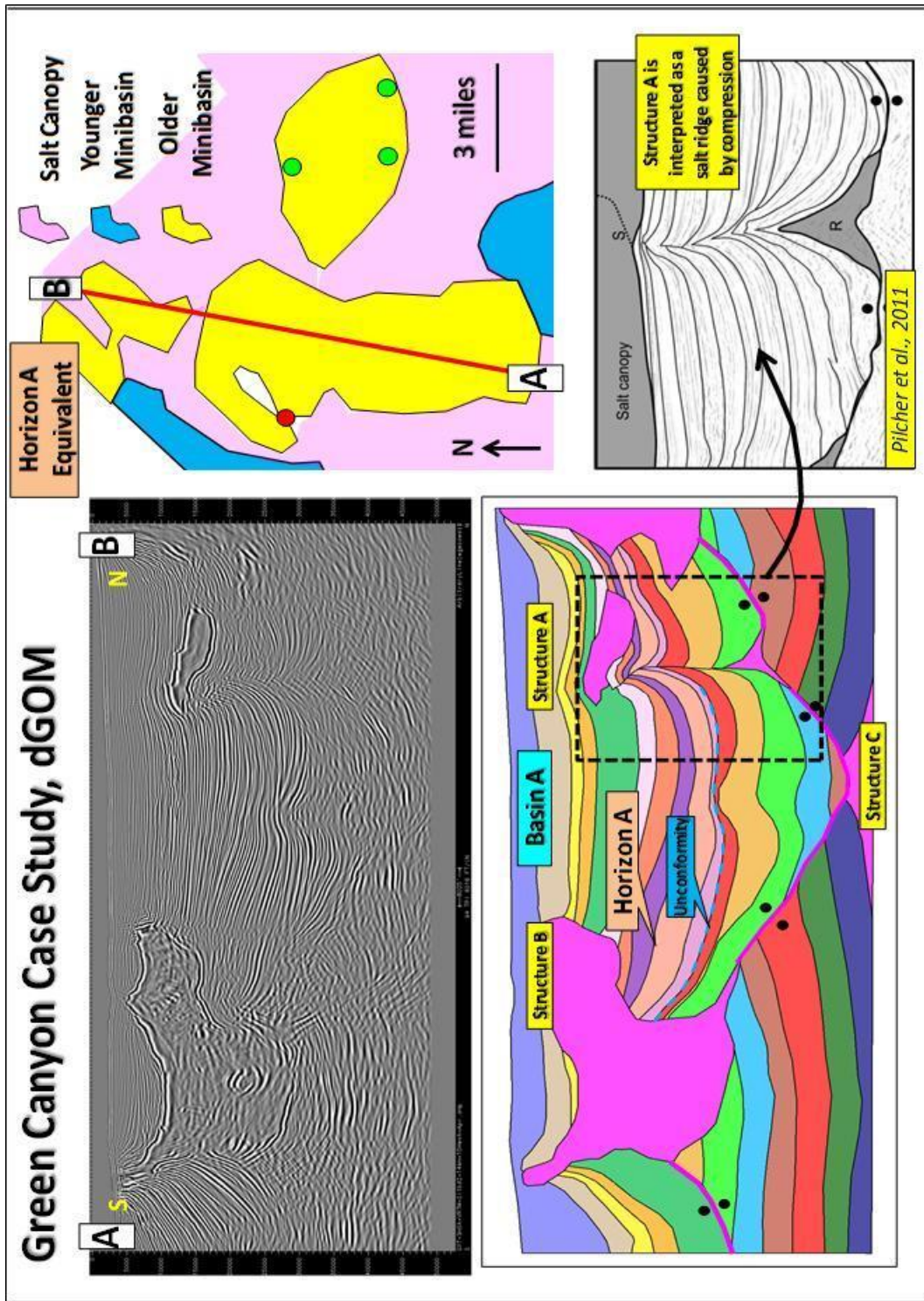


Figure 3.12. Case Study on the Green Canyon, deepwater GOM, salt structures and trap

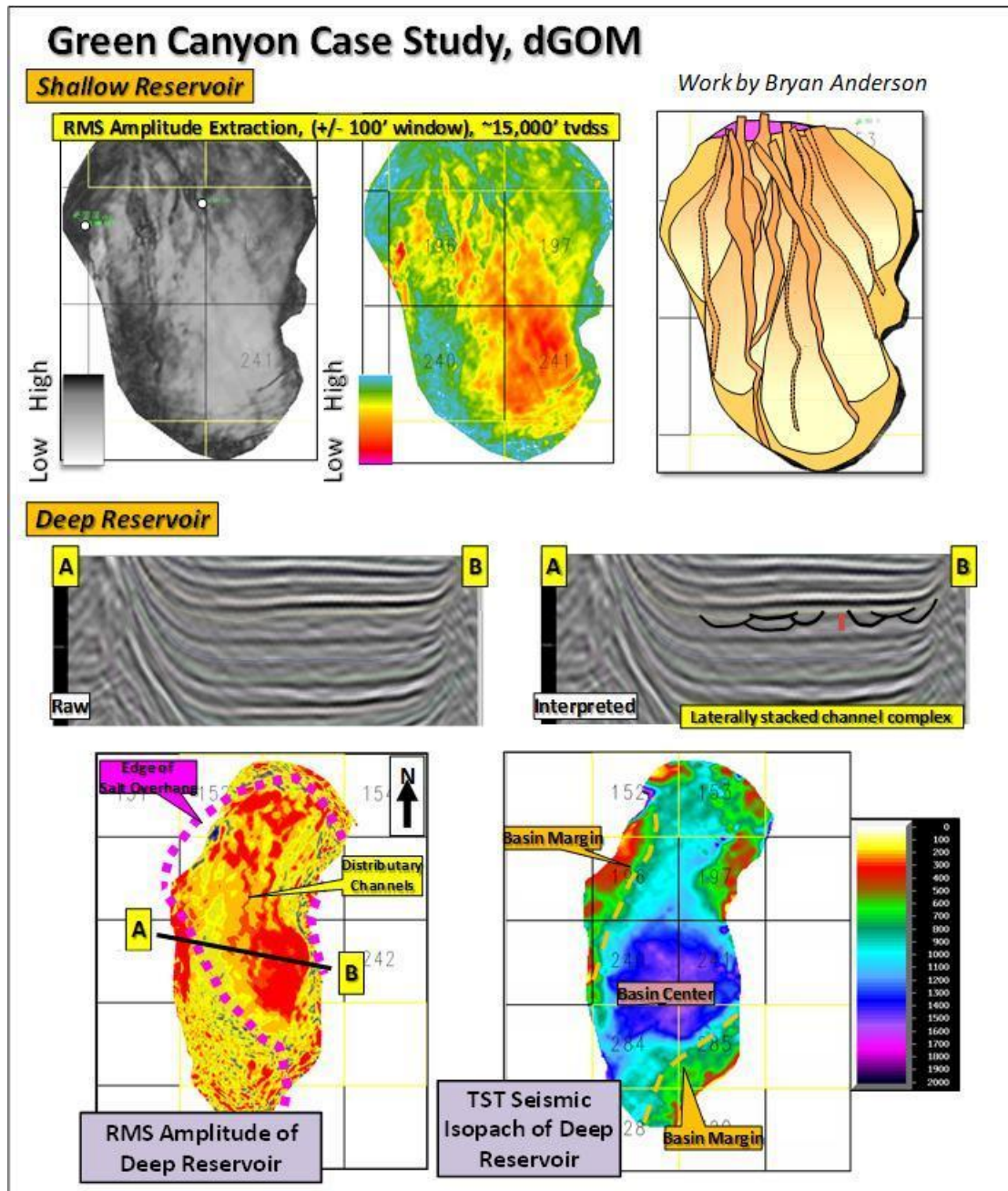


Figure 3.13. Case Study on the Green Canyon, deepwater GOM, turbidite deposition for shallow and deep reservoirs

MIOCENE	LOWER TERTIARY	SALT CANOPY
<p>Targets in the deepwater Miocene trend have generally been influenced by salt intrusion, making reservoir geology difficult to understand. Projects in the development phase must balance increased well complexity with a desire to reduce drilling and completion costs.</p>	<p>The Lower Tertiary trend is generally characterized by older sediments with lower porosities, ultra-deepwater depths, reservoir depths greater than 26,000 ft and high bottomhole pressures.</p>	<p>The extensive Salt Canopy greatly impacts seismic imaging quality. Salt bodies present unique well planning demands, slow drilling progress and require highly engineered completion solutions to ensure long-term well productivity.</p>
<p>EXPLORATION:</p> <ul style="list-style-type: none"> • Seismic imaging in narrow mini-basins • Sand identification 	<p>EXPLORATION:</p> <ul style="list-style-type: none"> • Limited geologic/analogue well information • Lack of reservoir modeling 	<p>EXPLORATION:</p> <ul style="list-style-type: none"> • Seismic attenuation • Depth imaging below salt • Defining base of salt • Locating and identifying inclusions
<p>DRILLING:</p> <ul style="list-style-type: none"> • Narrow drilling margin • Borehole stability challenges • Complex well trajectories in development projects • Improving drilling efficiency 	<p>DRILLING:</p> <ul style="list-style-type: none"> • High well costs • Narrow drilling margin • Extreme reservoir depth 	<p>DRILLING:</p> <ul style="list-style-type: none"> • Drilling optimization through salt • High vibration and shock • Salt exit strategy • Unexpected "tar" deposits
<p>COMPLETION AND PRODUCTION:</p> <ul style="list-style-type: none"> • Unconsolidated formations • Cross flow between wells due to extensive faulting • Production declines that must be offset with methods to enhance recovery 	<p>COMPLETION AND PRODUCTION:</p> <ul style="list-style-type: none"> • High completion cost • Low reservoir porosity and variances in permeability • Economic challenges due to reservoir quality and flow capability 	<p>COMPLETION AND PRODUCTION:</p> <ul style="list-style-type: none"> • Casing size limitations • Salt creep • Reservoir compartmentalization • Reservoir compaction with pressure depletion

Figure 3.14. Summary of deepwater GOM reservoir development challenges (Halliburton Corp., 2010).

Field name	Location	Year of Discovery	Water Depth (ft)	Operator	Status	(Projected) Onstream	Production Type
Anduin West	Mississippi Canyon 754	2008	2,696	ATP	Producing	2010	Subsea
Appaloosa	Mississippi Canyon 459	2008	2500	ENI	Producing	2011	Subsea
Condor	Green Canyon 448	2008	3,266	LLOG	Producing	2011	Subsea
Coronado	Walker Ridge 143	2008	5,722	Chevron	Appraisal	N/A	N/A
Dalmatian	DeSoto 48	2008	5,876	Murphy	Development	2013	Subsea
Freedom (Gunflint)	Mississippi Canyon 948	2008	6,100	Noble Energy	Appraisal	2014	FPS
Geauxpher	Garden Banks 462	2008	2,820	Apache	Producing	2009	Subsea
Gladden	Mississippi Canyon 800	2008	3,116	Newfield	Producing	2011	Subsea
Kodiak	Mississippi Canyon 771	2008	5,000	BP	Appraisal	2013	N/A
Mississippi Canyon 72	Mississippi Canyon 72	2008	2,013	LLOG	Producing	2009	Subsea
Sargent	Garden Banks 339	2008	2,240	Newfield	Producing	2010	Subsea
Shaft	Green Canyon 141	2008	1,016	LLOG	Producing	2010	Subsea
Tortuga	Mississippi Canyon 561/605	2008	6,500	Noble Energy	Development	2012	N/A
Buckskin	Keathley Canyon 872	2009	6,920	Chevron	Appraisal	N/A	N/A
Bushwood	Garden Banks 463	2009	2,700	Apache	Appraisal	2015	N/A
Ewing Bank 998	Ewing Bank 998	2009	1,000	Walter	Producing	2011	Subsea
Hadrian	Keathley Canyon 919	2009	7,425	ExxonMobil	Appraisal	N/A	N/A
Heidelberg	Green Canyon 903	2009	5,000	Anadarko	Appraisal	2014	N/A
Jake	Green Canyon 490	2009	3,740	Helix (ERT)	Development	2012	Subsea
Lucius	Green Canyon 875	2009	7,100	Anadarko	Development	2014	N/A
Pyrenees	Garden Banks 293	2009	2,100	Newfield	Development	2012	Subsea
Samurai	Green Canyon 432	2009	3,400	Anadarko	Appraisal	N/A	N/A
Santa Cruz	Mississippi Canyon 563	2009	6,515	Noble Energy	Development	2012	Subsea
Shenandoah	Walker Ridge 52	2009	5,750	Anadarko	Appraisal	N/A	N/A
Tiber	Keathley Canyon 102	2009	4,132	BP	Appraisal	N/A	N/A
Vito	Mississippi Canyon 984	2009	4,038	Shell	Appraisal	N/A	N/A
Wide Berth	Green Canyon 490	2009	3,700	Apache	Development	2012	N/A
Winter	Garden Banks 605	2009	3,400	Newfield	Appraisal	N/A	N/A
Appomattox	Mississippi Canyon 392	2010	7,290	Shell	Appraisal	N/A	N/A
Deep Blue	Green Canyon 723	2010	5,040	Noble Energy	Appraisal	N/A	N/A
Logan	Walker Ridge 969	2011	7,750	Statoil	Appraisal	N/A	N/A
Moccasin	Keathley Canyon 736	2011	6,739	Chevron	Appraisal	N/A	N/A
Santiago	Mississippi Canyon 519	2011	6,500	Noble Energy	Development	2012	Subsea
Mandy	Mississippi Canyon 199	2012	2,096	LLOG	Development	2012	Subsea
Coronado 2	Walker Ridge 98	2013	6,127	Anadarko	Appraisal	N/A	N/A
North Platte	Garden Banks 959	2013	4,400	Cobalt	Appraisal	N/A	N/A
Phobos	Sigsbee Escarpment 39	2013	8,500	Anadarko	Appraisal	N/A	N/A
Shenandoah 2	Walker Ridge 51	2013	5,750	Anadarko	Appraisal	N/A	N/A
Vicksburg	De Soto Canyon 393	2013	7,446	Shell	Appraisal	N/A	N/A
Katmai	Green Canyon 40	2014	2,100	Noble Energy	Exploration	N/A	N/A
Dantzer-2	Mississippi Canyon 782	2014	6,600	Noble Energy	Appraisal	N/A	N/A
Gila	Keathley Canyon 93	2014	5,000	BP/Conoco	Appraisal	N/A	N/A
Rydberg	Mississippi Canyon 525	2014	7,479	Shell	Exploration	N/A	N/A

Figure 3.15. Summary of major discoveries from 2008-2014 in the deepwater Gulf of Mexico (Halliburton Corp., 2010). N/A = Not Available

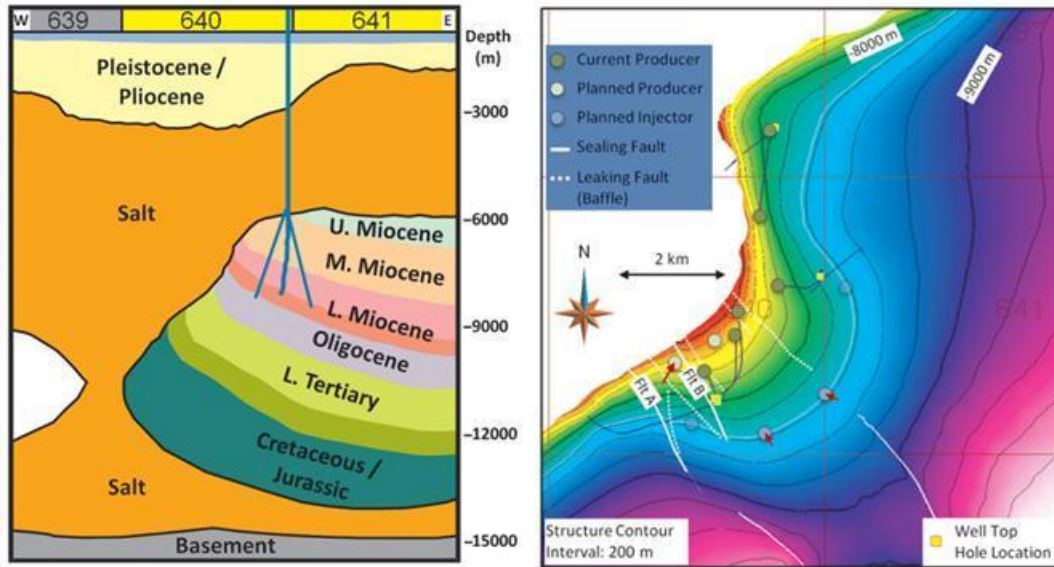


Figure 3.16. The structural model and map of the Tahiti field, Green Canyon Block 640, deepwater GOM (Swaston *et al.*, 2012).

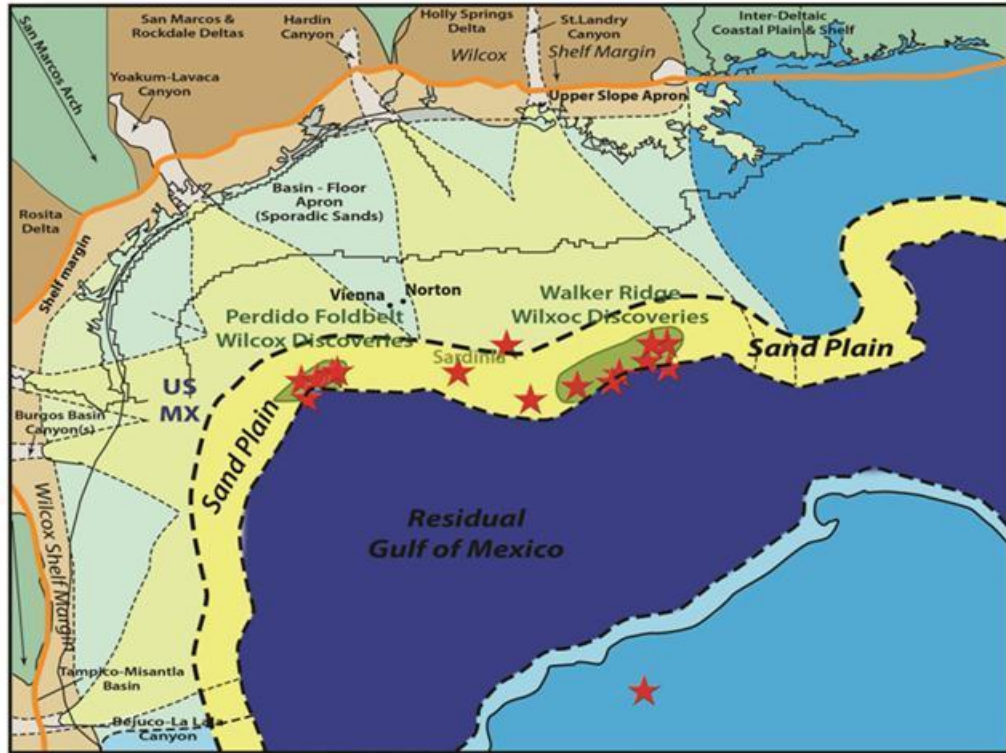


Figure 3.17. Lower Tertiary paleogeography and depositional styles in the northern Gulf of Mexico. Some discoveries are shown by red stars (Berman and Rosenfeld, 2007).

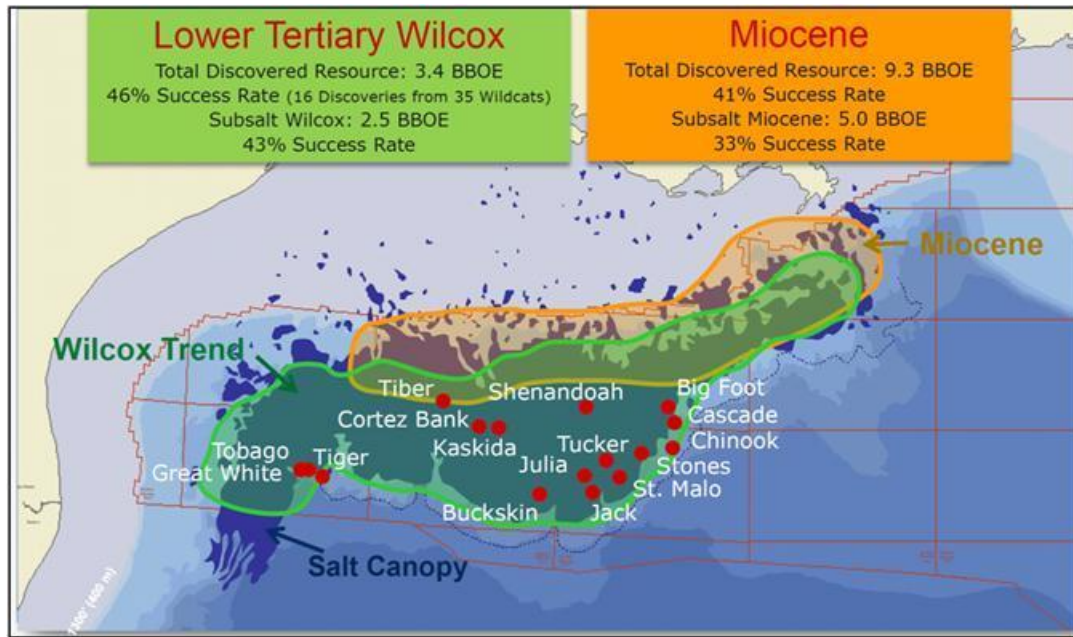


Figure 3.18. Wilcox discoveries and deepwater GOM resource potential (Chevron Corp., 2011). Orange color is the Miocene Trend, Green Color is the Paleogene (Lower Tertiary Wilcox) Trend, Deep purple color is the salt canopy, small red circles are key Paleogene fields.

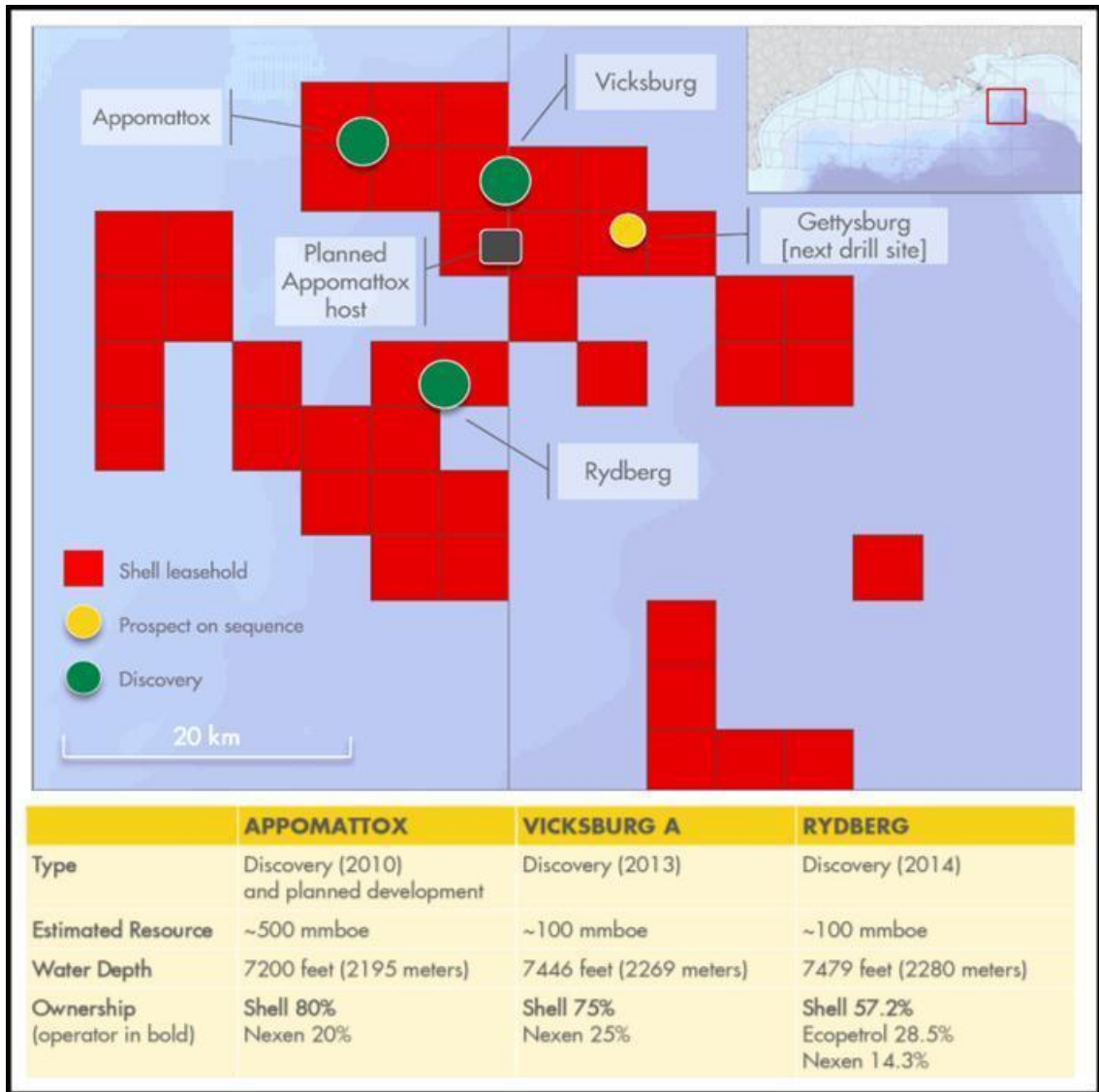


Figure 3.19. The Norphlet play area in the eastern Mississippi Canyon and Desoto Canyon and the three most important discoveries by Shell (Shell Oil Company, 2014).

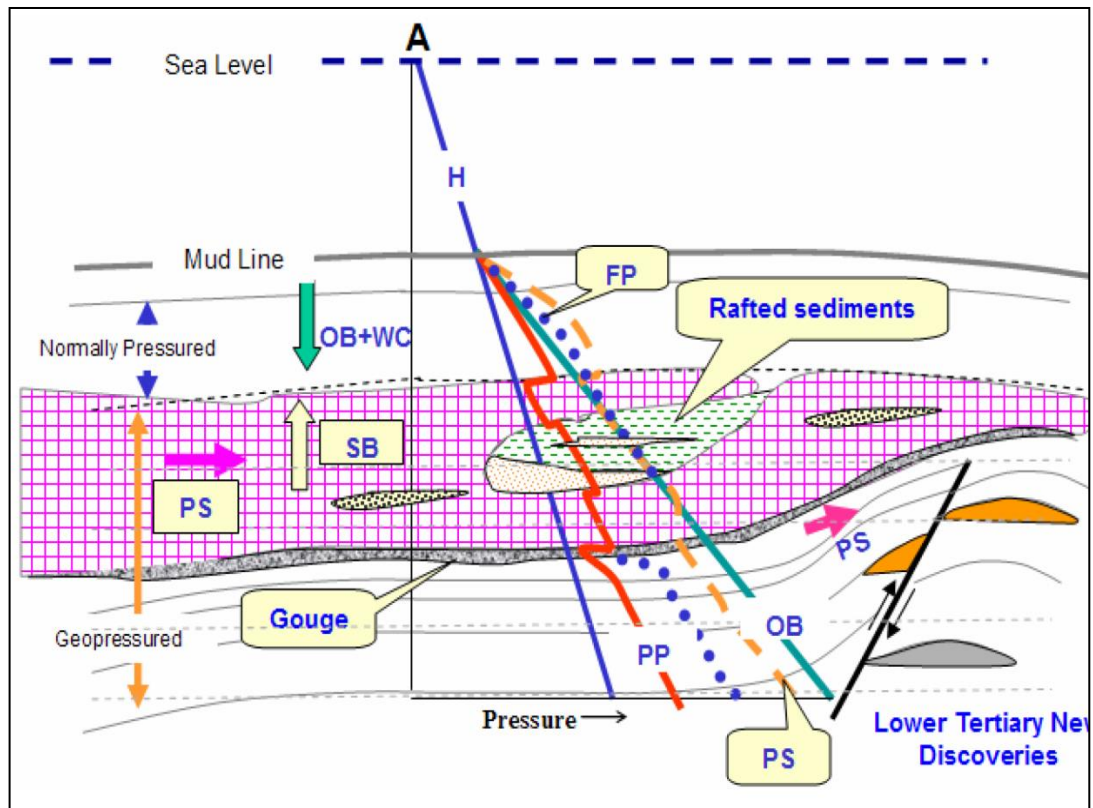


Figure 3.20. Summary of Wilcox pressure challenges (Shaker, 2010). PS = principle stress, FP= fracture pressure, OB = overburden, PP = pore pressure, SB = salt buoyancy

Jack & St. Malo: Deep Water Development Sanctioned in October 2010



Drill Rig *Cajun Express* performing the Jack Well Test

Conceptual Facility Design

Conceptual Subsea Design

- Emerging Lower Tertiary Wilcox trend discoveries with reservoir depths in the order of ~26,500 feet
- Co-development with subsea completions at each location flowing back >10 miles to a centrally-located semi-submersible facility
- Facility design initial capacity for 170,000 barrels of oil and 42.5 million cubic feet of natural gas / day
- Estimated >500 MMBOE of recoverable resources
- Startup: expected in 2014; Expected development cost: \$7.5 billion

Key Enabling Technologies

- Will be one of the largest hulls ever constructed
- Seafloor boosting for late field life operations
- Efficient multi-zone frac equipment for complex completions over very large reservoir intervals

28

Figure 3.21. Summary of the Wilcox reservoir development in Perdido fold belt (Chevron Corp., 2011)

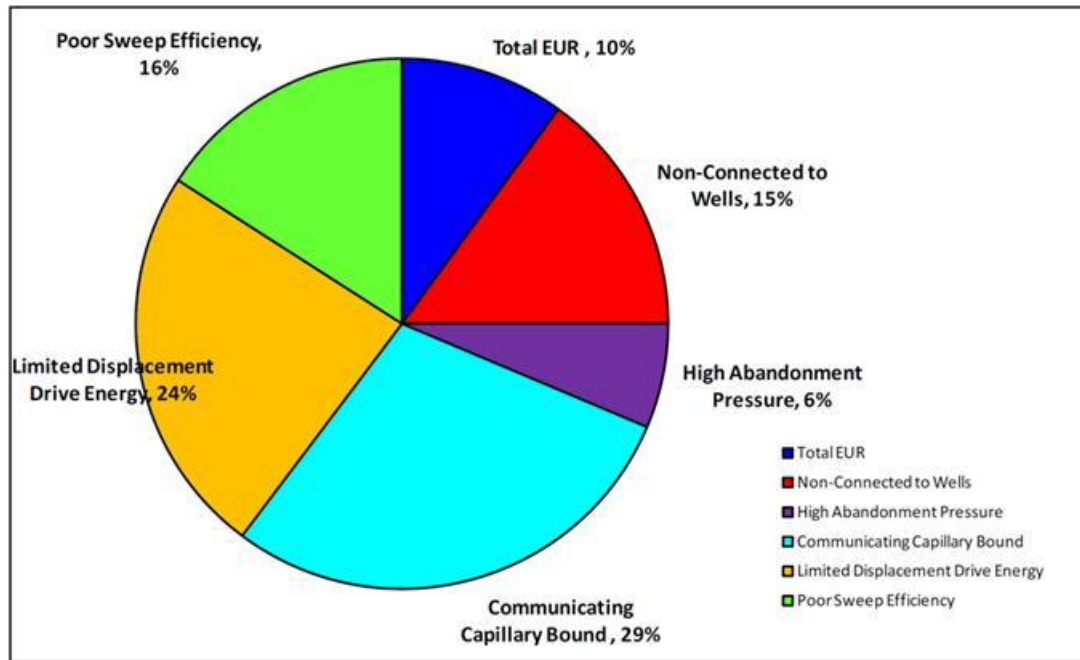


Figure 3.22. Major trapped oil mechanisms for Paleogene Wilcox reservoirs in dGOM (Lach, 2010).

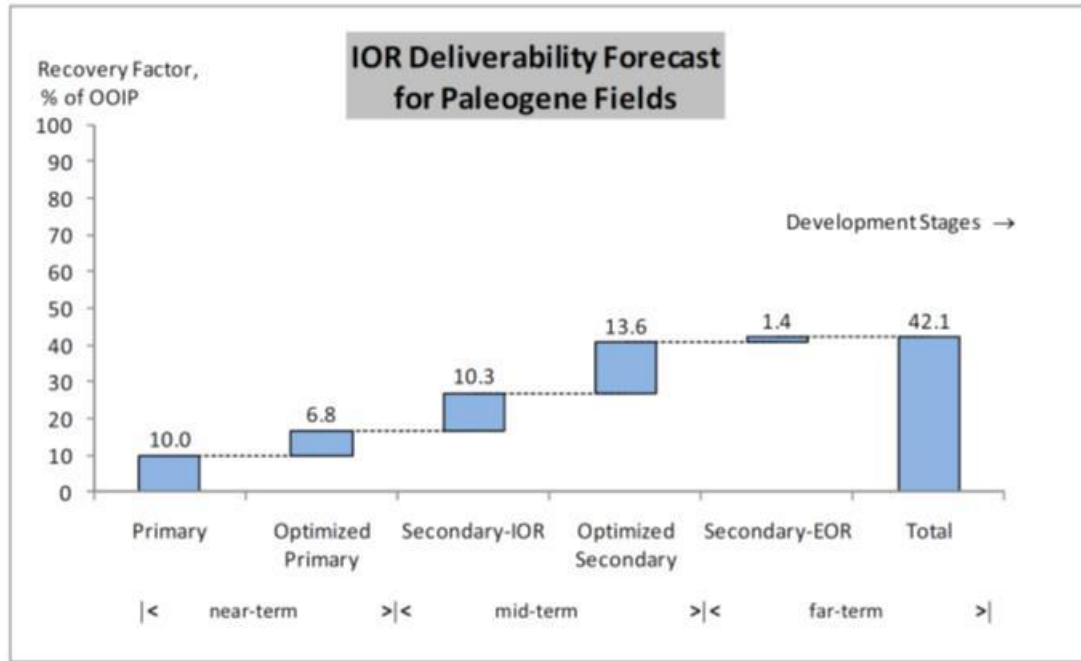


Figure 3.23. IOR deliverability forecast for Paleogene fields (Lach, 2010).

Total near-term, mid-term and far-term IOR can contribute up to 42.1% of oil recovery by forecast. From a practical standpoint, the IOR process during Wilcox reservoir development should use the technology having a mature technical level and lower costs. Among the methods mentioned above, conventional water flood, subsea multiphase pumping, conventional hydrocarbon gas injection, in well ESP, and directional or horizontal drilling have the highest “technical readiness level”, and they should be applied regularly during the reservoir development phase. In the IOR process ranking, conventional water flooding and subsea multiphase pumping rank the highest. A combination of these IOR methods will unlock the recovery step by step through near, mid to far term field life cycle. Ideally, the ultimate recovery factor through the life cycle of the field can be up to 42%.

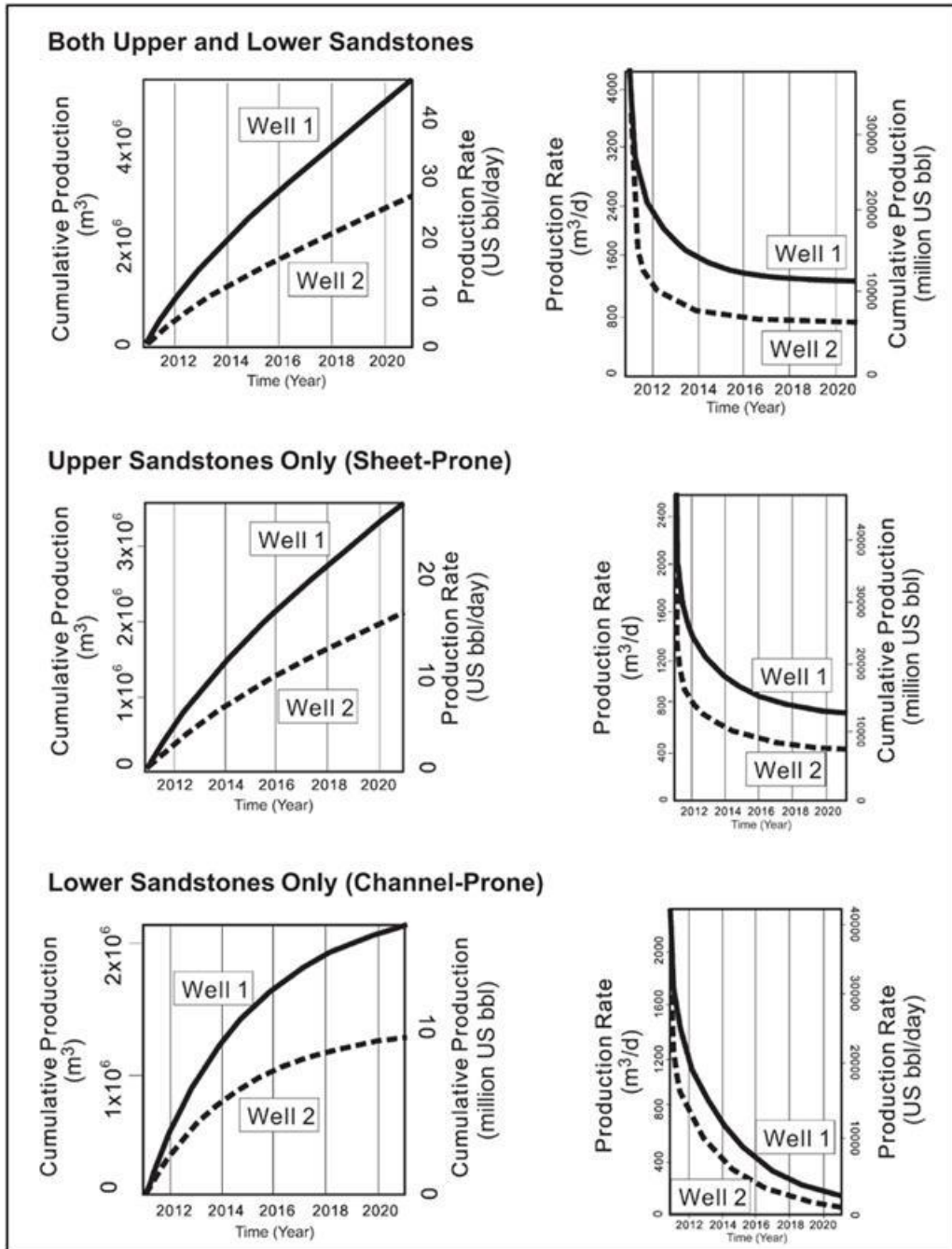


Figure 3.24. Reservoir simulation results from both upper and lower sandstones, upper sandstones only, and lower sandstones only, including cumulative production and production rate from producing well 1 (solid line) and well 2 (dashed line). Note that the (1) production volume and rate in well 1 is 60% more than those in well 2 in all cases; (2) the lower channelized sandstone package shows a larger drop in production rate than does the upper sheet sandstone; and (3) the upper sandstones are more sustainable during a 10-yr production period, whereas the rate of the lower sandstones is close to zero after 10 years (Zou *et al.*,2012).

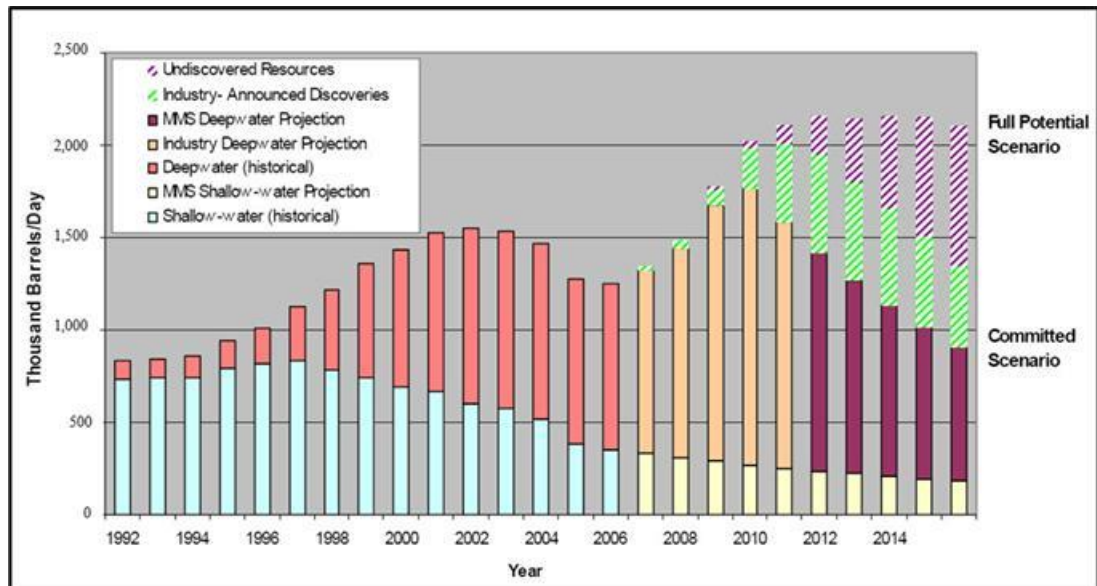


Figure 3.25. Oil production and prediction of dGOM (Paganie, 2009).

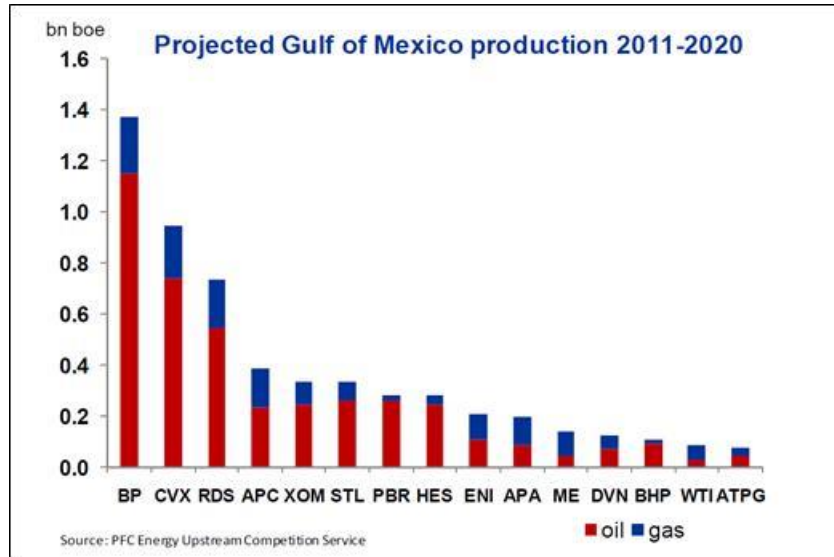


Figure 3.26. Production from 2010-2020 by companies (Wood Mackenzie, 2014). Bnboe = billion of barrels oil equivalent, BP = British Petroleum, CVX = Chevron Corporation, RDS = Royal Dutch Shell, APC = Anadarko Petroleum Corporation, XOM = ExxonMobil Corporation, STL = Statoil Corporation, PBR = Petrobras Corporation, HES = Hess Corporation, ENI = Eni Corporation, APA = Apache Corporation, ME = Murphy Oil Company, DVN = Devon Corp, BHP = BHP Corp.

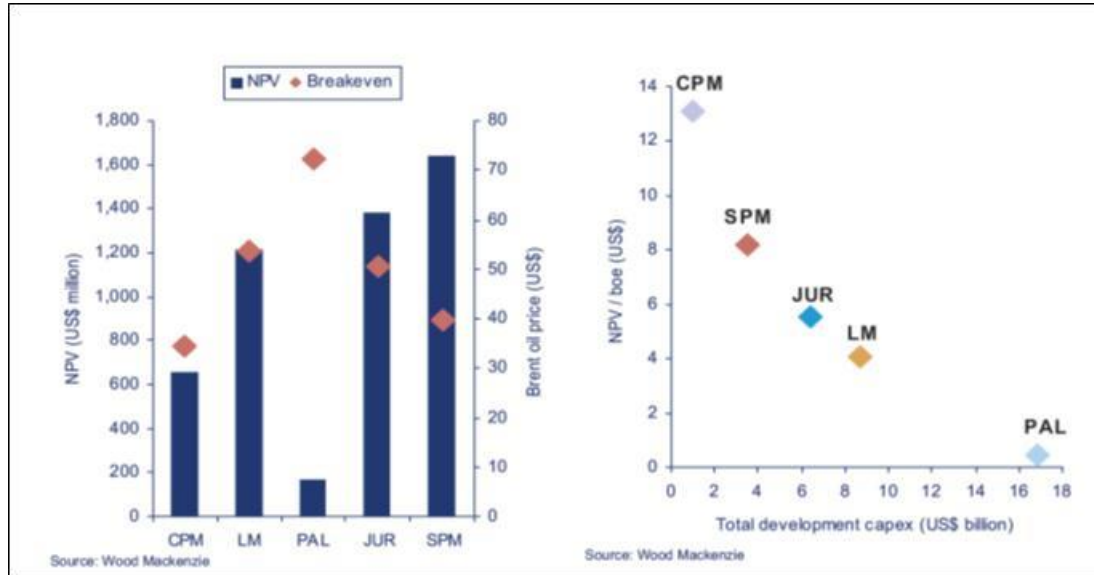


Figure 3.27. NPV and breakeven oil prices (left), and NPV/boe and total Capex (right) for deepwater GOM plays (Wood Mackenzie, 2014). BOE = Barrel of Oil Equivalent, NPV = Net Present Value

REFERENCES

- Bureau of Ocean Energy Management, Regulation and Enforcement (BOEMRE), Gulf of Mexico Oil and Gas Production Forecast: 2007-2016.
- Berman, A.E and J.H. Rosenfeld, 2007, A new depositional model for the deepwater Wilcox-equivalent Whopper sand - changing the paradigm, *World Oil*, Vol. 228, No.6.
- Daly, M. and A. Hopwood, 2011, Upstream break-out, Longer term investments, BP 2011 Results and Strategy Presentation.
- Dooley, T. P., M. R. Hudec, and M. P. A. Jackson, 2012, the structure and evolution of sutures in allochthonous salt, *AAPG Bulletin*, v. 96, no. 6, pp. 1045–1070
- Haughton, P.D.W., 2000, Evolving turbidite systems on a deforming basin floor, *Tabernas, SE Spain: Sedimentology*, v. 47, p. 497–518.
- Halliburton's, 2010, Deepwater Gulf of Mexico Map,
http://www.halliburton.com/public/solutions/contents/Deep_Water/related_docs/GOM_DWMap.pdf
- Lach J., 2010, IOR for Deepwater Gulf of Mexico, Improved Recovery: Phase I, RPSEA Project 1701 Final Report, pp. 1-329.
- Lewis, J., Clinch, S., Meyer, D., Lewis, J., Richards, M., Skirius, C., Stokes, R., and Zarra, L. 2007. Exploration and Appraisal Challenges in the Gulf of Mexico Deep-Water Wilcox: Part 1 – Exploration Overview, Reservoir Quality, and Seismic Imaging. Presented at the 27th Annual GCSSEPM Foundation Bob F. Perkins Research Conference, Houston, Texas, 2-5 December.

- Mathur, V., 2008, The emerging Paleogene play: Deepwater Gulf of Mexico, 19th World Petroleum Congress, Spain 2008, Forum 01: New frontier exploration.
- Meyer, D., L. Zarra, D. Rains, B. Meltz and T. Hall, 2005, Emergence of the Lower Tertiary Wilcox trend in the deepwater Gulf of Mexico, *World Oil*, Vol. 226, No.5.
- Mount, V. S., K. Dull, and S. Mentemeier, 2007, Structural style and evolution of traps in the Paleogene play, deepwater Gulf of Mexico, in L. Kennan, J. Pindell, and N. C. Rosen, eds., *The Paleogene of the Gulf of Mexico and Caribbean basins: Processes, events, and petroleum systems: Proceedings of the SEPM Gulf Coast Section, 27th Annual Research Conference, Houston, Texas*, p. 54–80.
- Pilcher, R.S., B. Kilsdonk, J. Trude, , 2011, Primary basins and their boundaries in the deep-water northern Gulf of Mexico: Origin, trap types, and petroleum system implications, *AAPG Bulletin*, V. 95, No. 2, P. 219–240.
- Pyles, D.R., J.P.M. Syvitski, R.M. Slatt, 2011, Defining the concept of stratigraphic grade and applying it to stratal (reservoir) architecture and evolution of the slope-to-basin profile: An outcrop perspective: *Marine and Petroleum Geology*, 28(3), p. 675-697.
- Sawyer, 2006, Seismic geomorphology, lithology, and evolution of the late Pleistocene Mars-Ursa turbidite region, Mississippi Canyon area, northern Gulf of Mexico, Master Thesis of the Pennsylvania State University, pp. 1-200.
- SEPM STRATA Website, Deepwater Element Architect, <http://www.sepmstrata.org/page.aspx?pageid=39>.

- Siegele, P., 2007, Deepwater Gulf of Mexico presentation in Merrill Lynch global energy conference, Chevron Corporation.
- Shaker, 2008, Dirty vs. clean salt: their impact on the subsalt Wilcox deepwater exploration plays, Gulf Coast Association of Geological Societies Transactions, v. 59, p. 689-696.
- Slatt, R.M., C.G. Stone, and P. Weimer, 2000, Characterization of slope and basin facies tracts, Jackfork Group, Arkansas, with applications to deepwater (turbidite) reservoir management, in Weimer, P., Slatt, R.M., Coleman, J. L. Jr. and., Bouma, A.H (eds.), Deep-water reservoirs of the world, Gulf Coast Sect. Soc. Econ. Paleon. & Mineral. Found. 20th Ann. B.F. Perkins Research Conference, p. 940-980.
- Sullivan, M. D., J. L. Foreman, D. C. Jennette, D. Stern, G. N. Jensen, and F. J. Goulding, 2004, An integrated approach to characterization and modeling of deep-water reservoirs, Diana field, western Gulf of Mexico, in Integration of outcrop and modern analogs in reservoir modeling: AAPG Memoir 80, p. 215–234.
- Swanston, A. M., M. D. Mathias, and C. A. Barker, 2011, Subsalt Exploration and Development: Wide-azimuth TTI imaging at Tahiti: Reducing structural uncertainty of a major deepwater subsalt field, Geophysics, September, v. 76, p. WB67-WB78
- Thurston, S., 2011, Chevron Overview: OE, Global Upstream and Deepwater Gulf of Mexico, Citigroup Deepwater Houston Tour, Houston, TX.

Zou, F., R.M. Slatt, R. Bastidas, and B. Ramirez, 2012, Integrated outcrop reservoir characterization, modeling, and simulation of the Jackfork Group at the Baumgartner Quarry area, western Arkansas: Implications to Gulf of Mexico deep-water exploration and production, AAPG Bulletin, vol. 96, no. 8 (August 2012), pp. 1429-1448.

**Chapter 4: Relationship between Bioturbation, Microfacies and
Chemostratigraphy, and Its Implication on the Sequence Stratigraphic
Framework of the Woodford Shale, Oklahoma***

Fuge Zou^{1,2}, Roger Slatt¹

¹ConocoPhillips School of Geology and Geophysics, University of Oklahoma, Norman,
Oklahoma

²Marathon Oil Company, Oklahoma City, Oklahoma

**Part of this chapter has been accepted by:*

*Unconventional Resources Technology Conference (UrTEC) 2015, July 20-22, San Antonio,
Texas.*

*This paper is also going to be submitted to **AAPG Bulletin** after final editing and permission
from Marathon Oil*

ABSTRACT

The nanoscale porosities in shales have been widely studied by industry with emphasis on organo-porosity and its significant in migration (and generation) of hydrocarbons. However, less attention is paid to the next scale up, which would include burrows to provide potential migration pathways. The original intent of the work was to evaluate whether burrows were sufficiently abundant and interconnected to provide permeability pathways at the scale of the burrows. The final goal turned out to be comparing all the bioturbation types and abundance to reservoir properties.

The Devonian-Mississippian Woodford Shale in the Anadarko basin, Oklahoma has been one of the major unconventional plays in the United States for nearly a decade. This research has utilized ultra-high-resolution (625 micron increment per slice) and advanced 3-D Micro-CT scan technology to quantitatively describe and analyze the ichnofacies and microfacies in selected Woodford cores. The results of bioturbation analysis were tied to related data (chemostrata, XRD, SEM, geochemical analysis, and well logs etc.) to build a detailed sequence stratigraphic framework to correlate to the most productive zones for unconventional resources potential.

The ichnofacies in the Woodford Shale cores has been categorized into short and long *Chondrites*, *Paleodictyon*, *Thalassinoides* and *Planolites*. The 3-D geometries, abundance, and diversity of ichnofacies have been quantitatively described using Avizo Fire software. Bioturbation Index (BI) was calculated from the sum of the abundance of all ichnofacies in each stratigraphic interval. The BI was then compared with XRF data (including Al, Si, Ti, Zr, Mo, and U), XRD data (including quartz, clay, feldspar, pyrite, and dolomite) and geochemistry data to relate ichnofacies, paleo-redox environment, and sediment provenance. The stratigraphic distributions of these properties were found to be related to sea-level fluctuation, biostratigraphy from *Conodonts*, and sequence stratigraphy.

Our results indicate that bioturbation and bio-activities are more common in Woodford Shale than previously thought. But they are not sufficiently abundant and vertically interconnected to provide permeability pathways at the scale of the burrows. However, in some core sections, the horizontal burrows are sufficiently connected. There is not much in the way of vertical connectivity of burrows, but along some

bedding planes there are enough touching burrows to make a permeability pathway. Although burrows frequently develop in highstand systems tracts, they also occur in presumably anoxic environments conducive to preservation of high TOC content and biogenic quartz. These relationships can aid in targeting the best horizontal landing zones in the Woodford Shale.

INTRODUCTION

The nanoscale porosity in shales has been widely studied by industry with emphasis on organo-porosity and its significant in migration (and generation) of hydrocarbons (Loucks *et al.*, 2009; Slatt and O'Brien, 2011; Slatt *et al.*, 2012; Loucks *et al.*, 2012; Erdman and Drenzek, 2013; Slatt and O'Brien, 2014). However, less attention is paid to the next scale up for unconventional shales, which would include burrows to provide potential migration pathways. In addition, the abundance of smaller fractures are lithology dependent (brittle chert vs. ductile clay-mudstone), which would be the next scale up from the burrows. This feature at the microscale has also been largely neglected. The original intent of this work was to evaluate whether burrows were sufficiently abundant and interconnected to provide permeability pathways at the scale of the burrows.

The Devonian-Mississippian Woodford Shale in the Anadarko basin, Oklahoma has been one of the major unconventional plays in the United States for nearly a decade. To fully understand the distribution of the play and the best way to develop its remaining resources, a detailed sequence stratigraphic framework is needed from various disciplines. Methods such as routine core analysis, organic geochemistry,

chemostratigraphy, X-Ray Diffraction, SEM and Micro-CT scan are quite popular today in the unconventional energy industry. And we use applied these technologies to study in Woodford cores.

Since 2010, three key Woodford cores and numerous subsurface data (borehole images, well logs and 3-D seismic, Figure 4.1) have been collected by Marathon Oil Company that covered from proximal to distal parts across Anadarko basin based on our interpretation. Based on these data, this study is focused on characterizing these cores with emphasis on chemostrata, bioturbation, and depositional environments. Quantitative analysis on the relationship between bioturbation, micro-fossils and chemostrata further constrains the sequence stratigraphic framework from conventional methods such as well log interpretation, geochemical analysis or core description.

Chemostratigraphy, which has close connection to the depositional and paleoredox environment (aerobic, dysaerobic, and anoxic), has been widely used in the unconventional shale industry (Ratcliffe *et al.*, 2012; Mu *et al.*, 2013; Slatt *et al.*, 2015). Such a workflow has been proven to be an effective way to correlate shale sequences over long distances and to help geosteering of horizontal wells such as in the Eagle Ford play. Tribovillard *et al.* (2006) and Mu *et al.* (2013) summarized key elements and proxies used as paleoredox and productivity indicators. These proxies serve as a foundation of chemostrata analysis in shale. A few key elements, such as Mo, U, Th, Ni, Ti and V can indicate the paleo-environment of the (bottom) sea water, which has a major impact on bioactivities.

Trace fossils, or ichnofacies, are most commonly used to differentiate relative bottom-water oxygen levels and to discriminate anoxic, dysoxic, and oxic settings

preserved in Phanerozoic strata (Boyer and Droser, 2011). Traditionally, to study the 3-D ichnofacies with 2-D thin-sections and core cuts was always challenging. As more core data and advanced technology has become available in recent years, the study of bioturbation and ichnofacies has gained more attention in unconventional shale research. La Croix *et al.* (2012) used conceptual 3-D flow models of different trace fossils, which indicated that only 0-10% (volume) of bioturbation in a rock can greatly increase the horizontal and vertical connectivity. Bednarz and McIlroy (2012) used a serial grinding method to conduct a 3-D volume reconstruction of *Phycosiphon*-like burrows and investigates the possible fluid-flow paths caused by the ichnofabric. They concluded that the increased quartz content in burrows in their samples could increase the porosity and permeability by 13%-26% relative to undisturbed matrix. LaCroix *et al.* (2013) applied the spot-minipermeameter and micro-CT methods to quantify the dual-porosity and its relationship between bioturbation index and permeability. They further proved their model to support an arithmetic mean of flow contributions between bioturbation and permeability. Despite their abundance, economic importance and these recent studies, mudstones that were deposited under reduced bottom-water oxygen conditions remain poorly understood (Boyer and Droser, 2011; Spaw, 2013).

The research described in this paper has utilized ultra-high-resolution (625 micron increment per slice) and advanced 3-D segmentation and visualization technology to quantitatively describe and analyze the ichnofacies and microfacies in the Marathon Oil Woodford cores. We then correlated the results with all other related sources of data (chemostrata, SEM, geochemical analysis, geomechanics and well logs

etc.) to build a detailed sequence stratigraphic framework to better define the most productive zones for unconventional resources potential.

THE WOODFORD SHALE BACKGROUND

There is an industry and academic consensus that the Woodford Shale can be divided into three informal members referred to as the Upper, Middle and Lower Woodford (Slatt *et al.*, 2011, Figure 4.2). The Lower Woodford member (0-150ft thick) is primarily a black and silty claystone deposited during the beginning of transgression (back-fill sequence), thus it has the least areal extent. The Middle Woodford (0-200 ft thick) consists of a black, less silty claystone that has the highest overall Total Organic Carbon (TOC) content. It was deposited as a condensed section and has the greatest aerial extent. The Upper Woodford (0-150 ft) consists of a gray-black silty claystone with phosphate and calcareous nodules (Figure 4.2). It is interpreted to be a progradational highstand deposit during which the rate of deposition exceeded the rate of sea level rise, leading to a shallowing of marine waters (Slatt and Abousleiman, 2011; Chain, 2012; Slatt, 2013). However, such a generalized classification can be oversimplified such that: (1) log correlation may disagree with other data such as geochemistry, geomechanics, core analysis, and biostratigraphy; (2) the generalized members boundaries may not follow time equivalent (biostratigraphic) surfaces; and (3) intervals with lateral heterogeneity, such as the discontinuous Lower Woodford, are hard to correlate across the Anadarko basin (Spaw, 2013). Therefore, combinations of various data are needed in order to develop a reasonable, accurate and applicable sequence stratigraphic framework.

Slatt (2013) proposed the sequence stratigraphic framework of the Woodford Shale. The entire age of the Woodford covers a 29Ma time span from 388-359 million years ago, which is interpreted as a complete 2nd order depositional sequence. There are also several 3rd order sequences within the 2nd order sequence. The most significant transgression occurs at the Frasnian-Famennian boundary at about 372Ma. It is also defined as the lower part of the Middle Woodford. Above this boundary, the Woodford sequence shifts from transgressive to regressive deposition, resulting in the generally chert rich, nodular Upper Woodford regressive (highstand) interval.

Alternatively, Hemmesch *et al.* (2014) proposed that the entire Woodford is a second-order sea level fall with multiple third-level highstand shedding into the Permian Basin.. The stratigraphic progression is from organic-rich mudstone with no or little bioturbation, upward to heavily bioturbated, organic-poor mudstone. The paleo-environment shifted from a marine organic assemblage in the Lower Woodford and most of the Middle Woodford to a terrigenous-rich assemblage in the upper part of the Middle Woodford and the Upper Woodford. Hemmesch *et al.* (2014) also claimed to find no evidence of a major transgression with high clay or organic matter input. The reason for the discrepancy between the Woodford sequence stratigraphy in the Permian Basin and Anadarko Basin is unanswered. Thus a multi-disciplinary analysis is needed to study the similarities and differences in the Woodford deposited in these two basins, as well as in other basins within Oklahoma.

METHODS OF STUDY

The new Micro-CT scan and true 3-D processing and visualization technology using Avizo Fire™ provided a revolutionary tool to study the Woodford Shale. Through this technology we can conduct quantitative characterization and analysis on bioturbation and ichnofacies distribution. It bridges the gap between nanometer-micrometer scale features measured from SEM and conventional thin sections to the scale of human eyes. In our case, a full 3-D scale of bio-activity and microfacies leads to a more accurate sequence stratigraphic framework and interpretations of paleoenvironments than traditional core descriptions. The Micro-CT scan we use is a 0.625 millimeter per vertical scan, which is 1600 scans per meter of core (or 488 scans per foot of core). The 3-D visualization and analysis on the Micro-CT scan data are to characterize: 1) intensity of bioturbation (or Bioturbation Index, BI), which is defined by the abundance of all observed trace fossils over the entire core; 2) diversity and facies variance; 3) relative burrow diameter, length, geometry, density; and 4) succession of bioturbation colonization styles.

Fluctuations in the dysaerobic or oxygen-minimum zone (by whatever mechanism) contribute to periodic introduction of oxygen into a basin (Jordan, 1985). Boyer and Droser (2011) studied the Devonian trace and body fossils in marine black shale using a high resolution 2-D approach directly on outcrops in New York State, USA. Their classification and analysis serve as a good analog for the Woodford. By describing the trace and body fossils in outcrops on a centimeter scale, they established the relationship between bottom water oxygen conditions and the relative amount of bioturbation, estimated as an ichnofabric index (ii), maximum burrow diameter measurements and body-fossil species diversity. One significant observation they made

is that the bottom-water oxygen levels, associated with trace fossils present, fluctuated considerably within a narrow stratigraphic range (on a centimeter scale). This observation coincides well with our observation in the Woodford, as micro CT-scan can further extend the scale into millimeters in 3-D. In addition, the source of the oxygen which allowed burrowing animals to thrive in the sediments was possibly short-lived turbidity currents (Griffith, 1977).

Regionally in North America, the diversity of ichnofacies in Devonian black shales is low (Jordan, 1985; Boyer and Droser, 2011; Spaw, 2013). Only four ichnofacies were identified in the studied cores with confidence: *Chondrites*, *Planolites*, *Paleodictyon*, and *Thalassinoides*. Using the three Woodford core micro-CT-Scans, we described and classified the generalized ichnofacies into the following types:

Chondrites

Chondrites are root-like burrows, and one of the most common ichnofacies in the Woodford Shale (Figure 4.3 and 4.4). It consists of a horizontal to slightly inclined burrow system exhibiting branching (up to several orders) from a main stem (Jordan, 1985). It has been interpreted as the trace of a deposit-feeding sipunculid worm having a retractable proboscis which allowed the animal to work from a fixed point to efficiently mine the substrate for food (Simpson, 1956). In all cases *Chondrites* represents simple, shallow feeding burrows (Jordan, 1985). They were given different type designations (A, B, C and D) depending on their sizes (Jordan, 1985). Often in the Woodford Shale, *Chondrites* are relatively small (several millimeters to several centimeters long), and are typically 1 mm in diameter (ranging from 0.2 to 1.3 mm).

Spaw (2013) classified them into short versus long *Chondrites*. The burrow systems are filled with either mud similar to the surrounding sediment or silt without any internal structure. They are commonly associated with *Planolites* (Boyer and Droser, 2011). In some cases in the Woodford, its monospecific association is indicative of low oxygen conditions (Spaw, 2013).

Theoretically, the 3-D images of the *Chondrites* are branched and root like pipes in different sizes. However, in the Woodford cores, the short *Chondrites* (Figure 4.3) are the dominant ichnofacies. Often they are characterized by small (millimeter scale), irregular and isolated objects, which could be misidentified as radiolarian in cherts without knowing the context. Long *Chondrites* (Figure 4.3) are much less frequent, and their size can reach up to 3-5cm. Sometimes it is difficult to differentiate Long *Chondrites* from *Planolites*. The major difference of these two ichnofacies is whether they are branched and straight (*Chondrites*) or unbranched and curved (*Planolites*). In addition, *Chondrites* are sometimes dimmed (lack of contrast between burrows and matrix) in the argillaceous matrix and may not be resolvable by 3-D micro scan. In order to better detect them, it is needed to analyze on indirect evidence such as discrete laminations in thin sections (Figure 4.4).

Paleodictyon:

Paleodictyon is one kind of grazing trace on bedding planes that often co-exists with short *Chondrites* in deep water. By definition, it contains both an irregular and regular network of polygons resulting from systematic feeding along the bedding plane. In our analysis on micro-CT scan image (Figure 4.5), the *Paleodictyon* are "cookie" like

shaped bodies which usually have 2-3cm extension along the bedding planes. Most *Paleodictyon* are irregularly shaped without a specific orientation. Some of them are elongated, and some of them are more rounded. The aspect ratio (length/width) of these shapes are often less than 3:1.

Planolites

Planolites are also common in the Woodford Shale cores, but they are less common than *Chondrites* and *Paleodictyon*. It consists of horizontal to sub-horizontal, meandering and unbranched tubes, which are circular in cross section where uncompacted. It has been interpreted as the burrow of deposit-feeding worms (Jordan, 1985). The length of *Planolites* ranges from 1.25-17.5 cm and the diameter of burrows ranges between 0.25-1.25cm (Jordan, 1985). Although they are present in association with and crosscut all other ichnofacies recognized in the Woodford units (Boyer and Droser, 2011). The *Planolites* tend to be monospecific, which indicate low oxygen conditions (Spaw, 2013).

Figure 4.6 shows one example of *Planolites* ichnofauna in a micro-CT-Scan at 30-31 ft (9.5m) of Well A (top of the Middle Woodford). This example illustrates the advantage of 3-D imaging. One circular feature on the horizontal slice and several light gray dots on the vertical slice are seen with the 2-D images only (Figure 4.6, left). The 3-D images provide more detail of the *Planolites* including geometry, density and distribution. The *Planolites* are mostly horizontal burrows. Figure 4.7 is another example from 222ft (67.5m) of Core C. A major curved *Planolites* burrow is parallel to the bedding plane. Only a tiny piece of the burrow can be seen on 2-D vertical section

of the Micro-CT image, while the 3-D processing revealed the detail of the burrow associated with nearby barite and chert grains.

Figure 4.8 shows another example that *Planolites* co-developed with *Grazing Trails* (*Paleodictyon*) at 181ft (55m) in Well C (Middle Woodford) (red arrow). The lower burrow (indicated by red arrow) shows a sub-vertical geometry which are crossing a bedding plane. This is the only interval with sub-vertical burrows observed in Woodford Cores. This interval has very high quartz content (71wt.%). High quartz content and sub-vertical burrows may be the causes of high porosity (8.5%) and permeability (115,000 nd) measured for this interval. Another good example is a bioturbated interval at 98ft (30m) in Core C (Figure 4.9), which is a dolo-mudstone interval (38 wt.% dolomite) near the base of the Middle Woodford. Both 2-D and 3-D images indicate a good straight *Planolites* burrow. There are also 2-3cm thick chert beds above and below the burrow. This interval has low measured porosity (4.4%) and permeability (2990 nano-darcy). Organic content is also low. The interval is interpreted as the shallower water environment right above Frasnian-Famennian Boundary.

Thalassinoides

Thalassinoides belongs to the *Cruziana* ichnofacies. They are usually found in shallow marine, sub- to intertidal environments below wave base and above storm base. The presence of *Thalassinoides* often indicates quiet offshore environment with strong bioturbation activities. In Woodford Shale, the *Thalassinoides* are present in the Lower Woodford, and they are well recognized in Core B and C. The geometries are characterized by sandglass shape with the vertical burrow from 2-5cm. The materials filled in the vertical burrows are coarser grained than the surrounding matrix, with occasionally pyritized

framboids (Figure 4.10). No *Thalassinoides* has been found in Middle and Upper Woodford Shale, which imply that the Lower Woodford has unique shallower-water depositional environment.

Radiolarian Chert and Fecal Pellets

Radiolaria in cherts can be easily seen in segmentation images of Micro CT-Scan data. They are dense, small and spherical objects of millimeter scale that are scattered in 3-D space (Figure 4.11). They are often pyritized and can be easily recognized in core. The spherical geometry often helped to differentiate them from short *Chondrites*. Fecal pellets are also important spherical features in the Woodford Shale (Slatt and O'Brien, 2011; Chain, 2012). However, they often are of smaller size than radiolaria in cherts. In general, they are less than 1mm, which are smaller than the detectable range of Micro CT-Scan. The fecal pellets are better resolved using SEM methods (Slatt *et al.*, 2011; Chain, 2012).

Nodules

Phosphate and chert nodules are common features in the Upper Woodford. Their 3-D geometry can also be thoroughly resolved using segmentation of Micro-CT scan. They are interpreted to represent very shallow, low energy environments in the shelf of the Anadarko basin. The segmentation of Micro-CT scan can filter other noisy features such as artificially induced fractures, chips and cements, leaving only the 3-D bodies of the nodules (Figure 4.12). The nodules represent the large sea-level drop at the Early Mississippian boundary.

THE WOODFORD CORE STUDY

The three Woodford Shale cores collected by Marathon Oil Corporation in the past five years cover the proximal and distal parts of the northern Anadarko Basin in western central Oklahoma (Figure 4.1). Core A is located on the proximal shelf of the Anadarko basin with a 82ft (25m) thick Woodford section. Core B is located at the middle shelf with 202ft (61.5m) of Woodford section. Core C is located in the distal portion with 372ft (113.5m) of Woodford section. Core A and B have been studied by Chain (2012) using conventional thin section, SEM and organic geochemistry analysis within a preliminary sequence stratigraphic framework. These three cores were also studied by Hlava (2013) with emphasis on sedimentary features and micro-facies. Spaw (2013) conducted a revolutionary study on of the three Woodford cores using the micro-CT scan technology. Four main types of ichnofacies were identified: *Paleodictyon*, *Chondrites*, *Planolites* and *Thalassinoides*. Based on this previous work, Micro-CT scan data were input into the Avizo Fire™ software packages for 3-D processing, segmentation and rendering. Although such technology has been used in other basins, its application to the data produced the first clear and detailed, true 3-D geometry of the ichnofacies in the Woodford Shale of the Anadarko Basin.

Lithofacies and Ichnofacies of the Woodford Shale

The lithofacies of the Woodford cores have been defined by Slatt *et al.* (2011); Chain (2012); Hlava (2013); Spaw (2013); Mann (2014) and Hemmesch *et al.* (2014). Spaw (2013) pointed out that the lithofacies of the Woodford Shale are difficult to be defined and classified with traditional core description because: 1) they are very dark;

2) they are difficult to sample due to fissility; 3) many features are beneath normal resolution of standard petrographic equipment; and 4) different scales of sedimentary features are mixed which often requires upscaling. The descriptive terminology such as “fissile”, “massive” or “laminated” are not diagnostic to differentiate different shales (Hemmesch *et al.*, 2014).

Based on thin section petrology and X-ray diffraction data, there are 5 microfacies related lithologies defined by Spaw (2013). These are: (1) kerogen-rich, radiolarian-bearing, argillaceous chert; (2) agglutinated forams and transported debris-rich mudstone with laminae; (3) kerogen-rich, argillaceous, detrital silt-rich mudstone; (4) dolomitic, kerogen-rich, argillaceous, Tasmanites-rich mudstone; and (5) agglutinated foram mudstone.

Hemmesch *et al.* (2014) simply classified the Woodford lithology into organic-rich mudstone, radiolarian-rich lamina, dolomite or limestone, and chert. The Woodford Shale has a high quartz content ranging from 31-80% by volume, and the clay content varies from 6-32% by volume, with an average of 18% (Spaw, 2013). There are 3 types of quartz based on thin sections: (1) diagenetic chert (crystalline chert) dominates the Upper Woodford; (2) biogenic (radiolarian) quartz mudstone dominates the Middle Woodford; and (3) extrabasinal detrital quartz silt that dominates the Lower Woodford (Spaw, 2013).

The term mudstone covers a wide variety of rock components, fabrics and textures. It is the most common lithofacies in the Woodford Shale (more than 85%). Gamero-Diaz *et al.* (2012) proposed an effective classification scheme for organic mudstones based on bulk mineralogy (Figure 4.13). We plotted our XRD mineralogy

data from Core A, B and C on a Ternary diagram to show how Lower, Middle and Upper Woodford Shale fall into their categories. As the plot (Figure 4.13 Lower) indicates, most of the Woodford Shale are (mixed) siliceous shale. Only a few samples are (mixed) carbonate shale and NONE of the mudstones are in argillaceous mudstone categories.

For the purpose of this study, the lithofacies are divided into six mudstone categories or facies unit and classified as:

1. Organic-rich Mudstone

In core it is often dark to dark gray, laminated shales, that are soft and contain very high TOC (often times >6 weight %). Thin-sections often reveal the presence of *Tasmanites*.

2. Siliceous Mudstone

The siliceous mudstone category is further divided into two types of mudstones with high quartz content: radiolarian chert-rich and detrital quartz-rich. The detrital quartz grains are more frequent in the Lower Woodford while the radiolarian cherts are more common in the Middle and Upper Woodford. Radiolarian chert-rich mudstone tend to have the 2nd highest TOC content next to organic rich mudstone, and they are often interbedded with each other. Detrital quartz mudstone, common in the Lower Woodford, often has lower TOC values due to the abundance of quartz grains diluting the concentration of organic matter.

3. Nodular Chert Mudstone

The nodular chert mudstone consists of phosphate and chert nodules which usually occur in the Upper Woodford. Trace fossils are mostly absent in this facies.

Other micro-fossils and bioactivities are also rare or absent when phosphate nodules are present. This facies possibly represents a life-free zone, which is a typical character of the Upper Woodford.

4. Bioturbated Mudstone

In general, bioturbated mudstone often correlates to higher bottom water oxygen levels, lower TOC and lower reservoir quality (lower porosity and permeability). However, in some cases in the Middle Woodford, bioturbation can be correlated to the presence of higher TOC.

5. Silty Mudstone:

This facies is often present in the Lower Woodford with high detrital quartz content.

6. Dolomitic Mudstone:

In the Middle and Upper Woodford there are some dolomitic beds in the mudstone matrix as determined from X-ray diffraction data. The presence of dolomitic materials in the mudstone can indicate a shallow water (sub-tidal) environment. The water depth of Woodford time is not as deep as we previously thought. The dolomitic material is interpreted to be transported from the shelf during highstand (Spaw, 2013).

In addition to lithology, the relationship between the lithofacies and depositional environment has been interpreted by Hlava *et al.* (2013) and Spaw (2013). Their work shows that from the proximal Anadarko shelf (northeast) to the distal Anadarko basin (southwest), both detrital sediment and bulk density decreases while the total organic carbon (TOC) and biogenic quartz increases. In an offshore shelf environment, the lithofacies are dominated by bioturbated siltstone, silty, and siliceous mudstones. In

hemi-pelagic slope environments, the lithofacies are dominated by bioclastic mudstone with agglutinated forams and medium radiolarian cherts. The most distal pelagic environment is dominated by laminated (banded), siliceous mudstone, with fewer forams but more radiolarian cherts with higher TOC. There also were bottom currents and minor turbidite flows associated with these lithofacies, resulting in cross beddings and ripples.

Based on an integrated study on the Woodford core, we proposed a slope-to-basin depositional model within a sequence stratigraphic framework (Figure 4.14). It captures the lateral facies variations and the processes that are active in different portions of the basin. Thin-section photos of representative lithofacies seen in the interval are shown in Figure 4.14. Each individual micro-facies and trace fossils (mainly *Paleodictyon* and *Chondrites*) have been correlated to certain depositional environments, which helps to then develop an accurate sequence stratigraphic framework.

In the current study, 3-D segmentation and processing of the Micro-CT scan images enable us to quantify the abundance of the burrows foot-by-foot. We created a 3-D image for each foot of core, and chose to display all the ichnofacies by adjusting and filtering to a balanced color scale. There is background noise in these images such as fractures, mud plugs etc. This noise can be filtered using a certain color spectrum. In our analysis, each foot has 4 ichnofacies characterized: short *Chondrites*; long *Chondrites*; *Paleodictyon* and *Planolites*, with abundance values scaled to: 3 as abundant, 2 as common, 1 as sparse and 0 as absent (Figure 4.15). Following these measurements, all the values of the ichnofacies abundance for each foot have been

summed up as the total Bioturbation Index (BI). In addition, the radiolarian cherts, phosphate nodules and *Tasmanites* are also marked as flags. The core footage is described in feet beginning at the base of Woodford Shale.

Core A:

Core Summary

Core A cut 82ft (25m) of the Woodford section at the most proximal setting in the basin and penetrated the Upper Middle Woodford and the Upper Woodford (Figure 4.16-4.19). All of the Lower Woodford and lower part of the Middle Woodford are absent. Petrophysical logs indicate that the best reservoir quality is near the "Upper Woodford Chert Base" (Figure 4.16). The basal Woodford in this core (Upper Middle Woodford) is mud-rich and lies on top of the Hunton Group with a major erosional unconformity (Figure 4.17). Biogenic quartz (radiolarian chert) lithofacies is prevalent which has resulted in abundant interparticle and floccule porosity development (Slatt and O'Brien, 2011) in the dark laminated shale lithofacies. Radiolarian chert increases upward to a maximum concentration at 42ft (12.8m) indicating an upward deepening of water (i.e. transgression). Further up section, the radiolarian chert beds continue with additional high angle bedding, quartz-rich clasts and slump beds indicating detrital component of mudstones (Chain, 2012). Chert beds with phosphate nodules occur near the top of the Upper Woodford. Pyrite is dispersed throughout the core in varying sizes.

Bioturbation Summary

From the traditional core description, thin-section analysis and 2-D CT-Scan interpretation, common- to- abundant *Chondrites* burrows and wide *Grazing Trails*

occur throughout the core (Chain, 2012; Hlava *et al.*, 2013 and Spaw, 2013, Figure 4.17). From the base of the Woodford section, there is 20 feet of section with abundant *Chondrites*. The ichnofacies gradually shifts upward to smaller amounts of *Paleodictyon* and A-Type *Chondrites* to the top of the Middle Woodford. The Upper Woodford interval has a much lower concentration of ichnofacies, with only common-sparse *Paleodictyon* and short *Chondrites* sparsely present. In general, the Middle Woodford is definitely more bioturbated than the Upper Woodford. The highest bioturbation index is at 30ft (9.1m) just below the top of the Middle Woodford. Most bioturbation occurs in the dark mudstone facies. Much less bioturbation occurs in the radiolarian chert facies.

Integration to Other Core Data

All core sample test results with Gas Research Institute (GRI) porosity and permeability, X-Ray Diffraction (XRD) and geochemistry data are shown in Figure 4.18 to be compared to the results from bioturbation. The preferred facies for horizontal fracturing in Core A is characterized by high porosity, permeability and TOC that often correlate with BI \leq 2 intervals in Upper Woodford, while the high BI in Middle Woodford correlates to medium reservoir quality. There is no clear trend in this core that high or low bioturbation would contribute to reservoir quality(at least bioturbation is not a main control).

In addition to GRI, XRD and Geochemistry data, a high-resolution XRF (X-ray fluorescence) analysis was completed on Core A at every 0.3ft (0.1m) throughout the entire Woodford by Dr. Harry Rowe at University of Texas at Austin. Based on his data, we plotted key chemostrat proxies associated with description of lithofacies and

trace fossils in Figure 4.19. The key paleo-redox elements and ratios have been discussed by Tribovillard *et al.* (2006), Ratcliffe *et al.*, (2012), Turner and Slatt (2013) and Mu *et al.* (2013), so they are not repeated here in any detail.

Figure 4.19 clearly indicates a reverse relationship between BI and Zr/Al ratio. The highly bioturbated intervals correlate to lower Zr/Al ratio and vice versa. This can be explain by the fact that high detrital input into the basin would change the paleo-redox environment and disturb the bioturbation activities, especially in Upper Woodford time. Another detrital input indicator Ti/Al also reversely correlates to BI to some extent. Mo and U are proxies for redox environment and sea-water depth, they are related to TOC and transgression events. Mo positively follows the general trend of BI.

Core B:

Core Summary

Core B comprises 202ft (61.6m) of the Woodford section, and includes the entire Lower, Middle and Upper Woodford (Figure 4.20). It is 18 miles (28.8 kilometers) southwest (depositionally downdip) of Core A. 40ft of the uppermost Upper Woodford core is absent (failed to catch). SEM analysis indicates that the porosity in the core is dominated by fecal pellets and micro-channel porosity in multiple lithofacies (Chain, 2012). The Woodford section in Core B also unconformably overlies the Hunton Group. The basal Woodford Shale shows a higher silt content than the underlying Hunton Group. Further up section, the Lower Woodford is mainly silty mudstone with organic shale interbeds. Radiolarian cherts and *Tasmanites* rich shale from 27-37ft (8.5m) comprise a major condensed section with high TOC. The Frasnian-

Famennian boundary identified near the bottom of the Middle Woodford at 104ft (31.7m) in this core is also characterized by a combination of organic rich shale associated with radiolarian cherts and *Tasmanites*. The Middle Woodford has higher detrital quartz content and TOC than the Lower Woodford. The last major condensed section occurs at 167ft (51m), which also contains large amounts of radiolarian cherts. Cherty and radiolarian-rich beds also appear with minor clasts present in the Upper Woodford. Pyrite is dispersed throughout the entire Woodford section ranging from microscopic in size to nodules >2 inches in diameter.

Bioturbation Summary

Paleodictyon and *Chondrites* are the dominant ichnofacies in Core B, they represent predominantly dysaerobic conditions with minor to common resident or background assemblages interspersed with allochthonous (turbidite) deposits (Spaw, 2013). There are clear reversed relationships at 32ft (9.7m) (Condensed Section 1), 104ft (31.7m) (Frasnian-Famennian Boundary) and 167ft (51m) (Condensed Section 3) that the TOC peak and organic-rich shale correlate to bioturbation-free zones. These three intervals with highest Gamma Ray (GR) and TOC are interpreted to be the most important condensed sections in Core B. The intervals with a high bioturbation index are also noticeable. In theory, the highest bioturbation zones often correlate to the most oxic environment associated with the lowest sea-level. Sequence Boundaries 1, 2 and 4 (Figure 4.21) are such examples. In the Middle Woodford, there are also distinct alternating intervals of high bioturbation and bioturbation-free beds from 97-157ft (29.5-47.8m). In this zone, the lithofacies with high bioturbation index is mudstone with higher clay content and detrital quartz. The lithofacies with low bioturbation index is

mudstone with higher organic content, radiolarian cherts and a small amount of dolomite [dolomite is probably cement or diagenesis related (Caldwell, 2011)].

Integration to Other Core Data

Figure 4.22 and 23 are core and chemostrata data integrated with Core B. Figure 4.22 indicate a unevenly distributed sample frequencies with samples largely focused on high-TOC condensed sections. Reservoir intervals with highest quality (porosity, permeability, TOC, QFM, HI etc.) often correlate with low BI. As for chemostrata data, again, the reverse relationship between Zr/Al and BI is well recognized. Fe/Al ratio also reversely relate to BI. Redox indicators such as Mo, U correlate well with TOC, they are indicators of major condensed sections.

Core C:

Core Summary

Core C cut 372ft (113.4m) of the Woodford Shale interpreted to have been deposited in a distal setting. It contains a complete Woodford section from bottom to top (Figure 4.24-4.27). Petrophysics indicate major thick reservoir presented in Middle and Upper Woodford (Figure 4.24). Interbedded chert, siliceous and silty mudstone are the dominant lithofacies from thin section analysis (Spaw, 2013; Hlava *et al.*, 2013). The lowermost part consists of bioturbated silty mudstone to interbedded chert and silty mudstone from 0ft (Top Hunton) to 93ft (28.3m). The silty mudstone is interpreted as part of the Misener sandstone sourced from the northern Anadarko shelf. From 93-320ft (28.3-97.5m), the lithofacies are mainly interbedded chert and mudstones with some barite and occasionally dolomite. This interval has the best reservoir quality in the study

area. The amount of chert increases upward into the Upper Woodford, with phosphate and chert nodules becoming common above 3591ft (109.4m).

Bioturbation Summary

Chondrites and *Paleodictyon* (*Grazing Trails*) are the main ichnofacies, and other burrows (*Planolites* etc.) are minor to moderate in abundance throughout the core (Figure 4.25). Paleo-redox conditions are interpreted to have been predominantly dysaerobic. The ichnofauna is characterized by resident or background assemblages with rare allochthonous deposits (Spaw, 2013). The silty interval in the lowermost Woodford (Misener) contains a moderate amount of trace fossils (e.g., *Thalassinoides*). In the upper part of the Lower Woodford and the lower part of the Middle Woodford (80-140ft, 24.4-42.7m), the bioturbation index is low (0-1) which correlates to siliceous mudstone. There are large amounts of chert and barite in this interval with high TOC, indicating a distal oxygen-deficient deepwater environment.

The Bioturbation Index (BI) increases closer to and above the Frasnian-Famennian boundary (F-F boundary) (140-220ft, 42.7-67m). The lithofacies changes from chert and barite rich siliceous mudstone to bioturbated mudstones. The increase of bioturbation indicates a regression occurred above the F-F boundary. Above 220ft (67m), the BI decreases while TOC and Gamma Ray increase, indicating another transgression. A condensed section is from 240-260ft (73.2-79.2m) with barite-rich mudstone beds present. The overlying Upper Woodford is similar to that in Core B, having massive phosphate nodules and cherts at the uppermost Woodford without bioturbation. Four sequence boundaries and four condensed sections have been

interpreted in Core C shown in Figure 4.11, with related transgression and regression cycles supported by the bioturbation analysis.

Integration to Other Core Data

There is no clear and unique relationship between reservoir quality and BI (Figure 4.26). As for XRF data: from the base of the Woodford, the Misener detrital deposits show very high Th/U---an indicator of significant detrital input during lowstand time. The transition from the Misener to the Lower Woodford is characterized by higher Mo, Si/Al, Zr/Al and U, indicating both a transgressional sequence and a large amount of detrital input into the system. Pyrites and radiolarian cherts are not common in this interval, resulting in lower Fe/Al measurements (Figure 4.27).

In the Middle Woodford, the geochemical detrital indicator such as Th/U, Zr/Al and Ti/Al are significantly lower than in the underlying Lower Woodford, indicating a lack of detrital input. Fe/Al and Mn peaks from 120-160ft (36.6-48.8m) in Core C correlates to high amounts of radiolarian cherts and pyrite in an interpreted super-anoxic and deepwater marine bottom environment. This anomaly, which occurs right above the Frasnian-Famennian boundary, is interpreted to be a consequence of the Kellwassere extinction event. During the event, over 30% of all species disappeared due to multiple causes including global cooling, carbon dioxide decrease and anoxic marine environments. The general decrease of Mo from the base to the top of the Middle Woodford indicates the shallowing of sea water, which correlates to the global cooling and glacial event during Late Devonian time. A decrease in radiolarian cherts and increase in trace fossils in the Upper Middle Woodford indicate a shallowing of sea water, where more large organisms thrived after the Kellwasser mass extinction. The

radiolarians were food sources for many large organisms which build burrows, thus ichnofacies and radiolarians can co-exist in Upper Middle Woodford strata. In addition, a calcium spike correlates to the lower gamma ray measurements, indicating that the lowest sea-level during HST may have received some carbonate input either from external transport or in situ precipitation. The decrease of silica-replaced fossils (cherts) upward in the Middle Woodford might also be an effect of the Late Devonian extinctions (Kidder and Erwin, 2001). In summary, the chemostrat and bioturbation data enhanced the biostratigraphic interpretation from *Conodonts*. Anomalies from Fe/Al, Mo and Mn with a cyclic bioturbation behavior all support the Kellwasser extinction events in Late Devonian time peaked from 100-120ft (30.4-36.6m).

The Upper Woodford contains the boundary between Devonian and Mississippian strata. Another important extinction event (Hangenberg) is located at this boundary. From the chemostrat chart, the Mo, Fe/Al, U and Ca peaks can all be correlated to an interval with high gamma ray readings from 290-330ft (88.4-100.6m). This implies that 1) this interval belongs to a super-anoxic interval from Fe/Al, U and Gamma ray; 2) a bump in the Mo values indicate deepwater marine environment; 3) a sudden decrease of gamma ray above 330ft(100.6m) and an increase of Si/Al and Th/U indicate a siliciclastic input caused by relative sea-level drop; 4) a lack of trace fossils further supports that the Hangenberg extinction event has resulted in a life-free zone from 290-330ft(88.4-100.6m) where there are neither evidence of bio-activities nor trace fossils; and 5) a large amount of phosphate nodules and calcium indicate that the system is transforming into a stable carbonate shelf environment.

Cross-plotting of All Results

Figure 4.28 shows the results integrating reservoir quality, lithofacies and bioturbation. In these cross plot, the total Bioturbation Index (BI, which ranges from 0-10) was divided into: unbioturbated (BI=0), bioturbated ($0 < BI < 4$), and heavily bioturbated ($BI > 4$). Data points of permeability (in nano darcy, nd) from core plugs and measured gas-filled porosity (in %) have been plotted using these bioturbation categories. The plot results indicate that 1) the heavily bioturbated group often have $< 100,000$ nd permeability while the porosity covers a wider range from 2-9% and 2) bioturbated and unbioturbated results all cover wide ranges of porosity and permeability. These plots indicate that heavy bioturbation in the most oxic environments would cause a decrease of reservoir quality due to bio-mixing and homogenization. The upper right figure indicates the lithofacies of the data points, with most of the higher porosity and permeability rocks being mudstone and radiolarian chert. Silty mudstones and nodular shale all have low porosity, low permeability and low bioturbation index because: 1) silty mudstones received muddy and detrital (turbidite) input from the shelf, which diluted both organic material and suppressed bio-activity (Spaw, 2013) and 2) phosphate nodules are indicators of bioactivity and organic material free zones from chemostrat studies (Turner, 2013). The lower figure is the porosity vs. permeability plot colored by bioturbation types. *Chondrites* and *Grazing Trails (Paleodictyon)* both have moderate reservoir quality, while *Thalassinoides* has poor reservoir quality. Non-bioturbated intervals have wide range of reservoir quality. All the relationships between bioturbation and reservoir parameters are summarized in Table 4.1.

SEQUENCE STRATIGRAPHIC FRAMEWORK

After a thorough interpretation of the three Woodford cores, a detailed sequence stratigraphic framework has been built by combining core results with the massive amount of subsurface well log data (500+ wells) in the Anadarko Basin (Figure 4.29). In the well logs, the entire Woodford was divided into 10 intervals from bottom to top as: Hunton Group, Misener, Lower Woodford, Frasnian-Famennian Boundary, Lower Famennian TST, Upper *Crepida* Zone (*Conodonts* defined), Middle Woodford, Upper Woodford Chert, Top Woodford and Mississippian Limestone. Each well top was chosen because it has significant meanings for sequence stratigraphic correlation. A North-South stratigraphic cross section including the three Woodford cores is shown in Figure 4.18. The section was flattened on the top of key time horizons in time order.

At the first stage of deposition, the Lower Woodford consists of the Misener Sandstone unit, which is a low-stand incised valley fill (IVF) deposit, and a TST (Transgressive System Tract) with back-filled deposits above. The thickness of the Lower Woodford ranges from 0-150ft (0-45m) depending on the sea floor topography and tectonically controlled by the distribution of Hunton Group and the pre-Woodford erosional events (Slatt *et al.*, 2014). It is commonly agreed that where the underlying Hunton is thick, the overlying Woodford is thin. This is due to the down-cutting at the pre-Woodford erosional event. The thick lower Woodford shale is where the incised valley fill developed. Bioturbation and bio-activities in this interval are low.

The second stage includes intervals from the Top of the Lower Woodford to the Lower Famennian TST. It also corresponds with the lower portion of the Middle

Woodford. This stage has significant importance that is related to the Frasnian-Famennian Boundary and the Late Devonian Mass Extinction (Kellwasser Event). The deposition was continuous hemipelagic "rain" or hyperpycnal flows (Scheibere *et al.*, 2010) which follows sea-floor topography. Bioturbation and bio-activities in this interval is low to absent because of the confined, super-anoxic environment during Late LST and Early TST filling.

During the third stage, bioturbation abundance is medium to high with all *Chondrites*, *Paleodictyon* and *Planolites* present in the cores. These are the "survivors" from the Kellwasser mass extinction. The environment is dysoxic with medium TOC content. Deposition rate is also very low, following a similar pattern as stage 2 without major thickness variations. The highest abundance of trace fossils have been found consistently from the top of the "Lower Famennian TST" to the top of the "Upper *Crepida*" zone.

The fourth stage (Upper Woodford) is where relative sea-level drops significantly and the Hangenberg extinction event occurs. Phosphate nodules and cherts are the dominate lithologies with no trace fossils found. The one TST above the Middle Woodford is correlated to the beginning of the Hangenberg extinction event, when sea-level dropped significantly and this is interpreted as the transition from Devonian shale to Mississippian Limestone deposition.

The derived Woodford sequence stratigraphic framework can be correlated to the global sea-level curve (Haq and Shutter, 2008). Within that interval there are 8 medium-major sea-level changes from the Upper Frasnian to the Upper Famennian. This is similar to what has been derived from our data. By matching the key markers

including the Frasnian-Famennian Boundary and the Devonian-Mississippian boundary, we can confidently correlate to the global sea level curve. Figure 4.30 is the gross isochore maps of Lower Middle and Upper Woodford Shale, showing the transition of more restricted deposition in Lower Woodford to more extended deposition in Upper Woodford.

Correlation in Anadarko Basin

The established sequence stratigraphic framework of Woodford Shale can be extended to other parts of the basin. Figure 4.31 shows an effort to correlate Core C to Hunton Anticline Quarry (measured by Bryan and Slatt, 2013) that is 25 miles (40km) southeast to Core C. In this correlation, note that the two locations contain the most similar gamma ray patterns to match. This correlation is confirmed with examination on wells drilled in between these two locations. All the key horizons, including top of Middle Woodford, F-F Boundaries, Lower Woodford transgression etc. are shown. The bioturbation activities are focused in between top of Middle Woodford and F-F boundaries. Although we did not check the bioturbation in the Hunton Anticline Quarry section, we can predict that the time equivalent interval in that section also have the highest bioturbation index. Other parameters such as Mo, Ti, Si/Al and Zr all follow similar patterns.

Another example is from the measurements of Hall 2B core (Bryan and Slatt, 2013) which is 30 miles (48km) southwest from Core B. Hall 2B only penetrated the Upper and Upper Middle Woodford, however, the correlation can give us valuable information on how the chemostrata and sequence change towards the basin. Unlike

Core C and Hunton Anticline Quarry, the gamma ray curves do not match very well. However, comparing all trace and major elements can help better correlate time equivalent intervals. Si/Al increased upward from both locations indicate an increase in chert.

Correlation with Woodford Shale in Permian Basin

Hemmesch *et al.* (2014) proposed that the entire Woodford Shale belongs to a 2nd-order sea-level drop and 10+ 3rd sea-level fluctuations which coincides with Haq and Schutter (2008). We generally agree with this conclusion based on the fact that the lithology eventually changed from Woodford Shale into Mississippian Limestone. However, we would also argue that during Lower and Middle Woodford, there are significant transgressions such as F-F boundary, and top Middle Woodford that can cause a significant rise in sea-level. The rising sea-level is also backed by the bioturbation and chemostrata analysis. These transgressions cannot be emphasis enough that they are closely related to the unconventional resources. We disagree with the claim that Hemmesch made that "the high TOC zones are regression and no major transgression have been found" because they used insufficient data to draw the conclusion. These transgressions in Woodford Shale have been backed-up by our core analysis, bioturbation studies, biostratigraphy and chemostrata work.

CONCLUSION

The Woodford Shale in the Anadarko basin, Oklahoma has been one of the major unconventional plays in the United States for nearly a decade. To fully

understand the lateral and vertical heterogeneity of the play and the best way to develop its remaining resources, a detailed sequence stratigraphic framework derived from various disciplines is needed. This research has fully utilized ultra-high-resolution (625 micron increment per slice) and advanced 3-D Micro-CT scan technology to quantitatively describe and analyze the ichnofacies and microfacies in selected Woodford cores. The results of trace fossil analysis were related to chemostrata, XRD, SEM, geochemical analysis, and well logs etc. to build a detailed sequence stratigraphic framework in order to better correlate to the most productive zones for unconventional resources potential.

The ichnofacies in the Woodford Shale cores have been categorized into short and long *Chondrites*, *Paleodictyon*, and *Planolites*. The 3-D geometries, abundance, and diversity of ichnofacies have been quantitatively described using Avizo Fire™ software. Bioturbation Index (BI) was calculated from the sum of the abundance of all ichnofacies in each stratigraphic interval. The BI was then compared with XRF data (including Al, Si, Ti, Zr, Mo, and U), XRD data (including quartz, clay, feldspar, pyrite, and dolomite) and geochemistry data (including TOC) to relate ichnofacies and paleo-redox environment. The stratigraphic distributions of these properties were found to be related to sea-level fluctuation. A new sequence stratigraphic framework was built using these data with Conodonts biostratigraphy.

To our knowledge, this research is the first published effort to quantitatively study the detailed ichnofacies in the Woodford Shale using advanced 3-D Micro-CT scan technology. The results indicate that bioturbation and bio-activities are more common in the Woodford Shale than previously thought. Although burrows frequently

develop in highstand systems tracts, they also occur in presumably anoxic environments conducive to preservation of high TOC content and biogenic quartz. These relationships can aid in targeting the best horizontal landing zones in the Woodford Shale.

LIST OF FIGURES

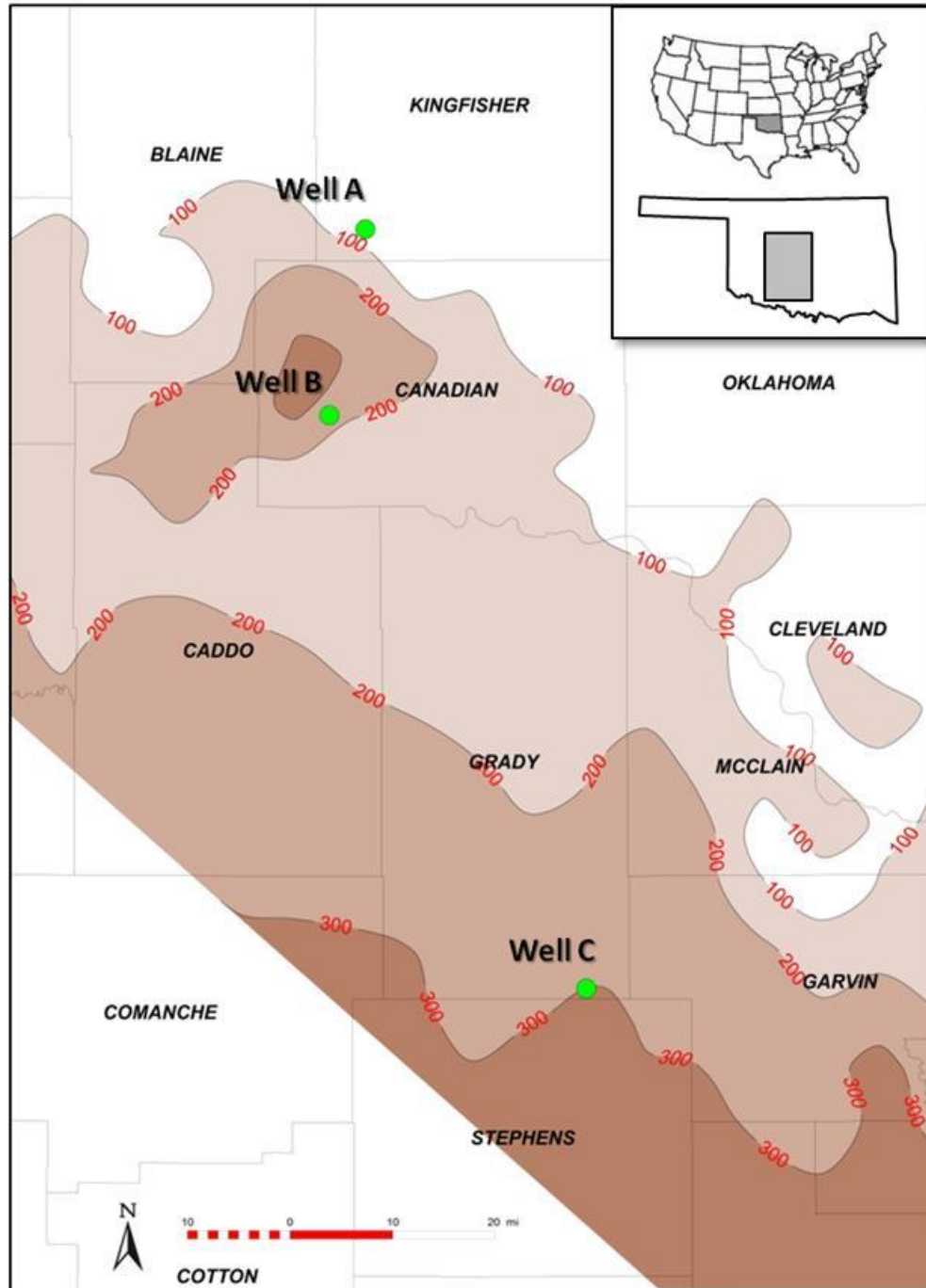


Figure 4.1. Gross isochore thickness map from top Woodford Shale to top Hunton Group in the study area (in feet, 100ft = 30m), with three well locations marked as A, B and C.

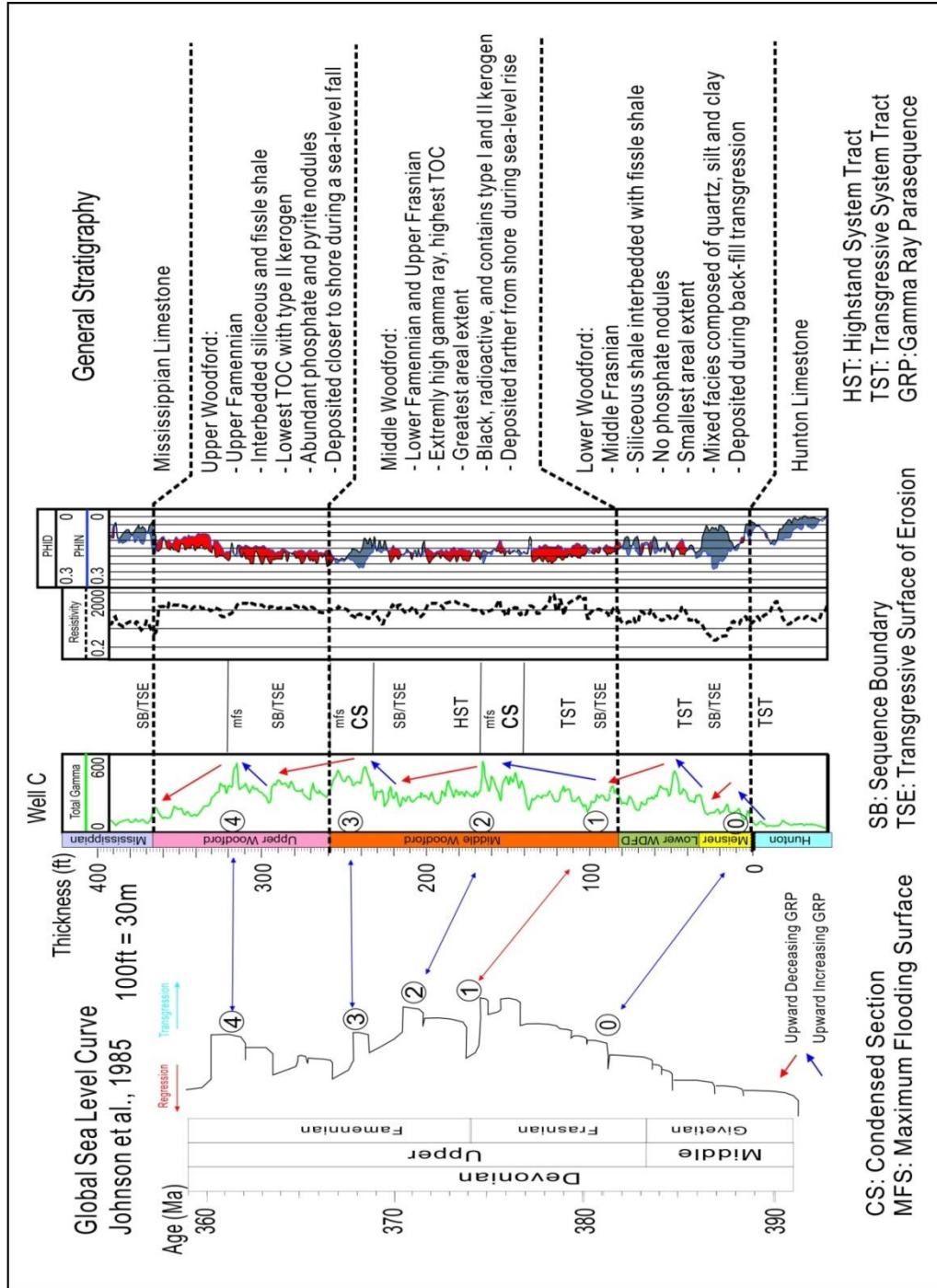


Figure 4.2. Stratigraphic column of the Woodford Shale based on global sea-level (Johnson *et al.* (1985), Slatt *et al.* (2013), and Spaw (2013)), biostratigraphy work is mainly from Conodonts by Dr. Jeffrey Over, Kerogen Type from Corelab.

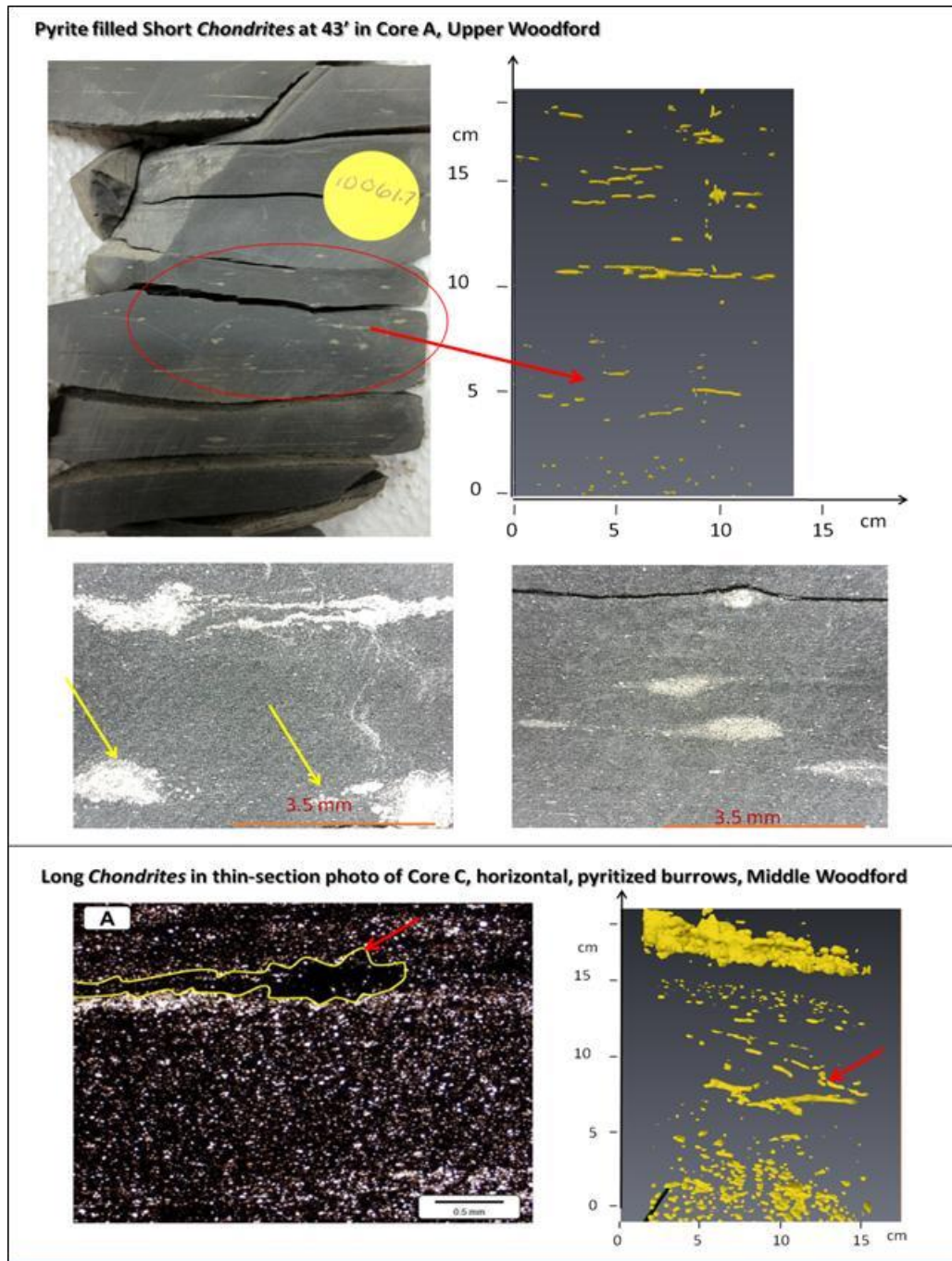
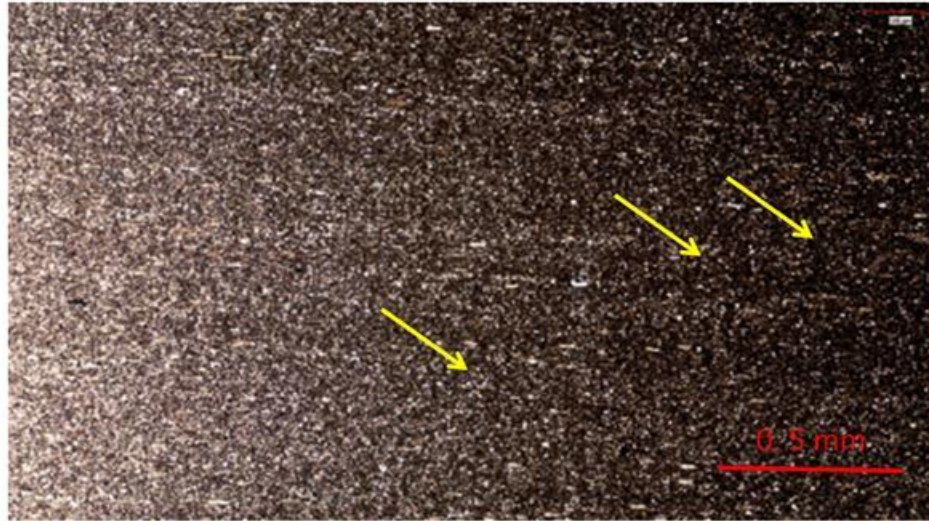


Figure 4.3.Upper Left: Core photo of short *Chondrites* from Upper Woodford of Core A (43'). Upper Right: The same short *Chondrites* in the segmentation images of Micro CT-Scan. Middle: Zoom in photos of the pyritized *Chondrites*. Lower Left: Thin-Section photo of the long *Chondrites* from Middle Woodford in Core C, Lower Right: 3-D CT Scan Segmentation images of the same interval. (Thin-Section and 2-D Core photos by Kimberly Hlava and Joan Spaw.)

97' in Core B: faintly lamination with discrete burrows



118' in Core B: Abundant pyrite-filled short *Chondrites*

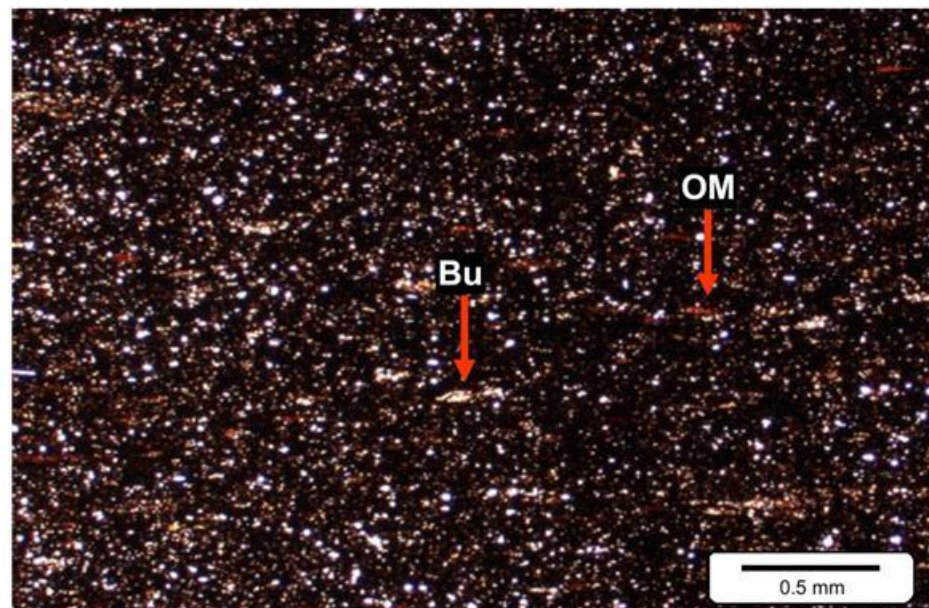


Figure 4.4. Upper: Thin-section of short *Chondrites* in argillaceous shales from Middle Woodford of Core B (97'). Lower: Abundant pyritized short *Chondrites* in Middle Woodford of Core B (118') . (Thin-Section photos by Joan Spaw and CoreLab.)

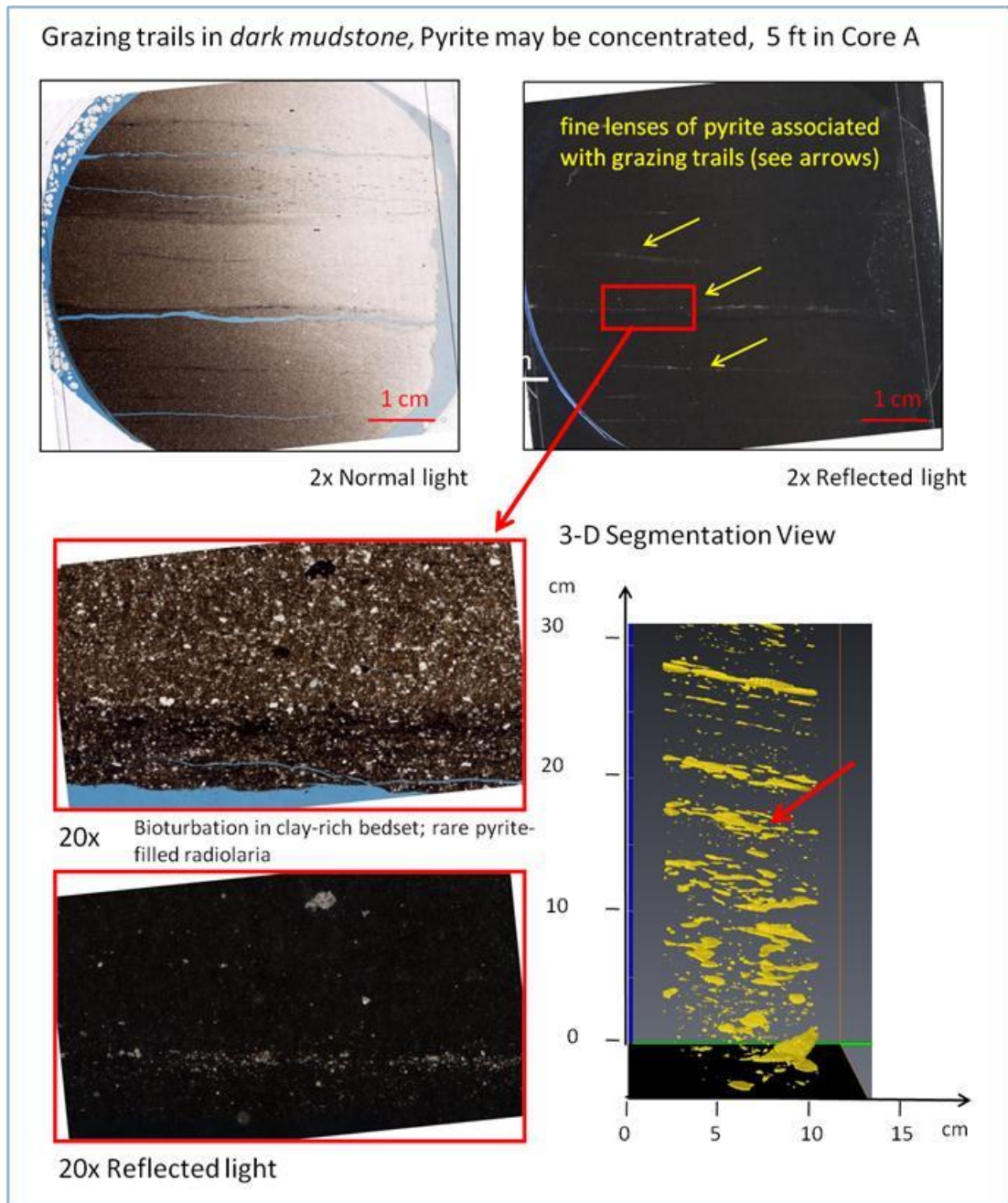


Figure 4.5.Upper Left: Core photos of the *Grazing Trails* from Upper Middle Woodford of Core A. Upper Right: 2X reflected light of the same photo. Lower Left: Thin section photo of the same intervals. Note the burrows are filled by cherts. Lower Right: 3-D CT Scan Segmentation image of the same intervals.

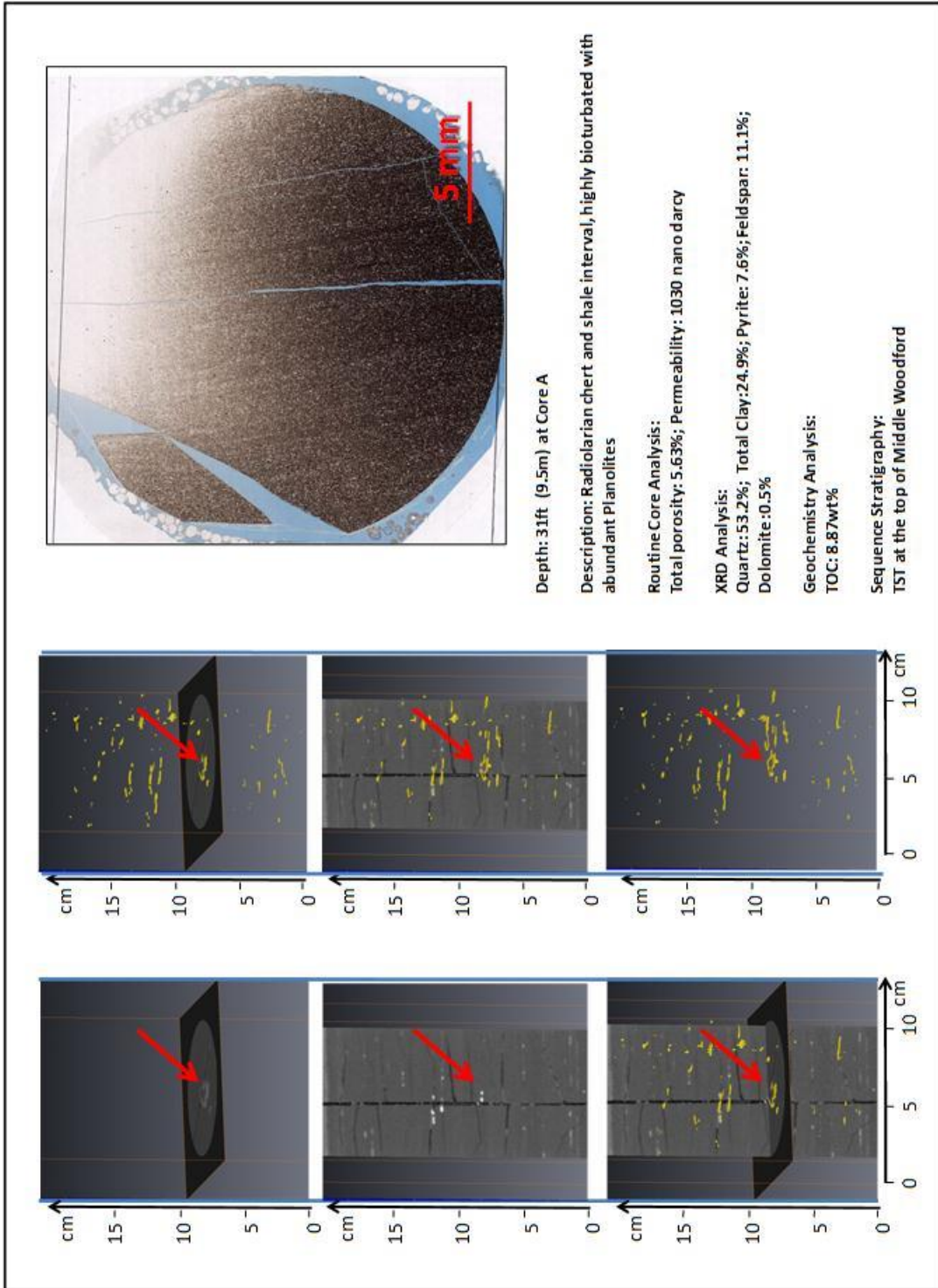


Figure 4.6. Integrated trace fossil analysis at 30-31 ft (9.5m) of Core A. Left: 3-D segmentation of the *Planolites* with 2-D intersections. Red arrows points to the same *Planolites* feature to compare. Right: thin-section photo of the same interval, with Corelab parameters (lithology, XRD, TOC, and sequence).

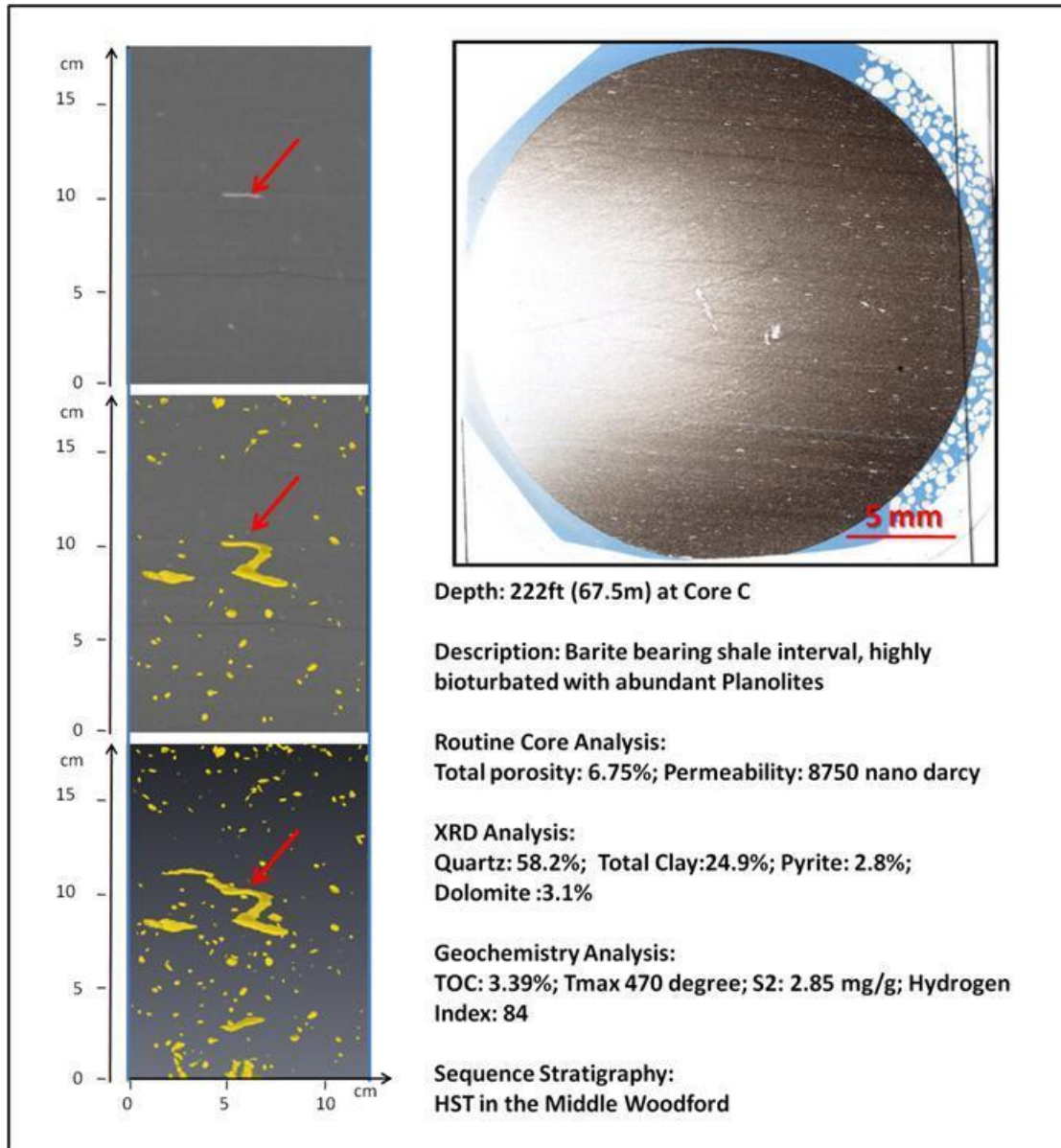


Figure 4.7. *Planolites* example at 222ft (67.5m) of Core C. Upper Left: 2-D Micro CT image; Middle Left: 2-D Micro-CT image with 3-D Segmentation; Lower Left: 3-D Segmentation showing the 3-D geometry of *Planolites*. Upper Right: Core Photo at the same interval. There is obvious advantage of 3-D Micro CT-Scan in viewing the burrows.

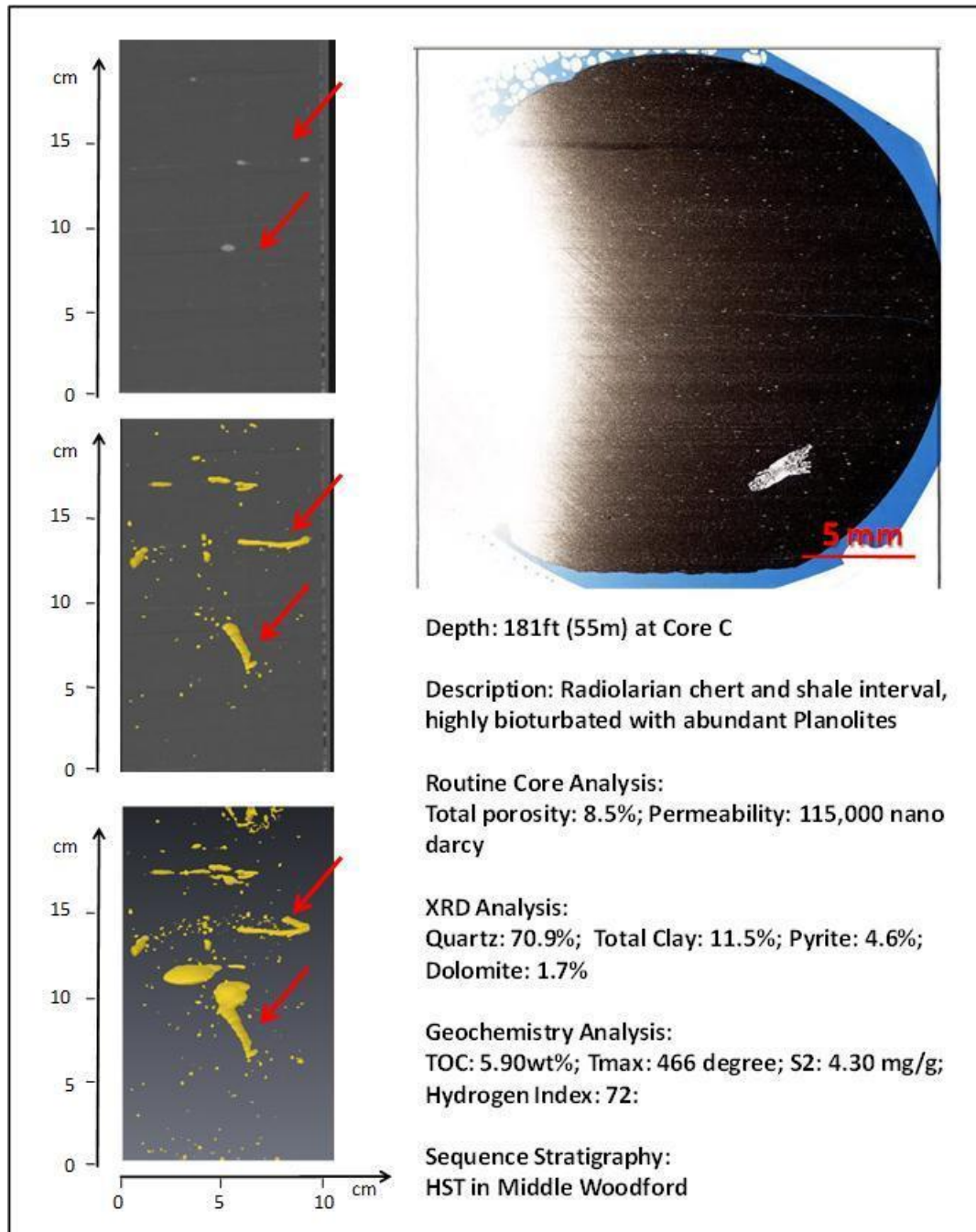


Figure 4.8. Integrated trace fossil analysis at 181ft (55m) of Core C. Left: 3-D segmentation of the Planolites with 2-D intersections. Red arrows points to the same Planolites features to compare. Right: thin-section photo of the same interval, with Corelab parameters (lithology, XRD, TOC, and sequence).

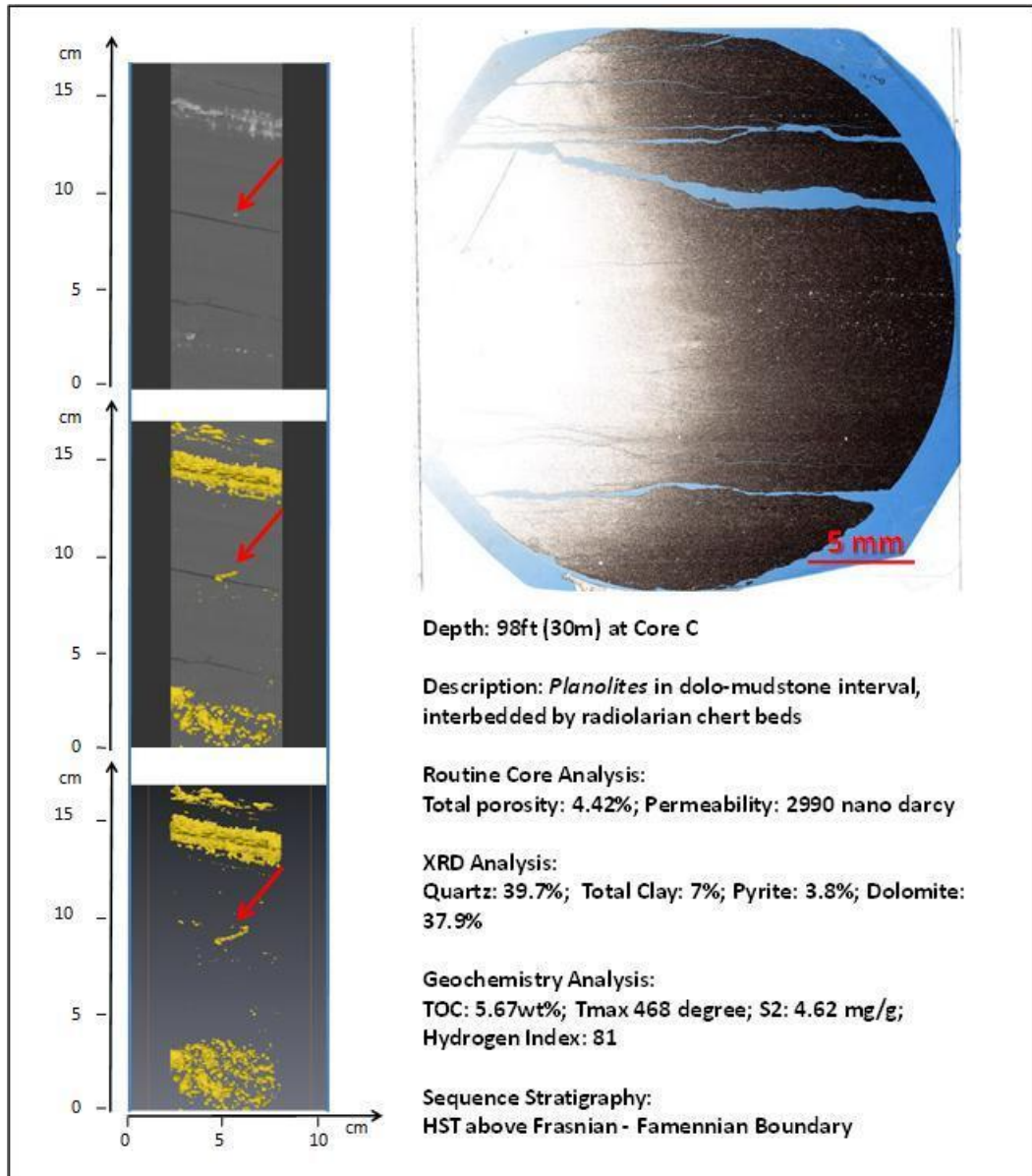


Figure 4.9. Integrated trace fossil analysis at 98ft (30m) of Core C. Left: 3-D segmentation of the *Planolites* with 2-D intersections. Red arrows points to the same *Planolites* features to compare. Right: thin-section photo of the same interval, with Corelab parameters (lithology, XRD, TOC, and sequence).



Figure 4.10. Examples of *Thalassinoides* in Core B and C, both examples are in Lower Woodford. The materials in vertical burrows are coarser grained than surrounding matrix, with occasionally pyritized framboid in them (Photos by Kimberly Hlava).

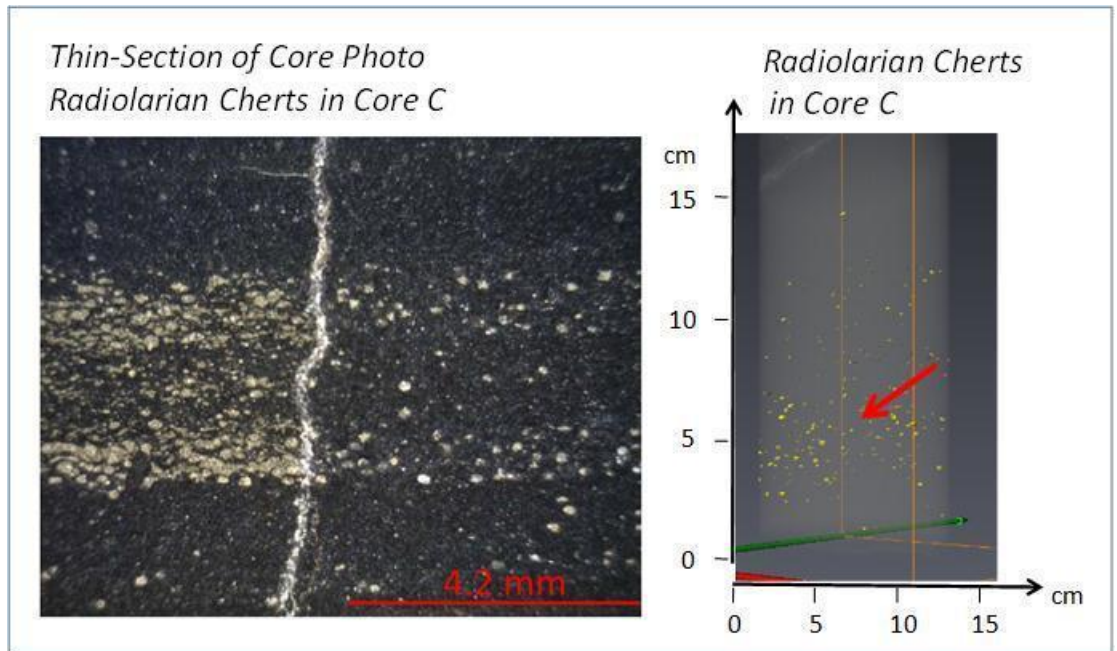


Figure 4.11.Pyritized radiolarian chert examples in Core C. Left: thin-section photos by Kimberly Hlava. Right: 3-D Micro-CT-Scan Segmentation of the same interval.

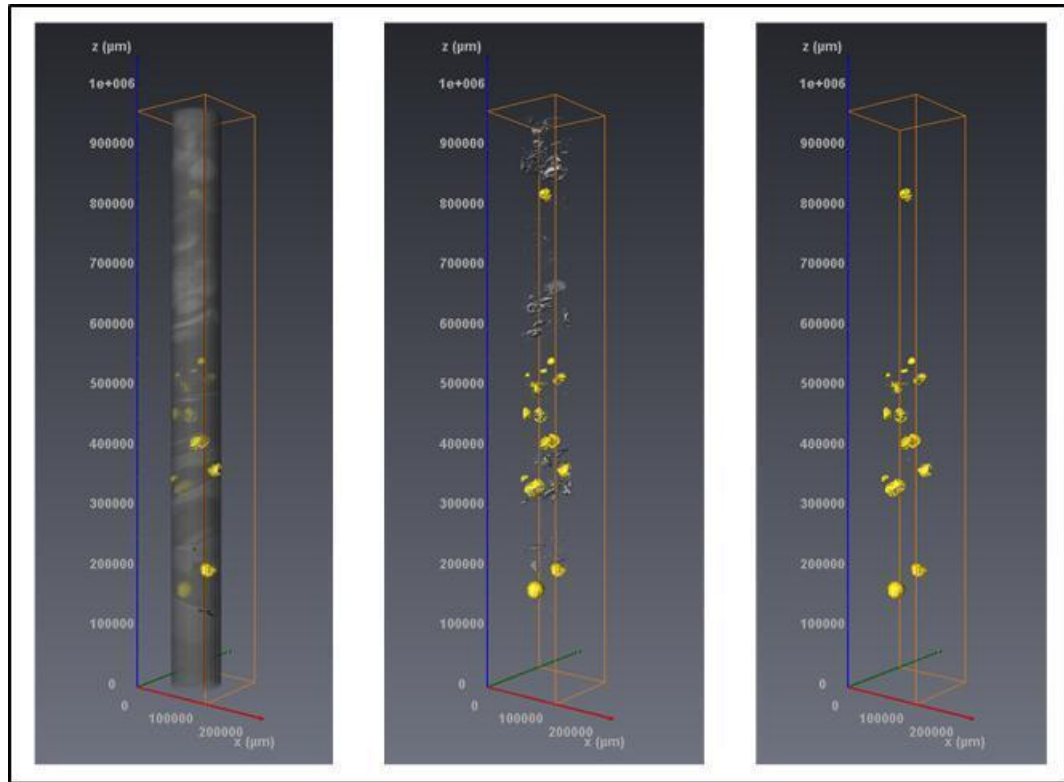


Figure 4.12. An example of the 3-D Micro-CT segmentation of nodules of 347-350ft (106m) in Core C (Upper Woodford). Left is the whole core image combined with nodules; middle is the noise and nodules; right is the filtered nodules

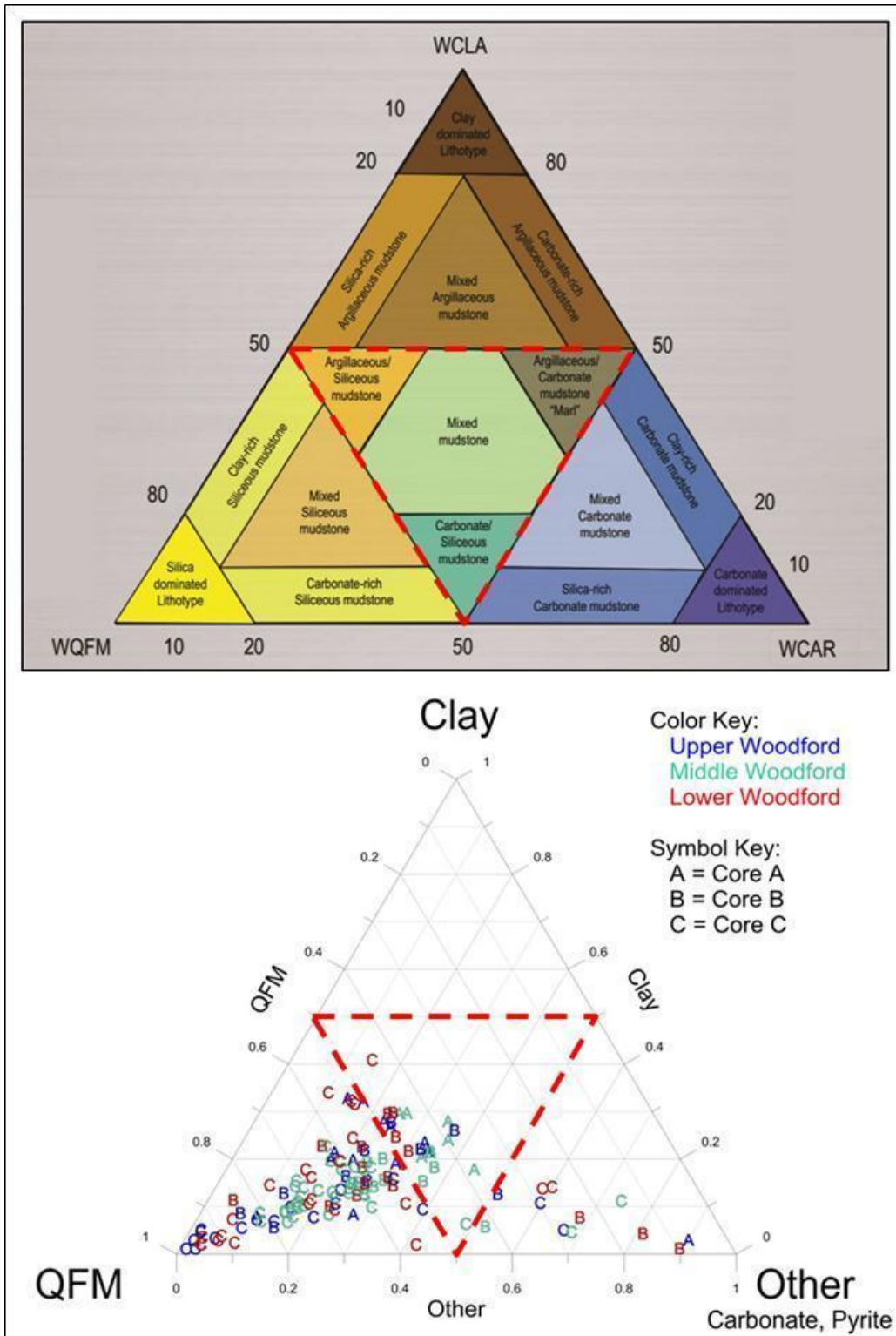


Figure 4.13. Upper: Shale classification by Gamero-Diaz *et al.* (2012) Lower: Ternary diagram plots showing how Lower, Middle and Upper Woodford Shale fall into their categories for Core A, B and C.

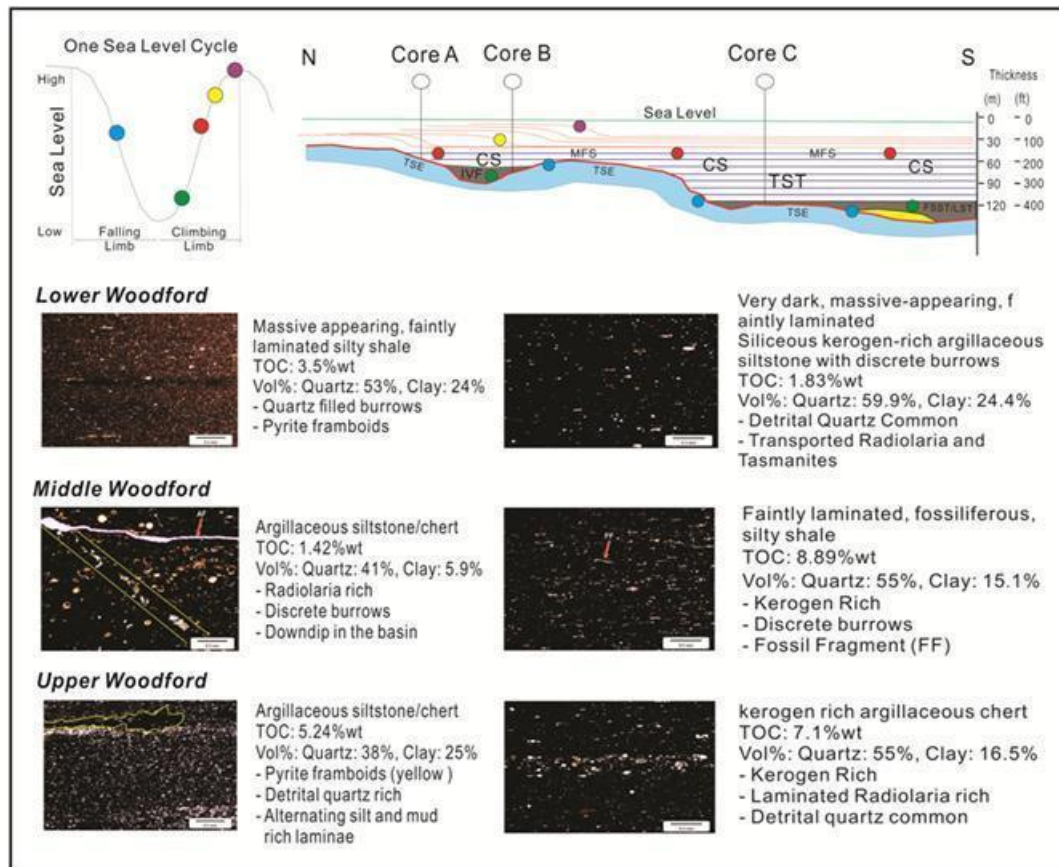


Figure 4.14. A sophisticated slope-to-basin depositional model for the Woodford Shale within a sequence stratigraphic framework. Modified from Slatt, 2013. Thin-section data by Joan Spaw, Kimberly Hlava and Corelab.

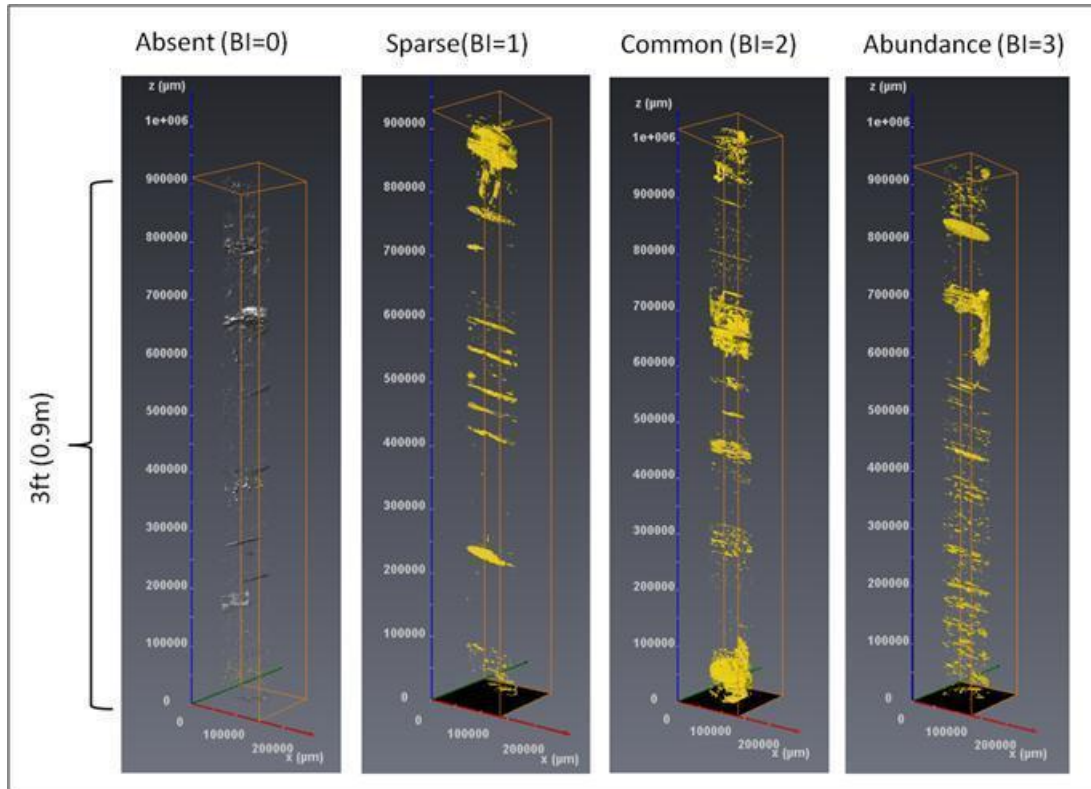


Figure 4.15. Examples of the criteria of the abundance of trace fossils, using a Bioturbation Index (BI) measured from Micro-CT scan 3-D segmentation image and thin-section description. From left to right are: Absent (BI=0), Sparse (BI=1), Common (BI=2), and Abundance (BI=3). The values of the BI have been used for statistics and calculations.

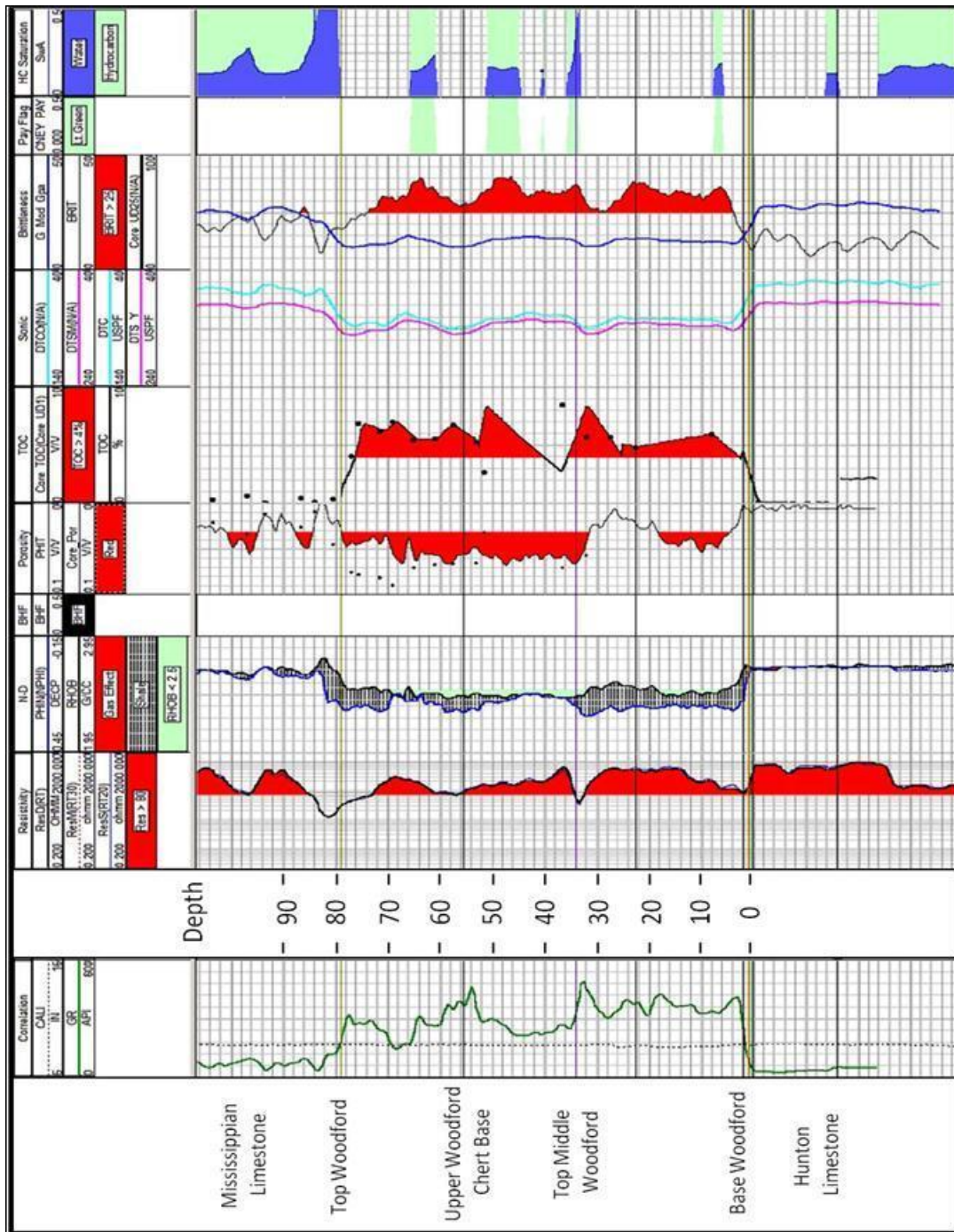


Figure 4.16. Petrophysics logs of Corer A, including GR, Resistivity, Neutron-Density, Calculated TOC, Vclay, Brittleness from dipole sonic logs and calculated water saturation.

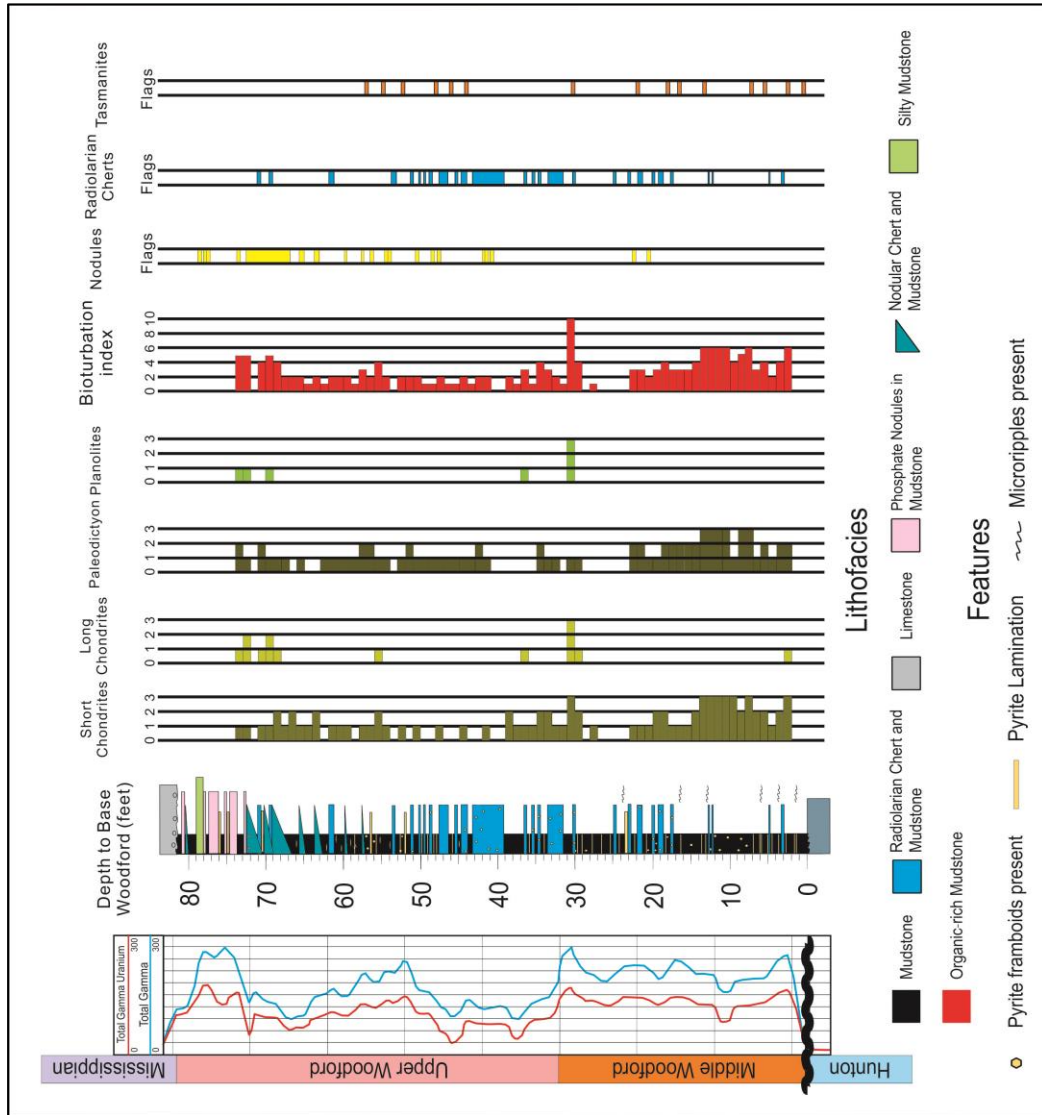


Figure 4.17. Integrated description of Core A, with emphasis on bioturbation. Bioturbation Index (BI) is the sum of all four trace fossils (short *Chondrites*, long *Chondrites*, *Paleodictyon*, *Planolites*). Description and Interpretation are based on Dr. Joan Spaw, Kimberly Hlava and Fuge Zou’s work.

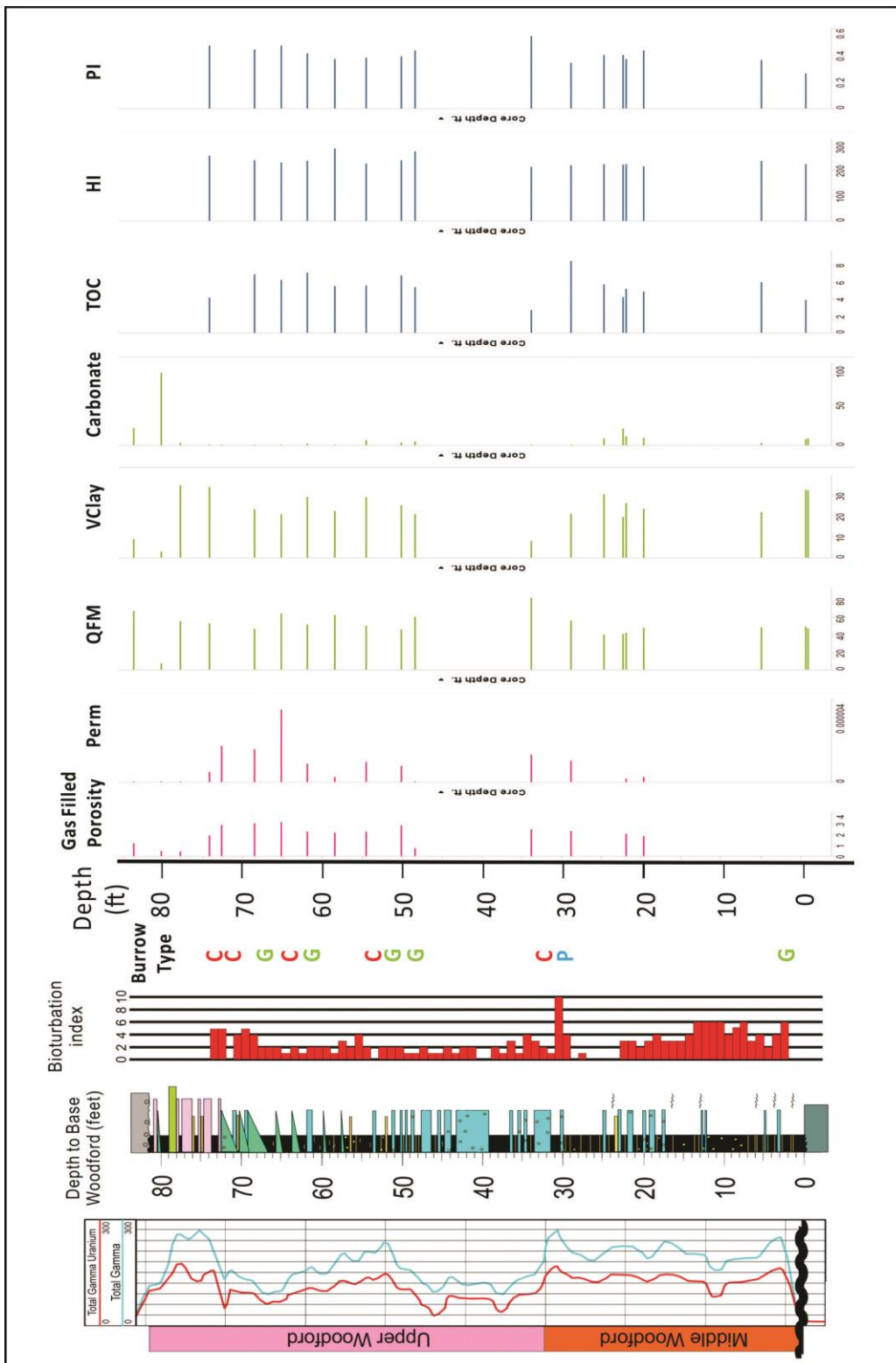


Figure 4.18. Integration of bioturbation data for Core A, including GRI (Gas Research Institute) porosity, permeability, XRD and Geochemistry from CoreLab. Burrow Type: Chondrites (C), Paleodictyon and Grazing Trails (G), Planolites (P) and *Thalassinoides* (T)

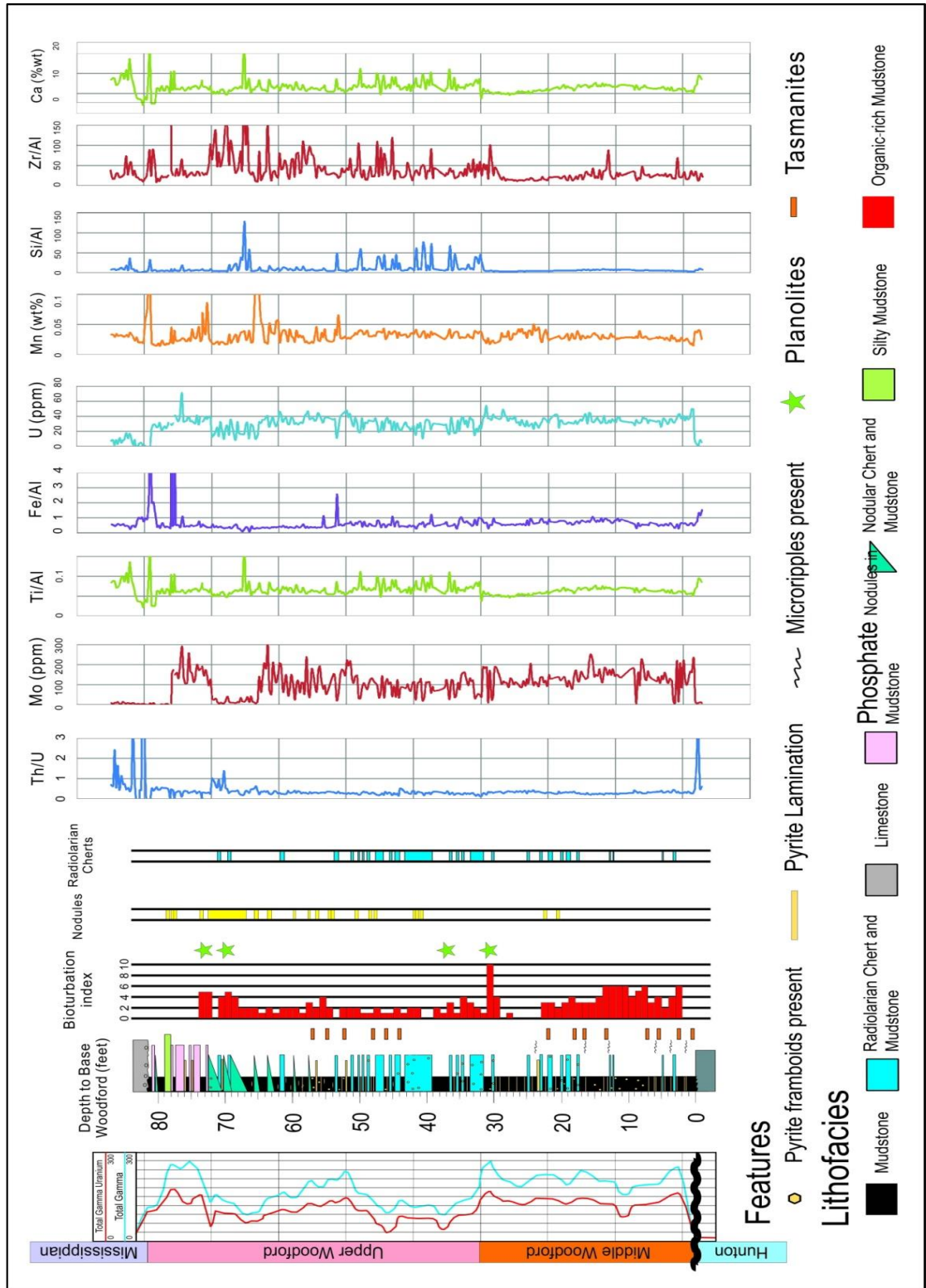


Figure 4.19. Integration of bioturbation data for Core A with chemostrata data. The high resolution hand held X-Ray Fluorescence (XRF) data is from Dr. Harry Rowe of University of Texas at Austin.

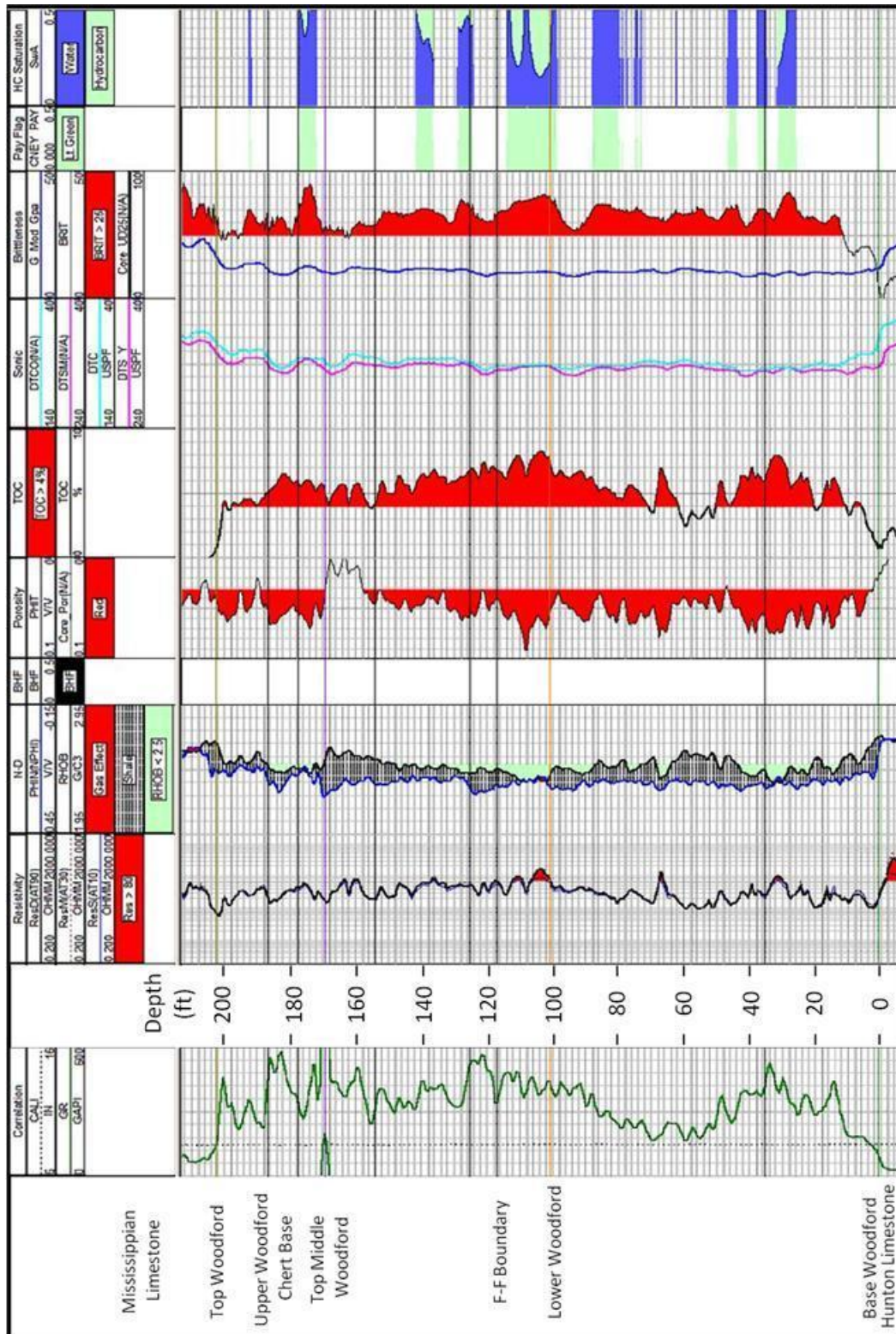


Figure 4.20. Petrophysics logs of Corer B, including GR, Resistivity, Neutron-Density, Calculated TOC, VClay, Brittleness from dipole sonic logs and calculated water saturation.

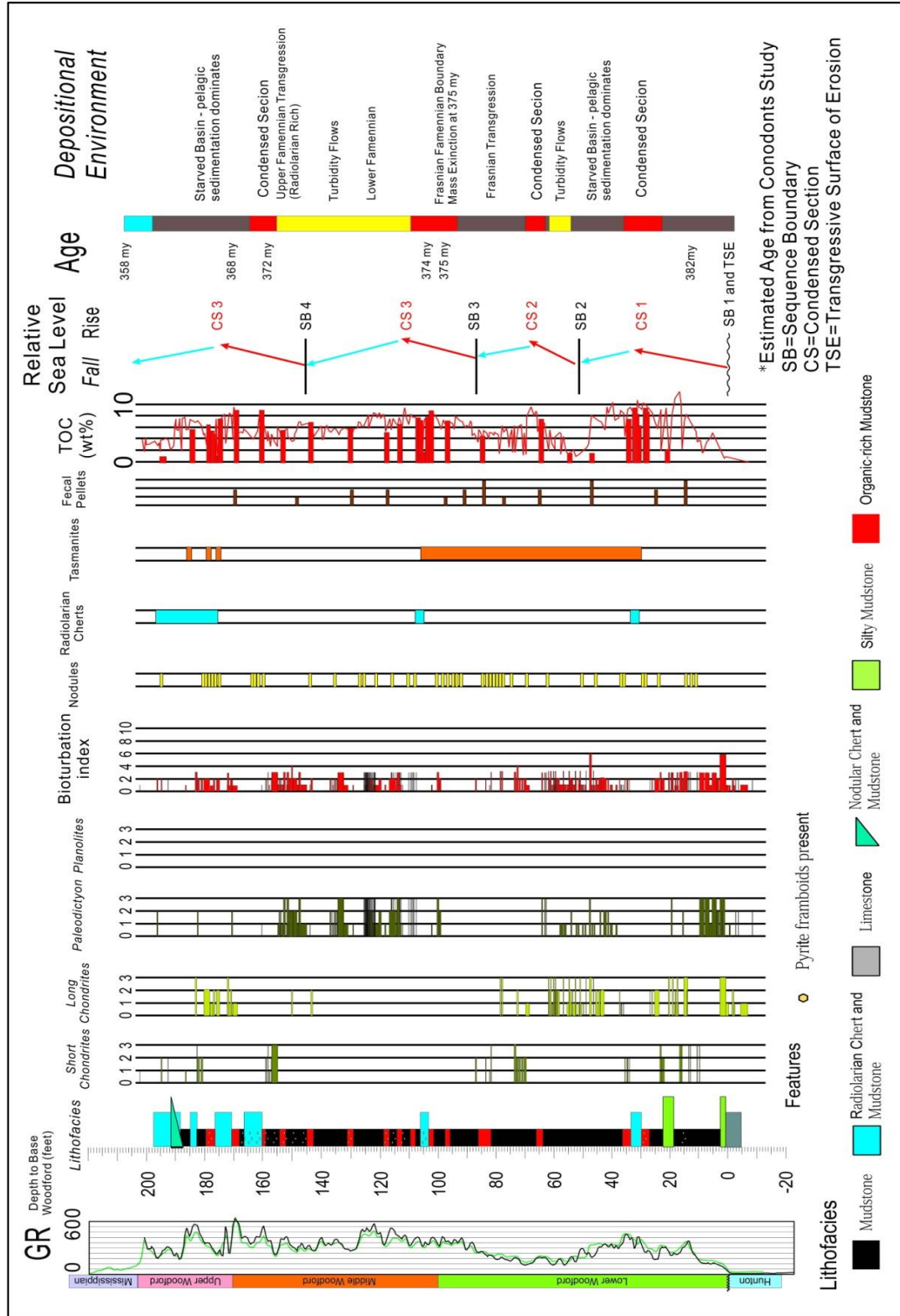


Figure 4.21. Integrated description of Core B, with emphasis on bioturbation. Bioturbation Index (BI) is the sum of all four trace fossils (short *Chondrites*, long *Chondrites*, *Paleodictyon*, *Planolites*). Description and Interpretation are based on Dr. Joan Spaw, Kimberly Hlava and Fuge Zou's work.

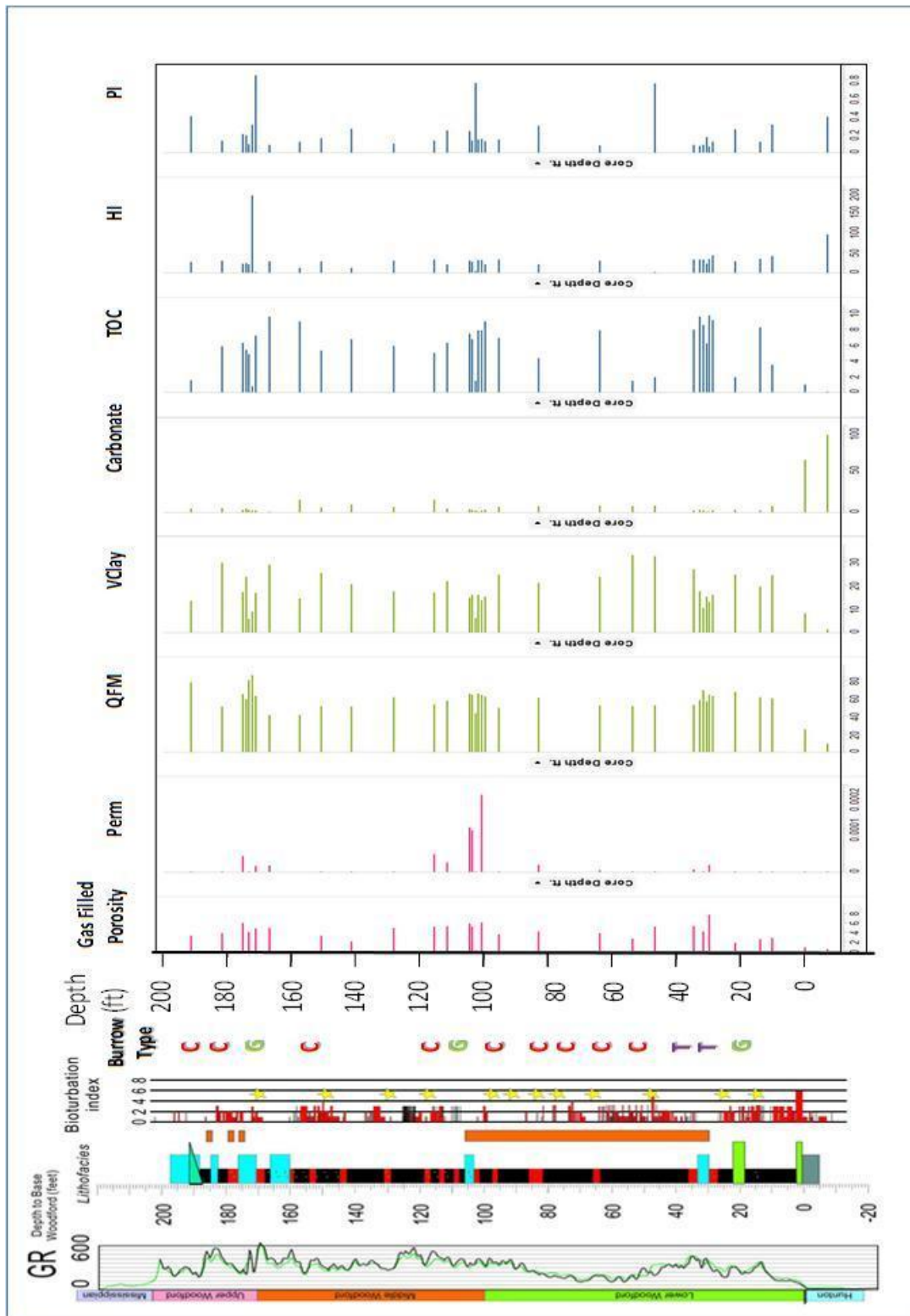


Figure 4.22. Integration of bioturbation data for Core B with chemostrata data. The high resolution hand held X-Ray Fluorescence (XRF) data is from Dr. Harry Rowe of University of Texas at Austin. Burrow Type: Chondrites (C), Paleodictyon and Grazing Trails (G), Planolites (P) and *Thalassinoides* (T)

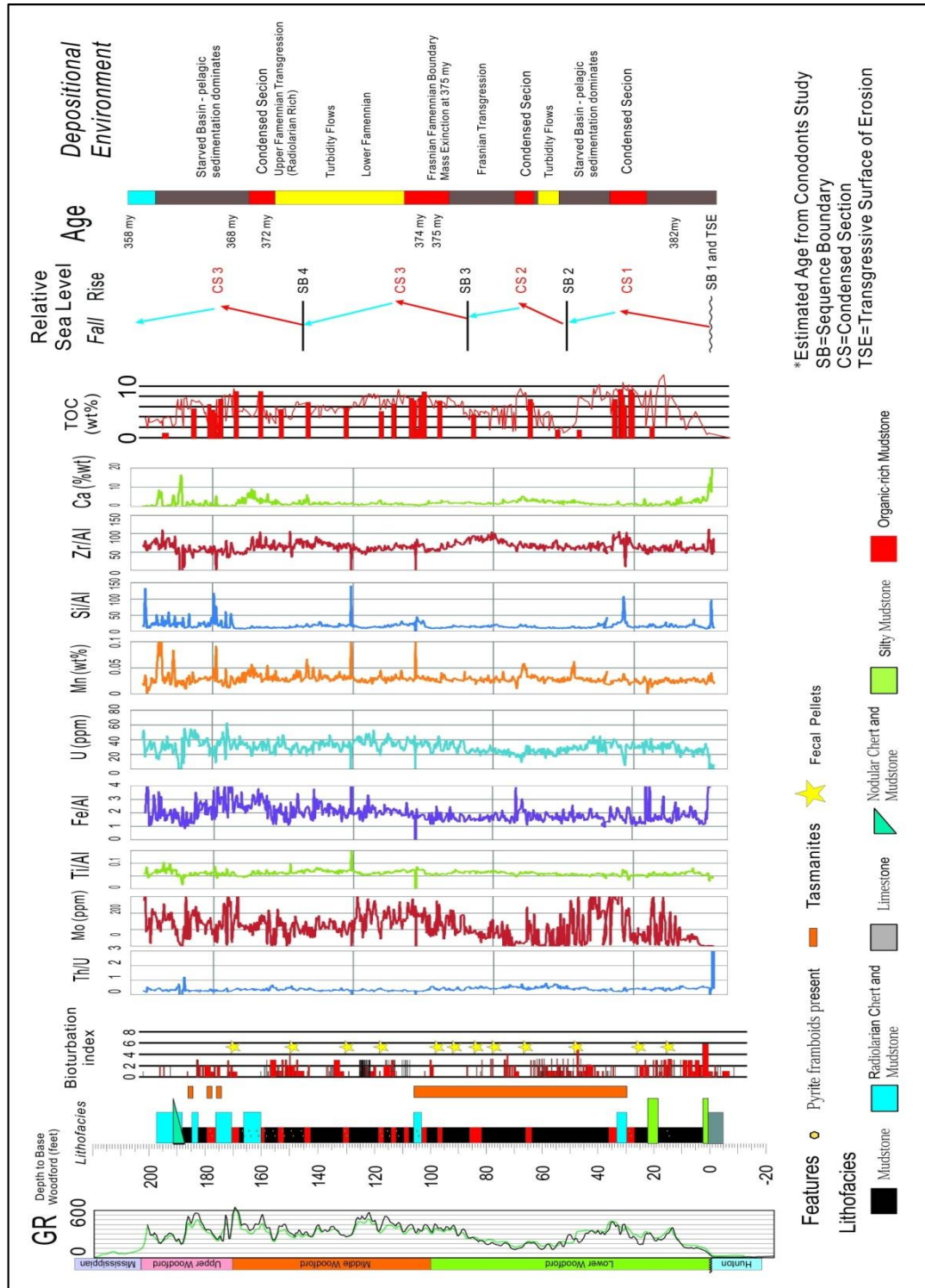


Figure 4.23. Integration of bioturbation data for Core B with chemostrata data. The high resolution hand held X-Ray Fluorescence (XRF) data is from Dr. Harry Rowe of University of Texas at Austin.

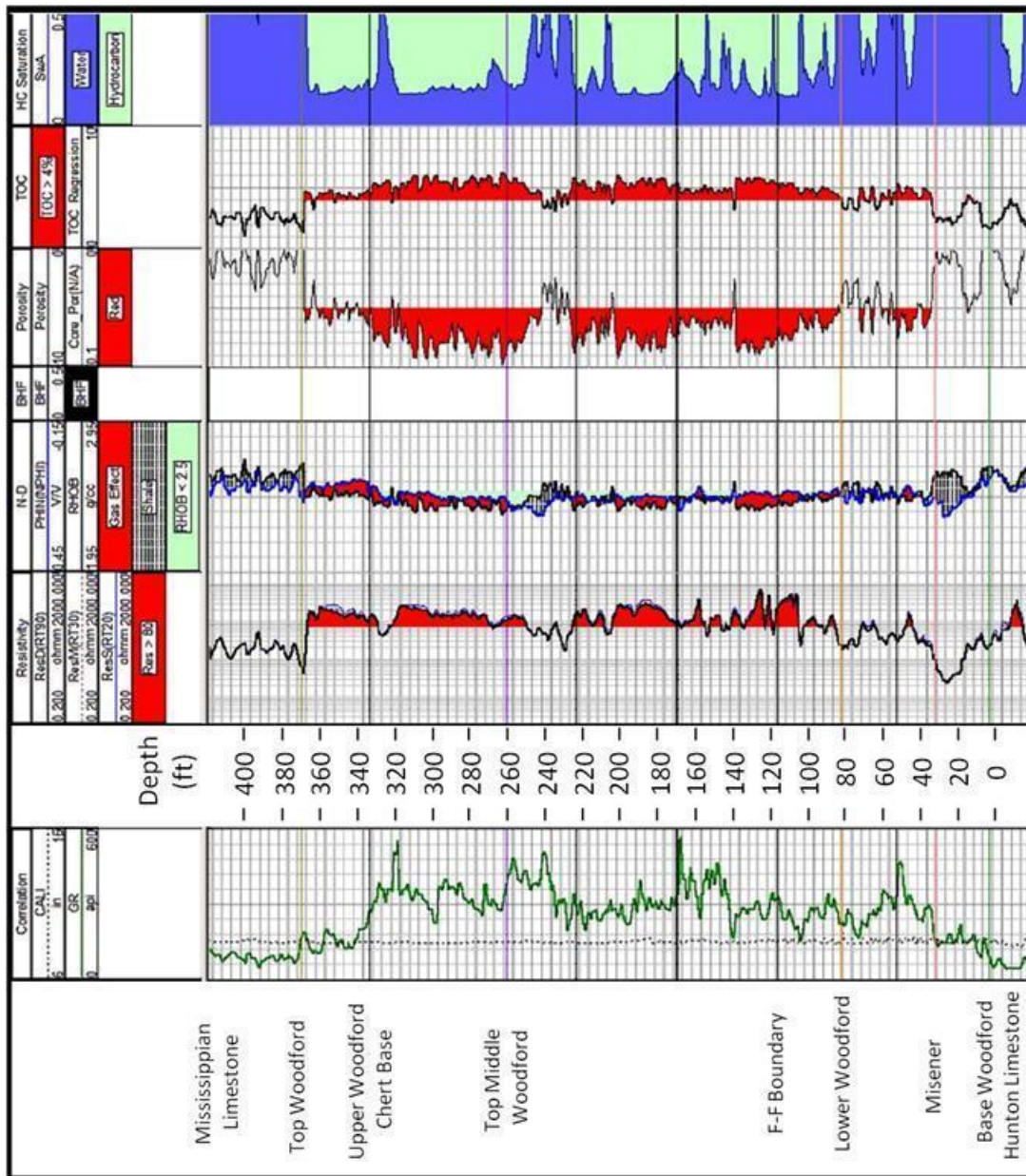


Figure 4.24. Petrophysics logs of Corer C, including GR, Resistivity, Neutron-Density, Calculated TOC, VClay, and calculated water saturation.

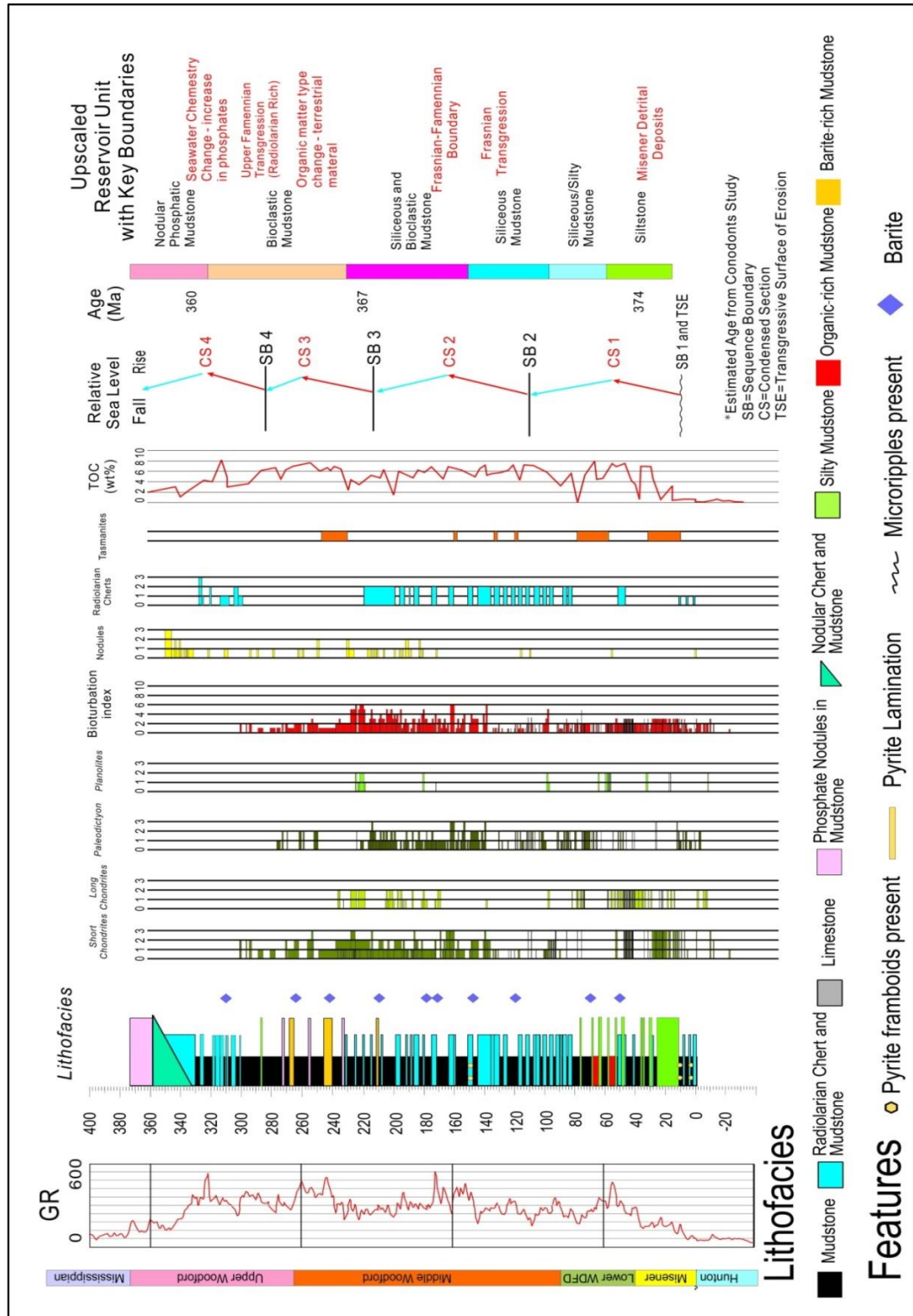


Figure 4.25. Integrated description of Core C, with emphasis on bioturbation. Bioturbation Index (BI) is the sum of all four trace fossils (short *Chondrites*, long *Chondrites*, *Paleodictyon*, *Planolites*). Description and Interpretation are based on Dr. Joan Spaw, Kimberly Hlava and Fuge Zou's work.

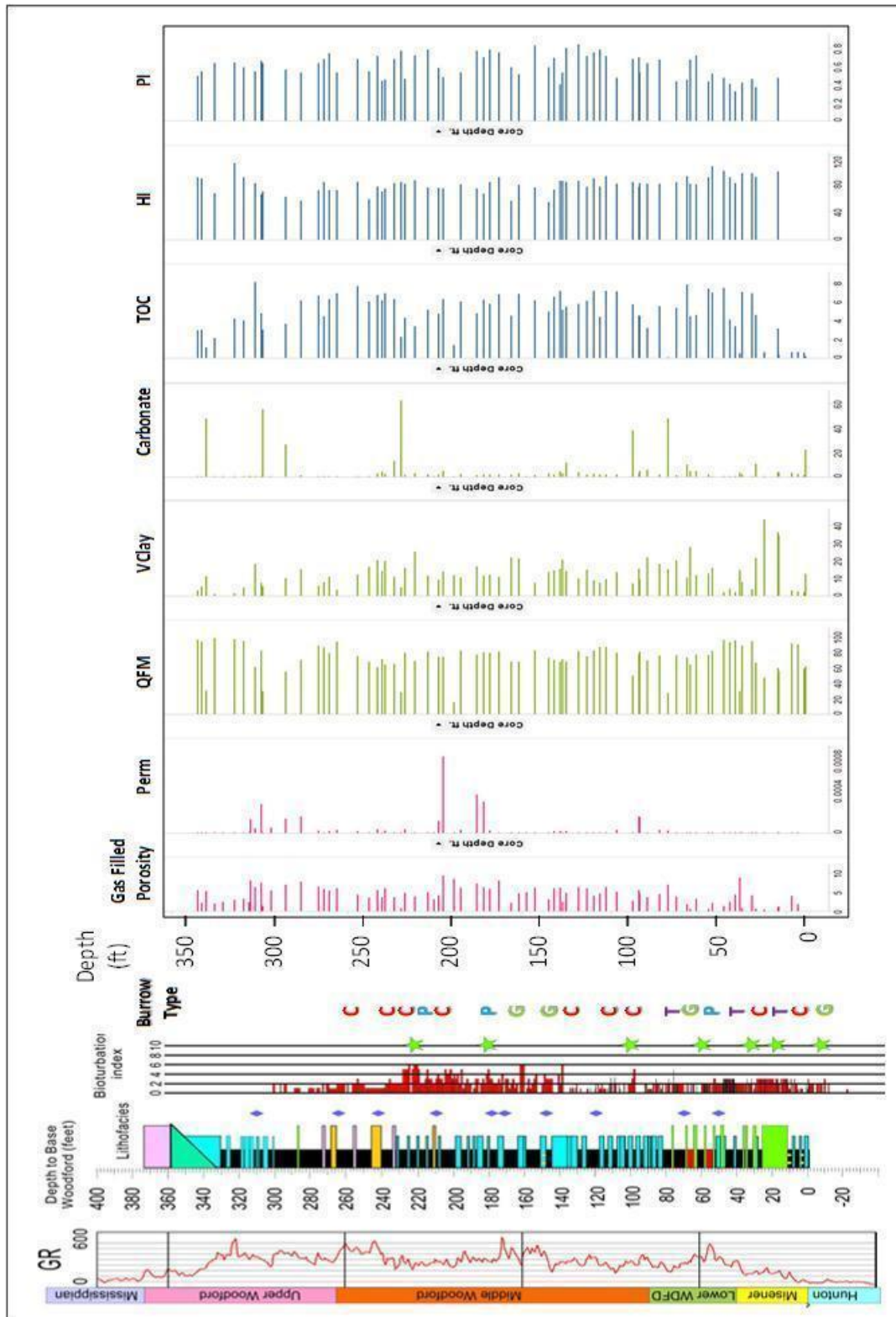


Figure 4.26. Integration of bioturbation data for Core C with chemostrata data. The high resolution hand held X-Ray Fluorescence (XRF) data is from Dr. Harry Rowe of University of Texas at Austin. Burrow Type: Chondrites (C), Paleodictyon and Grazing Trails (G), Planolites (P) and *Thalassinoides* (T)

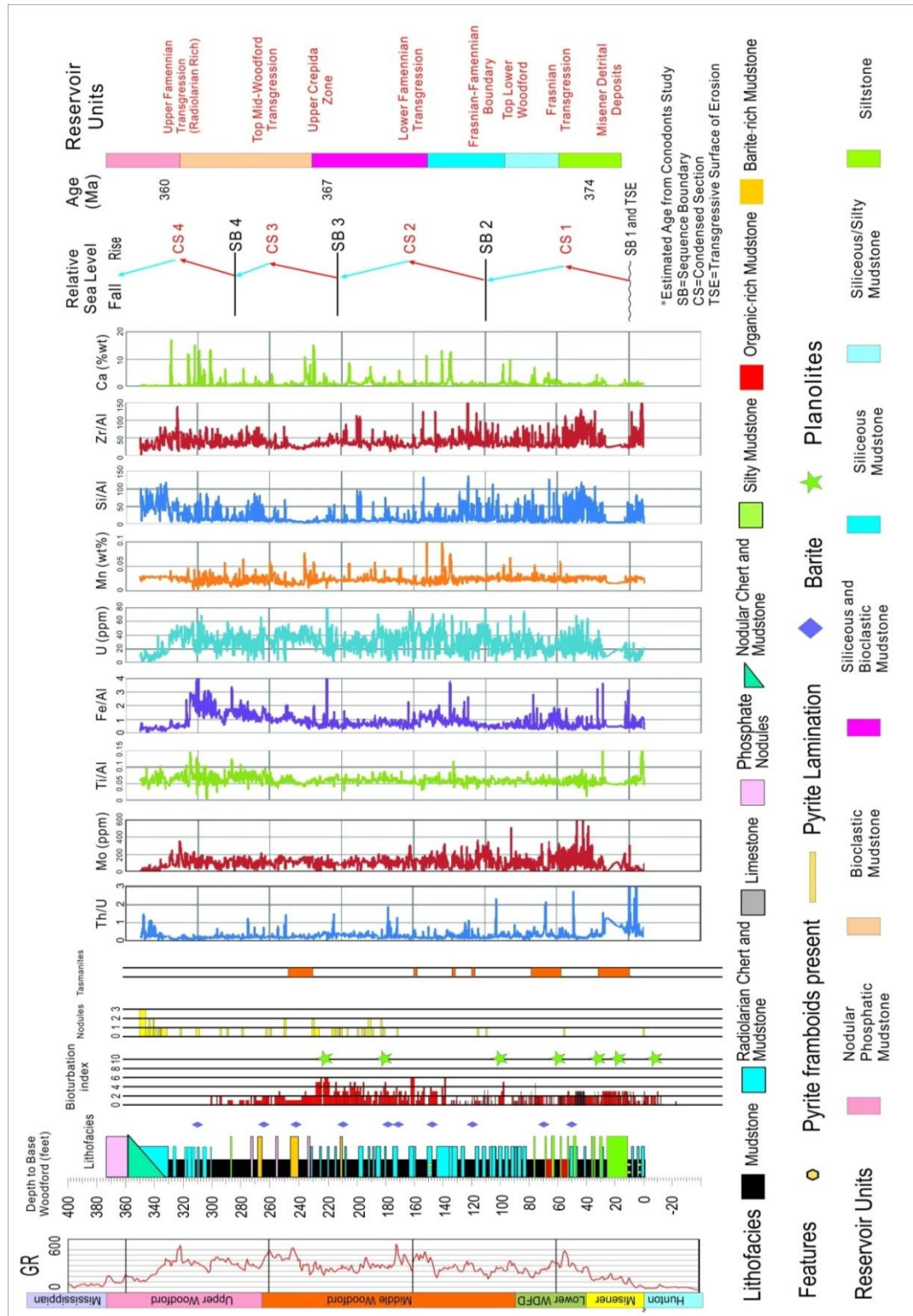


Figure 4.27. Integration of bioturbation data for Core B with chemostrata data. The high resolution hand held X-Ray Fluorescence (XRF) data is from Dr. Harry Rowe of University of Texas at Austin.

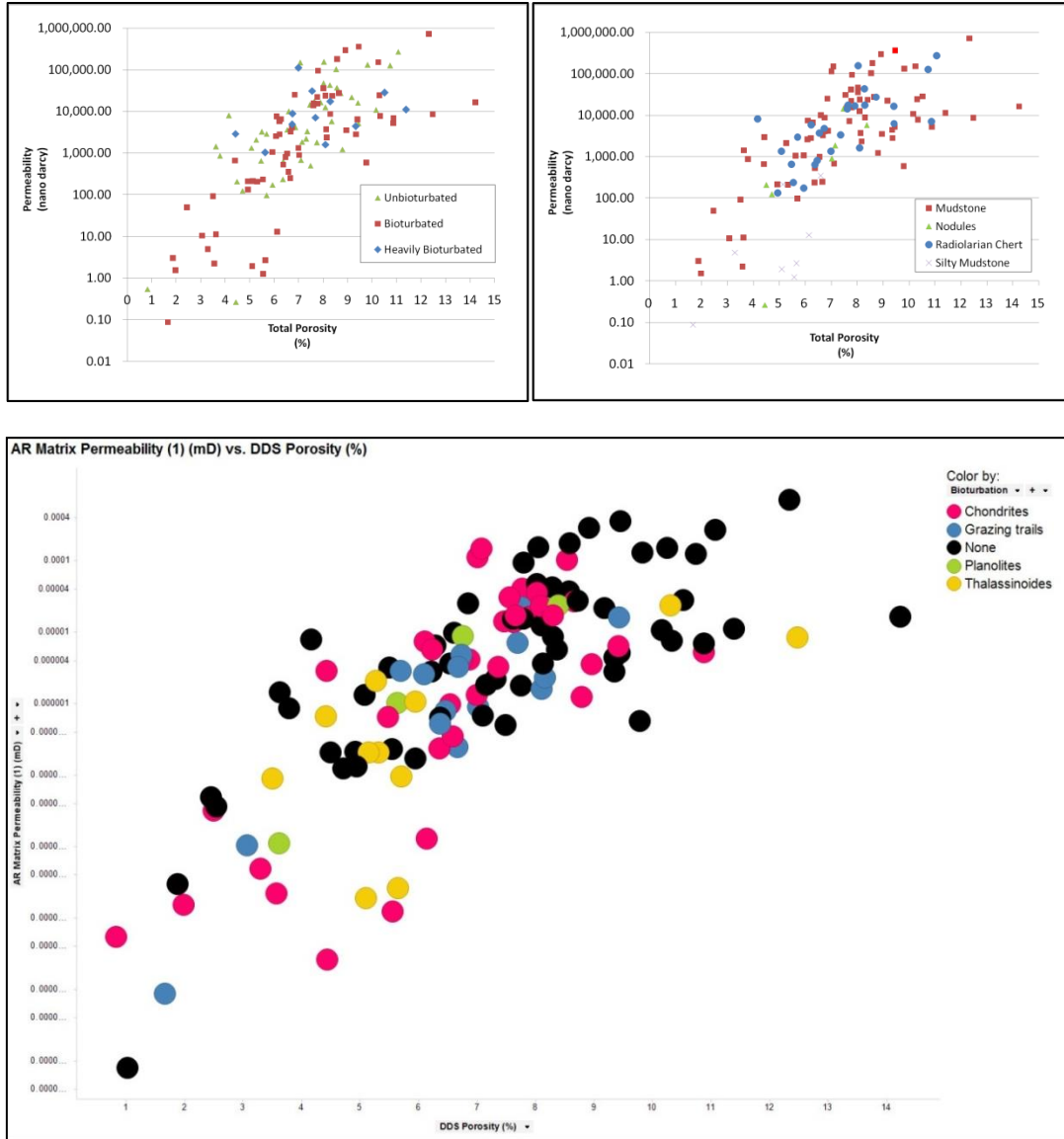


Figure 4.28. Cross-plotting of bioturbation intensity, permeability, porosity and lithofacies of 149 samples from three the Woodford corers. Upper Left is the permeability-porosity plot colored by bioturbation index. Upper Right is the permeability-porosity plot colored by lithofacies. Lower is the plotting of Porosity vs. Permeability colored by bioturbation types.

Bioturbation Type	Chondrites	Paleodictyon (Grazing Trails)	Thalassinoidae	Planolites
Bioturbation Presence and Abundance	None to abundant across the entire Woodford shale interval, short Chondrites are small short pipes and long Chondrites are branched and large straight pipes	None to abundant across the entire Woodford shale interval, parallel to the bedding plane, "cookie" like geometry indicate parallel laminations	Low to Medium Abundance in the Lower Woodford only	None to Medium, mostly present in the Middle Woodford Shale
Lithofacies	Mostly in Siliceous shales in Middle and Upper Woodford shale which is often pyritized.	Clay-rich laminated shales with pyrite filled radiolaria	Mudstones with higher clay content (30%) in the Lower Woodford shale.	Radiolarian Cherts with high quartz content n
Total Organic Carbon	3-9.5%wt, Average = 5%wt	0.18-7%wt, Average = 5.1%	0.09-8.13%wt, Average = 3.5%	3.3-8.5%wt, Average = 6.2%
Porosity	4-11%, Average = 6.7%	1.7-9.4%, Average = 6.5%	3.5-12.5%, Average = 6.2%	3.6-8.4%, Average = 6.1%
Permeability	20-148000 nano darcy, Average = 17961 nano darcy	11-22200 nano darcy, Average = 4357 nano darcy	2-23900 nano darcy, Average = 3348 nano darcy	11-23700 nano darcy, Average = 8372 nano darcy
Mineralogy	Quartz: 43-93.5%wt, Average = 57.4%; Clay: 6-43.2%wt, Average = 17.3%	Quartz: 21-91.0%wt, Average = 50.8%; Clay: 3-32.3%wt, Average = 19.3%	Quartz: 21-94.6%wt, Average = 60.9%; Clay: 2.1-35.8%wt, Average = 17.2%	Quartz: 45.9-70.7%wt, Average = 60.6%; Clay: 11.8-24.9%wt, Average = 17.6%
Chemostrata Characters	Generally Correlates to Low Mo, Low Zr, and Low Si/Al	Generally Correlates to Low Fe/Al	Generally Correlates to Low Mo and High Zr/Al	Generally Correlates to High Fe/Al
Sequence Stratigraphic Position	Mostly in HST	Mostly in TST	Backfill stage during TST	Mostly in TST

Table 4.1: Comparing the relationship between type and abundance of Bioturbation in Woodford and key reservoir parameters.

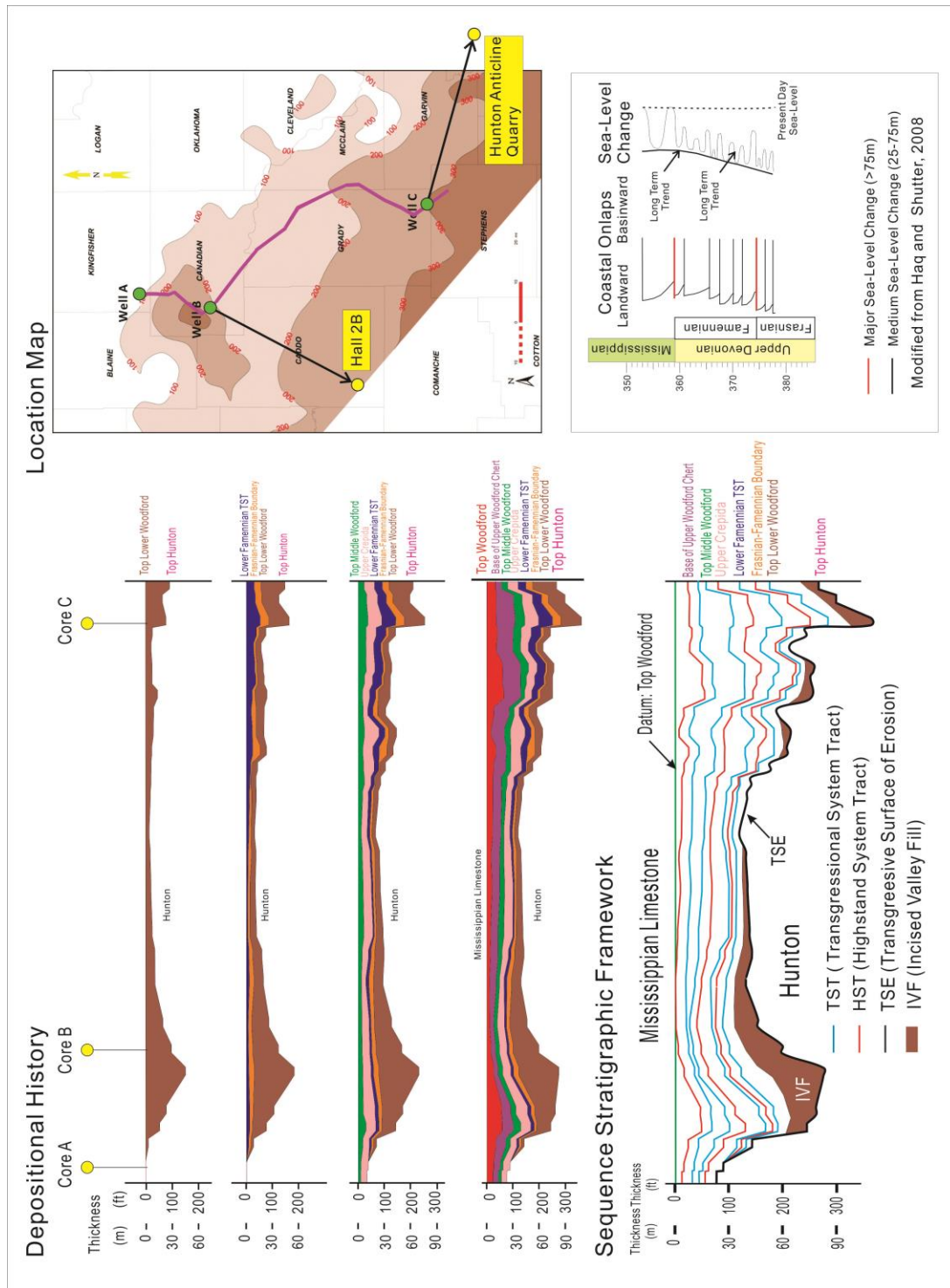


Figure 4.29. Regional stratigraphic framework of Woodford Shale in the study area. Left is the reconstruction of basin history. Right is location map (including correlation to the Hall 2B well and Hunton Anticline Quarry) and global sea-level curve.

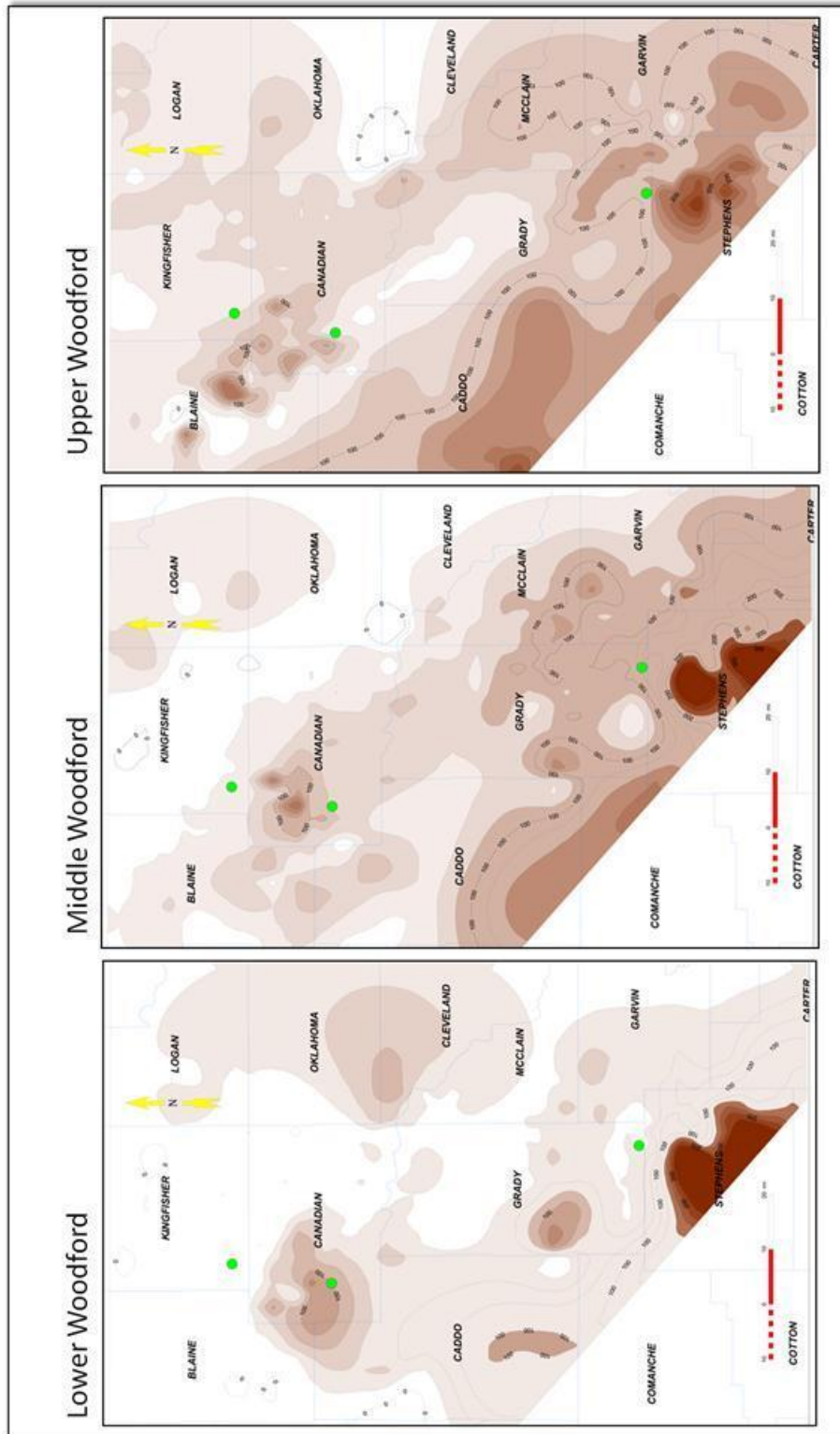


Figure 4.30. Gross isochore maps of Lower Middle and Upper Woodford Shale, showing the transition of more restricted deposition in Lower Woodford to more extended deposition in Upper Woodford.

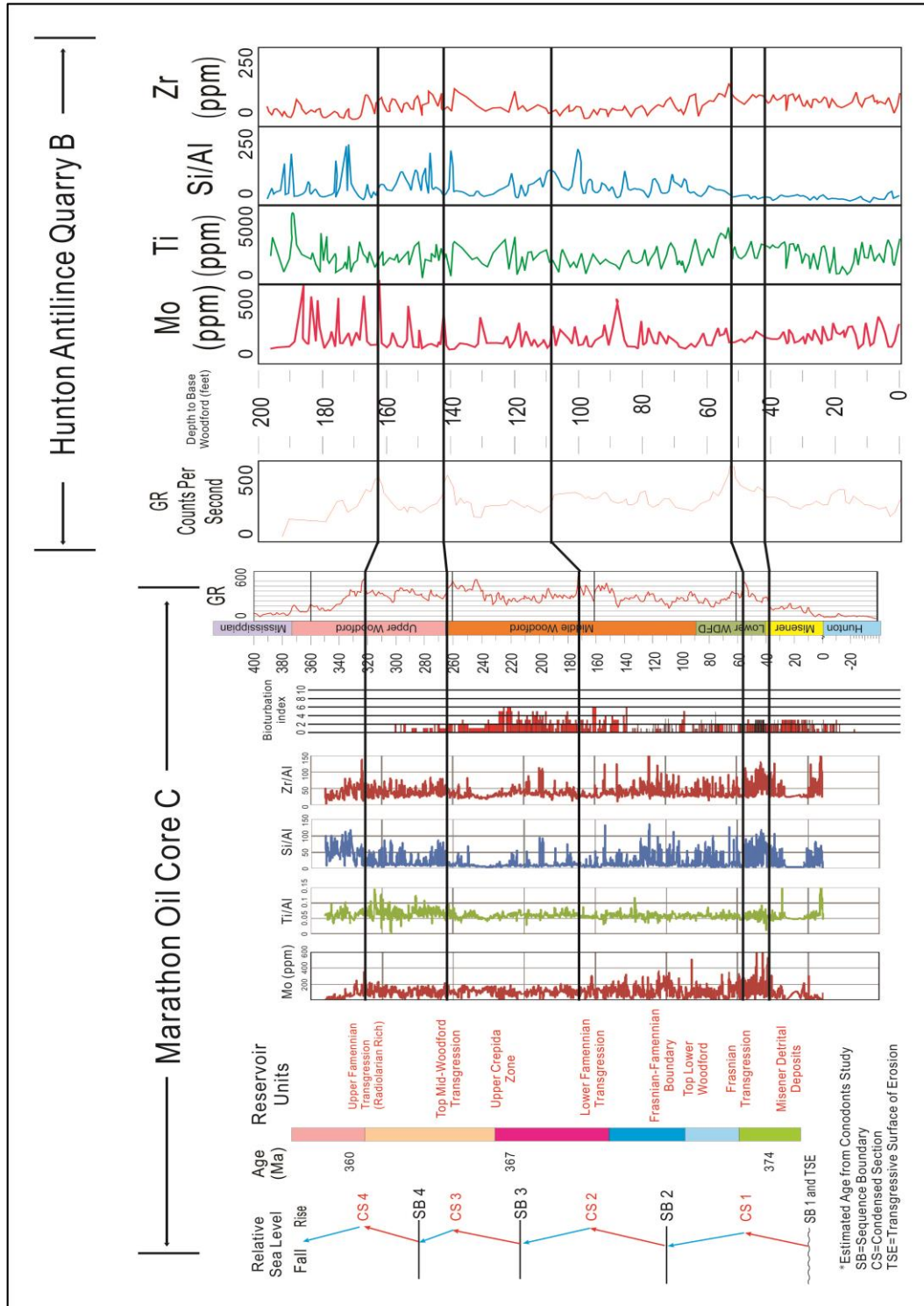


Figure 4.31. Correlation from Marathon Oil Core C to Hunton Anticline Quarry (measured by Bryan and Slatt, 2013) ~25 Miles (40km) southeast to Core C. Gamma Ray and key chemostrata parameters matches the sequence stratigraphic framework.

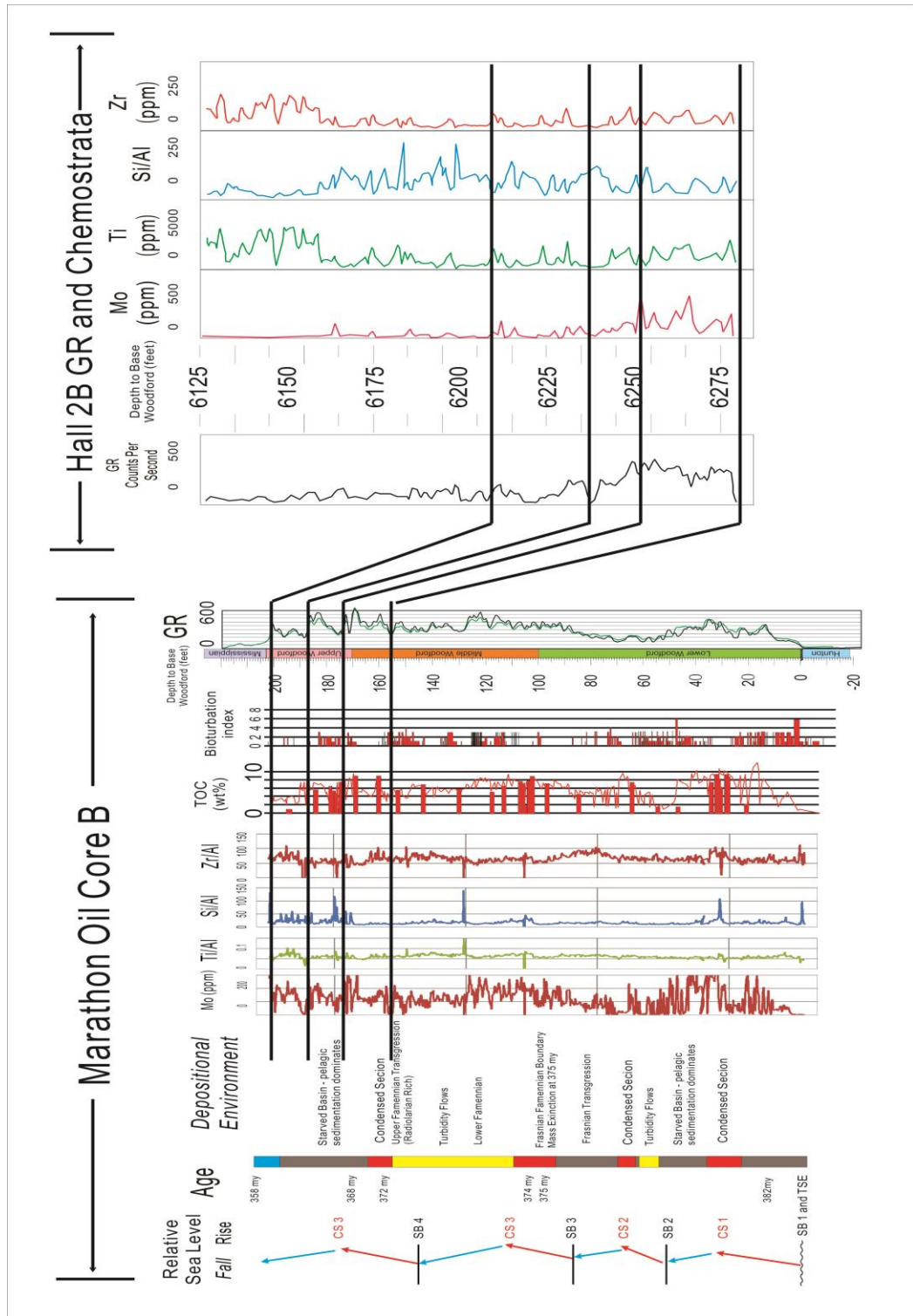


Figure 4.32. Correlation from Marathon Oil Core B to Hall 2B well (measured by Bryan and Slatt, 2013) ~30 Miles (48km) southwest to Core B. Gamma Ray and key chemostrata parameters matches the sequence stratigraphic framework. Note Hall 2B only cut Upper Woodford and Upper Middle Woodford Shale.

REFERENCES

- Bednarz, M. and D. McIlroy, 2012, Effect of phycosiphoniform burrows on shale hydrocarbon reservoir quality, *AAPG Bulletin*, v. 96, no. 10, pp. 1957–1980.
- Boyer, D.L. and M.L. Droser, 2011, A combined trace- and body-fossil approach reveals high-resolution record of oxygen fluctuations in Devonian seas, *PALAIOS*, v. 26, p. 500–508.
- Chain, A.R., 2012, Stratigraphy and composition of the Woodford Shale in positionally updip and downdip wells, Anadarko basin, Oklahoma, Master Thesis of the University of Oklahoma, pp.1-250.
- Erdman, N., and N. Drenzek, 2013, Integrated preparation and imaging techniques for the microstructural and geochemical characterization of shale by scanning electron microscopy, in Camp, W.K., E. Diaz, and B. Wawak (eds.), *Electron Microscopy of Shale Hydrocarbon Reservoirs*, Amer. Assoc. Petrol. Geol. Mem. 102, p. 7-14.
- Gamero-Diaz, H., C. Miller, and R. Lewis, 2012, sCore: A Classification Scheme for Organic Mudstones Based on Bulk Mineralogy, AAPG 2012 Southwest Section Meeting, Ft. Worth, Texas. AAPG Search and Discovery Article #40951.
- Griffith, C., 1977, Stratigraphy and paleoenvironment of the New Albany Shale Upper Devonian in north central Kentucky, M.Sc. thesis, University of Wisconsin at Madison, pp.214.
- Haq, B. U. and S. R. Shutter, 2008. A chronology of Paleozoic sea-level changes. *Science*, Vol. 322, October 2008, p. 64-68.

- Hlava, K., D. Alfred, B. Ramirez, and J. Rodriguez, 2013, Application of a Depositional and Sequence-Stratigraphic Model for Geocellular Modeling of the Woodford Formation, Oklahoma, Abstract of AAPG Annual Convention and Exhibition, May 19-22, Pittsburgh, PA.
- Hemmesch, N.T., N. B. Harris, C. A. Mnich, and D. Selby, 2014, A sequencestratigraphic framework for the Upper Devonian the Woodford Shale, Permian Basin, west Texas, AAPG Bulletin, v. 98, no. 1, pp. 23–47
- Jordan, D.W., 1985, Trace fossils and depositional environments of Upper Devonian black shales, east-central Kentucky, U.S.A. the SEPM Biogenic Structures: Their Use in Interpreting Depositional Environments (SP35), pp.279-298.
- Kidder, D.L. and D.H. Erwin, 2001, Secular Distribution of Biogenic Silica through the Phanerozoic: Comparison of Silica-Replaced Fossils and Bedded Cherts at the Series Level, The Journal of Geology, Vol.109, No.4, pp.509-522.
- La Croix, A.D., M.K. Gingras, S.E. Dashtgard, and S. G. Pemberton, 2012, Computer modeling bioturbation: The creation of porous and permeable fluid-flow pathways, AAPG Bulletin, Vol.96, No.3, pp.545-556.
- La Croix, A.D., M.K. Gingras, S.G. Pemberton, C.A. Mendoza, J.A. Maceachern and R.T. Lemiski, 2013, Biogenically enhanced reservoir properties in the Medicine Hat gas field, Alberta, Canada, Marine and Petroleum Geology, Vol.43, pp.464-477.
- Loucks, R.G., R.M. Reed, S.C. Ruppel, and D.M. Jarvie, 2009, Morphology, Genesis, and Distribution of Nanometer-Scale Pores in Siliceous Mudstones of the

- Mississippian Barnett Shale: *Journal of Sedimentary Research*, v. 79/12, p. 848–861.
- Loucks, R.G., R.M. Reed, S. C. Ruppel, and U. Hammes, 2012, Spectrum of pore types and networks in mudrocks and a descriptive classification for matrix-related mudrock pores, *AAPG. Bull.*, v. 96, p. 1071-1098.
- Mann, E., 2014, Stratigraphic study of organic-rich microfacies of the Woodford Shale, Anadarko basin, Oklahoma, Master Thesis of the University of Oklahoma, pp.1-200.
- Mu., G., N. Singh, S. Wang, M. Wright, E. Davies, B. Liu, 20113, Chemostratigraphy and Sequence Stratigraphic Investigation of the Lower Silurian - Upper Ordovician Hot Shale, Southeastern of the Sichuan Basin, *SPE 167022*, pp. 1-10.
- Ratcliffe, K. T., A.M. Wright and K. Schmidt, 2012, Application of inorganic whole-rock geochemistry, to shale resource plays: an example from the, Eagle Ford Shale Formation, Texas, *the Sedimentary Record*, Vol. 10, No.2, pp. 4-10.
- Schieber, J., J.B., Southard and A., Schimmelmann, 2010, Lenticular Shale Fabrics Resulting From Intermittent Erosion Of Water-Rich Muds: Interpreting The Rock Record In The Light Of Recent Flume Experiments: *Journal Of Sedimentary Research*, V. 80, P. 119–128.
- Simpson, S., 1956, On the trace fossil *Chondrites*, *Quart. Journal of Geological Society of London*, v.112, p. 475-499.
- Slatt, R. M., N. Buckner, Y. Abousleiman, R. Sierra, P. Philp, A. Miceli-Romero, R. Portas, N. O'Brien, M. Tran, R. Davis, and T. Wawrzyniec, 2011, Outcrop/behind

outcrop (quarry), multiscale characterization of the Woodford Gas Shale, Oklahoma, in J. Breyer, ed., Shale reservoirs - Giant resources for the 21st century: AAPG Memoir 97, p. 1–21.

Slatt, R. M., and N. R., O'Brien, 2011, Pore types in the Barnett and the Woodford gas shale: Contribution to understanding gas storage and migration pathways in fine-grained rocks: The American Association of Petroleum Geologists, v. 95, no. 12, p. 2017-2030

Slatt, R. M., and Y. Abousleiman, 2011, Merging sequence stratigraphy and geomechanics for unconventional gas shales: The Leading Edge, v. 30, p. 274–282, doi:10.1190/1.3567258.

Slatt, R. M., 2013, Sequence stratigraphy of the Woodford Shale and application to drilling and production, Oral presentation given at AAPG the Woodford Shale forum, Oklahoma City, Oklahoma in April, 11, 2013. AAPG Search and Discovery Article #50792.

Slatt, R.M., N. O'Brien, C. Molinares-Blancos, A. Serna-Bernal, E. Torres, and P. Philp, 2013, Pores, spores, pollen and pellets: small, but significant constituents of resource shales, URTeC 2013 ext. abs. Control No. 1573336, 17p.

Slatt, R.M. and N. O'Brien, 2014, Variations in Shale Pore Types and their Measurement, Unconventional Resources Technology Conference, Denver, Colorado, 25-27 August 2014: DOI 10.15530/urtec-2014-1921688.

Spaw, J.M., 2013, Recognition of Ichnofacies Distributions and their Contributions to Matrix Heterogeneity in Mudstones. Unconventional Resources Technology Conference, Denver, Colorado, 12-14 August 2013: pp. 664-668.

Tribovillard, N., T.J. Algeo, T. Lyons, and A. Riboulleau, 2006, Trace metals as paleoredox and paleoproductivity proxies: An update, *Chemical Geology*, Vol. 232, pp.12-32.